The Functional Role of Cardiac Non-Neuronal Cholinergic System in the Diabetic Heart

By

Eng Leng SAW

Department of Physiology

University of Otago

A thesis submitted for the degree of Doctor of Philosophy at the University of Otago, Dunedin, New Zealand

August 2019

Abstract

In type-2 diabetes mellitus (T2DM), insulin resistance and metabolic derangements reduce glucose transporter-4 (GLUT-4) expression to decrease glucose uptake, and hence the glucose oxidation in the diabetic heart. Further, the diabetic heart displays reduced basal myocardial energy status while diminished glucose oxidation further aggravates this condition in myocardial ischemia. Previous studies showed that normalization of glucose metabolism via increasing GLUT-4 expression attenuated diabetes-induced cardiac dysfunction. Cardiomyocytes possess a non-neuronal cholinergic system (NNCS) that consists of choline acetyltransferase (ChAT), choline transporter 1 (CHT1), vesicular acetylcholine transporter (VAChT), and acetylcholinesterase (AChE) to synthesize, release and degrade acetylcholine (ACh), respectively. The released ACh binds to type-2 muscarinic ACh receptor (M_2AChR) and mediates pro-survival phosphatidylinositol-3-kinase (PI3K)/protein kinase B (Akt) /hypoxia-inducible factor1α (HIF1α) signaling cascade to promote glucose metabolism through increasing GLUT-4 expression in normoxic condition. However, the expression and function of cardiac NNCS are not known in the diabetic heart. Therefore, the main aim of this thesis was to examine the role of cardiac NNCS in the diabetic heart.

The first aim was to investigate if the expression of cardiac NNCS (i.e., ChAT, CHT1, VAChT, AChE, and M_2AChR) and glucose transporters (GLUT-1 and GLUT-4) are affected in the diabetic *db/db* mouse and the diabetic human heart. The novel findings showed that the expression of the components of cardiac NNCS were altered in the diabetic *db/db* mouse (i.e., increased AChE and decreased M_2AChR expression) and diabetic human heart (i.e., decreased CHT1 expression). Besides, the findings also confirmed that T2DM decreased GLUT-4 expression in the diabetic *db/db* mouse and the diabetic human heart. Interestingly, the alteration of cardiac NNCS preceded the decrease in GLUT-4 expression and diastolic dysfunction in the *db/db* mice. Also, the findings showed that the diabetic cardiomyocytes

altered cardiac NNCS (i.e., increased VAChT and CHT1 expression; decreased AChE and M_2AChR expression) possibly to enrich the *db/db* mouse heart with ACh after developing diastolic dysfunction.

The next aim was to examine if cardiac NNCS activation can increase GLUT-4 expression and enhance the LV function of the diabetic heart. In this case, this study used diabetic *db/db* mice with ventricular-specific overexpression of *ChAT* gene (*db/db-ChAT-tg*). The findings showed that cardiac NNCS activation significantly enhanced the LV systolic function and contractibility in the diabetic heart. Further, western blot analysis confirmed that the superior LV function was associated with increased GLUT-4 expression, which was activated by pro-survival PI3K/Akt/HIF1α signaling cascade in the diabetic heart. As previous studies showed that cardiac NNCS plays a role in angiogenesis, I next investigated if activation of cardiac NNCS enhances the vascular function of the diabetic heart. The findings showed that activation of cardiac NNCS preserved the coronary macro- and micro-vasculature and endothelial function in the diabetic heart. Western blot analysis confirmed that the preserved vascular function was associated with increased VEGF-A expression in the diabetic heart.

Having demonstrated the role of cardiac NNCS in the diabetic heart, I further investigated if cardiac NNCS activation increases GLUT-4 expression and in return, attenuates the hypoxic injury in the diabetic cardiomyocytes *in-vitro*. The *in-vitro* insulin resistance diabetic cardiomyocytes model showed impaired Akt phosphorylation induced by 400 μM palmitate and 30.5 mM glucose. The findings revealed that cardiac NNCS activation by overexpression of the *ChAT* gene did not alleviate hypoxia-induced apoptosis, although it preserved membrane GLUT-4 expression in the diabetic cardiomyocytes model. Further, the findings also revealed that palmitate and glucose treatment, as well as hypoxia, decreased cardiac NNCS activation, as indicated by reduced ChAT expression. On a side note, my results also showed that insulin could be an inducer of cardiac NNCS activation. However, insulin resistance abolished the effect.

In conclusion, this thesis provides the first evidence that cardiac NNCS is altered in diabetes heart. Such alteration may contribute to decreased GLUT-4 and glucose uptake, and eventually causing cardiac dysfunction in the diabetic heart. The thesis also shows the protective effect of cardiac NNCS on the cardiovascular function of diabetic heart. Taken together, targeting cardiac NNCS to increase GLUT-4 and VEGF-A can be a potential therapeutic intervention to enhance glucose metabolism and angiogenesis, respectively, can be a potential therapeutic intervention to prevent the development of DHD in the diabetic heart.

Acknowledgments

To begin with, I would like to thank my supervisors – A/Prof. Rajesh Katare and Dr. Martin Fronius for their constant support, advice, and care. Thank you so much for all the critical feedback on writing, experimental design, and data analysis, and not to forget, for stopping me from entering the laboratory and reminding me to write thesis! Apart from this, I would like to thank the chair of my Ph.D. committee - Dr. Regis Lamberts for his time to conduct annual meetings and giving suggestions. I would also like to thank Prof. Alison Heather and Dr. Andrew Bahn for allowing me to carry out experiments in their laboratory. I much appreciate A/Prof. Alex Tups and Aline for providing me some samples of sodium palmitate and BSA as well as sharing protocol with me. A special appreciation to A/Prof. Daryl Schwenke for performing surgical preparation in SPring-8 facility, Japan.

I thank Jaya for ordering all the reagents and consumables for my experiment and keeping the laboratory clean and tidy. A special thanks to Emani for helping me in the laboratory and teaching me LC/MS analysis. Besides, I would like to express my appreciation to Mr. Andrew McNaughton from Otago Micro and Nanoscale Imaging (OMNI) for the training on confocal microscopy. I want to thank Mr. Andrew Gray and Dr. Claire Cameron from The Centre for Biostatistics for their advice in statistical analysis.

I will never forget my research training at Nippon Medical School, Japan (Oct-Dec 2017 & Mar-Apr 2019). It was such a privileged opportunity to work with Prof. Yoshihiko Kakinuma, who is the pioneer researcher in cardiac NNCS. I want to thank Prof. Yoshihiko Kakinuma for hosting me and being a great mentor during my stay. I thank Ms. Shino Oikawa and Ms. Yuko Kai for the technical support in the laboratory. I will never forget Dr. Takahiro Nemoto, Dr. Yasuhiro Takenaka, and Dr. Shuei Sugama for lending me western blot apparatuses and giving me tips and advice. Thank you to all the members in the department for helping me to settle down well in Tokyo, sharing oishii (delicious) foods and giving me omiyage (souvenir). A special appreciation to Ms. Shino Oikawa and Dr. Asuka Mano for arranging the hanami (viewing cherry blossoms)! Besides, having an opportunity to work in the SPring-8 facility was a valuable research training as well. I want to thank Prof. James Pearson and Dr. Hirotsugu Tsuchimochi from National Cerebral and Cardiovascular Center for assisting us in the SPring-8 facility. I certainly remembered all the good foods and fun chats we had after a hectic day! A special thanks to Dr. Hirotsugu Tsuchimochi for performing the surgical procedures.

I want to express my deepest gratitude to my parents and my sisters (Elaine and Evonne) for unconditional support and love. I hope they would be proud of me for completing my Ph.D.

journey. I will not skip the graduation ceremony this time so that all of you can witness me wearing the gown and cap in Dunedin and travel around in New Zealand.

I would also like to thank my friends – Joel, Ryan, Rachel, Charmaine, Vee-Liem SAW (my pseudo-cousin), Lucy, Kim, Chris, Shruti, Susan, Prashanth, Sumit and Mazhar for all the fun moments and road trips! Thank you Shruti and Prashanth for picking me up from Dunedin airport when I first arrived in New Zealand. Thanks, Shruti for being such a great friend, accompanying and helping me to settle down in Dunedin. A special thanks to my friends – Pei Thing, Chee Wei, and Kai Hui for bringing me around in Japan for good foods and translating Japanese for me! Thank you to my friends – Gui Ping, Hui Hoon, Hui Ting, and Edmond who came to visit me while traveling in New Zealand.

I would also like to thank departmental staffs for the support and assistance, especially Tracey, Karla, Fran, Heather, Karen, Janine, Rachel, Aaron, Chris, Mandy, Maureen, and Ray. I thank the Ph.D. peers – Aline, Chidima, Esther, Puja, Aram, Sajida, Sama, Adam, Pete, Daniel, Nilanjan, and Akash for the encouragement. A special appreciation goes to Pinky for offering me medicines when I was sick and lending me her vehicle to escape from the laboratory. I would especially like to thank Tanya for giving advice and tips in bacterial work, giving me gift samples of transfection reagent as well as all the encouragements!

Last but not least, I would like to thank the University of Otago for providing the prestigious Doctoral scholarship. I appreciate the Department of Physiology for providing funding for research and travel support. I thank Division of Health Sciences, School of Biomedical Sciences and RSNZ for providing travel funding to attend conferences and conduct research training in Japan.

Author contributions

I performed all the experiments as well as collected, analyzed, and interpreted all the data presented in Chapter 3 to 5, except the following works:

1. In Chapter 3, Dr. Shruti Rawal [1] collected all the mouse ventricular tissues.

2. In Chapter 4, Prof. Yoshihiko Kakinuma measured the body weight (Figure 4.1), blood glucose level (Figure 4.1), and LV function (Figure 4.2 & 4.3) of *db/db-ChAT-tg* mice (8- to 20-weeks of age). I analyzed all the data. After the measurement, Prof. Yoshihiko Kakinuma collected the ventricular tissues for western blot analysis.

3. In Chapter 4, Prof. James Pearson and Dr. Hirotsugu Tsuchimochi from National Cerebral and Cardiovascular Center assisted the works performed in the SPring-8 facility (Japan). Prof. Yoshihiko Kakinuma provided the *db/db* and *db/db-ChAT-tg* mice (12- and 24-weeks of age). A/Prof Rajesh Katare, A/Prof Daryl Schwenke, and Dr. Hirotsugu Tsuchimochi performed surgical preparation for Synchrotron radiation microangiography. I recorded data and collected the mouse ventricular tissues for immunofluorescence analysis and western blot analysis.

Besides, all the illustrative diagrams were generated by me, except Figure 2.6, and 3.1 were taken from the manufacturer's website with permission.

List of prior publications

Saw EL, Kakinuma Y, Fronius M, and Katare R**.** The non-neuronal cholinergic system in the heart: A comprehensive review. *J Mol Cell Cardiol* 125: 129-139, 2018.

Fomison-Nurse I, **Saw EEL**, Gandhi S, Munasinghe PE, Van Hout I, Williams MJA, Galvin I, Bunton R, Davis P, Cameron V, and Katare R**.** Diabetes induces the activation of pro-ageing miR-34a in the heart, but has differential effects on cardiomyocytes and cardiac progenitor cells. *Cell death and differentiation* 25: 1336-1349, 2018.

Statement of contributions: I wrote the manuscript drafts of the first author article.

Note: According to J. Mol. Cell Cardiol.'s policies, I retain the right to include the published review article in my thesis, provided it is not published commercially (https://www.elsevier.com/about/our-business/policies/copyright#Author-rights).

Table of Contents

List of Figures

List of Tables

Abbreviations

A’	Late ventricular filling velocity
ACh	Acetylcholine
AChE	Acetyolcholinesterase
ADP	Adenosine diphosphate
AGEs	Advanced glycation end prodcts
Akt	Protein kinase B
AMP	Adenosine monophosphate
AMPK	5’ AMP-activated protein kinase
AMPKα	5’ AMP-activated protein kinase α-subunit
APS	Ammonium persulfate
AS160	Rab GTPase-activating protein
Asp	Aspartic acid
ATP	Adenosine triphosphate
BMI	Body mass index
BP	Blood pressure
BSA	Bovine serum albumin
CABG	Coronary artery bypass grafting
CAD	Coronary artery disease
ChAT	Choline acetyltransferase
CHF	Chronic heart failure
CHT1	Choline transporter 1
CMVD	Coronary microvascular disease
CO	Cardiac output
CPT-1	Carnitine palmitoyltransferase-1
CTNI	Cardiac troponin I
DAG	Diacylglycerol
DAPI	4’, 6’-diamidino-2-phenylindole
db/db	C57BL/KsJ-Lepr$^{db/db}$ mice
db/db-ChAT-tg	C57BL/KsJ-Lepr$^{db/db}$ –ChAT-tg mice
decT	Early ventricular deceleration time
DHD	Diabetic heart disease
DM	Diabetes mellitus
DMEM	Dulbecco’s modified Eagle’s medium
E’	Early ventricular filling velocity
EF	Ejection fraction

End-diastolic pressure	EDP
End-diastolic volume	EDV
End-systolic pressure	ESP
End-systolic volume	ESV
eNOS	Endothelial nitric oxide synthase
FA-CoA	Long chain fatty acyl-CoA
FBS	Fetal bovine serum
FFA	Free-fatty acid
G6P	Glucose 6-phosphate
GLUTs	Glucose transporters
GLUT-1	Glucose transporter-1
GLUT-4	Glucose transporter-4
$HbAI_C$	Glycated hemoglobin
HCL	Hydrochloric acid
HDL	High-density lipoprotein
HF	Heart failure
HIF1α	Hypoxia-inducible factor 1 α-subunit
HIF1β	Hypoxia-inducible factor 1 beta-subunit
HR	Heart rate
IR	Insulin receptor
IRES	Internal ribosome entry site
IRS1-3	Insulin receptor substrate family protein 1-3
IRX4	Iroquois homeobox 4
IVSd	Interventricular septal diameter diastole
KO	Knockout
LAD	Left anterior descending artery
LC 3-KA	Long chain 3-ketoacyl CoA thiolase
LDL	Low-density lipoprotein
LV	Left ventricle
M_2AChR	Type-2 muscarinic acetylcholine receptor
mAChR	Muscarinic acetylcholine receptor
MI	Myocardial infarction
mRNA	Messenger ribonucleic acid
MVO_2	Myocardial oxygen consumption
nAChR	Nicotinic acetylcholine receptor
NaCl	Sodium chloride

NaOH	Sodium hydroxide
ND	Non-diabetic
NNCS	Non-neuronal cholinergic system
O_2	oxygen molecule
OCT	Optimal cutting temperature
PAGE	Polyacrylamide gel electrophoresis
PBS	Phosphate-buffered saline
PDK	Pyruvate dehydrogenase kinase
PDK1	Phosphoinositide-dependent protein kinase 1
PFA	Paraformaldehyde
PI3K	Phosphatidylinositol-3-kinase
PIP_2	Phosphatidylinositol 4, 5-biphosphate
PIP_3	Phosphatidylinositol 3, 4, 5-triphosphate
PKC	Protein kinase C
PMSF	Phenylmethane sulfonylfluoride
PPARα	Peroxisome proliferator activated receptor alpha
qPCR	Quantitative polymerase chain reaction
RIPA	Radioimmunoprecipitation assay
RNA	Ribonucleic acid
Rpm	Revolutions per minute
RT	Reverse transcription
SDS	Sodium dodecyl sulfate
Ser	Serine
SNP	Sodium nitroprusside
SEM	Standard error of mean
SV	Stroke volume
T1DM	Type-1 diabetes mellitus
T2DM	Type-2 diabetes mellitus
TAG	Triglyceride
TEMED	N, N, N’, N’-Tetramethylethylenediamine
Thr	Threonine
VAChT	Vesicular acetylcholine transporter
VEGF-A	Vascular endothelial growth factor A
VHL	von Hipple-Lindau tumor suppressor
WT	Wild type

Chapter 1 : General Introduction

1.1 Type-2 diabetes mellitus (T2DM)

In the first part of the literature review, I introduce type-2 diabetes mellitus, which is the strong contributing factor of diabetic heart disease (DHD). Then, I will discuss the diabetes-induced alteration in cardiac metabolism and myocardial energy production and how such changes contribute to DHD. Also, the therapeutic options aiming to restore the cardiac metabolism are discussed.

1.1.1 T2DM and diabetic heart disease

Diabetes mellitus is a chronic metabolic disorder characterized by the inability to maintain blood glucose level (reviewed in [2]). The prevalence of DM is increasing at an alarming rate, affecting 425 million individuals (1 in 11 individuals) globally in 2017 [3]. This estimate is projected to further increase to 637 million in 2045 [3]. The standard classifications of DM include type-1 DM (T1DM), type-2 DM (T2DM) and gestational DM (reviewed in [2]). Notably, over 90% of diabetes cases are T2DM, which is characterized by insulin resistance (i.e., defective insulin action) [4]. The pathogenesis of T2DM is complex and entails different elements such as genetic factor, sedentary lifestyle, and dietary factor (reviewed in [5]).

T2DM is associated with more than a two-fold greater risk of developing cardiovascular diseases, which is termed diabetic heart disease (DHD) [6-9]. DHD includes coronary artery disease (CAD), diabetic cardiomyopathy, and heart failure (HF) (reviewed in [10]). The etiology of DHD is multifactorial as DM has different impacts on the cardiovascular system [6, 9, 11-13]. This includes hypertension [14, 15], macro- and microvascular dysfunction [16, 17], impaired cardiac metabolism [18-24], cardiac autonomic neuropathy [25] and increased oxidative stress as well as apoptosis [26, 27].

1.1.2 Cardiac metabolism in the healthy and diabetic heart

1.1.2.1 The healthy heart

The heart is an aerobic organ that relies on the oxidation of substrates such as free fatty acid (FFA), glucose, and lactate to produce ATP [28, 29]. Notably, the heart predominantly metabolizes FFA as it is an energy-dense substrate and contributes to 70% of ATP production in the heart (Figure 1.1A) [28, 29]. Conversely, glucose and lactate contribute to 20% and 10% of ATP production, respectively [28, 29]. As shown in Figure 1.1A, FFA is transported by fatty acid transporter CD36 and enters mitochondria to undergo β-oxidation, Krebs cycle, and oxidative phosphorylation to generate ATP (reviewed in [30, 31]). Further, a healthy heart can flexibly switch substrates to allows adaptation in different physiological [28, 29, 32-34] or pathological conditions [35-37] in response to altered hormones, substrates availability, myocardial oxygen supply, and cardiac workload. For examples, in normal physiological conditions, FFA utilization is predominant in fasted-state [38-40]; glucose utilization is predominant in fed-state [40]; and lactate utilization is predominant during exercise [38, 41].

In a pathological condition such as acute ischemia, the heart prefers to metabolize glucose [42-45] (Figure 1.1B). This preference is because glucose requires lesser oxygen molecules for oxidation (ATP/O_2 ratio = 5-5.3) in comparison to FFA oxidation (ATP/O_2 ratio = 4.6) to generate ATP (reviewed in [46]). However, whether glucose is aerobically or anaerobically metabolized depends on the severity of ischemia. In mild-to-moderate ischemia such as a 60% reduction in left anterior descending (LAD) coronary artery blood flow, glucose oxidation, but not anaerobic glycolysis, is essential to maintain contractile function [45]. In this case, glucose transporter-4 (GLUT-4) transport glucose into the cells where it undergoes glycolysis to be converted into pyruvate, thereby leading to generation of ATPs (Figure 1.1B; reviewed in [31]). Pyruvate is further converted by pyruvate dehydrogenase (PDH) and enters the Krebs cycles, where it subsequently will be further processed and oxidized to generate ATPs (Figure 1.1B; reviewed in [31]).

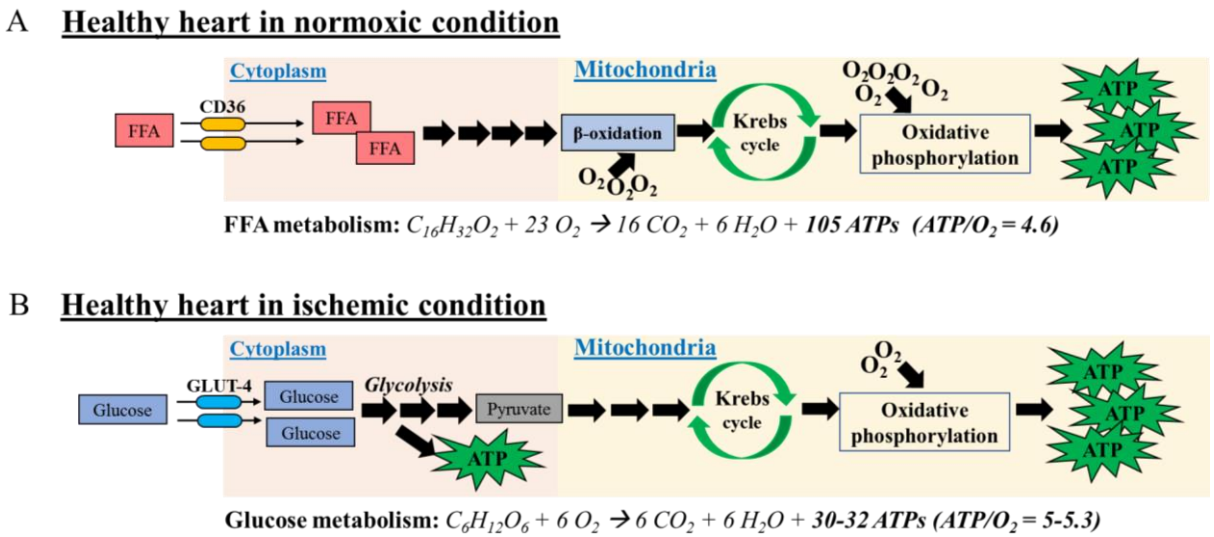

Figure 1.1 Schematic illustration of the cardiac metabolism of a healthy heart under normoxic and ischemic condition.
(A) *A healthy heart predominantly metabolizes FFA to generate ATPs in normoxic condition.* ***(B)*** *In ischemic condition, the heart switches to glucose for ATP generation due to lower oxygen consumption required to complete oxidation in mitochondria.*

1.1.2.2 The diabetic heart

In contrast, the diabetic heart is metabolically inflexible as it mainly relies on FFA to produce ATP (Figure 1.2A) [47-51]. The increase in FFA reliance is due to loss of insulin action, which leads to increased lipolysis from the adipose tissue, and thus increasing the release of FFA into circulation [52]. Hyperlipidemia promotes cardiac FFA uptake, storage, and oxidation in the diabetic heart [53-57]. Further, increased FFA oxidation and insulin resistance reduce expression and membrane translocation of GLUT-4 that is responsible for cardiac glucose uptake, thus suppressing glucose oxidation [56-64]. Therefore, this alteration indicates that the diabetic heart is unable to utilize glucose to generate ATP. Consequently, increased FFA oxidation increases basal myocardial oxygen consumption (MVO_2), thereby reducing cardiac efficiency (a ratio between cardiac work/MVO_2) [19, 20, 65-68]. However, whether reduced cardiac efficiency *per se* alters cardiac function remains inconclusive. This is because the diabetic individuals reported as having normal cardiac morphology and contractility [19, 68] while the diabetic animal models exhibited cardiac dysfunction [51, 65, 67, 69].

1.1.3 Impaired ATP production in the diabetic heart

Multiple studies showed the basal myocardial energy status was decreased in diabetic animal models [70, 71], diabetic patients with normal cardiac function [19] or with abnormal cardiac function [21, 72]. Further, Scheuermann-Freestone et al. [19] showed that decreased basal myocardial energy status was associated with increased plasma FFA in diabetic patients. In line with this, emerging evidence suggests that excessive FFA utilization decreased mitochondrial oxidative capacity, thereby reducing ATP production in the diabetic heart [35, 73-76]. Thus, these studies indicate that increased FFA utilization increased ATP concentrations before the onset of DHD (Figure 1.2A).

As diabetes mellitus progresses, prolonged exposure to metabolic derangements contributes to endothelial dysfunction, contributing to CAD and coronary microvascular disease (CMVD) [16, 17, 77, 78]. CAD and CMVD reduce coronary artery blood flow and myocardial perfusion, thereby reducing the availability of oxygen to the myocardium [68]. In this case, the combinational effects of defective glucose utilization [56-62, 79], decreased oxygen availability [68], excessive FFA utilization [19, 20, 65-68] and reduced mitochondrial oxidative capacity [35, 73-76] impair ATP production and contractile function of the diabetic heart, contributing to cardiac dysfunction [45, 68, 80, 81] (Figure 1.2B).

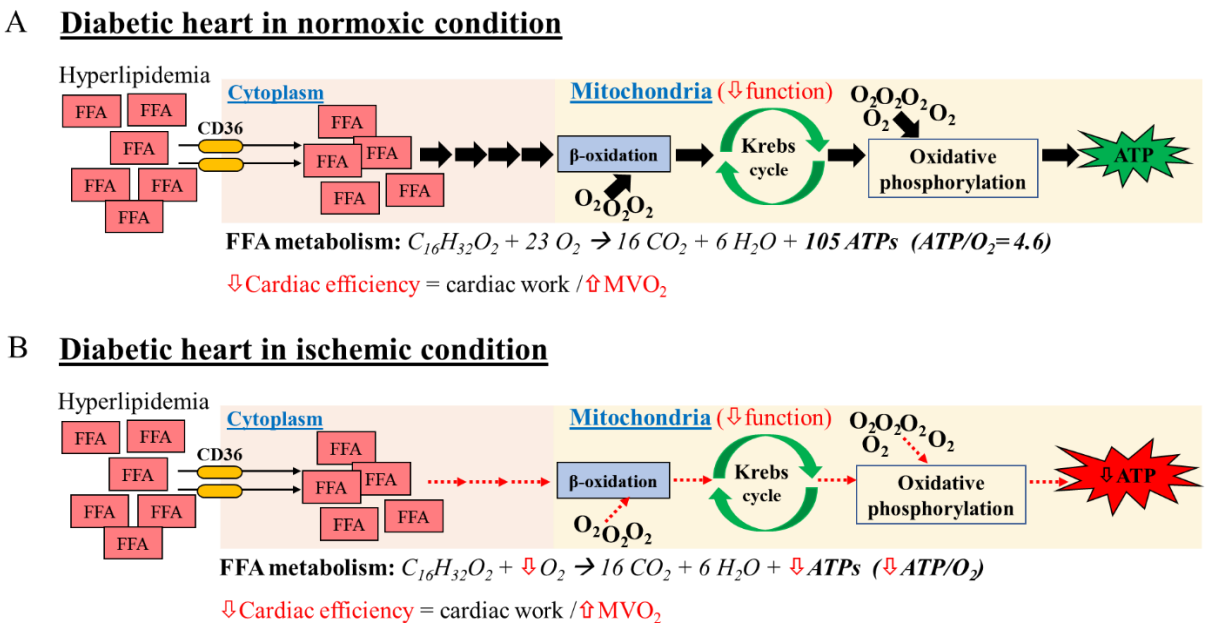

Figure 1.2 Schematic illustration of the cardiac metabolism of a diabetic heart under normoxic and ischemic condition.
(A) *FFA oxidation is increased in the diabetic heart due to insulin resistance and metabolic derangement. Thus, elevated FFA oxidation increases MVO_2 and decrease mitochondrial function, thus leading to decreased cardiac efficiency and ATP production in normoxic condition.* ***(B)*** *In ischemic condition, the availability of oxygen is insufficient for FFA oxidation, thus further impairing the production of ATP. Energy deficit affects the contractile function and subsequently leads to cardiac dysfunction. Red dashed lines indicate diminished FFA oxidation.*

1.1.4 Normalization of cardiac metabolism by pharmacological approaches

As the occurrence of altered cardiac metabolism and energetics precedes the onset of DHD, early normalization of this derangement has been demonstrated to be effective in preventing the onset of DHD in T2DM animal models [19, 20, 23]. In this section, commercially available pharmacological agents that either promote glucose uptake and oxidation or suppress FFA uptake and oxidation are discussed (reviewed in [82]). However, as some of these drugs were developed in the setting of CAD or HF only [83-86], the effect of these drugs in the diabetic population is yet to be elucidated.

1.1.4.1 Targeting the glucose uptake and oxidation

Increased glucose uptake and oxidation can be targeted to normalize the altered cardiac metabolism in the diabetic heart (Table 1.1). For example, glucose-insulin potassium (GIK)

solution increases the insulin concentration in the circulation and stimulate the peripheral organs, including the heart to uptake glucose for oxidation, which in return, reduce the oxygen consumption in the ischemic heart [87, 88]. However, this may not apply to diabetic individuals as the plasma glucose level is already high and accompanied by insulin resistance. Besides, pyruvate dehydrogenase kinase (PDK), which inhibits PDH and prevents the conversion of pyruvate to acetyl-CoA for oxidation, can be inhibited by dichloroacetate, SDZ048-619, and PS10 [86, 89, 90]. However, the effect of these inhibitors was only tested in animal models, while the effect is unknown in diabetic individuals.

Table 1.1 Examples of drugs promote glucose uptake and oxidation

Therapeutic goal	Treatment [Reference]
Increase in glucose uptake from circulation	Glucose-insulin potassium solution [87, 88]
Increase in glucose oxidation	PDK inhibitor – dichloroacetate, SDZ048-619 and PS10 [86, 89, 90]

1.1.4.2 Targeting the FFA uptake and oxidation

Reduction of FFA oxidation can be another approach to prevent FFA uptake from circulation as well as by inhibition of mitochondrial FFA uptake and oxidation (Table 1.2). The β-adrenoceptor antagonists (e.g., carvedilol and propranolol) reduce catecholamine-induced lipolysis and thus, the extraction of FFA from circulation [91, 92]. Also, it reduces sympathetic-stimulated cardiac workload, thereby reducing oxygen consumption. Besides, peroxisome proliferator-activated receptor alpha (PPARα) agonists (e.g., ciprofibrate and fenofibrate) decrease circulating FFA availability by inducing hepatic enzymes that are involved in hepatic FFA breakdown [93, 94].

On the other hand, etomoxir [95] and perhexiline [85] have been developed to inhibit the activity of carnitine palmitoyltransferase-1 (CPT-1), which is responsible for mitochondrial FFA uptake. Trimetazidine directly inhibits the mitochondrial long-chain 3-ketoacyl CoA thiolase (LC 3-KA), which is the terminal enzyme of FFA β-oxidation [83, 84]. Nevertheless,

as the diabetic heart predominantly utilizes FFA for ATP production, suppression of FFA utilization and oxidation alone may further reduce the ATP production as the diabetic heart is unable to use other substrate fuels (i.e., glucose and lactate). Thus, it may seem reasonable to postulate that the suppression of FFA utilization may not be ideal for diabetic individuals. However, the effectiveness and potential side effects of these drugs are still yet to be studied in diabetic individuals. This suggests that more therapeutic interventions are required to be developed for the diabetic population.

Table 1.2 Examples of drugs prevent FFA uptake and oxidation

Therapeutic goal	Treatment [Reference]
Inhibition of FFA uptake from circulation	β-adrenoceptor antagonists – carvedilol & propranolol [91, 92]
	PPARα agonists – ciprofibrate & fenofibrate [93, 94]
Inhibition of mitochondrial FFA uptake	CPT-1 inhibitors - etomoxir & perhexiline [85, 95]
Inhibition of β-oxidation	LC 3-KA inhibitor – trimetazidine [83, 84]

1.2 The cardiac non-neuronal cholinergic system (NNCS)

The cardiac NNCS is known as an intrinsic defensive mechanism to allow the heart to adapt to changes in physiological and pathological condition [96-101]. In this part of the introduction, I first provide an overview of cardiac NNCS and discuss its physiological role focusing on the regulation of glucose metabolism. Then, I discuss the signaling cascade mediated by cardiac NNCS in the heart. *(a part of the literature presented in this section has been modified from the published literature review in the Journal of Molecular and Cellular Cardiology [102])*

1.2.1 Discovery of NNCS in the heart

The cholinergic neurons transmit electrical impulses from the brain to the heart through acetylcholine (ACh) to regulate cardiac function [103-107]. In the last decade, several researchers have provided evidence that the cardiomyocytes possess a functional intrinsic cholinergic machinery to synthesize, release, and degrade ACh [96, 99, 108]. Kakinuma et al.

[96] employed immunogold electron microscopy to demonstrate the presence of vesicle-like structure with positive vesicular ACh transporter (VAChT) immunoreactivity in the muscle fibers of the rat hearts, indicating ACh storage and release via vesicles. This finding is further supported by Rocha-Resende et al. [99] who showed co-localization of VAChT with recycling vesicles in the isolated adult mouse ventricular cardiomyocytes. Also, Rana et al. [108] used bromoacetylcholine, an inhibitor of choline acetyltransferase (ChAT), to treat isolated atrial and ventricular rat cardiomyocytes and found that ACh secretion from cardiomyocytes was significantly reduced, supporting that ChAT is the main ACh-synthesizing enzyme in the cardiomyocytes. Rocha-Resende et al. [99] identified the presence of choline transporter 1 (CHT1) by treating the mouse cardiomyocytes with hemicholinium-3, a CHT1 inhibitor, to observe a reduced activity of cardiac NNCS. Moreover, the ACh derived from cardiomyocytes was detected intracellularly and extracellularly in the presence of acetylcholinesterase (AChE) inhibitors such as donepezil, physostigmine, and pyridostigmine [96, 97, 108]. In addition to rodent models, the presence of cardiac NNCS represented by VAChT and ChAT was detected in human LV [101]. Thus, all these findings indicate that cardiomyocytes do possess proteins for ACh synthesis (ChAT), reuptake of choline for synthesis (CHT1), storage and release (VAChT) and degradation (AChE). On a side note, the cardiac NNCS possess the same enzymes and transporters as the neuronal cholinergic system. A schematic illustration of the cardiac non-neuronal cholinergic system compared to the classical neuronal cholinergic system is shown in Figure 1.3.

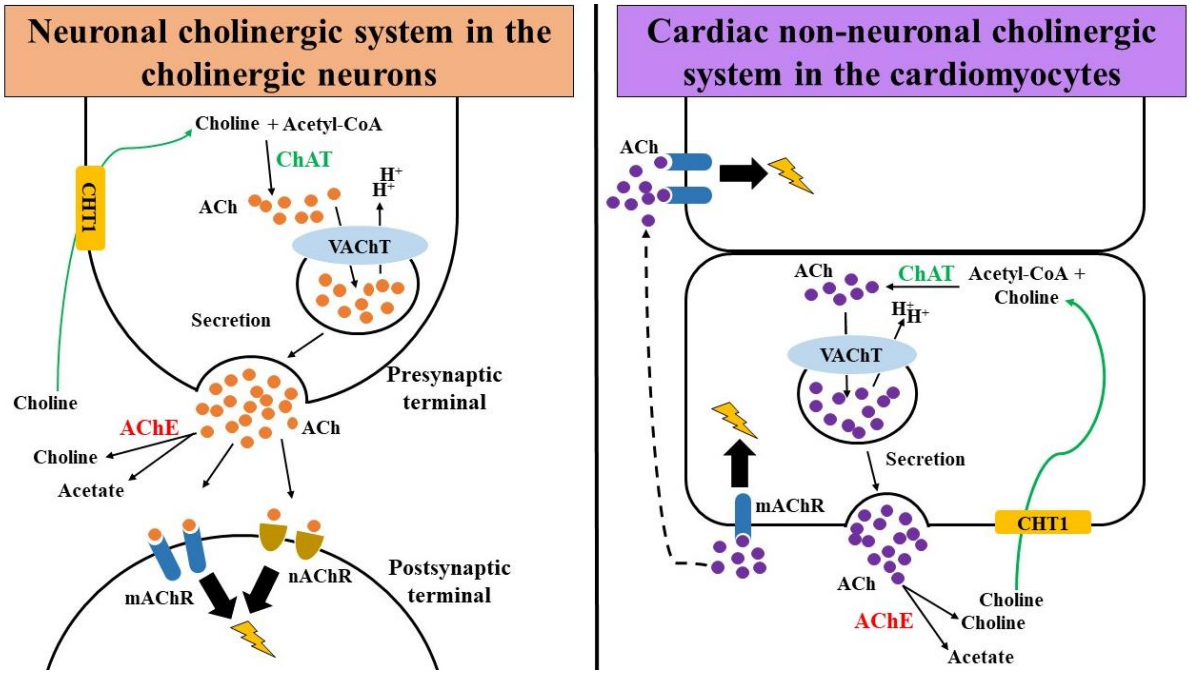

Figure 1.3 Schematic illustration of the comparison between the cardiac NNCS and the classical neuronal cholinergic system.

In the cardiomyocytes and cholinergic neurons, ACh is synthesized by ChAT by combining acetyl-CoA and choline. ACh is stored and released by VAChT upon stimulation. The ACh released from cholinergic neurons binds to nicotinic or muscarinic ACh receptor present in the postsynaptic terminal. The non-neuronal ACh released from cardiomyocytes binds to the muscarinic ACh receptor expressed on the membrane in an auto/paracrine manner to mediate signaling. AChE is present in the extracellular space and terminate the effect of ACh by hydrolysis. CHT1 is responsible for the reuptake of free choline from the extracellular space into the cholinergic neurons and cardiomyocytes for ACh synthesis.

1.2.2 Type-2 muscarinic ACh receptor mediated signaling

In the mammalian heart, the cholinergic system regulates the cardiac function via muscarinic receptors [109]. There are five subtypes of muscarinic ACh receptor (mAChR), and the quantitation of the mRNA expression of these receptors have revealed that type-2 muscarinic ACh receptor (M_2AChR) is the major receptor while other subtypes are expressed at very low level in the rodent and human heart [110-112].

M_2AChR is a G protein-coupled receptors (GPCR) which is bound to a heterotrimeric G protein complex. Activation of this receptor leads to dissociation of the $G_{\alpha i/o}$ subunit from the complex and eventually changes in cardiac ion channel activity in two folds. First, $G_{\beta\gamma}$ subunit interacts with G-protein coupled inward rectifying K^+ (GIRK) channel that predominantly expressed in atrial, sinoatrial node and atrioventricular node cells, thus opening up an inwardly rectifying

potassium channel (K_{ACh}) [113]. This leads to hyperpolarization and therefore reducing the heart rate (HR). Second, $G_{\alpha i/o}$ subunit inhibits adenylyl cyclase activity and thereby reducing the generation of cyclic adenosine monophosphate (cAMP). A reduction in this cyclic nucleotide decreases the ion activity of the hyperpolarization-activated cyclic nucleotide-gated channels (HCN, also known as pacemaker channels) that solely expressed in the cardiac conduction system, hence reducing spontaneous depolarization in pacemaker action potentials and hence the HR [114]. Also, a reduction in cAMP decreases the ion activity of L-type Ca^{2+} channels (LCC), thereby decreasing the contraction force of cardiomyocytes [115-118].

Apart from this, it has been reported that cardiomyocytes release ACh as a mediator to trigger autocrine/paracrine signaling independent of the abovementioned bradycardia mechanism. Upon ACh binding to M_2AChR, the $G_{\beta\gamma}$ subunit is released and binds directly to activate phosphatidylinositol-3-kinase (PI3K) [119]. PI3K is an upstream key player of a pro-survival signaling pathway, which subsequently activates protein kinase B (Akt) and hypoxia-inducible factor 1-alpha (HIF1α) [120, 121]. The effect of this signaling cascade is further discussed in Section 1.2.4.

1.2.3 The physiological role of cardiac NNCS in glucose metabolism

Previous studies showed that inactivation of cardiac NNCS decreased intracellular ATP level, increased oxygen consumption, and increased mitochondrial activity in the ChAT-KO HEK293, ChAT-KO HL-1 cardiomyocytes, and hemicholinium-3 treated H9c2 cells [96, 98, 122]. Conversely, activation of cardiac NNCS via overexpression of *ChAT* gene or exogenously added ACh to the HEK293 cells led to decreased mitochondrial function, increased intracellular ATP level and resistance to chronic serum deprivation [96, 122]. In line with this, overexpression of *ChAT* gene increased GLUT-1 and GLUT-4 protein expression, as well as the glucose content, in the left ventricle (LV) of *ChAT-tg* mice compared to the wild-type mice [100]. Further, immunohistochemistry analysis showed strong GLUT-4 immunoreactive signal,

but not GLUT-1, in the LV of *ChAT-tg* mice [100]. This evidence suggests that cardiac NNCS promotes glucose metabolism through enhancing GLUT-4 expression, therefore physiologically modulating cardiac metabolism and energetics in the heart.

In addition to this, cardiac NNCS is involved in other physiological role such as *(1)* production of pro-angiogenic factor vascular endothelial growth factor (VEGF) to maintain coronary vasculature [100, 123]; *(2)* maintaining action potential propagation through increasing connexin43 [98, 100]; *(3)* regulation of HR with the neuronal cholinergic system [97, 101]; *(4)* offsetting hypertrophic signals induced by hypersympathetic stimulation [97, 99, 101, 124]. ACh activates these effects through M_2ACh receptor-mediating signaling (Figure 1.4). The ACh released from cardiomyocytes or cholinergic neurons stimulate the neighboring cardiomyocytes to synthesize ACh further to maintain or propagate the effects in the heart in an auto/paracrine manner [96].

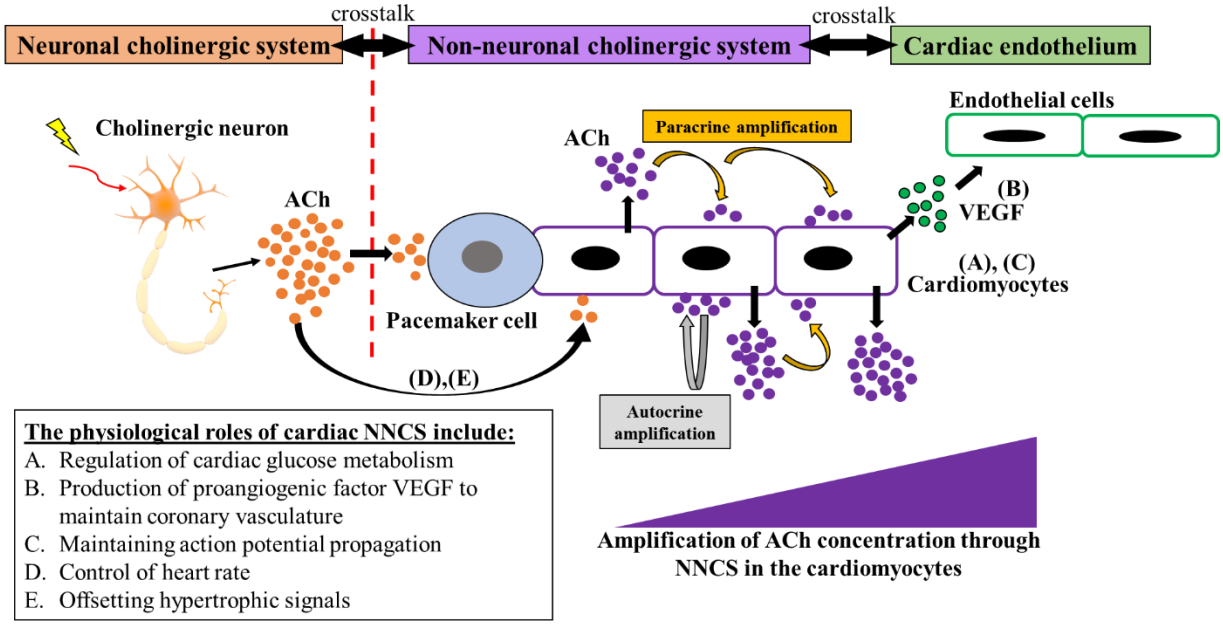

Figure 1.4 Cardiac NNCS exerts its effect by an auto/paracrine amplification mechanism to initiate and propagate neuronal- and non-neuronal effects.
(A) *The ACh released from cardiomyocytes activates pro-survival signaling to promote glucose metabolism through GLUT-4 expression, as well as* ***(B)*** *to promote angiogenesis by increasing pro-angiogenic factor VEGF-A expression in an auto/paracrine manner.* ***(C)*** *Besides, the ACh released from cardiomyocytes enhances the expression of connexin43 to preserve the gap-junction function and maintain action potential propagation.* ***(D)*** *Further, the ACh released from parasympathetic cholinergic neurons activates the NNCS in the cardiomyocytes to synthesize and release ACh. The ACh released from cardiomyocytes is thought to maintain and amplify the neuronal cholinergic effects to reduce heart*

*rate and possibly contraction force of the heart as well as **(E)** to counteract hypertrophic signals induced by hypersympathetic stimulation. The schematic purple bar represents the ACh concentrations being amplified through NNCS in the cardiomyocytes.*

1.2.4 Cardiac NNCS activates pro-survival signaling to regulate GLUT-4 expression

ACh-M_2AChR interaction activates the pro-survival phosphatidylinositol-3-kinase (PI3K)/protein kinase B (Akt) signaling cascade, thereby increasing the availability of hypoxia-inducible factor 1-alpha (HIF1α) under normoxic condition [100, 120, 125]. Activation of Akt prevents the binding of von Hipple-Lindau tumor suppressor (VHL) to the HIF1α protein [100, 120, 125]. Thus, this prevents ubiquitin-mediated proteasomal degradation of the HIF1α protein, thus increasing its availability [126]. HIF1α and HIF1β dimerize to form HIF1, a master transcription factor, to transcriptionally activate a broad spectrum of hypoxia-responsive genes that eventually being translated to proteins to facilitate the adaption to ischemic stress, such as glycolysis to balance oxygen demand (Figure 1.5; reviewed in [127]).

The HIF1 transcription factor regulates glycolysis through transcriptionally activating *GLUT-1* and *GLUT-4* genes to promote glucose uptake [128-131]. In particular, GLUT-4 is the major glucose transporter in the adult heart [132, 133]. An upregulation of GLUT-4 expression in the heart of *ChAT-tg* mice increased cardiac glucose content and ATP content [100]. Thus, these studies demonstrated that activation of cardiac NNCS increases ACh content, which in turn mediates PI3K/Akt/HIF1α signaling cascade to promote glucose metabolism through increasing GLUT-4 expression.

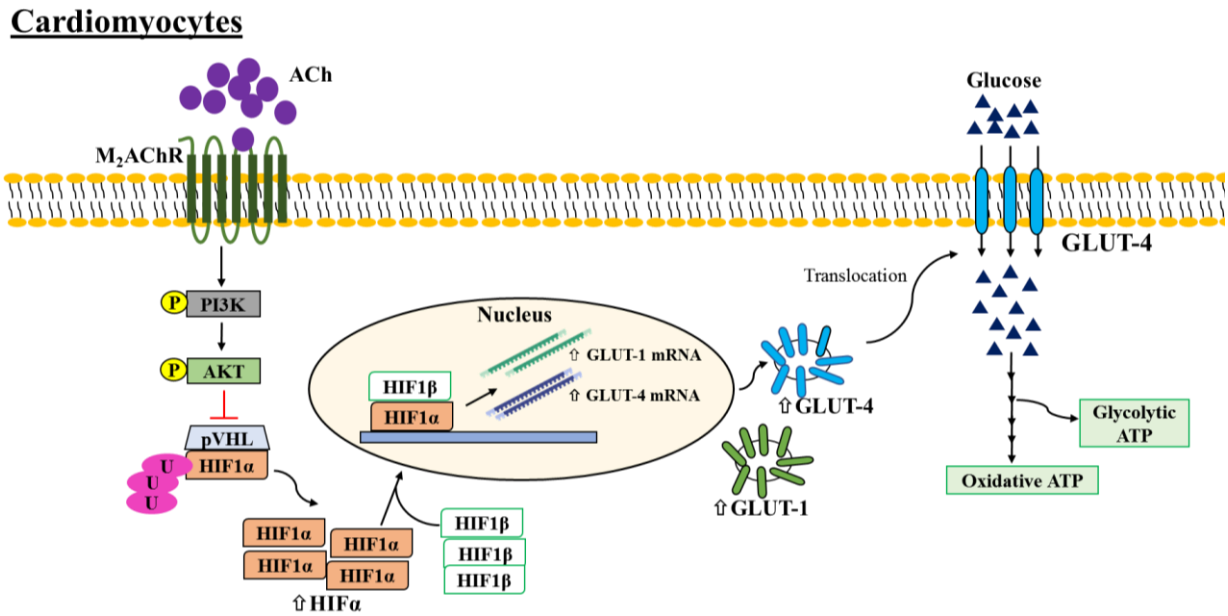

Figure 1.5 Cardiac NNCS activates pro-survival PI3K/Akt/HIF1α signaling cascade.
Inhibition of ubiquitin-mediated proteasomal degradation by ACh increases HIF1α protein in normoxic condition. Subsequently, HIF1α and HIF1β dimerize to form a master transcription factor HIF1 to transcriptionally activate a broad spectrum of hypoxia-responsive genes which are eventually translated to proteins that are involved in glucose uptake (GLUT-1 & GLUT-4). P indicates phosphorylation; U indicates ubiquitination.

1.3 Overview and outline of the Ph.D. thesis

Before the onset of DHD, altered cardiac metabolism (i.e., increased FFA utilization and decreased glucose utilization) decreases the basal myocardial energy status and cardiac efficiency in the diabetic heart. Also, an ischemic condition induced by CAD or CMVD reduces oxygen availability to the myocardium, thus, limiting FFA oxidation and ATP production. In this case, the diabetic heart is unable to maintain its contractile function, thereby suffering extensive myocardial damage. Although there are guidelines and treatment in place for managing DHD [134], it remains the leading cause of death in the diabetic population worldwide [135]. The alarming increase in the incidence of DHD urges for alternative therapeutic options. However, the lack of understanding in the molecular mechanism involved in the disease progression hamper the progress in the development of new therapy.

The heart consists of both neuronal and non-neuronal cholinergic system. It is now well established that cardiac NNCS physiologically modulates glucose and energy metabolism [96, 98, 100, 122]. However, the role of cardiac NNCS in diabetic heart has yet to be elucidated.

Based on the current knowledge - *(1)* activation of cardiac NNCS results in an increase in GLUT-4 expression and *(2)* the diabetic heart displays reduced GLUT-4 expression and glucose utilization before the onset of DHD [58, 60, 64]. Therefore, it seems logical to postulate that T2DM could decrease cardiac NNCS before the onset of DHD.

Therefore, it is essential to examine *(1)* whether the expression of various components (i.e., ChAT, CHT1, VAChT, AChE, and M_2AChR) that are involved in the cardiac cholinergic machinery are altered in diabetes mellitus and *(2)* if activation of cardiac NNCS could prevent or attenuate the detrimental effect of diabetes on the heart.

1.3.1 Aims and hypotheses

The aim of my thesis is to examine the role of cardiac NNCS in the diabetic heart. Thus, I divided this project into five specific objectives.

i. *Examining the temporal expression changes in the components of cardiac NNCS and glucose transporters in the diabetic db/db heart.*

I hypothesized that the expression changes in the components of cardiac NNCS (ChAT, CHT1, VAChT, AChE, and M_2AChR) and GLUTs (GLUT-1 and GLUT-4) would be dysregulated in the diabetic *db/db* heart. Also, I hypothesized that dysregulation of the components of cardiac NNCS would precede the decrease in GLUT-4 expression in the *db/db* mice. To test this hypothesis, I measured gene and protein expression of the components of cardiac NNCS and GLUTs in the ventricular tissues of type-2 diabetic *db/db* mice at different ages (i.e. 8-, 12-, 16-, 20-, 24-, 28- and 32-weeks of age).

ii. *Examining the expression changes in the components of cardiac NNCS and glucose transporters in the diabetic human heart*

I hypothesized that the expression changes in the components of cardiac NNCS (ChAT, CHT1, VAChT, AChE, and M_2AChR) and GLUTs (GLUT-1 and GLUT-4) would be dysregulated in the diabetic human heart. To test this hypothesis, I measured the protein expression of the components of cardiac NNCS and GLUTs in the ventricular tissues of type-2 diabetic human who underwent coronary artery bypass surgery (CABG).

iii. Investigating the beneficial effect of cardiac NNCS activation via overexpression of the ChAT gene on the cardiovascular function of the diabetic heart

I hypothesized that ventricular-overexpression of *ChAT* gene would lead to activation of PI3K/Akt/HIF1α/GLUT-4 signaling pathway to promote glucose metabolism, thus improving the cardiac function of the diabetic heart. To test this hypothesis, the blood glucose level, LV function, protein expression of targets (ChAT, M_2AChR, Akt, HIF1α, GLUT-4, AMPKα) were assessed in the diabetic *db/db* mice with ventricular-overexpression of *ChAT* gene at 8-, 12-, 16- and 20-weeks of age. Also, I hypothesized that the ventricular-overexpression of *ChAT* gene would lead to an increase in VEGF-A expression and promote angiogenesis, thus improving vascular function of the diabetic heart. To test this hypothesis, the coronary circulation, microvascular density, protein expression of VEGF-A were assessed in the diabetic *db/db* mice with ventricular-overexpression of *ChAT* gene at 12- and 24-weeks of age.

iv. Establishing an in-vitro diabetic cardiomyocytes model using AC16 cells

I hypothesized that palmitate and glucose treatment would impair insulin signaling and lead to insulin resistance in the AC16 cells. To test this hypothesis, I treated the AC16 cells with palmitate and glucose for 48 hours and followed by insulin stimulation for 30- and 60-minutes to test the insulin responsiveness. The cytosolic and membrane proteins were isolated and assessed the expression changes in Akt, GLUT-4, and ChAT in the diabetic AC16 cells.

v. Investigating the protective effect of cardiac NNCS in the diabetic AC16 cells under the hypoxic condition

I hypothesized that activation of cardiac NNCS via overexpression of the *ChAT* gene would lead to an increase GLUT-4 expression, thus sustaining energy production and reducing apoptosis under hypoxic condition. To test this hypothesis, I first overexpressed *ChAT* gene in the AC16 cells for 24 hours, followed by palmitate and glucose treatment for 48 hours, and finally exposing the cells to 24 hours of hypoxic conditions. The cytosolic and membrane proteins were isolated and assessed the expression changes in GLUT-4, ChAT, AMPKα, and cleaved caspase-3 in the diabetic AC16 cells.

Chapter 2 : General materials and methods

This chapter outlines the general materials and methods for the techniques applied in this Ph.D. study. The specific details of the materials and methods are described in the corresponding chapter.

2.1 Ethics

The Animal Ethics Committee from the University of Otago (AEC25/12) and Nippon Medical School approved the animal studies conducted in this Ph.D. study (section 2.2.2 and 2.2.4). Health and Disability Ethics Committee in New Zealand approved the use of human LV tissues (LRS/12/01/001/AM13; section 2.2.1). The human tissues samples of patients with or without type-2 diabetes with CAD who underwent CABG in Dunedin hospital were collected following their informed consents.

2.2 The study models and experimental design

This Ph.D. study included animal and human ventricular tissues as well as a cardiomyocyte cell line for investigation (Figure 2.1). The ventricular tissues from type-2 diabetic *db/db* mouse model (C57BL/KsJ-Lepr$^{db/db}$) and type-2 diabetic human with CAD were used to investigate the expression changes of cardiac NNCS (ChAT, VAChT, CHT1, AChE, and M_2AChR) as well as GLUTs (GLUT-1 and -4). Next, the type-2 diabetic *db/db* mice with ventricle-specific overexpression of *ChAT* gene (C57BL/KsJ-Lepr$^{db/db}$-ChAT-tg) and AC16 cells were used to investigate the functions of cardiac NNCS in the *in-vivo* and *in-vitro* condition.

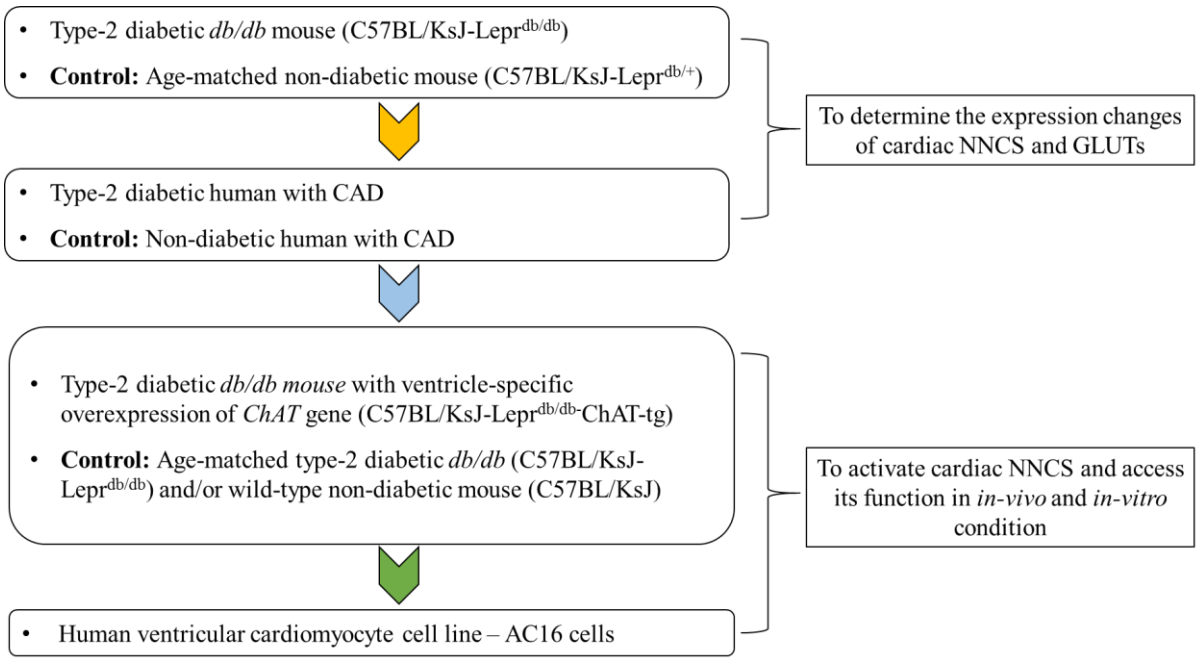

Figure 2.1 A brief overview of the use of animal and human ventricular tissues as well as AC16 cells in this thesis.
The use of ventricular tissues from type-2 diabetic db/db mice and type-2 diabetic human with CAD was used to investigate the expression changes of cardiac NNCS and GLUTs. Then, I validated the function of cardiac NNCS using type-2 diabetic db/db mice with ventricle-specific overexpression of ChAT gene and AC16 cells to NNCS in the in-vivo and in-vitro condition.

2.2.1 Type-2 diabetic *db/db* (C57BL/KsJ-Lepr$^{db/db}$) mouse model

The *db/db* mouse model served as the model of type-2 diabetes mellitus [1, 136, 137]. This mouse model develops spontaneous diabetes due to homozygous transverse point mutation (G→T) in the intron 18 of the leptin receptor (Lepr) [138, 139]. Before termination, these mice had free access to the food pellets. The tissue collection was performed between 3 pm to 4 pm by Dr. Shrtui Rawal as part of her Ph.D. study. The atrial tissues were removed, and the ventricular tissues were equally cut into three parts (Figure 2.2). These ventricular tissues were available (8-, 12-, 16-, 20-, 24-, 28- and 32-weeks of age; mixed gender) and used in my study [1]. Immunofluorescence analysis performed on the upper part of the ventricular tissues. RT-qPCR analysis and western blot analysis performed on the middle and lower parts of the ventricular tissues, respectively.

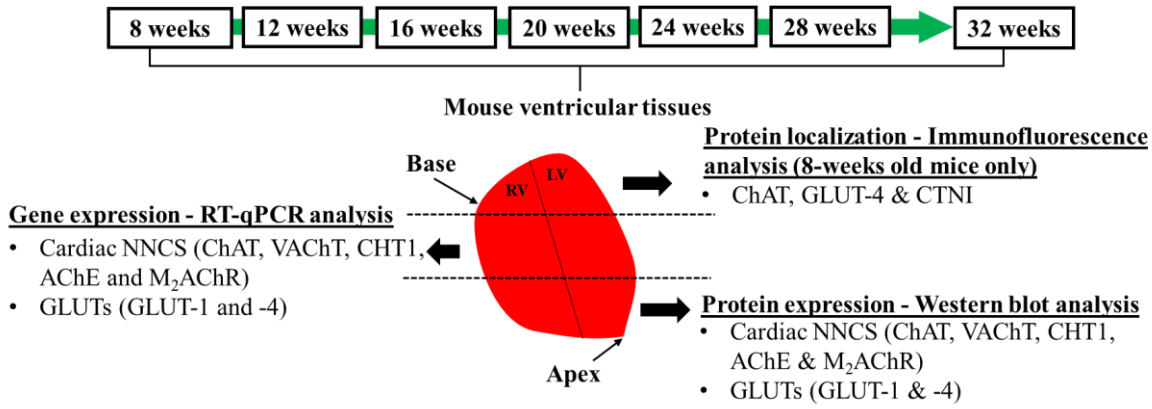

Figure 2.2 An overview of ventricular tissue collection and analytic techniques performed on type-2 diabetic *db/db* mice.
The ventricular tissues were cut into three parts after removal of the atrial tissues. The upper part of the ventricular tissue was harvested and fixed in 4% formaldehyde for immunofluorescence analysis. The middle and lower parts were collected for RNA and protein analysis, respectively.

2.2.2 Type-2 diabetic human with CAD

Through the HeartOtago research network, I had access to human left ventricular (LV) samples from type-2 diabetic and non-diabetic patients with CAD. These patients were admitted to Dunedin Hospital to undergo coronary artery bypass graft (CABG) surgery. The selection criteria of diabetic patients were hemoglobin A1C (HbA1C) level ≥ 50nmol/mol and diabetic duration of more than one year [140]. Besides, the samples were restricted from those aged between 60-84 years old. The LV samples were used for the western blotting experiment. The information about the cardiac functions of the recruited participants was retrieved from the database maintained by HeartOtago.

2.2.3 Type-2 diabetic *db/db* mouse with ventricular-specific overexpression of *ChAT* gene

Prof. Yoshihiko Kakinuma (Nippon Medical School, Japan) generated and provided this unique model. As shown in Figure 2.3, the generation of this model was performed by crossing the heterozygous db/+ mouse ($Lepr^{db/+}$) with the mouse model of cardiac NNCS (i.e., ventricular-specific overexpression of *ChAT* gene; *ChAT-tg*) [100]. The heterozygous db/+ littermates with

ChAT-transgene (*db/+-ChAT-tg* mice) were further crossbred to generate homozygous *db/db* littermates with ChAT-transgene (*db/db-ChAT-tg* mice).

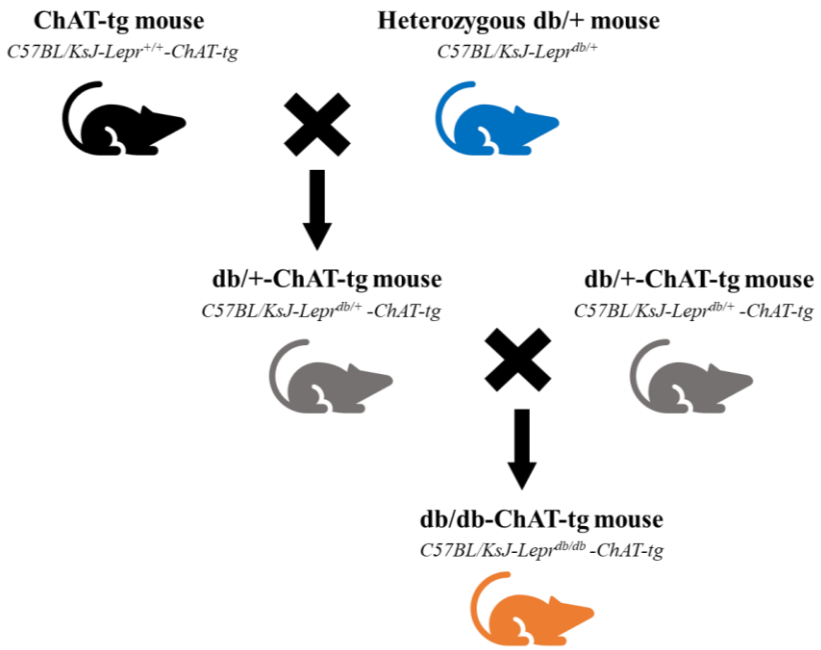

Figure 2.3 Type-2 diabetic *db/db* mouse with ventricular-specific overexpression of *ChAT* gene.
The mouse model of cardiac NNCS and heterozygous Lepr$^{db/+}$ mouse was crossbred. Heterogenous littermates with ventricle-specific ChAT transgene were further crossbred to obtain homogenous littermates with ventricle-specific ChAT transgene.

The body weight, blood glucose level, LV function of the *db/db-ChAT-tg* mice were assessed. The age-matched diabetic *db/db* mice were used as control. After the measurement, the hearts from *db/db* and *db/db-ChAT-tg* mice (8-, 12-, 16-, and 20-weeks of age; mixed gender) were retrieved. This procedure was performed between 9.00 am to 10.30 am. The atrial tissues were removed and the ventricular tissues were equally cut into three parts (i.e. upper, middle and lower) and collected by Prof. Yoshihiko Kakinuma as described in Figure 2.2. The lower part of the ventricular tissues was used for western blot analysis to measure the protein expression of the selected targets in my study (Figure 2.4). The wild type non-diabetic (ND) mice were included for western blot analysis only to allow comparison with *db/db* and *db/db-ChAT-tg* mice.

Also, the coronary vascular function was performed on *db/db* and *db/db-ChAT-tg* mice (12- and 24-weeks of age) in the SPring-8 facility in Japan. After Synchrotron radiation microangiography, the hearts were retrieved. The atrial tissues were removed and the ventricular tissues were equally cut into three-part (i.e. upper, middle and lower) and collected (Figure 2.2). The upper part of the ventricular tissue was used to assess the density of arterioles and capillaries in *ex-vivo* while the lower part of the ventricular tissues was used for western blot analysis (i.e., VEGF-A).

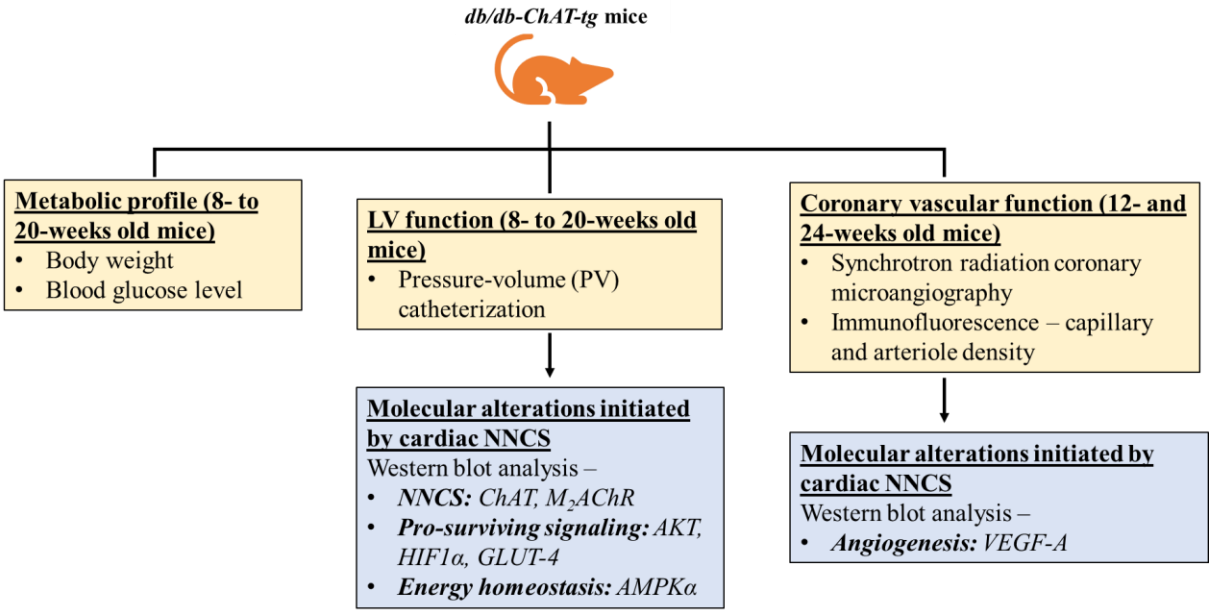

Figure 2.4 An overview of the experimental setup and analytical techniques to assess the cardiovascular function and molecular alterations initiated by cardiac NNCS in the *db/db-ChAT-tg* mice.
The body weight and blood glucose level were examined. The LV function was examined by admitting the pressure-volume catheter to the cardiac apex. The coronary vascular function was examined by microangiography as well as immunofluorescence to measure the capillary and arteriole density. Finally, western blot was performed to assess the expression changes in the proteins involved in the cardiac NNCS-mediated signaling.

2.2.3 Human ventricular cardiomyocyte cell line – AC16 cells

AC16 cells were purchased from Dr. Mercy M. Davidson from Columbia University. This cell line was generated by fusing SV40 transformed, uridine auxotroph human fibroblasts, devoid of mitochondrial DNA, with the primary cells from human ventricular tissues [141]. This model was used to overexpress human *ChAT* gene, followed by the induction of insulin resistance and

hypoxic treatment (Figure 2.5). At the end of the experimental time point, the cytosolic and membrane proteins were separated and collected. Western blot analysis was performed to measure the protein expression of selected targets (Figure 2.5).

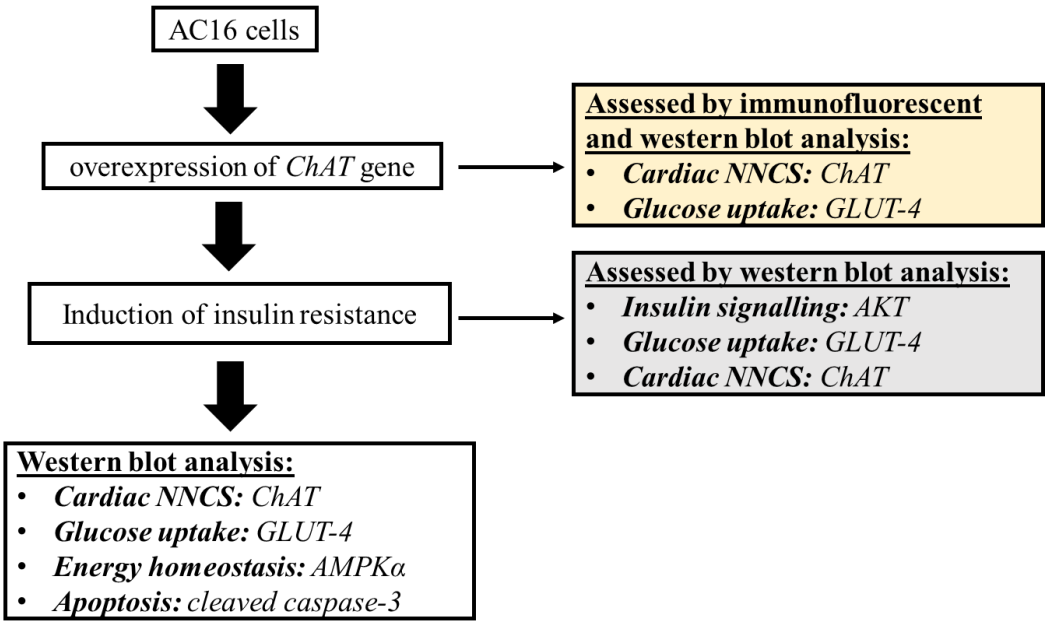

Figure 2.5 An overview of the experimental setup and analytical techniques used to study the function of cardiac NNCS in AC16 cells.
The experiment was designed to demonstrate the protective effect of cardiac NNCS in diabetic AC16 cells under hypoxic condition. The function of cardiac NNCS was assessed by protein targets that involved in glucose uptake, energy homeostasis and apoptosis.

2.3 Molecular analyses of gene and protein expression

2.3.1 Determination of gene expression from mouse ventricular tissues

2.3.1.1 Isolation of ribonucleic acid (RNA)

RNA was isolated using Trizol reagent (Invitrogen, 15596026) according to the manufacturer's instruction. Briefly, mouse ventricular tissues were lysed and homogenized in Trizol reagent using 2.0 mm stainless steel beads (Next Advance, SSB14B-RNA) in a homogenizer (Next Advance, BBX24). The lysate was cleared by centrifugation at 12,000 g at 4°C and followed by phase separation using chloroform (in the ratio of 1:5, chloroform: Trizol). The aqueous phase containing RNA was then transferred to a fresh tube and precipitated by isopropanol (in the ratio of 1:2, isopropanol: Trizol). The precipitated RNA was washed using 75% ethanol (in

the ratio of 1:1, 75% ethanol: Trizol) and solubilized by RNA-free water. The concentration of RNA was measured using a NanoDrop-1000 spectrophotometer (NanoDrop Technologies, USA). The purity of the RNA was evaluated by the absorbance ratio of 260 over 280 and 260 over 230 nm. A 260/280 ratio between 1.8 and 2.1 and 260/230 ratio of above 2 indicate pure RNA quality and no protein and organic solvent contamination. All RNA samples in my study had 260/280 and 260/230 ratio of 1.8 and above.

2.3.1.2 Synthesis of complementary deoxyribonucleic acid (cDNA) by reverse transcription

Before reverse transcription, isolated RNA was treated with recombinant DNase (rDNase) to remove genomic DNA. In brief, 3.5 µg of RNA was treated with rDNase at 37ºC for 30 minutes, followed by incubation at 75ºC for 10 minutes to inactivate rDNase. Then, the concentration of DNase-treated RNA was measured as described above. One microgram of the rDNase-treated RNA was mixed with PrimeScript™ buffer, oligo dT primer, random hexamers and PrimeScript™ RT enzyme mix 1 (Takara, RR037A; Table 2.1) to reverse transcribe the RNA to cDNA. The reaction mixture was incubated at 37ºC for 15 minutes to synthesize cDNA, and 85ºC for five seconds to inactivate the reverse transcriptase in a thermal cycler (BioRad, T100).

Table 2.1 The concentration and volume of components required for reverse transcription

Reagent	Initial concentration	Final concentration/volume
PrimeScript™ buffer	5X	1X
Oligo dT primer	50 µM	5 µM
Random hexamers	100 µM	10 µM
PrimeScript™ enzyme mix I (0.5 µl per 500 ng RNA)	-	2 µl
rDNase-treated RNA	-	1 µg

2.3.1.3 Quantitative polymerase chain reaction (qPCR)

After reverse transcription, PCR amplification was performed to measure the gene expression of selected targets. Briefly, the synthesized cDNA was mixed with SYBR Premix Ex Taq™

(Takara, RR420L), KiCqStart forward and reverse primer (Sigma-Aldrich), nuclease-free water and then plated in a 96-well plate in triplicates (Table 2.2). Then, the reaction was initiated by incubating the reaction mixture at 95ºC for two minutes for to activate the enzyme, followed by 40 cycles of denaturation at 95ºC for five seconds and primer annealing at 54-60ºC for 30 seconds in StepOnePlus Real-time PCR system (ThermoFisher Scientific; 4376600). The primer sequences, optimized concentrations, and annealing temperature of each primer are listed in Chapter 3. After amplification, the PCR amplicons were subjected to the gradual increment of temperature to measure the melting temperature. Such measurement provides an indication of the specificity of amplification.

Table 2.2 The concentration and volume of components required for qPCR amplification

Reagent	Initial concentration	Final concentration/volume
SYBR Premix Ex Taq™	2X	1X
Forward primer*	10 µM	0.2 – 1 µM
Reverse primer*	10 µM	0.2- 1 µM
Synthesized cDNA	-	2 µl

**Primer sequences, optimized concentrations, and annealing temperature of each primer are listed in Chapter 3.*

2.3.1.4 qPCR data analysis

The qPCR experiment was performed one time for each sample as this analysis was to detect the presence of selected targets in the mouse ventricular tissues. The gene expression of selected targets was normalized to ribosomal RNA 18S by the 2^{-ddCt} method [142] and any samples showing a C_T value of >35 were excluded from the analysis.

2.3.2 Determination of protein expression from mouse, human ventricular tissues and AC16 cells

2.3.2.1 Total protein isolation

Total proteins were isolated using RIPA buffer (150 mM NaCl, 0.1% SDS solution, 1% Triton X-100, 1% sodium deoxycholate in 50 mM Tris-HCl, pH 8.0), supplemented with 1X

cOmplete™ protease inhibitor cocktail (Roche, 4693159001) and 100 mM phenylmethane sulfonyl fluoride (PMSF; Sigma-Aldrich, 10837091001) [137]. Mouse and human ventricular tissues were lysed and homogenized in RIPA buffer by 2.0 mm stainless steel beads (Next Advance, SSB14B-RNA) in a homogenizer (Next Advance). For AC16 cells, RIPA buffer was added to the culture dish to lyse the cells. Then, the protein lysates were collected and cleared by centrifugation at 13,400 rpm at 4ºC for 30 minutes. Purified protein lysates were then transferred to a fresh tube and quantified by Bradford assay described in the following section.

2.3.2.2 Membrane and cytosolic protein isolation from AC16 cells

The fraction of membrane and cytosolic protein from AC16 cells was isolated using the Mem-PER™ Plus Membrane Protein extraction kit (Thermo Scientific, 89842). Briefly, 5 x 10^6 cells were washed once with cell wash solution supplied from kit followed by scraping the cells with 0.75 mL of permeabilization buffer supplemented with 1X cOmplete™ protease inhibitor cocktail, 1X PhosSTOP™ phosphatase inhibitor cocktail (Roche, 4906845001) and 100 mM PMSF. The cell lysates were collected in a microcentrifuge tube and incubated for 10 minutes at 4ºC with constant mixing. After centrifugation at 16,000 g for 15 minutes, the supernatant containing cytosolic proteins was collected, and the pellet was resuspended in 0.5 mL of solubilization buffer with the addition of 1X cOmplete™ protease inhibitor cocktail, 1X PhosSTOP™ phosphatase inhibitor cocktail and 100 mM PMSF. The cell lysates were then incubated for 30 minutes at 4ºC with constant mixing. After centrifugation at 16,000 g for 15 minutes, the supernatant containing solubilized membrane and membrane-associated proteins was transferred to a new microcentrifuge tube and quantified by Bradford assay described in the following section. The protein expression of pan-cadherin (a membrane protein) was examined via western blot analysis to confirm the successful separation of cytosolic and membrane proteins.

2.3.2.3 Determination of protein concentration by Bradford assay

Bradford assay was performed to determine protein concentration by extrapolating against bovine serum albumin (BSA) standard. First, BSA powder (Sigma-Aldrich, A7906) was dissolved in PBS to make 2 mg/mL stock solution. Serial dilutions of this stock solution were made according to Table 2.3. Then, five microlitres of BSA standards or purified protein lysates from test samples were added to wells containing 250 µL of Bradford dye reagent in a 96-well plate (BioRad, 5000205). The absorbance of BSA standards and test samples were measured at 595 nm by SpectraMax i3x microplate reader (Molecular Device, USA). A standard graph was plotted by using the absorbance of BSA standards versus the final concentration, thus allowing determination of the protein concentration of test samples.

Table 2.3 Preparation of BSA standards for Bradford assay

Tube #	BSA volume (µL)	BSA solution (2 mg/mL stock)	Diluent volume (µL)	Final BSA concentration (µg/mL)
1	20	2 mg/mL stock	0	2,000
2	30	2 mg/mL stock	10	1,500
3	20	2 mg/mL stock	20	1,000
4	20	Tube 2	20	750
5	20	Tube 3	20	500
6	20	Tube 5	20	250
7	20	Tube 6	20	125
8	-	-	20	0

2.3.2.4 Sodium dodecyl sulfate-polyacrylamide gel electrophoresis (SDS-PAGE) and immunoblotting

Following the quantification, the protein lysates were mixed with 6X Laemmli samples buffer (12% SDS, 60% glycerol, 30% β-mercaptoethanol, 0.012% bromophenol blue, 0.375 M Tris-HCl, pH 6.8) and incubated at 95ºC for five minutes to denature the proteins. Then, an equal amount of denatured protein lysates was loaded to discontinuous polyacrylamide gel (Table 2.4) and subjected to electrophoresis in Tris-glycine buffer (25 mM Tris base, 192 mM glycine and

0.1% SDS, pH 8.3). Precision plus Kaleidoscope prestained protein ladder (BioRad, 1610375) was used to determine the molecular weight of the proteins.

Table 2.4 Composition of discontinuous polyacrylamide gel

Component	Stacking gel	Resolving gel
0.5 M Tris-HCl, pH 6.8	0.0625 M	-
1.5 M Tris-HCl, pH 8.8	-	0.4 M
30% Acrylamide/Bis solution	5%	7.5% - 12%
10% SDS	0.1%	0.1%
10% APS	0.1%	0.1%
TEMED	0.1%	0.1%

After separation, the proteins were transferred onto polyvinylidene difluoride (PVDF) membrane (BioRad, 1620264) in Tris-glycine transfer buffer (25 mM Tris base, 192 mM glycine and 20% (v/v) methanol, pH 8.3) at 110 voltage for 90 minutes. Successful transfer of total proteins was confirmed by staining the PVDF membrane with Ponceau S solution (0.1% (w/v) Ponceau S in 5% (v/v) acetic acid), and the image was captured using Syngene Pxi imaging system (USA). Next, the PVDF membrane was washed with TBST buffer (20 mM Tris base, 137 mM NaCl, 2.7 mM KCl, and 0.1% (v/v) Tween-20) to remove the Ponceau S dyes. The membrane was blocked with 5% (w/v) of BSA/TBST solution for one hour at room temperature, followed by incubation of primary antibody at 4ºC overnight. Following day, the membrane was washed with TBST buffer and incubated with horseradish peroxidase (HRP)-conjugated secondary antibody for one hour at room temperature. Finally, the membrane was washed with TBST buffer to remove any unbound secondary antibody, followed by incubation with enhanced chemiluminescence (ECL) substrate reagent (BioRad, 1705060). The chemiluminescence signal was captured by Syngene Pxi imaging system (USA) to visualize the target protein expression.

2.3.2.5 Western blot data analysis

The western blot experiment was performed two to four times for each sample. The band intensity was quantified using ImageJ analysis software (https://imagej.nih.gov/ij/index.html). The band intensity of protein of interest was normalized to the band intensity of a prominent band between 37 kDa and 50 kDa from Ponceau S stained blot (total protein expression level) [143, 144] and expressed as fold changes towards the control group [145]. This particular approach was taken because the protein expression of housekeeping genes such as α-tubulin and β-actin showed a decreasing trend in the *db/db* mice while the selected band between 37 kDa and 50 kDa (from Ponceau S stained blot) showed consistent expression in the ND, *db/db* and *db/db-ChAT-tg* mice (Appendix 2, Figure S2.1). Although it is unknown why α-tubulin and β-actin expression showed a decreasing trend, this could be due to enhanced protein degradation that is associated with diabetes mellitus [146-150].

2.4 Immunofluorescence

2.4.1 Processing of mouse ventricular tissues

2.4.1.1 Tissues fixation and cryosection

Mouse ventricular tissues were excised and fixed in 4% paraformaldehyde (PFA) solution overnight. The tissues were then washed with PBS and dehydrated by immersing it in a 30% sucrose solution until it sank to the bottom of the tube. After dehydration, the tissues were washed in PBS, embedded in optimum cutting temperature (OCT) medium (Thermo Scientific, 6769006) and stored at -80ºC. OCT-coated ventricular tissues were cut into 7 µm section on the short axis using cryostat-microtome (Leica, CM1950) at -20ºC. The sectioned tissues were adhered onto the superfrost plus microscope glass slides (LabServ, LBS4951plus) and stored in -20ºC until used.

2.4.1.2 Pre-staining treatment

The tissues were treated with ice-cold acetone for five minutes in -20ºC, followed by air-drying for 30 minutes in the room temperature. The use of acetone is to remove lipids and dehydrate the cells. Next, permeabilization was performed by treating the tissue sections with PBS solution containing 0.1% Triton-X 100 for 30 minutes in the room temperature. Tissues were washed thrice by PBS containing 0.03% Triton X-100 for five minutes in between each step. After permeabilization, tissue sections were incubated with 5% goat serum for one hour in the room temperature to block non-specific antigens.

2.4.2 Processing of AC16 cells

2.4.2.1 Fixation

AC16 cells were cultured in 8-well chamber slide. Upon reaching 70% confluency or after 24 hours of transfection, the culture medium was removed and washed with PBS. The cells were then incubated in 4% PFA solution for 15 minutes at room temperature, after which the cells were washed with PBS thrice and left in PBS and ready for the following treatment.

2.4.2.2 Pre-staining treatment

Permeabilization was performed by treating the cells with PBS solution containing 0.1% Triton-X 100 for 30 minutes in the room temperature. Cells were washed thrice by PBS containing 0.03% Triton X-100 for five minutes in between each step. After permeabilization, the cells were incubated with 5% goat serum for one hour in the room temperature to block non-specific antigens.

2.4.3 Immunostaining of ventricular tissue section and cells

This section describes the general protocol of single immunostaining or multicolor immunostaining (double or triple staining of multiple targets in a sequential manner) in the

same sample (original protocol provided by Abcam). The specific antibody, concentration, and methods are described in the corresponding chapter.

Briefly, the tissue sections/cells were incubated with primary antibody diluted in 0.1% goat serum in PBS in a humidified chamber at 4ºC overnight. Next day, the tissue sections/cells were incubated with secondary antibody conjugated with a fluorophore for two hours in the room temperature protected from light. If multicolor immunostaining was performed, the second blocking step was required and followed by incubation with second primary antibody diluted in 0.1% goat serum in PBS in a humidified chamber at 4ºC overnight. On the following day, the tissue sections/cells were incubated with second secondary antibody conjugated with a fluorophore that was different from the one used for the first antibody for two hours. For triple staining, a third blocking step followed by the third primary and secondary antibody was performed.

After immunostaining, tissue sections/ cells were counterstained with DAPI (Santa Cruz, SC3598; 1:1,000) to stain the nucleus for one minute. The tissue section/cells were washed with PBS containing 0.03% Triton X-100 three times in between each step. Finally, slides were mounted on the coverslip with fluorescent mounting medium (Invitrogen, 00495802) and dried overnight.

2.4.4 Secondary antibody-only control for immunofluorescence

Tissue sections or cells used as secondary antibody-only control underwent the same steps described above except the addition of primary antibody.

2.4.5 Microscopic imaging

Nikon A1 confocal laser microscope or Olympus BX51 fluorescent microscope was used to visualize and capture fluorescent images. The images were captured in four or ten random areas per section under the 20X or 60X objective lens, respectively.

2.4.6 Immunofluorescence data analysis

ImageJ software was used to process and quantify the fluorescent images. No analysis was performed for fluorescent images captured to identify the localization and confirm the expression of selected targets.

2.5 Cell culture

AC16 cells were maintained and grown in cell culture media composed of Dulbecco's modified Eagle's medium (DMEM; Gibco, 31600034), 5% fetal bovine serum (FBS; Hyclone, SH30406.02) and 1X antibiotic-antimycotic solution (Gibco, 15240062) in 75cm^2 flask, under 37ºC and 5% CO_2. The complete DMEM medium was changed every two days.

2.5.1 Subculture

Upon reaching 90-100% confluency, AC16 cells were passaged and subcultured at 1:5 ratio. Briefly, the cells were dissociated from the surface of the flask using TrypLE (Gibco, 12604021) for one minute at 37ºC, followed by centrifugation at 300 g for five minutes. The cell pellet was resuspended in fresh complete DMEM medium and seeded in a new 75cm^2 flask or 60mm dish.

2.5.2 Cryopreservation

In brief, cells were dissociated from the surface of the flask using TrypLE for one minute at 37ºC, followed by centrifugation at 300 g for five minutes. Next, the cell culture medium was removed, and the cell pellet was resuspended in freezing medium (10% dimethyl sulfoxide (DMSO; Sigma-Aldrich, D8418) in complete DMEM medium) and transferred to a cryovial. The cryovial was frozen in cell freezing container (Biocision, BCS405) at -80°C overnight before moving to vaporized liquid nitrogen tank on the following day.

2.6 Overexpression of human ChAT gene in AC16 cells

2.6.1 Mammalian expression plasmid

The pReceiver-M83 expression plasmid with the insertion of human *ChAT* gene (NM_001142929) was purchased from GeneCopoeia™ (Figure 2.6). The same plasmid without open reading frame served as the negative control. This plasmid is bicistronic as it contains an internal ribosome entry site (IRES) to allow simultaneous expression of the mCherry fluorescent protein as well as ChAT. The mCherry fluorescent protein was used as a reporter to determine transfection efficiency.

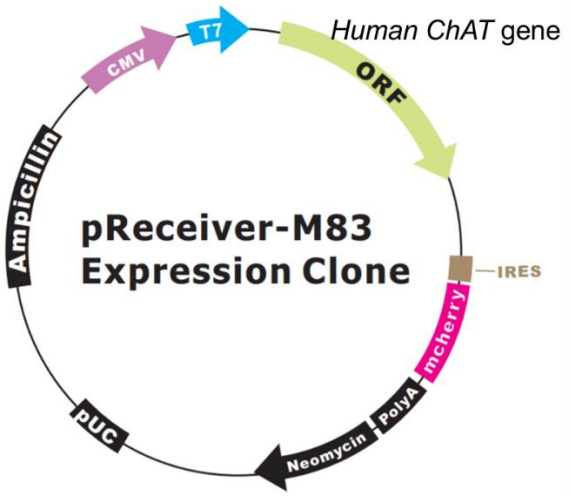

Figure 2.6 The construct of the pReceiver-M83 plasmid
The promoter for cytomegalovirus (CMV) was used to overexpress human ChAT gene. The presence of IRES allows the gene expression of mCherry, which eventually translated to a fluorescent protein. The image was adapted from GeneCopoeia™ and modified with permission (source: https://www.genecopoeia.com/wp-content/uploads/oldpdfs/tech/omicslink/pReceiver-M83.pdf).

2.6.2 Amplification of expression plasmid

2.6.2.1 Bacterial transformation

DH5-α competent *E. coli* (Invitrogen, 18265017) were used to amplify the pReceiver-M83 plasmid to generate a sufficient amount of plasmid that is required for the downstream experiment. Briefly, the bacteria were pre-incubated with 200 ng of the plasmid on ice for 30

minutes. Then, the bacteria were heat-shocked at 42ºC for 45 seconds to induce uptake of plasmid, followed by two minutes incubation on ice. A pre-heated super optimal broth (SOC) medium (Invitrogen, 15544034) was added to the bacteria and incubated at 37ºC for an hour in a shaking incubator at 235 rpm.

After incubation, 100 µL of the bacterial suspension was streaked on LB-ampicillin agar plates (Table 2.9), which was incubated at 37ºC overnight (>16 hours). On the following day, a single bacterial colony was picked and incubated in 100 mL of LB-ampicillin medium (Table 2.9) to further culture the colony at 37ºC overnight (>16 hours) in a shaking incubator at 235 rpm.

2.6.2.2 Extraction and purification of plasmid

A large scale extraction of plasmid from bacteria grown overnight was performed using NucleoBond Xtra Midi plus kit (Macherey-Nagel, 740412) as per manufacturer's instruction. After overnight culture, the bacterial cells were harvested and pelleted at 6,000 g for 10 minutes at 4ºC. Next, the pellet was vigorously resuspended in 8mL of RES buffer in the presence of RNase, followed by addition of 8 mL LYS buffer to lyse the cells with gentle mixing. The mixture was incubated at room temperature for five minutes. While incubating, NucleoBond Xtra column together with inserted column filter was set up and equilibrated with 12 mL of EQU buffer. Next, 8mL of NEU buffer was added to neutralize the mixture with gentle mixing, followed by loading the mixture to the equilibrated column filter. The NucleoBond Xtra column and the column filter was washed with 5 mL of EQU buffer. After the buffer entirely flowed through the column, the column filter was removed. Next, the column was washed with 8 mL of WASH buffer, followed by elution using 5 mL of ELU buffer and collected in a fresh 50 mL falcon tube.

Next, the plasmid present in the eluted buffer was precipitated using 3.5 mL of room-temperature isopropanol and centrifuged at 15,000 g for 30 minutes at 4ºC. The supernatant was discarded, and the pellet was washed with 2 mL of room-temperature 70% ethanol at

15,000 g for five minutes at 4ºC. The supernatant was discarded, and the pellet was dry at room temperature for 15 minutes. Finally, the plasmid was reconstituted in DNase-free water. The concentration of plasmid was measured by using a NanoDrop-1000 spectrophotometer (NanoDrop Technologies, USA). The purity of the plasmid was evaluated by the absorbance ratio of 260 over 280 and 260 over 230 nm.

2.6.3 Lipofectamine-mediated transfection of pReceiver-M83 expression plasmid

Lipofectamine-mediated transfection was performed to overexpress the human *ChAT* gene in the AC16 cells. The cell seeding density was optimized at $0.75x10^5$ cells/$cm^{2,}$ which resulted in approximately 90% confluency after overnight attachment. Lipofectamine™ 3000 kit (Invitrogen, L3000015) was used to transfect AC16 cells with pReceiver-M83 expression plasmid with human *ChAT* gene (M83-hChAT) or without an open reading frame (M83-neg) as a negative control. Briefly, for each well of the 24-well culture dish, 1 µg of M83-hChAT or M83-neg plasmid was mixed with 1.5 µL of Lipofectamine™ 3000 reagent and 2 µL of P3000™ reagent and incubated for 15 minutes to form DNA-lipid complex. The mixture was then added to the cells and incubated for 24 hours.

2.6.3.1 Transfection efficiency analysis

After 24 hours of transfection, AC16 cells were fixed with 4% PFA solution for 15 minutes. Images were captured at random areas (four images per sample) using an Olympus BX51 fluorescent microscope under a 40X objective lens. The results were expressed as the mean values of the two independent experiments. The transfection efficiency was determined using the following formula:

$$\frac{Number\ of\ cells\ with\ mCherry\ expression}{Total\ number\ of\ cells}\ x\ 100\%$$

2.7 Induction of insulin resistance in AC16 cells

An *in-vitro* diabetic cardiomyocyte model was established using AC16 cells to investigate the role of cardiac NNCS in regulating GLUT-4 in diabetic condition .

2.7.1 Preparation of palmitate/BSA complex solution

Palmitate was used to induce insulin resistance in AC16 cells. Palmitate is a saturated fatty acid which is insoluble in the cell culture medium. Thus, conjugation of palmitate to FFA-free BSA solution (Sigma-Aldrich, A8806) is required to create an aqueous solution that can be absorbed and utilized by cells. Briefly, a 100 mM of sodium palmitate solution (Sigma-Aldrich, P9767) was prepared in 0.1 M NaOH (BDH, 10252) at 70^0C. A 10% (w/v) FFA-free BSA solution was prepared in H_2O and filtered using 0.2 μM syringe filter. Next, 100 mM of palmitate was conjugated to 10% FFA-free BSA solution in the ratio of 1:9 at 55ºC to obtain the final concentration 10 mM palmitate/ 10% BSA complex solution [151].

2.7.2 Preparation of cell culture medium for induction of insulin resistance

The cell seeding density was optimized at $0.6x10^5$ cells/cm^2, which resulted in approximately 70% confluency after overnight attachment. Then, the cells were cultured in DMEM serum-free medium containing 30.5 mM glucose, 400 μM palmitate/4% BSA complex, 1X antibiotic-antimycotic solution to induce insulin resistance. The cells cultured in DMEM serum-free medium containing 5.5 mM glucose, 25 mM mannitol (osmotic control), non-conjugated BSA solution, and 1X antibiotic-antimycotic solution was served as vehicle control.

2.8 Oil Red O staining of AC16 cells

Oil Red O (ORO) staining was performed to confirm the uptake of palmitate in the cells. 0.35% (w/v) ORO/isopropanol stock solution was prepared and filtered using 0.2 μM syringe filter [152]. The ORO working solution was prepared by mixing six part of the stock solution and four-part of distilled water, which was then filtered using 0.2 μM syringe filter. After 48 hours of palmitate incubation in the cells, AC16 cells were harvested and fixed with 4% PFA solution for 15 minutes and washed with PBS for 5 minutes thrice. Next, the cells were treated with 60% isopropanol thrice and incubated with 250 μL of ORO working solution for one hour in room temperature. After incubation, the cells were rinsed with 60% isopropanol for five minutes and distilled water for one minute. Next, the cells were incubated with Mayer's hematoxylin solution (Sigma-Aldrich, MHS-16) for 10 minutes to stain the nucleus followed by washing with distilled water for three minutes thrice to remove unbound hematoxylin solution. Slides were mounted on the coverslip with mounting medium and dried overnight.

2.8.1 ORO staining analysis

Five images were captured at random areas from each sample using an Olympus BX61 Montaging light microscope under a 40X objective lens. The results were expressed as the mean values of the two independent experiments. The palmitate uptake was determined using the following formula:

$$\frac{Number\ of\ cells\ with\ positive\ ORO\ staining}{Total\ number\ of\ cells}\ x\ 100\%$$

2.9 Statistical analyses

This section describes the general workflow to carry out statistical analyses. The use of the specific statistical test is described in each chapter. All data were tabulated in Microsoft Excel™

and statistically analyzed using GraphPad Prism software (version 7). The type of analysis performed was consulted with biostatistician Dr. Claire Cameron and Mr. Andrew Gray from the Centre for Biostatistics (University of Otago).

D'Agostino-Pearson and Shapiro-Wilk tests tested the assumption of the normal distribution of the data. Parametric tests (unpaired T-test, One-way, and Two-way ANOVA) were used if the data were normally distributed. Non-parametric tests (Mann-Whitney and Kruskal-Wallis test) were used if the data were not normally distributed. Then, a post-hoc analysis (such as Tukey's and Sidak's test) was performed for multiple's group comparisons. The data are expressed as mean ± standard error of the mean (SEM), and the numbers of samples are presented as *n*. A p-value <0.05 was considered as statistically significant.

Chapter 3 : Characterization of cardiac NNCS and glucose transporters in the diabetic heart

3.1 Introduction

As described in chapter 1, cardiac NNCS regulates glucose metabolism by inducing GLUT-4 expression [100, 122]. However, if this regulation is impaired in diabetes mellitus is unknown. Since glucose metabolism is diminished in the diabetic heart [48, 58, 61-63, 153, 154], this chapter investigated the hypothesis that cardiac NNCS could be dysregulated in the diabetic heart, and such dysregulation could occur in the early stage of diabetes.

3.1.1 Cardiac dysfunction in the diabetic heart

A reduction in diastolic function (i.e., myocardial relaxation) is one of the early diabetes-induced alterations, which may later progress to systolic dysfunction and ultimately HF [20, 65, 69, 155-159]. The incidence of diastolic dysfunction is usually high in the diabetic population with preserved systolic function [156, 160-162]. This prevalence is because the myocardial relaxation is a high ATP-consuming process while the myocardial energy status in the diabetic heart is reduced and unable to provide enough ATP to relax the chamber [21, 72, 163]. In addition, Gopal et al. [164] showed that impaired myocardial glucose oxidation was associated to the development of diastolic dysfunction in a mouse model. Moreover, it has also been reported that increased circulating AGEs promotes cardiac fibrosis as well as LV stiffness, subsequently impairing the diastolic function [165-169]. Further, altered cardiac metabolism and energetics decreases cardiac efficiency and progressively decreases the contractile function of the diabetic heart [20, 65, 69, 159, 170]. Also, diabetes adversely alters the cardiac structure, which ultimately affects the contractile function [171-174].

3.1.2 Cardiac glucose transporters in the diabetic heart

Glucose is the dominant fuel substrate for ATP production in the postprandial condition. The uptake of glucose is facilitated by glucose transporters (GLUTs) in an ATP-independent mechanism (reviewed in [175]). In the human heart, GLUT-4 is the most abundantly expressed GLUT in the LV, followed by GLUT-1 [132]. GLUT-4 is responsible for insulin-stimulated glucose uptake [176] while GLUT-1 is responsible for the basal glucose uptake [177]. In a pathological condition such as diabetes, GLUT-4 expression is reduced [58, 63, 153], thereby decreasing glucose uptake and oxidation [48, 61, 62, 154]. Such a reduction is caused by insulin resistance and elevated FFA oxidation [56-61, 79].

3.1.3 Cardiac NNCS

3.1.3.1 Bioavailability of ACh

As outlined in Chapter 1, the cardiomyocytes possess an intrinsic cholinergic machinery. The functionality of this machinery can be categorized into three aspects – synthesis, release, and degradation of ACh. There are two components involved in ACh synthesis – namely ChAT and CHT1. ChAT is an enzyme involved in ACh synthesis by combining acetyl-CoA and choline [108]. CHT1 is a transporter that engages in the uptake of choline from extracellular space for ACh synthesis [99]. As choline is the precursor of ACh, the uptake of choline is the rate-limiting step for ACh synthesis (reviewed in [178]). ACh is stored and released from VAChT [96, 99]. Lastly, AChE is an enzyme present in extracellular space to hydrolyze ACh [96, 97, 108]. These components collectively maintain the homeostasis of ACh in cardiomyocytes.

3.1.3.2 ACh mediated signaling through muscarinic ACh receptors (mAChR)

ACh released from the cardiomyocytes mediates signaling via binding to the muscarinic ACh receptor (mAChR) expressed on the plasma membrane of cardiomyocytes. Thus far, five subtypes of mAChR ($M_{1\text{-}5}$AChR) have been identified. In the human atrium and ventricle, the

gene expression of these five subtypes is readily detectable; however, the protein expression of M_4AChR cannot be detected [112]. Furthermore, gene expression studies revealed that M_2AChR is the predominant subtype in both the atrium and ventricle of the mouse and rat, however, the expression of other subtypes is relatively low [111, 179].

The initiation of ACh-mAChR mediated signaling in the heart can be a result of both neuronal and non-neuronal ACh origin. The neuronal effect is initiated in the atrial region by ACh released from cholinergic neurons that decrease heart rate (HR) and cardiac contraction by modulating the activity ion channels [113, 180]. It is suggested that this neuronal effect is further amplified and propagated by the intrinsic cardiac NNCS [96, 97]. This could help in transmitting neuronal cholinergic signals in the sparsely innervated ventricular myocardium [181-185]. Besides, it is well established that M_2AChR mediates this neuronal effect [113, 180], but emerging evidence suggests that M_1- and M_3AChR also play a role in regulating the HR and contraction [186, 187].

On the other hand, the non-neuronal effects induced by the cardiac NNCS include increased ACh synthesis through increased cardiomyocytes ChAT expression [96]; and activation of pro-survival PI3K/Akt/HIF1α signaling cascade in the cardiomyocytes via auto/paracrine manner [96, 100]. It is still unknown which subtype of mAChR is responsible for the non-neuronal effect. However, it is reasonable to postulate that M_2AChR is likely the main receptor responsible due to its abundance compared to other muscarinic subtypes in the heart [186, 187].

3.2 Study aim

The aims of this chapter are *(1)* to investigate the expression changes in cardiac NNCS (ChAT, CHT1, VAChT, AChE and M_2AChR) and glucose transporters (GLUT-1 and GLUT-4) in the ventricles of type-2 diabetic *db/db* mouse and human, and *(2)* to investigate if the expression changes in cardiac NNCS precedes the expression changes in GLUT-4 in the ventricles of type-2 diabetic *db/db* mouse of different ages.

I hypothesized that the components of cardiac NNCS and GLUTs would be dysregulated - particularly *(1)* ChAT, CHT1, and VAChT expression would be decreased; *(2)* AChE expression would be increased, *(3)* M_2AChR expression, as well as *(4)* GLUT-1 and GLUT-4 expressions, would be decreased in the ventricles of diabetic *db/db* mouse and diabetic human. Further, I hypothesized that dysregulation of cardiac NNCS would precede the downregulation of GLUT-4 in the ventricles of diabetic *db/db* mice.

3.3 Materials and methods

This section only outlines the specific reagents, concentration, and conditions used for each of the general methodologies. Detailed experimental procedures for general methods are described in 'Chapter 2: General materials and methods'.

3.3.1 Type-2 diabetic *db/db* mouse

The ventricular tissues from type-2 diabetic *db/db* mice of 8-, 12-, 16-, 20-, 24-, 28-, and 32-weeks old were available [1] and used in this study to investigate the gene and protein expression changes in cardiac NNCS and GLUTs. These aged-matched non-diabetic *db/+* mice (ND) were used as a control (see Section 2.2.2). The echocardiographic data of these ND and *db/db* mice are available in a recent publication from Katare laboratory [1].

3.3.2 Type-2 diabetic human LV tissues

The LV tissues taken from non-diabetic (ND-CAD) and type-2 diabetic (D-CAD) human patients who underwent coronary artery bypass graft were used in this study to investigate the protein expression changes in cardiac NNCS and glucose transporters (see Section 2.2.1). The corresponding echocardiographic data from ND-CAD and D-CAD patients were retrieved from the patient database of HeartOtago.

3.3.3 Immunofluorescence analysis

Triplet-labelling immunofluorescence of ChAT, GLUT-4 and CTNI was performed on ND mouse ventricular tissues, and followed by counterstained with DAPI (1:1,000) to stain nuclei (described in Chapter 2, Section 2.4). The purpose of performing multicolor immunofluorescence was to identify if ChAT and GLUT-4 are localized in the mouse ventricular cardiomyocytes. The specificity of anti-ChAT antibody was tested on the ventricular tissue of *db/db-ChAT-tg* mice (served as positive control; Appendix 3, Figure S3.1) while anti-CTNI antibody was tested on the skeletal muscle of ND mouse (served as negative control; Appendix 3, Figure S3.2). Unfortunately, there was no appropriate control to test the specificity of anti-GLUT-4 antibody, hence, this is one of the limitations of the study.

Besides, as anti-ChAT and anti-GLUT-4 primary antibodies were produced in rabbit (Table 3.1), an additional blocking step is required to prevent the second secondary antibody from binding to the first primary antibody. In this case, after labeling ChAT with secondary antibody (Figure 3.1, step 2), the sections were incubated with 10% rabbit serum (Sigma-Aldrich, R9133; Figure 3.1, step 3) for two hours and followed by AffiniPure anti-rabbit Fab fragment (Jackson ImmunoResearch, 111-007-003; Figure 3.1, step 4) at 1:15 for two hours. In Appendix 3, Figure S3.3 shows the fluorescent images of co-labelling ChAT and GLUT-4 in the same ventricular tissue with and without AffiniPure anti-rabbit Fab fragment to demonstrate successful blocking. Besides, single staining of ChAT, GLUT-4 and CTNI on mouse ventricular tissues was

individually performed to serve as a control to compare with the images obtained from triple-labelling staining (Appendix 3, Figure S3.4).

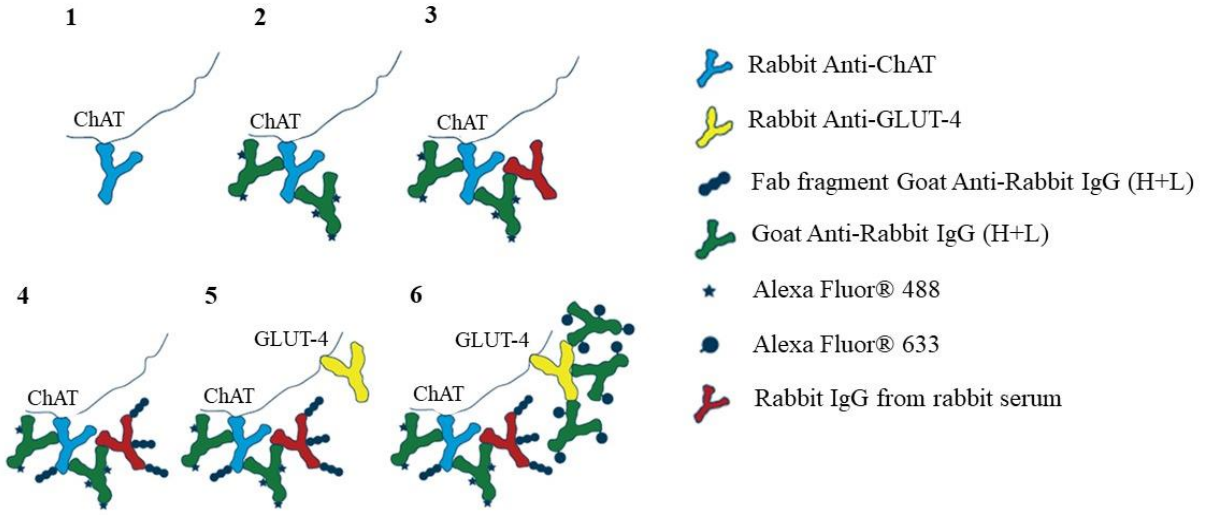

Figure 3.1 Double labeling of primary antibodies produced from the same host species
Immunostaining of ChAT was first performed (1-2) and followed by blocking with rabbit serum and Fab fragments (3-4). Then, immunostaining of GLUT4 was performed (5-6). The image was taken from Jackson ImmunoResearch and modified with permission (source: https://www.jacksonimmuno.com/technical/products/protocols/double-labeling-same-species-primary/example-c).

Table 3.1 Information on antibodies for triplet-labelling immunofluorescence

Antigen	Source	Dilution	Manufacturer/Catalogue number
Primary antibodies			
ChAT	Rabbit	1:100	Abcam, AB181023
GLUT-4	Rabbit	1:100	NovusBio, NBP1-49533
CTNI (antibody is biotinylated)	Mouse	1:100	NovusBio, NB110-2546B
Secondary reagents			
AlexaFluor® 488 conjugated anti-rabbit IgG	Goat	1:100	Invitrogen, A32731
AlexaFluor® 633 conjugated anti-rabbit IgG	Goat	1:200	Invitrogen, A21070
Streptavidin-AlexaFluor® 568	-	1:200	Invitrogen, S11226

3.3.4 Quantitative polymerase chain reaction (qPCR) analysis

Total RNA extraction from the middle part of the mouse ventricular tissues was performed as described in Section 2.3.1.1. The isolated RNAs were treated with rDNase to remove genomic DNA and followed by reverse transcription (Section 2.3.1.2) and real-time amplification (Section 2.3.1.3) were performed to detect gene expression of ChAT, CHT1, VAChT, AChE, M_2AChR, GLUT-1, and GLUT-4. The successful rDNase treatment was confirmed by directly

subjecting the rDNase-treated RNA to real-time amplification and ensuring no amplification (Appendix 1, Figure S1.1B). Also, gradient PCR was performed at annealing temperature of 50°C, 54°C and 58.4°C (CHT1, AChE, M_2AChR, GLUT-1, and GLUT-4) or 50°C, 55°C and 60°C (ChAT and VAChT) to determine the optimal annealing temperature of each primer (Appendix 1, Figure S1.1A). Besides, the melt curve analysis showed the melting temperature of each PCR amplicons, which was used as an indicator to examine the specificity of PCR amplification (Appendix 1, Figure S1.1C). Table 3.2 summarizes the primer sequences, the primer binding exon-exon junction/exon, optimal annealing temperature, concentration and amplicon size. The gene expression of the selected target was normalized to the expression of reference gene RN18S and expressed as $2^{-\Delta\Delta Ct}$ [142].

Table 3.2 Predesigned KiCqStart mouse primers used for qPCR amplification

Gene	Ref Seq ID	Primer sequences		Exon-exon junction/Exon	Annealing Temp (°C)	Primer Conc. (µM)	Amplicon length (bp)
ChAT	NM_009891	F=	GGACAGCCAATCCATTCCCAC	6-7	55	0.2	194
		R=	CAAAGAACTGGTTGCAGCAGG	7-8	55	0.2	
CHT1	NM_022025	F=	TCAGACAAAATGCATCAGAC	8-9	54	1.0	145
		R=	ATGATGTAGACAAGGTCAGAG	9	54	1.0	
VAChT	NM_021712	F=	ATGGCTGTGAGGACGACTAC	NA	60	0.2	149
		R=	ACTCATTAGAGGAGGTGGGC	NA	60	0.2	
M_2AChR	NM_203491	F=	AGTCAGTGACAGGTTTAAATG	2-3	54	0.2	102
		R=	GGACTGGTAATAGCCAAAC	3	54	0.2	
AChE	NM_009599	F=	GTATCTTCCGATTTTCCTTCG	2	54	0.2	99
		R=	CCTGCAGGTCTTGAAAATC	2-3	54	0.2	
GLUT-1	NM_011400	F=	AAGTCCAGGAGGATATTCAG	10	54	0.2	163
		R=	CTACAGTGTGGAGATAGGAG	10	54	0.2	
GLUT-4	NM_009204	F=	CAATGGTTGGGAAGGAAAAG	3-4	54	0.2	108
		R=	AATGAGTATCTCATAGGAGGC	4	54	0.2	
RN18S	NR_003278	F=	CAGTTATGGTTCCTTTGGTC	NA	54-60	0.2	198
		R=	TTATCTAGAGTCACCAAGCC	NA	54-60	0.2	

bp, basepair; Conc., Concentration; NA, Not applicable; Temp, Temperature

3.3.5 Western blot analysis

Total protein extraction from mouse (lower part) and human ventricular tissues was performed as described in Section 2.3.2.1. Ten micrograms of mouse and human protein samples were separated using SDS gel electrophoresis following which the membrane was probed for antibodies against ChAT, CHT1, VAChT, AChE, M_2AChR, GLUT-1, and GLUT-4. The specificity of anti-AChE, anti-ChAT, anti-CHT1, anti-M_2AChR and anti-VAChT antibodies were examined on a full blot with the use of positive control (i.e. mouse brain) and compared to the predicted molecular weight recommended by manufacturer and UniProt (Appendix 2, Figure S2.2-2.5). Unfortunately, there was no positive control to test anti-GLUT-1 and anti-GLUT-4 antibodies, hence, this is one of the limitations of the study. The band intensity of the target protein was normalized to a prominent band between 37 kDa and 50 kDa on the Ponceau S stained blot as described in Chapter 2 (section 2.3.2.5) [143, 144] and expressed as fold changes towards the control group [145]. The information of antibodies are listed in Table 3.3. The full blot for each antibody is shown in Appendix 2.

Table 3.3 Primary and secondary antibodies for western blot

Antigen	Host/Clone	Dilution factor	Predicted molecular weight (kDa)	Manufacturer/ Catalogue number
Primary antibodies				
AChE	Rabbit/polyclonal	1:1,000	68	Bioss, BS-2511R
ChAT	Goat/polyclonal	1:1,000	70/74	Chemicon, AB144P
CHT1	Rabbit/polyclonal	1:1,000	70-75	Merck Millipore, ABN458
GLUT-1	Rabbit/polyclonal	1:1,000	54	Merck Millipore, 07-1401
GLUT-4	Rabbit/polyclonal	1:1,000	55	NovusBio, NBP1-49533
M_2AChR	Rabbit/monoclonal	1:1,000	52	Abcam, AB109226
VAChT	Rabbit/polyclonal	1:1,000	70	Sigma-Aldrich, SAB4200560
Secondary antibodies				
Anti-goat IgG, HRP conjugated	Mouse	1:3,000	-	Santa Cruz, SC2354
Anti-rabbit IgG, HRP conjugated	Goat	1:5,000	-	Sigma-Aldrich, A6154

Recombinant mouse IgGκ light chain binding protein, HRP conjugated	-	1:3,000	-	Santa Cruz, SC516102

Note: the predicted molecular weight of protein is recommended by the manufacturer

3.3.6 Statistical analyses

All statistical analyses were performed using GraphPad Prism (version 7) in consultation with biostatistician Mr. Andrew Grey and Dr. Claire Cameron (Centre for Biostatistics, University of Otago). Data are expressed as the mean ± SEM. For the gene expression and protein expression data from the ND and *db/db* mice, there were data from some specific age groups that failed the normality test. However, there is no single non-parametric test equivalent to Two-way ANOVA. In this case, a non-parametric Mann-Whitney U test was used. This particular approach was consulted with biostatistician Dr. Claire Cameron and Mr. Andrew Gray. Besides, unpaired T-test was used to analyze all the parameters of patient characteristics and western blot data derived from human LV tissues

3.4 Results

3.4.1 Characterization of cardiac NNCS and glucose transporters in the ventricles of type-2 diabetic *db/db* mice

3.4.1.1 Cardiac function and structures

The echocardiographic results of *db/db* mice have already been published [1]. The results shown here is for referencing purposes. The *db/db* mice showed a progressive deterioration of cardiac function with marked ventricular remodeling. The early diastolic dysfunction was observed at 20-weeks of age (i.e. E/A ratio and deceleration time; Figure 3.2A&B) and severely impaired at 28-weeks of age. The systolic function (i.e. EF and FS; Figure 3.2C&D) began to deteriorate at 20-weeks of age and gradually progress to systolic dysfunction at 28-weeks of age (EF<50%). In terms of the cardiac structure, cardiac hypertrophy as evidenced by an increase in LV mass developed at 16-weeks of age (Figure 3.2E). Subsequently, increased LV internal diameter at systole and diastole as well as increased relative wall thickness was observed at 20- and 24-weeks of age, respectively (Figure 3.2F-H). Changes in these indices indicate cardiac remodeling.

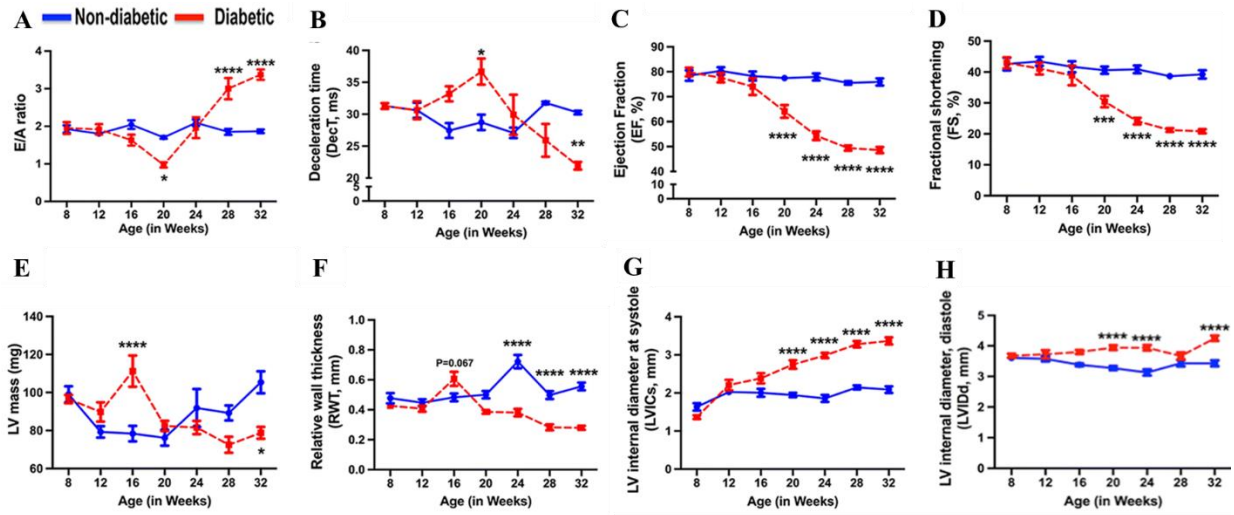

Figure 3.2 Diabetes-induced progressive cardiac dysfunction and remodeling in the type-2 diabetic *db/db* mice

Line graphs showing the temporal changes of diastolic function indicated by ***(A)*** *E/A ratio and* ***(B)*** *deceleration time; systolic function indicated by* ***(C)*** *ejection fraction (EF) and* ***(D)*** *fractional shortening (FS) as well as the temporal changes in LV structure indicated by* ***(E)*** *LV mass,* ***(F)*** *relative wall thickness,* ***(G)*** *LV internal diameter at systole and* ***(H)*** *LV internal diameter at diastole in 8- to 32-weeks*

*old db/db mice. Data are presented as mean ± SEM and are from eight animals in each group. Two-way ANOVA with Tukey's multiple comparisons test was performed. *p<0.05; **p<0.01; ***p<0.001; ****p<0.0001 VS age-matched ND (Non-diabetic) group. These results were collected and analyzed by Rawal et al. [1].*

3.4.1.2 Localization of ChAT and GLUT-4 in the ventricular tissue

Triplet-labeling immunofluorescence was performed to co-stain the ventricular tissues with antibodies against ChAT and GLUT-4 together with cardiomyocyte-specific marker cardiac troponin-I (CTNI) and counterstained with DAPI (nuclear marker). The confocal image showed positive staining of CTNI in the mouse ventricular tissues (Figure 3.3A). Further, positive staining of ChAT was detected in the ventricular tissues, confirming that ChAT was expressed by the ventricular cardiomyocytes (Figure 3.3B, white arrows). The localization of GLUT-4 was observed in two regions. First, intracellular GLUT-4 vesicles were close to the nucleus in the ventricular cardiomyocytes (Figure 3.3B, red arrows). Second, membrane GLUT-4 was on the surface of the ventricular cardiomyocytes (Figure 3.3B, yellow arrows). The representative images for secondary-antibody only controls for CTNI, ChAT, and GLUT-4 staining are in Appendix 3 (Figure S3.5). These findings confirm that ChAT and GLUT-4 were expressed and localized in the mouse ventricular cardiomyocytes.

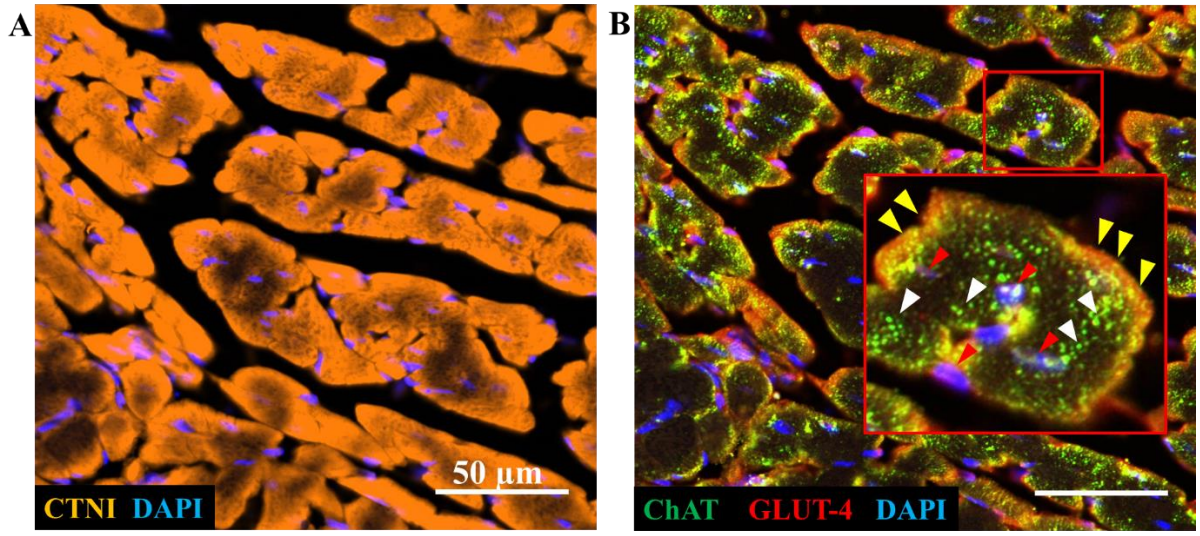

Figure 3.3 Localization of ChAT, GLUT-4, and CTNI in the mouse ventricular tissue
*The representative confocal images showing **(A)** the staining of CTNI as a cardiac marker and **(B)** the staining and localization of ChAT (white arrows), intracellular GLUT-4 (red arrows) and membrane GLUT-4 (yellow arrows) in the mouse ventricular tissue.*

3.4.1.3 Cardiac NNCS in the ventricles of type-2 diabetic *db/db* mice

The next aim was to investigate if the cardiac NNCS is altered in diabetes mellitus. The gene and protein expression of the components of cardiac NNCS (i.e., ChAT, CHT1, VAChT, AChE, and M_2AChR) were examined. The gene expression was measured by quantitative PCR analysis, while protein expression was measured by western blot analysis.

3.4.1.3.1 ACh synthesis - ChAT

Gene expression

The expression changes in *ChAT* gene was not statistically different between the ND and *db/db* mice at 8- to 32-weeks of age (Figure 3.4A).

Protein expression

The goat anti-ChAT antibody resulted in multiple bands (Appendix 2, Figure S2.2). As the manufacturer recommends the ChAT-positive bands to be 70/74 kDa, and overexpression of *ChAT* gene in the ventricles (Chapter 4) and AC16 cells (Chapter 5) resulted in a strong band at 70 kDa. Thus, I quantified the band intensity from the area between 70 to 74 kDa. One possible reason why there were multiple bands could be due to post-translational modification. ChAT protein expression was not statistically different between the ND and *db/db* mice at 8-, 12-, 16-, 20-weeks of age (Figure 3.4B). At 24-weeks of age, there was an increasing trend in ChAT expression ($p=0.09$). At 28-weeks of age, the expression was significantly decreased in the *db/db* mice, indicating a reduction in ACh synthesis and bioavailability. At 32-weeks of age, ChAT expression was comparable between the ND and *db/db* mice.

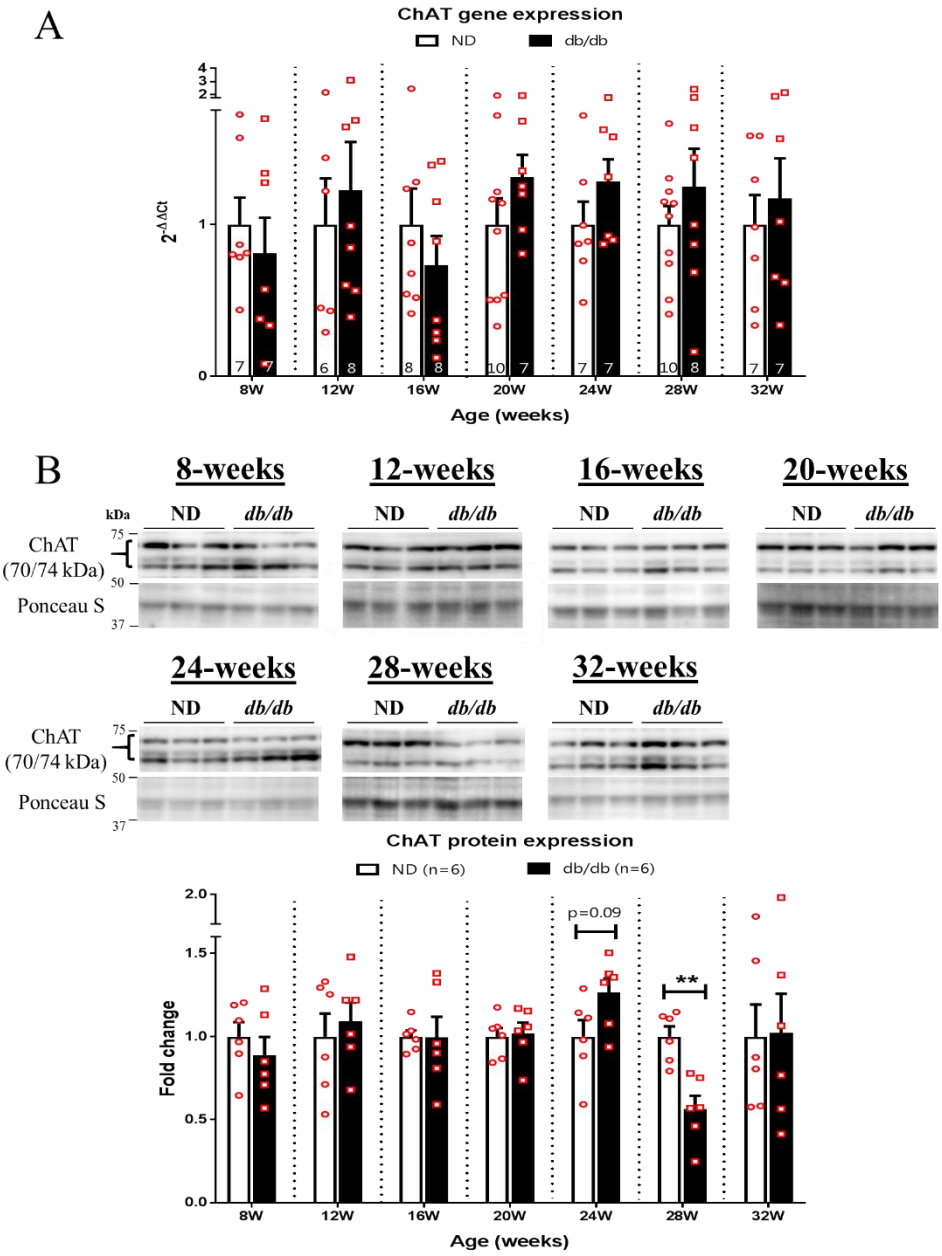

Figure 3.4 Decreased ChAT protein expression in the *db/db* mice at 28-weeks of age.
(A) *Quantitative bar graphs with scatter plot showing the gene expression of ChAT in the ND and db/db mice at 8- to 32-weeks of age.* ***(B)*** *Representative blots and quantitative bar graphs with scatter plot showing the protein expression of ChAT in the ND and db/db mice at 8- to 32-weeks of age. Data are presented as mean ± SEM. A non-parametric Mann-Whitney U test was performed. **p<0.01 VS age-matched ND mice. The number of samples per group is indicated in the figure.*

3.4.1.3.2 Reuptake of choline for ACh synthesis - CHT1

Gene expression

The expression changes in *CHT1* gene was not statistically different between the ND and *db/db* mice at 8- and 12-weeks of age (Figure 3.5A). The expression was significantly increased in the *db/db* mice at 16-weeks of age. Subsequently, CHT1 gene expression was decreased in the *db/db* mice at 24-weeks of age. However, the gene expression was increased in the *db/db* mice at 32-weeks of age.

Protein expression

The anti-CHT1 antibody resulted in two bands between 70 to 75 kDa (Appendix 2, Figure S2.3). The manufacturer specified that the CHT1-positive bands can be 70 and 75 kDa. This is because one N-linked glycosylation site has been reported (https://www.uniprot.org/uniprot/Q9GZV3), thus, resulting in molecular weight of 75 kDa. In this case, I quantified the band intensity from the area between 70 to 75 kDa.

CHT1 protein expression was not statistically different between the ND and *db/db* mice at 8-, 12-, 16- and 20-weeks of age (Figure 3.5B). At 24-weeks of age, the expression was significantly increased in the *db/db* mice. An increase in CHT1 protein expression suggests increased uptake of choline for ACh synthesis, hence increasing the ACh bioavailability. At 28- and 32-weeks of age, the expression was not statistically different between the ND and *db/db* mice.

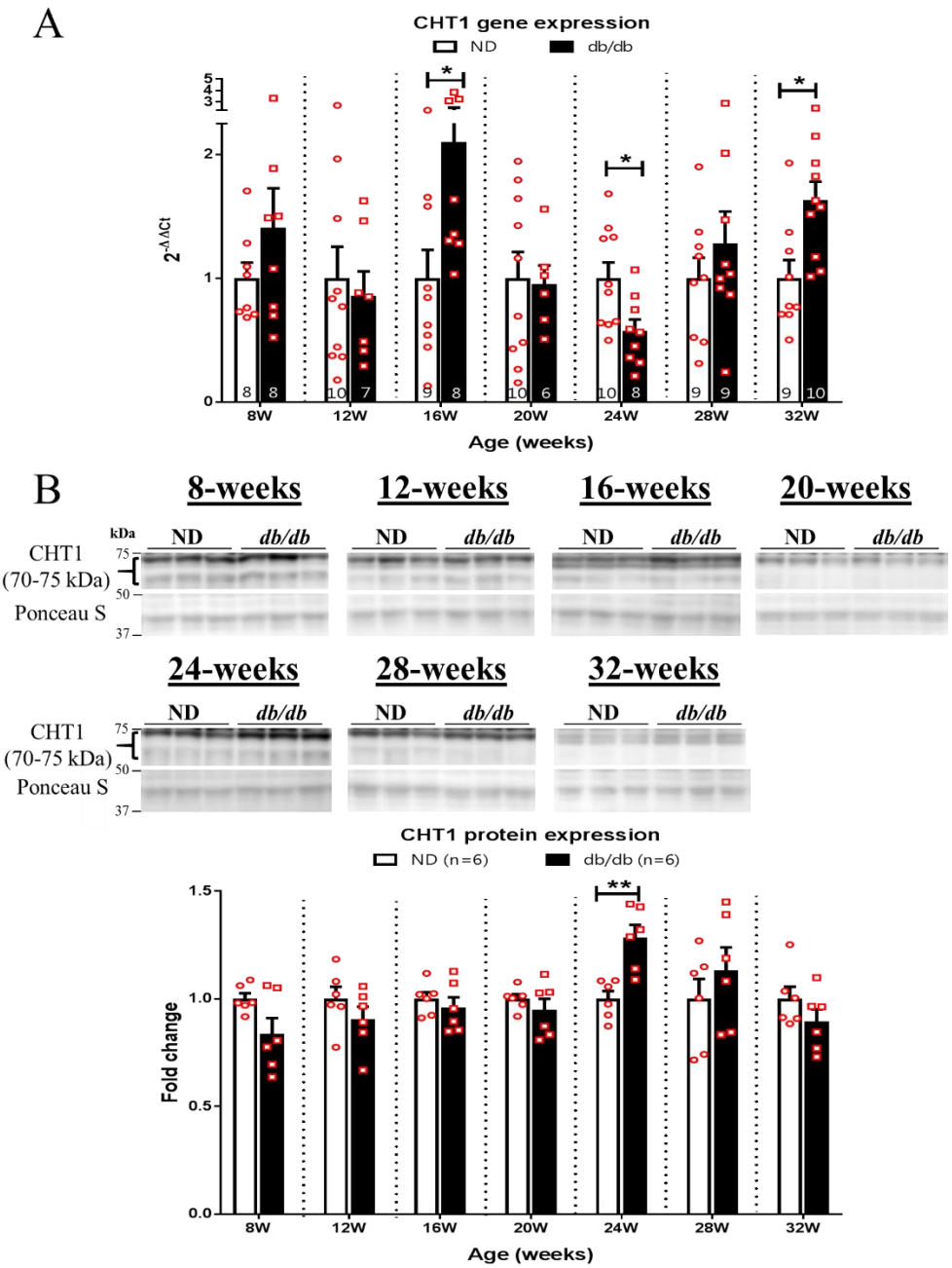

Figure 3.5 Altered CHT1 gene and protein expression in the *db/db* mice at 16-, 24- and 32-weeks of age.

(A) *Quantitative bar graphs with scatter plot showing the gene expression of CHT1 in the ND and db/db mice at 8- to 32-weeks of age.* ***(B)*** *Representative blots and quantitative bar graphs with scatter plots showing the protein expression of CHT1 in the ND and db/db mice at 8- to 32-weeks of age. Data are presented as mean ± SEM. A non-parametric Mann-Whitney U test was performed. *p<0.05, **p<0.01 VS age-matched ND mice. The number of samples per group is indicated in the figure.*

3.4.1.3.3 ACh release - VAChT

Gene expression

The expression changes in *VAChT* gene was not statistically different between the ND and *db/db* mice at 8-, 12-, 16-, 20-, 24- and 32-weeks of age (Figure 3.6A). However, the gene expression was significantly increased in the *db/db* mice at 28-weeks of age.

Protein expression

The polyclonal anti-VAChT antibody resulted in multiple bands on blot (Appendix 2, Figure S2.3). The manufacturer recommends that the VAChT-positive band is approximately 70 kDa. Further, this particular antibody was used by Guzman et al. [188] and they did not detect a band in the striatum-specific VAChT knockout mice.

VAChT expression was not statistically different between the ND and *db/db* mice at 8-, 12-, 16- and 20-weeks of age (Figure 3.6B). However, the expression was significantly increased in *db/db* mice in comparison to the ND mice at 24- and 28-weeks of age. An increase in VAChT expression suggests increased ACh release, thus, increasing the ACh bioavailability in the extracellular space. At 32-weeks of age, the expression was significantly decreased, suggesting a reduction in ACh release and bioavailability in the extracellular space in the diabetic heart.

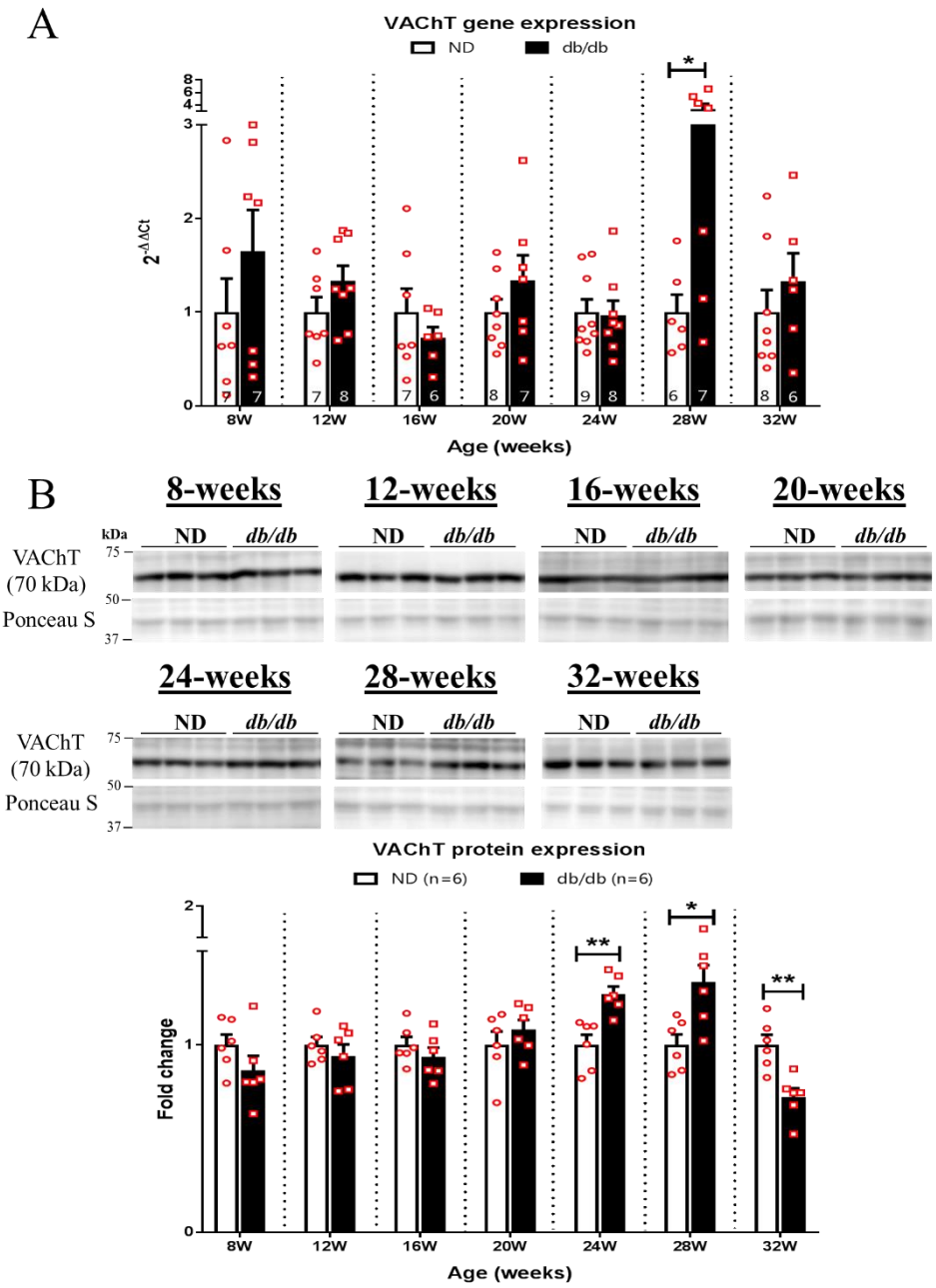

Figure 3.6 Altered VAChT gene and protein expression in the *db/db* mice at 24-, 28- and 32-weeks of age.

(A) *Quantitative bar graphs with scatter plot showing the gene expression of VAChT in the ND and db/db mice at 8- to 32-weeks of age.* ***(B)*** *Representative blots and quantitative bar graphs with scatter plots showing the protein expression of VAChT in the ND and db/db mice at 8- to 32-weeks of age. Data are presented as mean ± SEM. A non-parametric Mann-Whitney U test was. *p<0.05, **p<0.01 VS age-matched ND mice. The number of samples per group is indicated in the figure.*

3.4.1.3.4 ACh degradation - AChE

Gene expression

The expression changes in *AChE* gene was not statistically different between the ND and *db/db* mice at 8- to 32-weeks of age (Figure 3.7A). On a side note, there are three AChE variants,

namely AChE-S (synaptic variant), AChE-R (readthrough variant) and AChE-E (erythrocytic variant) (reviewed in [189]). The primers used in this study is unable to differentiate these variants as the primers anneal to exon 2 (forward primer) and exon 2-3 junction (reverse primer) that are commonly present in all variants (reviewed in [189]). However, it has previously been reported that AChE-S is present in the heart [190].

Protein expression

Although the polyclonal anti-AChE antibody resulted in multiple bands, I observed only one band around 75 kDa on the blot (Appendix 2, Figure S2.4). I identified this band as AChE-positive as the predicted molecular weight is approximately 68 kDa.

AChE protein expression was significantly increased in the *db/db* mice at 8-weeks of age (Figure 3.7B). This result indicates an increase in ACh degradation, and hence the ACh bioavailability was possibly decreased. At 12-, 16- and 24-weeks of age, the expression was not statistically different between the ND and *db/db* mice. However, at 20-, 28- and 32-weeks of age, AChE expression was significantly decreased in the *db/db* mice compared to the age-matched ND mice. This result indicates a reduction in ACh degradation, and thus the ACh bioavailability was possibly increased in the extracellular space in the diabetic heart.

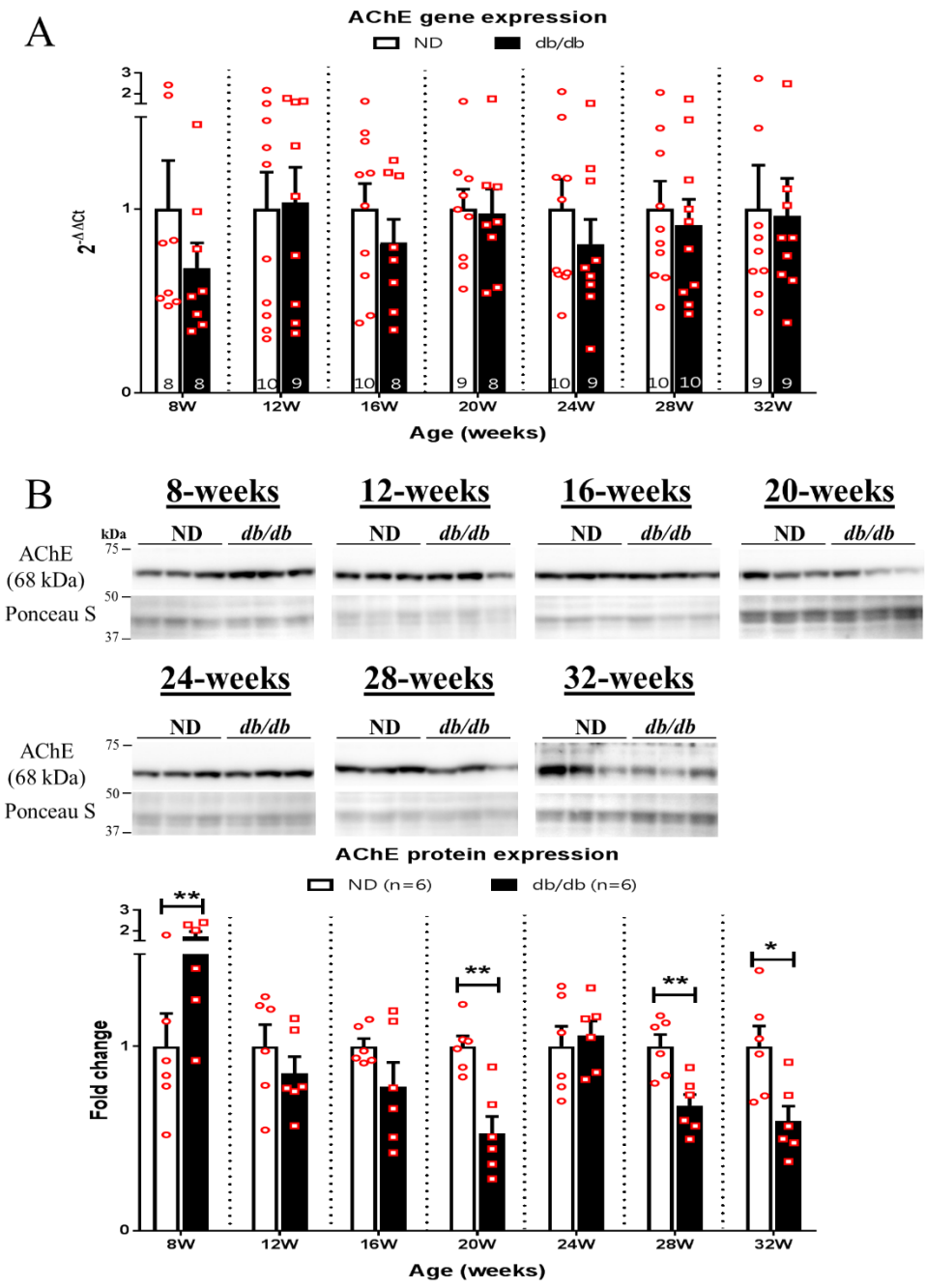

Figure 3.7 Altered AChE protein expression in the *db/db* mice at 8-, 20-, 28- and 32-weeks of age. ***(A)*** *Quantitative bar graphs with scatter plot showing the gene expression of AChE in the ND and db/db mice at 8- to 32-weeks of age.* ***(B)*** *Representative blots and quantitative bar graphs with scatter plots showing the protein expression of AChE in the ND and db/db mice at 8- to 32-weeks of age. Data are presented as mean ± SEM. A non-parametric Mann-Whitney U test was performed. *p<0.05, **p<0.01 VS age-matched ND mice. The number of samples per group is indicated in the figure.*

3.4.1.3.5 ACh binding receptor - M_2AChR

Gene expression

The expression changes in *M_2AChR* gene was not statistically different between the ND and *db/db* mice at 8- to 32-weeks of age (Figure 3.8A).

Protein expression

The monoclonal anti- M_2AChR antibody detected only one band that was close to 50 kDa on the blot (Appendix 2, Figure S2.2). I identified this band as M_2AChR-positive as the predicted molecular weight is approximately 52 kDa.

M_2AChR protein expression was significantly decreased in the 8- to 32-weeks old *db/db* mice (Figure 3.8B). This result suggests reduced receptor density for ACh binding, and thus ACh activated M_2AChR signaling was possibly reduced in the diabetic heart.

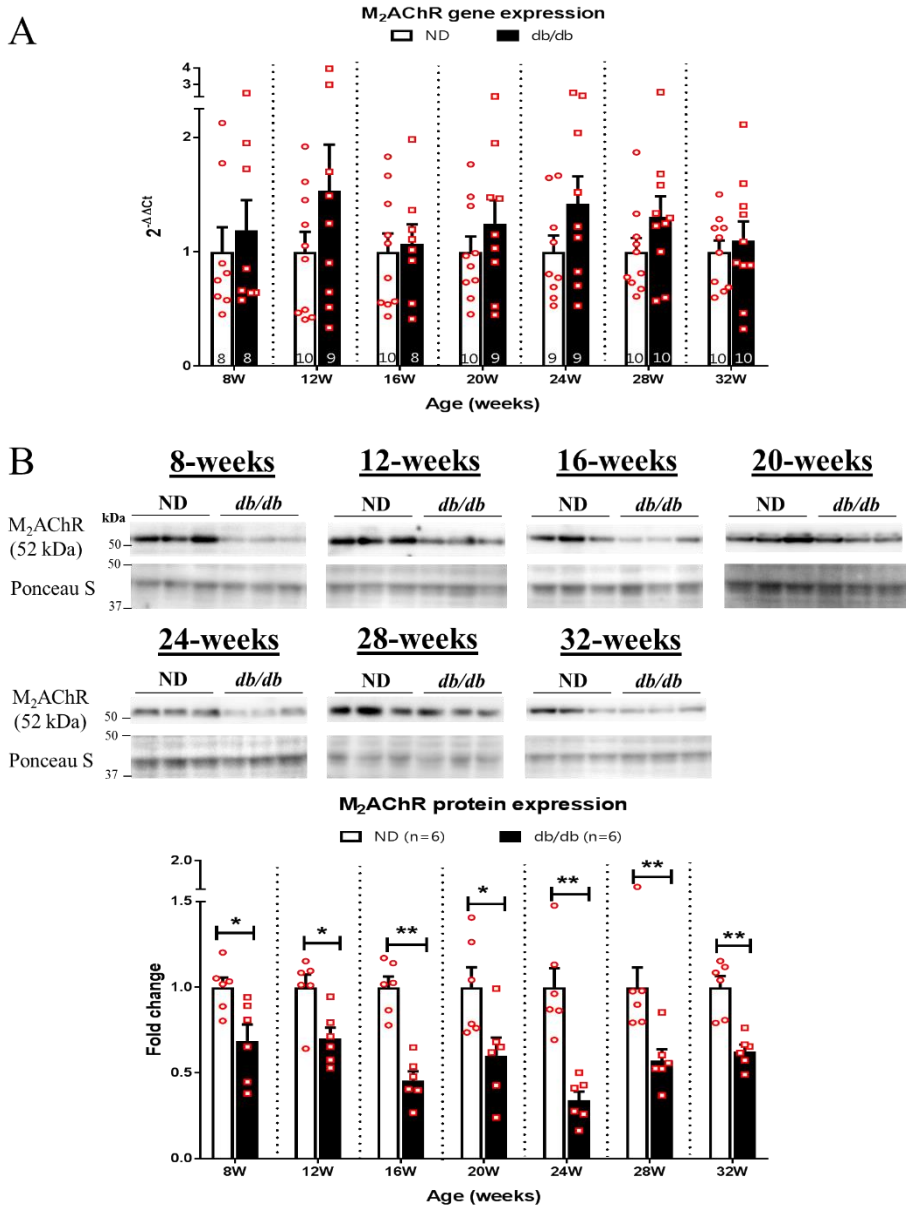

Figure 3.8 Decreased M_2AChR protein expression in the *db/db* mice at 8- to 32-weeks of age.
(A) *Quantitative bar graphs with scatter plot showing the gene expression of M_2AChR in the ND and db/db mice at 8- to 32-weeks of age.* ***(B)*** *Representative blots and quantitative bar graphs with scatter plots showing the protein expression of M_2AChR in the ND and db/db mice at 8- to 32-weeks of age. Data are presented as mean ± SEM. A non-parametric Mann-Whitney U test was performed. *p<0.05, **p<0.01 VS age-matched ND mice. The number of samples per group is indicated in the figure.*

In summary, the findings from this section show that *(1)* CHT1 and VAChT gene expression and *(2)* ChAT, CHT1, VAChT, AChE, and M_2AChR protein expression were altered in the ventricles of *db/db* mice.

3.4.1.4 GLUTs in the ventricles of type-2 diabetic *db/db* mice

Since insulin resistance decreases cardiac glucose utilization, the next aim was to investigate if T2DM affects GLUT-1 and GLUT-4 expressions in the ventricles of diabetic *db/db* mice. Quantitative PCR and western blot analyses were carried to measure the gene and protein expression of GLUT-1 and GLUT-4.

3.4.1.4.1 Basal glucose uptake - GLUT-1

Gene expression

The expression changes in *GLUT-1* gene was not statistically different between the ND and *db/db* mice at 8- to 32-weeks of age (Figure 3.9A).

Protein expression

The polyclonal ani-GLUT1 antibody detected multiple bands, however, there was only one band between 50 kDa and 75 kDa (Appendix 2, Figure S2.5). Thus, I identified this band as GLUT-1 positive based on the predicted molecular weight indicated by the manufacturer and UniProt. Further, Linz et al [191] used the same antibody and reported the same result.

There was an increasing trend in the GLUT-1 protein expression ($p=0.09$) in the *db/db* mice at 8-weeks of age (Figure 3.9B). At the 12-weeks of age, the expression was not statistically different between the ND and *db/db* mice. At 16- to 32-weeks of age, GLUT-1 expression was significantly decreased in the *db/db* mice in comparison to the age-matched ND mice. This result suggests that basal glucose uptake was reduced in the diabetic heart.

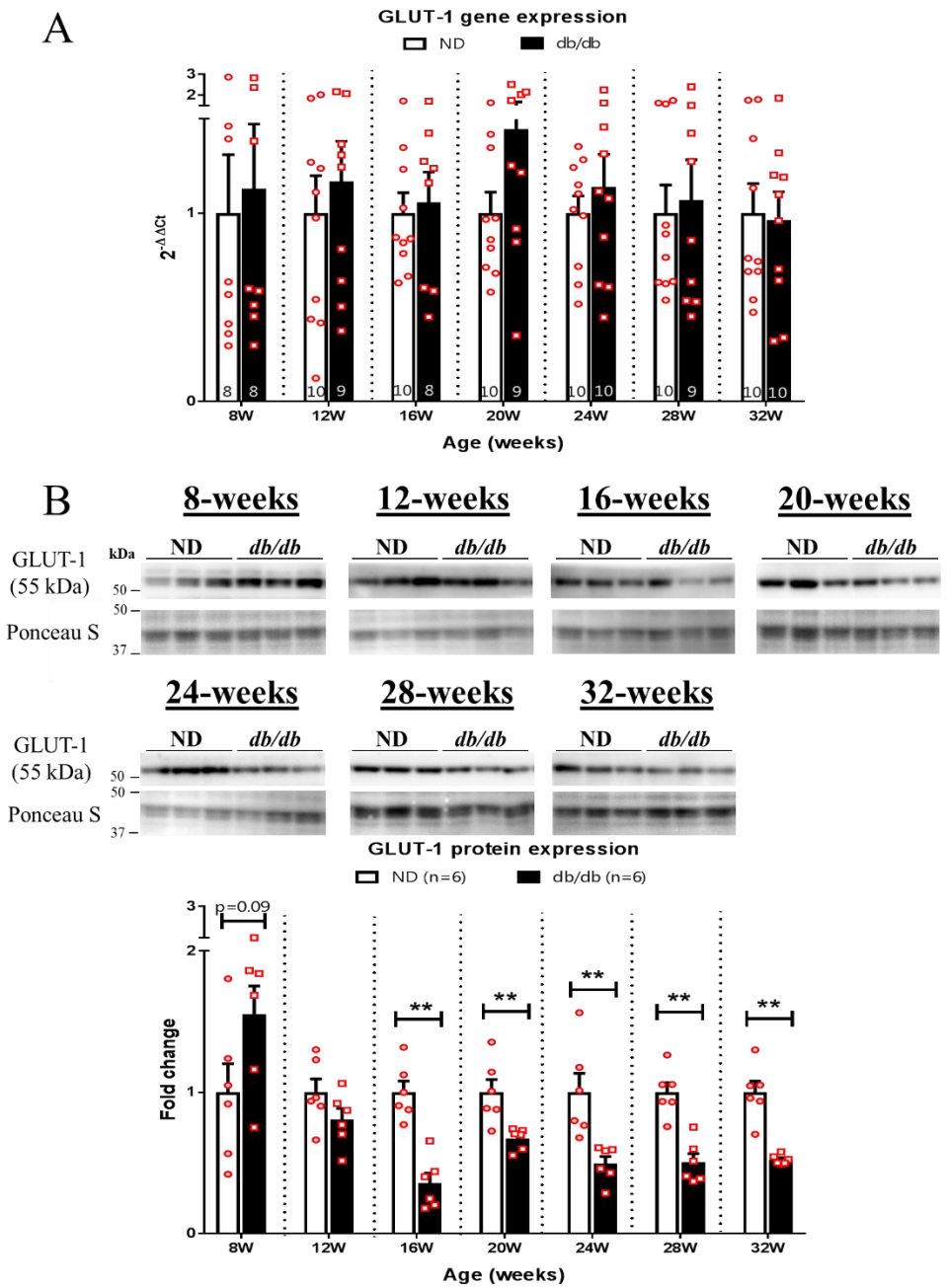

Figure 3.9 Decreased GLUT-1 protein expression in the *db/db* mice at 16- to 32-weeks of age.
(A) *Quantitative bar graphs with scatter plot showing the gene expression of GLUT-1 in the ND and db/db mice at 8- to 32-weeks of age.* ***(B)*** *Representative blots and quantitative bar graphs with scatter plots showing the protein expression of GLUT-1 in the ND and db/db mice at 8- to 32-weeks of age. Data are presented as mean ± SEM. A non-parametric Mann-Whitney U test was performed. **p<0.01 VS age-matched ND mice. The number of samples per group is indicated in the figure.*

3.4.1.4.2 Insulin-stimulated glucose uptake - GLUT-4

Gene expression

The expression changes in *GLUT-4* gene were not statistically different between the ND and *db/db* mice at 8- to 32-weeks of age (Figure 3.10A).

Protein expression

The polyclonal anti-GLUT-4 antibody detected multiple bands on the blot (Appendix 2, Figure S2.5). As the predicted molecular weight is 55 kDa, I identified the band that was closest to 50 kDa as GLUT-4-positive.

GLUT-4 protein expression was significantly increased in the *db/db* mice at 8-weeks of age (Figure 3.10B). At 12- and 16-weeks of age, the expression was not statistically different between the ND and *db/db* mice. However, GLUT-4 expression was significantly decreased in the *db/db* mice at 20-weeks of age, indicating decreased insulin-stimulated glucose uptake. Interestingly, there was an increasing trend in GLUT-4 expression in the *db/db* mice at 24-weeks of age. Subsequently, the expression was significantly decreased in the *db/db* mice at 28- and 32-weeks of age, indicating a reduction in insulin-stimulated glucose uptake.

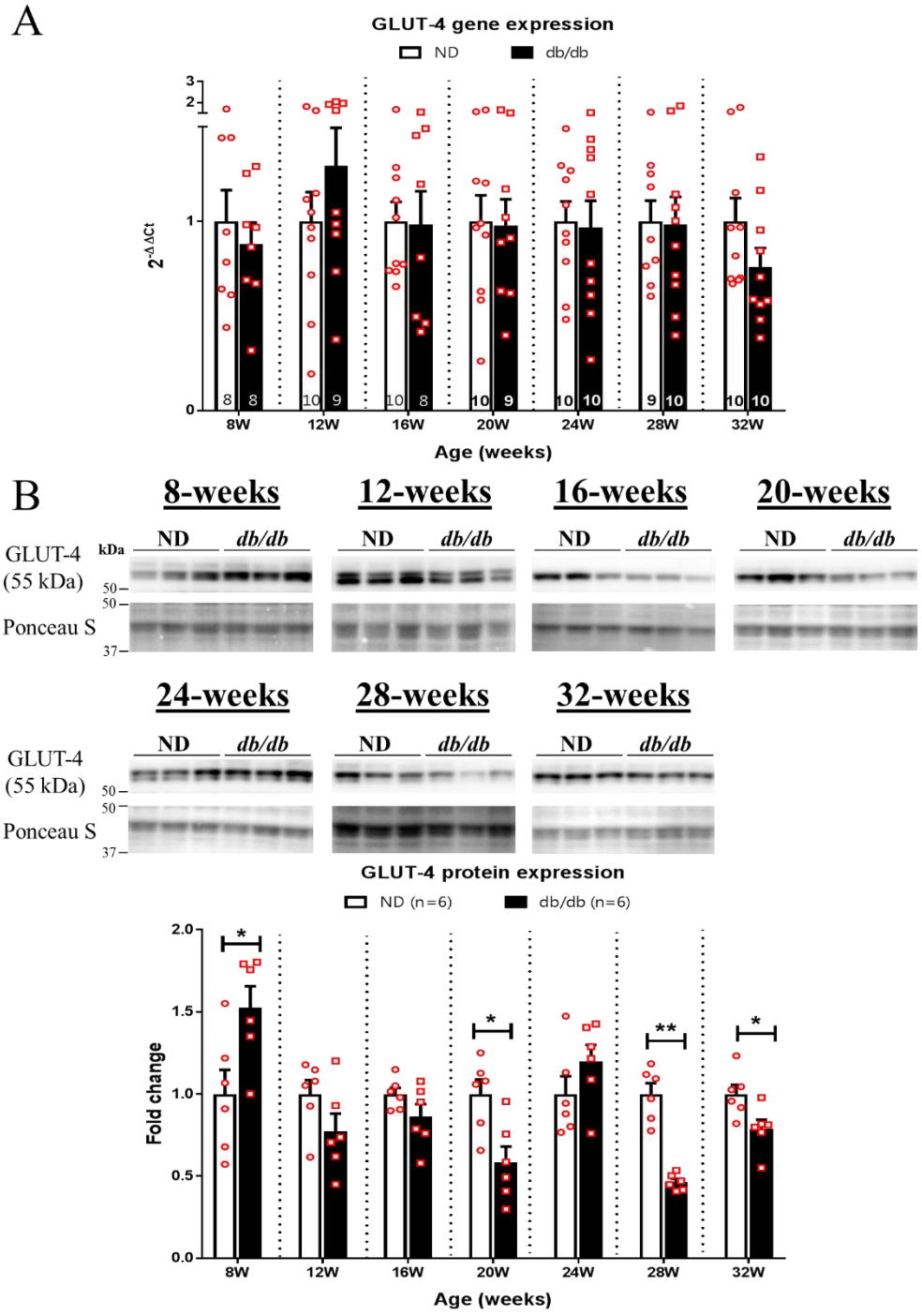

Figure 3.10 Altered GLUT-4 protein expression in the *db/db* mice at 8-, 20-, 28- and 32-weeks of age.

(A) *Quantitative bar graphs with scatter plot showing the gene expression of GLUT-4 in the ND and db/db mice at 8- to 32-weeks of age.* ***(B)*** *Representative blots and quantitative bar graphs with scatter plots showing the protein expression of GLUT-4 in the ND and db/db mice at 8- to 32-weeks of age. Data are presented as mean ± SEM. A non-parametric Mann-Whitney U test was performed. *p<0.05, **p<0.01 VS age-matched ND mice. The number of samples per group is indicated in the figure.*

In summary, the findings from this section show that GLUT-1 and GLUT-4 gene expression were not altered in the ventricles of *db/db* mice. However, GLUT-1 and GLUT-4 protein expression were altered in the ventricles of *db/db* mice.

3.4.2 Characterization of cardiac NNCS and glucose transporters in the ventricles of type-2 diabetic human patients

3.4.2.1 Clinical characteristic of type-2 diabetic human patients

Table 3.4 lists the metabolic, hemodynamic, cardiac function, and left ventricular (LV) structural profile of ND-CAD and D-CAD patients used in this study. D-CAD patients had increased BMI ($p=0.006$) and high level of glycated hemoglobin level ($HbA1_C$, $p>0.0001$) compared to ND-CAD patients. The functional profile based on LV end-diastolic volume (LVEDV), LV end-systolic volume (LVESV), heart rate (HR), stroke volume (SV), cardiac output (CO), the diastolic function (i.e. E/A ratio, E/e' ratio and deceleration time (decT)) and systolic function (i.e. ejection fraction and fractional shortening) were comparable between ND-CAD and D-CAD patients. Interestingly, the D-CAD patients exhibited diabetes-induced ventricular remodeling, as evidenced by significantly increased LV internal diameter at diastole (LVIDd, $p=0.006$). It is noteworthy that most of the patients in this study were treated with statins, beta-blockers, ACE inhibitors, calcium channel blockers. Additionally, D-CAD patients were treated with anti-diabetic agents such as metformin to control the blood glucose level.

Table 3.4 Patient characteristic

	ND-CAD (n=21)	D-CAD (n=16)	p-value
Age (year)	71.2 ± 1.6	70.7 ± 2.1	0.8
Gender (male/female)	15/6	12/4	
Metabolic profile			
BMI (kg/m^2)	28.0 ± 0.9	33.2 ± 1.7	<0.01**
Diabetic duration (years)	-	12.2 ± 1.5	
HbA1$_C$ (mmol/mol)	38.1 ± 0.7	55.1 ± 2.7	<0.0001*****
Hemodynamic profile			
LVEDV (mL)	91.3 ± 7.3	107.9 ± 10.6	0.22
LVESV (mL)	41.1 ± 4.7	49.2 ± 4.2	0.3
HR (beats/min)	69.7 ± 2.3	68.1 ± 2.3	0.63
SV (mL)	50.2 ± 3.4	58.7 ± 7.8	0.25
CO (L/min)	3.5 ± 0.2	3.9 ± 0.5	0.35
Diastolic profile			
E/A	1.0 ± 0.1	0.8 ± 0.1	0.43
E/e'	11.8 ± 0.9	12.2 ± 1.8	0.84
decT (msec)	251.1 ± 13.4	273.3 ± 22.8	0.38
Systolic profile			
Ejection fraction (%)	56.4 ± 2.1	51.1 ± 2.0	0.08
Fractional shortening (%)	32.9 ± 1.8	32.4 ± 2.1	0.86
Ventricular structure			
IVSd (cm)	1.2 ± 0.1	1.3 ± 0.1	0.44
LVPWd (cm)	1.0 ± 0.05	1.0 ± 0.1	0.92
LVIDd (cm)	4.2 ± 0.1	4.9 ± 0.2	<0.001**
LVIDs (cm)	2.9 ± 0.1	3.3 ± 0.2	0.059
Medications			
Statins	15/21 (71%)	15/16 (94%)	
Beta-blockers	17/21 (81%)	14/16 (88%)	
ACE inhibitors	11/21 (52%)	13/16 (81%)	
Calcium channel blocker	5/21 (24%)	9/16 (56%)	
Anti-diabetic agents	0/21 (0%)	11/16 (69%)	

*BMI, Body mass index; HbAI$_C$, Glycated hemoglobin; LVEDV, Left ventricular end-diastolic volume; LVESV, Left ventricular end-systolic volume; HR, Heart rate; SV, Stroke volume; CO, Cardiac output; E, Early ventricular filling velocity; A, Late ventricular filling velocity; e', Early ventricular myocardium relaxation velocity; decT, Early ventricular deceleration time; IVSd, Interventricular septal diameter diastole; LVPWd, Left ventricular posterior wall thickness at diastole; LVIDd, Left ventricular internal diameter at diastole; LVIDs, Left ventricular internal diameter at systole. Unpaired T-test was performed. **p<0.01; *****p<0.00001 VS ND-CAD patients.*

3.4.2.2 Cardiac NNCS in the ventricles of type-2 diabetic human patients

Having confirmed that the cardiac NNCS was altered in the type-2 diabetic *db/db* mice, the next aim was to assess the protein expression of ChAT, CHT1, VAChT, AChE, and M_2AChR in the type-2 diabetic human LV tissues by western blot analysis. *Note: I used the same antibodies to*

detect these targets in human LV tissues and the specificity of these antibodies and the reason to quantify multiple bands (i.e. ChAT and CHT1) have been discussed in previous section.

3.4.2.2.1 ACh synthesis - ChAT

There was a decreasing trend in ChAT protein expression (p=0.058) in D-CAD patients. However, it was not statistically significant (Figure 3.11).

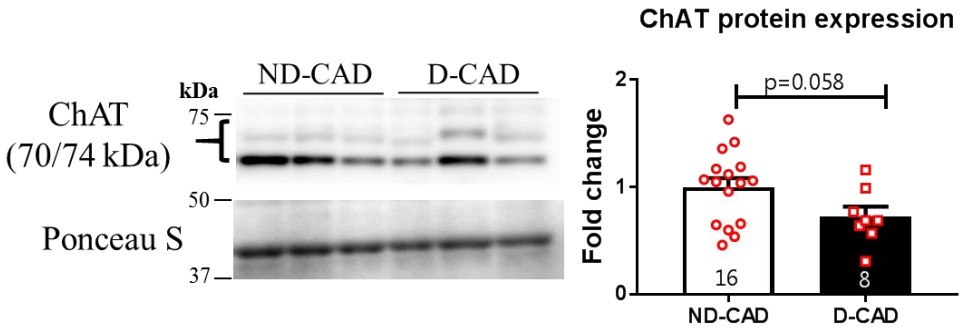

Figure 3.11 Unaltered ChAT protein expression in the LV tissues of D-CAD patients.
Representative blots and quantitative bar graphs with scatter plots showing the protein expression of ChAT. Data are presented as mean ± SEM. Unpaired T-test was performed. The number of samples per group is indicated in the figure.

3.4.2.2.2 Reuptake of choline for ACh synthesis - CHT1

CHT1 protein expression was significantly decreased in D-CAD patients (Figure 3.12). This result suggests a reduction in reuptake of choline for ACh synthesis. Hence the ACh bioavailability was reduced.

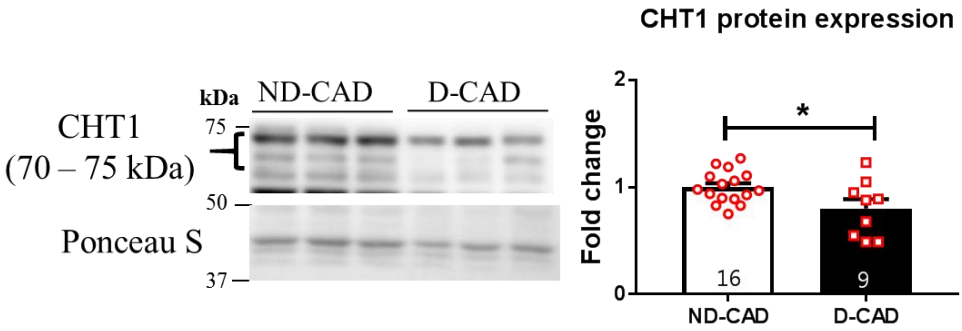

Figure 3.12 Decreased CHT1 protein expression in the LV tissues of D-CAD patients.
*Representative blots and quantitative bar graphs with scatter plots showing the protein expression of CHT1. Data are presented as mean ± SEM. Unpaired T-test was performed. *p<0.05 VS ND-CAD patients. The number of samples per group is indicated in the figure.*

3.4.2.2.3 ACh release - VAChT

The VAChT protein expression was not altered in the D-CAD patients in comparison to the ND-CAD patients (Figure 3.13).

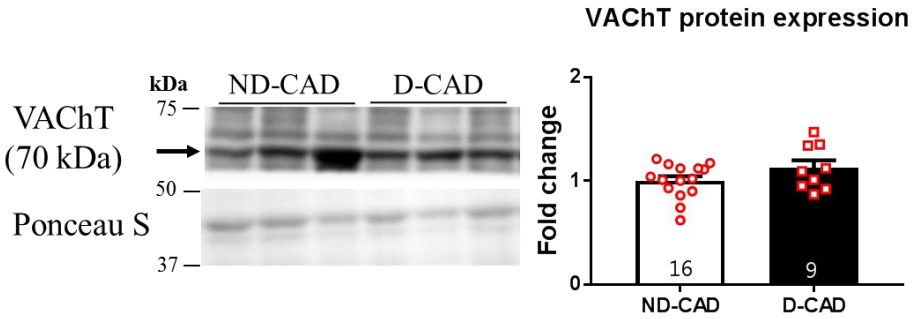

Figure 3.13 Unaltered VAChT protein expression in the LV tissues of D-CAD patients.
Representative blots and quantitative bar graphs with scatter plots showing the protein expression of VAChT. Data are presented as mean ± SEM. Unpaired T-test was performed. The number of samples per group is indicated in the figure.

3.4.2.2.4 ACh degradation - AChE

The AChE protein expression was not altered in the D-CAD patients in comparison to the ND-CAD patients (Figure 3.14).

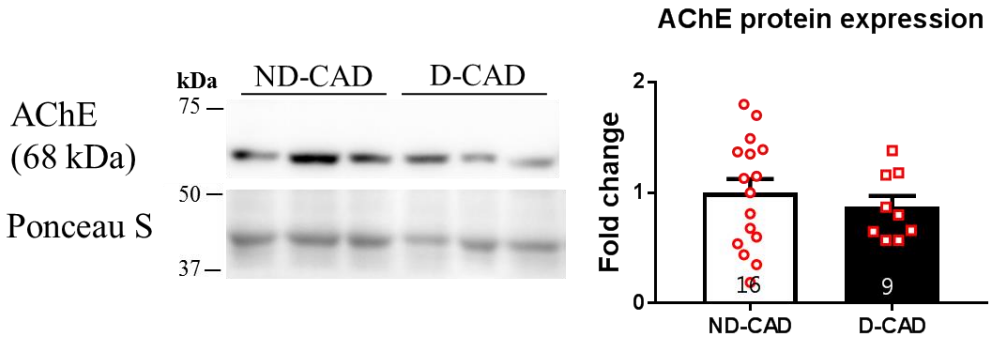

Figure 3.14 Unaltered AChE protein expression in the LV tissues of D-CAD patients.
Representative blots and quantitative bar graphs with scatter plots showing the protein expression of AChE. Data are presented as mean ± SEM. Unpaired T-test was performed. The number of samples per group is indicated in the figure.

3.4.2.2.5 ACh binding receptor - M_2AChR

The M_2AChR protein expression was not altered in the D-CAD patients in comparison to the ND-CAD patients (Figure 3.15).

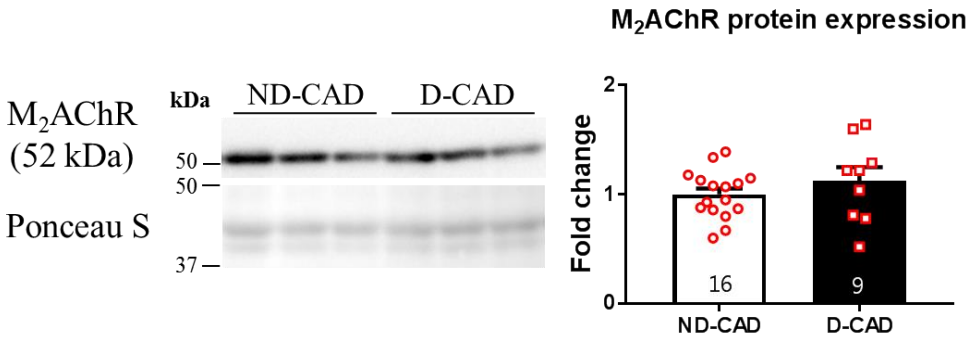

Figure 3.15 Unaltered M_2AChR protein expression in the LV tissues of D-CAD patients. *Representative blots and quantitative bar graphs with scatter plots showing the protein expression of M_2AChR. Data are presented as mean ± SEM. Unpaired T-test was performed. The number of samples per group is indicated in the figure.*

In summary, the findings from this section show that CHT1 protein expression was decreased in the D-CAD human LV tissues, while the protein expression changes in ChAT, VAChT, AChE, and M_2AChR were not statistically different.

3.4.2.3 GLUTs in the ventricles of type-2 diabetic human patients

Having confirmed that GLUT-1 and GLUT-4 protein expression were decreased in the *db/db* mice, the next aim was to examine the protein expression of these GLUTs in the ventricles of diabetic human patients by western blot analysis. *Note: I used the same antibodies to detect these targets in human LV tissues and the specificity of these antibodies have been discussed in previous section*

3.4.2.3.1 Basal glucose uptake - GLUT-1

The GLUT-1 protein expression was not altered in the D-CAD patients in comparison to the ND-CAD patients (Figure 3.16).

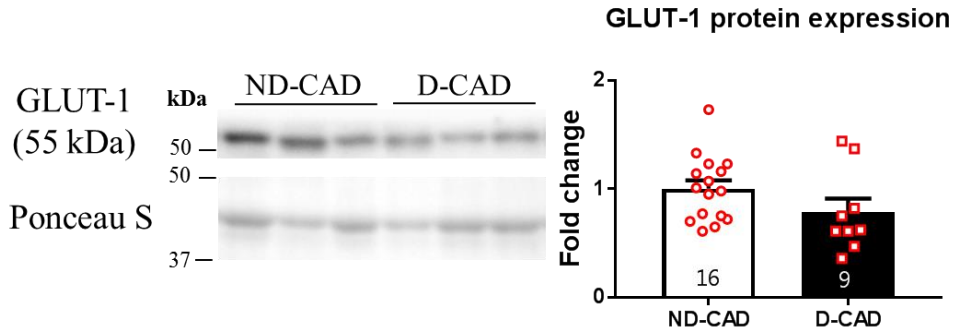

Figure 3.16 Unaltered GLUT-1 protein expression in the LV tissues of D-CAD patients.
Representative blots and quantitative bar graphs with scatter plots showing the protein expression of GLUT-1. Data are presented as mean ± SEM. Unpaired T-test was performed. The number of samples per group is indicated in the figure.

3.4.2.3.2 Insulin-stimulated glucose uptake - GLUT-4

The GLUT-4 protein expression was significantly decreased in the D-CAD patients, suggesting a reduction in insulin-stimulated glucose uptake (Figure 3.17).

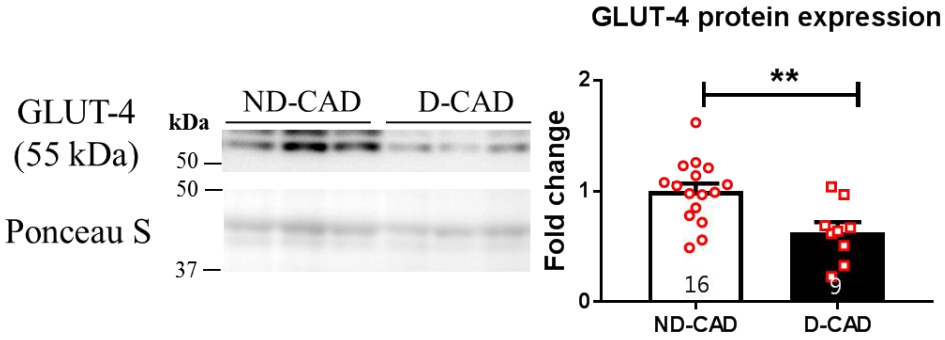

Figure 3.17 Decreased GLUT-4 protein expression in the LV tissues of D-CAD patients.
*Representative blots and quantitative bar graphs with scatter plots showing the protein expression of GLUT-4. Data are presented as mean ± SEM. Unpaired T-test was performed. **p<0.01 VS ND-CAD patients. The number of samples per group is indicated in the figure.*

In summary, the findings from this section show that GLUT-4 protein expression, but not GLUT-1, was decreased in D-CAD patients.

3.5 Discussion

In this chapter, the expression changes in the components of cardiac NNCS (i.e., ChAT, CHT1, VAChT, AChE, and M_2AChR), GLUT-1 and GLUT-4 were examined in the mouse model for type-2 diabetes represented by the *db/db* mouse. A recent publication from Katare laboratory showed that these *db/db* mice developed cardiac structural remodeling accompanied with activation of fetal genes, diastolic dysfunction, and systolic dysfunction at 16-, 20- and 28-weeks of age, respectively [1]. In another part of the study, human LV tissues from diabetic patients were investigated. The cardiac function and LV structural parameters measured by echocardiography were obtained from HeartOtago. One key reason of using both *db/db* mice and human LV tissues in this study is that the *db/db* mice of different ages allowed me to examine the expression changes in the components of cardiac NNCS over the progression of T2DM, which is not feasible in a human study. The young *db/db* mice (8- to 12-weeks of age) could represent the individuals with asymptomatic diabetes and remains undiagnosed for years, while the *db/db* mice at 16- to 24-weeks of age could represent the diabetic individuals with clinical symptoms such as marked hyperglycemia, polyuria, polydipsia, weight loss and potential complications such as diastolic dysfunction and diabetic cardiomyopathy [192]. Lastly, the *db/db* mice at 28- to 32-weeks of age could represent the diabetic individuals with end-stage complications such as heart failure (reviewed in [193]). However, the development of end-stage complications is often delayed/prevented in most of the diabetic individuals due to anti-diabetic therapy such as metformin (reviewed in [194]).

I hypothesized that cardiac NNCS, particularly *(1)* ChAT, CHT1, VAChT, and M_2AChR expression would be decreased while *(2)* AChE expression would be increased; as well as *(4)* GLUT-1 and GLUT-4 expressions would be reduced in the ventricles of both diabetic mouse and human patients. Apart from this, I hypothesized that dysregulation of cardiac NNCS would precede the decrease in GLUT-4 expression in the ventricles of *db/db* mice. The main findings of this study are summarized as follows and Table 3.5:

1. ***db/db* mice:**

- Cardiac function profile:
    - Diastolic and systolic dysfunction was remarkably evident at 20- and 28-weeks of age, respectively
- Gene expression:
    - Cardiac NNCS:
        - *At 16-weeks of age, CHT1 expression was increased*
        - *At 24-weeks of age, CHT1 expression was decrased*
        - *At 28-weeks of age, VAChT expression was increased*
        - *At 32-weeks of age, CHT1 expression was increased*
    - GLUTs:
        - *No changes in GLUT-1 and GLUT-4*
- Protein expression:
    - Cardiac NNCS:
        - *At 8-weeks of age, AChE expression was increased while M_2AChR expression was decreased*
        - *At 12- and 16-weeks of age, M_2AChR expression was decreased*
        - *At 20-weeks of age, AChE and M_2AChR expression were decreased*
        - *At 24-weeks of age, CHT1 and VAChT expression were increased while M_2AChR expression was decreased*
        - *At 28-weeks of age, ChAT, AChE and M_2AChR expression were decreased while VAChT expression was increased*
        - *At 32-weeks of age, VAChT, AChE and M_2AChR expression were decreased*
    - GLUTs:

- *At 8-weeks of age, GLUT-4 expression was increased*
- *At 16-weeks of age, GLUT-1 expression was decreased*
- *At 20-weeks of age, GLUT-1 and GLUT-4 expression were decreased*
- *At 24-weeks of age, GLUT-1 expression was decreased*
- *At 28- and 32-weeks of age, GLUT-1 and GLUT-4 expression were decreased*

2. **Diabetic human patients:**

- Significant increase in BMI and $HbA1_C$ level
- No sigificant changes in cardiac function
- LV remodelling was evident by increased LVIDd
- CHT1 expression was decreased
- GLUT-4 expression was decreased

The findings from gene and protein expression are not well correlated (e.g. Table 3.5: CHT1 expression at 24-weeks of age; or increased CHT1 gene expression but no change in protein expression at 16-weeks of age), suggesting that regulation of gene and protein expression of cardiac NNCS and GLUTs could be independent in the ventricles of diabetic heart. Another possible reason could be because of the different region of ventricles used for RT-qPCR and western blot analysis (Section 2.2.1, Figure 2.2). However, the underlying reason for this is not exactly clear. Considering that ACh released from cholinergic neurons can stimulate the cholinergic machinery in the cardiomyocytes [96], the presence and extend of cholinergic innervation in the epicardium and endocardium of ventricles could contribute to the difference in expression changes of RNA and protein [195-201]. In line with this, previous study showed that the thickness of epicardial AChE-positive nerves (i.e. parasympathetic nerves) decreases from base to apex of the ventricles [195]. Therefore, further investigation is required to

thoroughly examine the correlationship between the changes in parasympathetic nerve thickness and expression of cardiac NNCS. Additionally, Rana et al. [108] showed that there is not difference in the gene and protein expression of ChAT, VAChT and CHT1 between the left and right ventricles, thus ruling out the possible contribution from the left and right ventricles. Nonetheless, due to the divergent expression changes between the gene and protein, the following discussions only focus on the findings from protein expressions.

Table 3.5 Summary of gene and protein expression changes in the components of cardiac NNCS and GLUTs in the ventricles of diabetic mouse and human patients.

T2DM progression in *db/db* mice	Metabolic derangements and insulin resistance		Cardiac remodeling [1]	Diastolic dysfunction [1]		Systolic dysfunction [1]		D-CAD patients
	8W	12W	16W	20W	24W	28W	32W	
Cardiac NNCS								
ChAT						⇩		
CHT1			⇧		⇩ ⇧		⇧	⇩
VAChT					⇧	⇧ ⇧	⇩	
AChE	⇧			⇩		⇩	⇩	
M_2AChR	⇩	⇩	⇩	⇩	⇩	⇩	⇩	
GLUTs								
GLUT-1			⇩	⇩	⇩	⇩	⇩	
GLUT-4	⇧			⇩		⇩	⇩	⇩

Red arrows indicate gene expression changes; Black arrows indicate protein expression change; No arrows indicate no change in gene or protein expression.

3.5.1 Dysregulation of cardiac NNCS expression in DM

As outlined in Chapter 1, altered cardiac metabolism is indicated by a reduction in glucose uptake and oxidation with a concomitant increase in FFA uptake and oxidation in the diabetic heart [20, 48-51, 65, 159]. Further, the reduction in glucose uptake is associated with decreased GLUT-4 expression in the diabetic heart [58, 61, 63, 153]. Besides, elevated FFA oxidation decreases cardiac efficiency (a ratio between cardiac work/MVO_2) and basal myocardial energy status, thus contributing to cardiac dysfunction in the diabetic heart [19-21, 65-68, 70-72]. Notably, Kakinuma et al. [100] demonstrated that increased ACh bioavailability through activation of cardiac NNCS promoted glucose metabolism by increasing GLUT-4 expression in the *ChAT-tg* mice. Importantly, the shift of fuel substrate to glucose increased ATP production, decreased oxygen consumption, and mitochondrial activity in the *in-vitro* and *in-vivo* model of cardiac NNCS [96, 100, 122].

In my study, the cardiac NNCS was dysregulated at 8- to 16-weeks of age, as evidenced by increased AChE expression (8-weeks of age; Figure 3.7B) and decreased M_2AChR expression (8- to 16-weeks of age; Figure 3.8B). Further, GLUT-4 expression was significantly reduced in the *db/db* mice at 20-weeks of age (Figure 3.10B). In addition, the *db/db* mice progressively developed diastolic and systolic dysfunction at 20- and 28-weeks of age, respectively [1]. In line with this, ChAT (Figure 3.11, p=0.058), CHT1 (Figure 3.12), GLUT-4 expression (Figure 3.17) were decreased in the D-CAD patients, suggesting that reduced ACh bioavailability from cardiac NNCS could be related to the reduction of GLUT-4 expression in the diabetic heart. However, the diastolic and systolic functions of D-CAD patients were not different from that of the ND-CAD patients, which may be due to the prescribed medications masking the effect of DM on cardiovascular function (Table 3.4). Also, the changes in the components of cardiac NNCS were different in diabetic human patients and *db/db* mice. This discrepancy could be species-specific, but the reduced ACh bioavailability could possibly be the common outcome in both the diabetic human patients and *db/db* mouse heart. Kakinuma et al. [100] has previously

demonstrated the causal relationship between cardiac NNCS and GLUT-4 and based on the expression profiles obtained from my study, it is logical to postulate that early dysregulation of cardiac NNCS, together with insulin resistance, could contribute to reduced GLUT-4 expression and glucose uptake in the diabetic heart.

Apart from this, the *db/db* mice used in my study displayed a significant increase in LV mass at 16-weeks of age (Figure 3.1;[1]). The hypertrophied heart of these *db/db* mice showed a significant decreased α-myosin heavy chain (α-MHC) and increased β-myosin heavy chain (β-MHC) expression, indicating the development of cardiac remodeling in the diabetic heart [1]. Further, the D-CAD patients showed increased LVIDd (Table 3.4), which is an indication of ventricular dilation [202]. Other parameters such as IVSd, LVPWd, and LVIDs were comparable between the ND-CAD and D-CAD patients. However, as the ND-CAD and D-CAD patients had already had coronary artery disease, the extent of the altered cardiac structure may be similar in both groups. Also, medications such as ACE inhibitors or beta-blockers that was prescribed to most of the patients could have prevented diabetes-induced cardiac remodeling [203, 204]. Thus, the diabetes-induced LV structural changes may not be obvious.

Although metabolic derangements and insulin resistance are the known contributing factors to cardiac remodeling in diabetes [171-174, 205, 206], the underlying mechanism of how diabetes leads to cardiac remodeling is yet to be elucidated. Previous studies showed that a reduction of ACh bioavailability through inactivation of cardiac NNCS resulted in hypersympathetic-induced cardiac hypertrophy and molecular remodeling (i.e., increased β-MHC expression) in the rodent models [97, 99, 101, 124]. Conversely, increased ACh bioavailability through activation of cardiac NNCS prevented cardiac hypertrophy induced by MI in the *ChAT-tg* mice [100], suggesting that cardiac NNCS plays a role in offsetting hypertrophic signals. Interestingly, in my study, dysregulation of cardiac NNCS (increased AChE and decreased M_2AChR expression at 8- to 16-weeks of age) preceded the LV hypertrophy and molecular remodeling in the *db/db* mice [1]. These findings possibly suggest that early alteration in cardiac

NNCS could contribute to the development of LV hypertrophy and remodeling in the diabetic heart. However, further investigation is certainly needed to examine the role of cardiac NNCS in cardiac remodeling in the diabetic heart.

3.5.2 The compensatory effect of cardiac NNCS in the diabetic heart

In the diabetic *db/db* mice, decreased AChE expression (20-weeks of age; Figure 3.7B) and increased CHT1 and VAChT expression (24-weeks of age; Figure 3.5B and 3.6B) coincided with diastolic dysfunction [1]. Although M_2AChR expression remained decreased at 20- and 24-weeks of age (Figure 3.8B), the modulation of AChE, CHT1, and VAChT expression was likely able to boost the ACh bioavailability collectively. These changes would, in turn, activate M_2AChR-mediated signaling and result in non-neuronal effects (i.e., increased ChAT expression for ACh synthesis and PI3K/Akt/HIF1α pathway for survival) to compensate the diabetic heart with diastolic dysfunction.

The non-neuronal effects were observed in the *db/db* mice at 24-weeks of age. The effect was evidenced by an increasing trend in the ChAT (Figure 3.4B) and GLUT-4 expression (Figure 3.10B). In line with this, Kakinuma et al. [100] showed that overexpression of the *ChAT* gene in the ventricles increased ACh bioavailability and in turn, shifted the cardiac metabolism to glucose-dependent by increasing GLUT-4 expression. Thus, this suggests that the diabetic cardiomyocytes modulated cardiac NNCS, possibly to increase ACh bioavailability, which in turn promoted glucose uptake and oxidation for ATP production to sustain the contractile function. However, the measurement of cardiac ACh, glucose, and ATP content is undoubtedly required to confirm this postulation. Additionally, these findings also suggest that cardiac NNCS-mediated signaling remained intact and functional in the diabetic heart.

Apart from this, such compensatory effect through increasing ACh bioavailability has been reported previously [101, 207]. Roy et al. [101] showed that cardiac VAChT expression was significantly increased in HF patients with non-ischemic dilated cardiomyopathy. Further,

Kanazawa et al. [207] showed that cardiac sympathetic neurons transdifferentiated into cholinergic neurons in the LV of chronic HF patients and rat model. The cholinergic transdifferentiation suggests a compensatory mechanism to enhance ACh bioavailability in the failing heart. Thus, these findings underscore the vital role of ACh in the diseased heart. Modulation of cardiac NNCS is one of the mechanisms to increase the ACh bioavailability in the heart.

Importantly, the compensatory effect of cardiac NNCS is likely to be transient in the diabetic heart. The decline in cardiac NNCS machinery was evidenced by decreased ChAT expression in parallel with decreased AChE and increased VAChT expression in the *db/db* mice at 28-weeks of age. Further, decreased VAChT and AChE expression was observed in the *db/db* mice at 32-weeks of age. Gavioli et al. [124] showed that cardiomyocytes decreased ChAT, VAChT, and M_2AChR gene expression after subjecting to AChE inhibitor to increase ACh content. Thus, it is logical to postulate that the diabetic cardiomyocytes decreased ChAT and VAChT expression to prevent excessive ACh production, thus maintaining ACh homeostasis. Figure 3.18 summarizes the expression changes of ChAT, CHT1, VAChT, and AChE that are involved in ACh bioavailability in the *db/db* mice at 8- to 32-weeks of age.

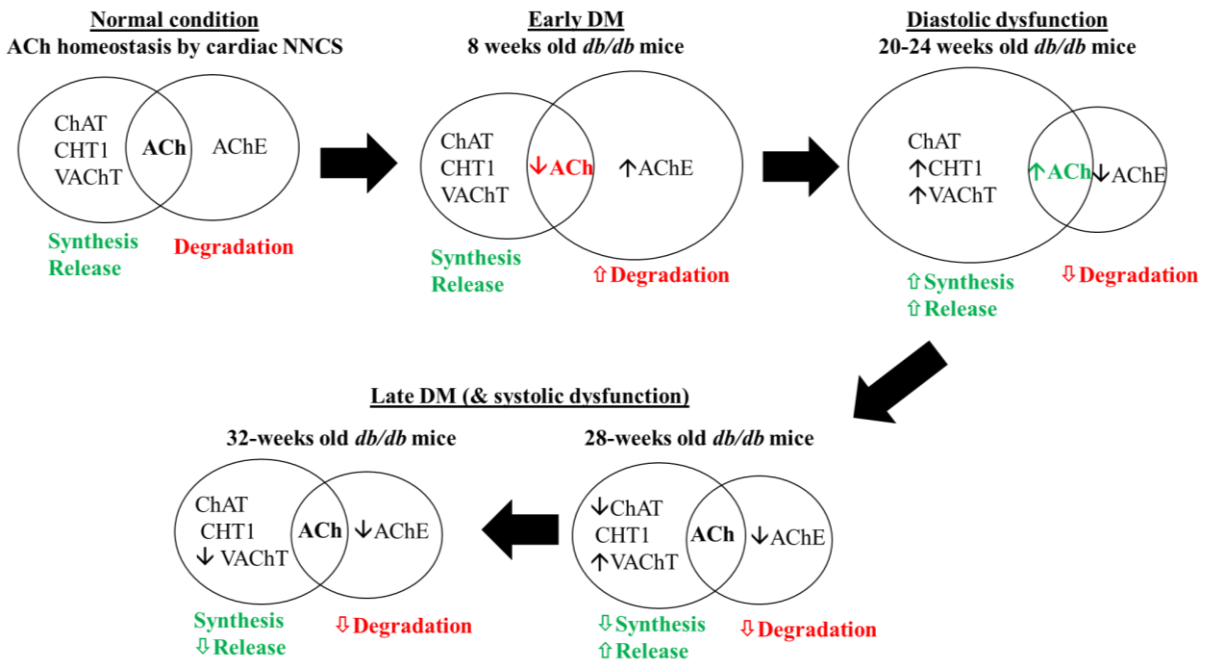

Figure 3.18 Summary of expression changes in the components of cardiac NNCS that are associated with the ACh bioavailability in the *db/db* mice.
The cardiomyocytes can synthesize, release, and degrade ACh. In early DM, the AChE expression was increased. In response to diastolic dysfunction, CHT1 and VAChT expression were increased to enrich the diabetic heart with ACh for protective effects. In late DM, the diabetic cardiomyocytes decreased ChAT and VAChT expression to reduce ACh bioavailability to maintain ACh homeostasis while AChE expression remained decreased.

Although the advantage of using *db/db* mice of different ages allowed me to examine the temporal expression changes in the components of cardiac NNCS, the results require careful interpretation. As there was an interval of 4-weeks between the mice of different age group and it is also logical that protein expression would take less than 4-weeks to change in the cardiomyocytes [208], this raises the question that whether the temporal changes represent the genuine biological changes in the *db/db* mice. Thus, future study should consider examining the temporal expression changes in a shorter age interval (e.g. difference of 1-week) and this would better represent the biological changes in cardiac NNCS and allow precise data interpretation.

Besides, the underlying mechanism of such temporal expression changes in the diabetic *db/db* mouse heart is not entirely clear. Whether T2DM *per se* alters the expression of these component at different stages of disease or the expression changes in one component lead to the expression changes of other components, this requires further investigation. Since AChE expression was first increased in the *db/db* mice at 8-weeks of age (Figure 3.18), one possible experiment to clarify the effect of T2DM could be achieved by injecting the AChE inhibitor such as physostigmine to inhibit the activity of AChE. If such inhibition does not prevent the expression changes of other components in later time point, this suggests that T2DM alone possibly influences the different components of cardiac NNCS as the disease progresses.

On a side note, Oikawa et al. [209] reported that cardiac NNCS possess a circadian rhythm that is similar to the neuronal cholinergic system (i.e. increased ChAT expression and ACh concentration when neuronal cholinergic system is predominant during light-off periods in

mice). However, the *db/db* mice and the age-matched ND mice were culled together between 3 pm to 4 pm (described in Section 2.2.1), hence, the influence of circadian rhythm in altering the expression of cardiac NNCS can be ruled out.

3.5.3 Altered glucose transporters expression in the diabetic heart

My findings showed a time-dependent increase and decrease in GLUTs in the diabetic mouse heart. The GLUT-4 expression was significantly increased in the *db/db* mice at 8-weeks of age (Figure 3.10B). Also, there was an increasing trend in GLUT-1 expression (not statistically significant, Figure 3.9B). Considering that glucose uptake and oxidation are reduced in the diabetic heart [20, 55, 210-214], the increase in GLUT-1 and GLUT-4 expression could be a compensatory effect to restore glucose uptake in the diabetic heart.

Progressively, GLUT-1 and GLUT-4 expression were significantly decreased in the *db/db* mice at 16- and 20-weeks of age, respectively, suggesting decreased basal and insulin-stimulated glucose uptake in the diabetic heart (Figure 3.9B and 3.10B). A reduction of GLUT-1 has previously been reported in a T1DM mouse model [215], while my study showed the reduction of GLUT-1 expression in a T2DM mouse model. However, GLUT-1 expression did not change in the diabetic human heart (Figure 3.16). Thus, whether GLUT-1 plays a role in the pathophysiology of T2DM is yet to be elucidated. Besides, previous studies showed that GLUT-4 expression was decreased in the diabetic animal models [20, 58, 63, 153] and diabetic human [61]. These are in agreement with my study that GLUT-4 expression was indeed decreased in the diabetic *db/db* mouse and the diabetic human heart.

Although the cardiac glucose content and glucose oxidation were not measured in this study, the reduction in GLUT-1 and GLUT-4 expression is likely to reduce glucose uptake and oxidation [20, 48, 59, 61, 154, 159]. Notably, GLUT-4 expression was normalized in the *db/db* mice at 24-weeks of age (Figure 3.10B). This normalization could be a compensatory effect

induced by cardiac NNCS to protect the diabetic heart (as discussed in Section 3.5.2; Figure 3.19).

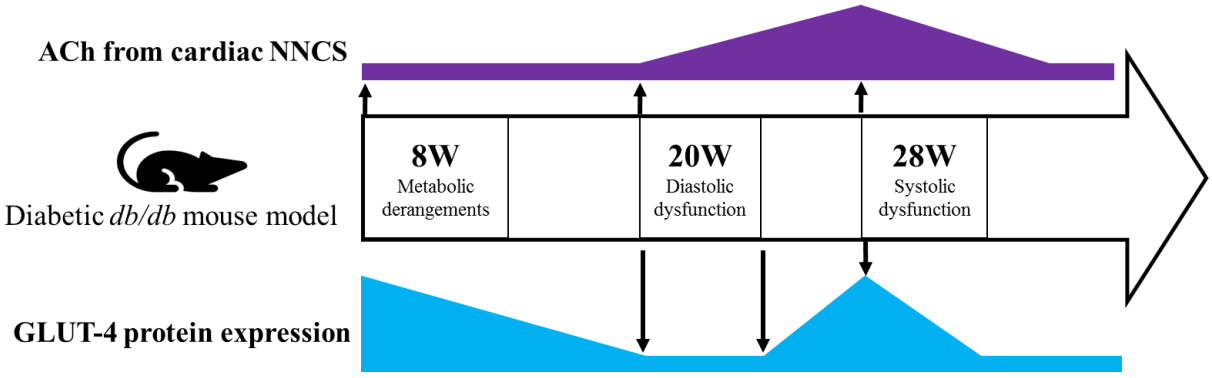

Figure 3.19 The association of cardiac NNCS with GLUT-4 expression in the diabetic heart. *The cardiac NNCS activity was decreased in the db/db mice at 8- to 16-weeks of age, while GLUT-4 expression was decreased at 20-weeks of age. The increase in cardiac NNCS activity started from 20-week of age while the rise in GLUT-4 protein expression was detected in 24-weeks of age. This may indicate a compensatory role of cardiac NNCS by promoting glucose metabolism through regulating GLUT-4 expression to protect the diabetic heart against diastolic dysfunction.*

3.6 Limitations

3.6.1 Assessing other possible components of cardiac NNCS

Although the cardiac cholinergic machinery has been completely established, it is still worthwhile to explore other proteins that could be involved in this machinery. Electrogenic cation transporters (OCTs) are engaged in ACh release in placental cells [216], urothelial cells [217], and airway epithelial cells [218]. However, OCTs have not been explored and studied in the cardiomyocytes. Similarly, AChE and butyrylcholinesterase (BChE) are reported to be complementary to each other (reviewed in [219]). Nonetheless, it would be interesting to investigate the presence and function of these proteins in cardiomyocytes. However, these are beyond the scope of my Ph.D. study, and it could be considered for future study.

3.6.2 Measurement of cardiac ACh level

Measurement of ACh level should have performed to support the western blot analysis of cardiac NNCS expression in the diabetic human patients and *db/db* mouse heart. However, the measure of ACh requires fresh myocardial tissues. Hence this was not possible in my study. This is because all the mouse and human ventricular tissues were previously snap-frozen and stored in the freezer.

3.6.3 Measurement of cardiac glucose level

Measurement of glucose level should have performed to support the western blot analysis of GLUT-1 and -4 in the diabetic mouse and human heart. However, due to limited availability of ventricular tissues, the tissues were prioritized for western blot analysis.

3.6.4 Aging effect in the diabetic *db/db* mouse model

To effectively compare the expression changes of cardiac NNCS and glucose transporters between *db/db* and age-matched ND mice, six protein samples isolated from ND and *db/db* mice of the same age group were loaded on the same gel and processed. By doing this, comparison of expression changes of the same protein target between different age groups had to be omitted as the experimental condition could vary from time to time. However, it is undeniable that aging is one of the factors that could alter the expression changes.

3.6.5 Assessing membrane GLUT-4 expression

The present study measured the total GLUT-4 expression (i.e. cytosolic and membrane GLUT-4) from the ventricular tissues of ND and *db/db* mice. The measurement of membrane GLUT-4 expression could have provided further insight on the function of GLUT-4 in transporting glucose in the cardiomyocytes. However, the separation of cytosolic and membrane protein was

not initially planned. Thus, this is one of the limitations of the study. Future study should carefully design the experimental layout considering this factor.

3.6.6 Specificity of antibodies

For immunofluorescence analysis, anti-ChAT and anti-CTNI antibodies were tested on positive and negative control, respectively. As GLUT-4 is commonly expressed even in the non-insulin sensitive tissues (e.g. liver and kidney), I was not able to identify an appropriate control to test the specificity of anti-GLUT-4 antibody. Also, due to limited resources and time, I was not able to test the antibody on purified antigen or obtain GLUT-4 knockout/overexpressing tissues/cells. However, the specificity of anti-GLUT-4 antibody has been validated by the manufacturer via biological strategy (i.e. positive and negative expressing cells; https://www.novusbio.com/products/glut4-antibody_nbp1-49533). Further, this particular antibody was also used in western blot analysis in Chapter 4 and Chapter 5, and the molecular weight of the GLUT-4 positive band was similar to predicted molecular weight. Particularly, in response to insulin stimulation in *in-vitro* model (Chapter 5), the intensity of the GLUT-4 positive band increased. Nevertheless, this is the limitation of the study. Future study should thoroughly examine the specificity of antibody and consider including absorption, positive and negative control to strengthen the outcome of the experimentation.

For western blot analysis, except anti-M_2AChR antibody, all the antibodies used for western blot analysis resulted in multiple bands on the full blot. I was able to identify the positive band(s) of ChAT, CHT1, VAChT and AChE based on the predicted molecular weight indicated by the respective manufacturer and UniProt as well as with the use of positive control such as mouse brain. There was no appropriate control to test anti-GLUT-1 and anti-GLUT-4 antibodies (same antibody used for immunofluorescence analysis) due to abovementioned reasons, thus, this is the limitation of the study. Future study should consider testing the antibody on purified antigen, overexpressing or knockout tissue/cells.

3.6.7 Different region of ventricular tissues used for qPCR and western blot analyses

As discussed earlier, the gene and protein expression changes of the components of cardiac NNCS and GLUTs were divergent. Whether T2DM regulates the gene and protein expression differently or the divergent results are caused by the different region of ventricular tissues, this is not clear. As the present study used different part of the ventricular tissues for qPCR and western blot analysis, this is one of the limitations of the study. Thus, future study should consider using the same part of tissues for examining the gene and protein expression.

3.6.8 Sample size

In the present study, I often observed an increasing or decreasing trend in protein expression, while these changes were not statistically significant. This could be due to the number of samples (i.e. 6 mice and 9-16 human LV tissues) was not powerful enough to detect the differences. For example, in order to detect the significant changes in ChAT expression in the *db/db* mice at 24-weeks of age (Figure 3.4) or diabetic patients (Figure 3.11), power analysis revealed that 14 mice per group and 24 human LV tissues per group are required (80% power), respectively (https://clincalc.com/stats/samplesize.aspx). Thus, future study should consider performing power analysis to determine the sample size required to detect significant expression changes.

3.7 Conclusion

In summary, the diabetic *db/db* heart exhibited decreased M_2AChR, GLUT-1, and -4 as well as increased AChE expression while the diabetic human heart exhibited decreased CHT1 and GLUT-4 protein expression. Thus, I partially confirm the hypothesis that cardiac NNCS and GLUTs were dysregulated in the diabetic *db/db* and the human heart. The changes in cardiac

NNCS (i.e., increased AChE and decreased M_2AChR expression) occurred in the *db/db* mice at 8- to 16-weeks of age, before the decrease in GLUT-4 expression at 20-weeks of age. Thus, I confirm the second hypothesis that dysregulation of cardiac NNCS would precede the decrease in GLUT-4 expression in the diabetic *db/db* heart. Therefore, this suggests that changes in cardiac NNCS, together with insulin resistance, contribute to decreased GLUT-4 expression in the diabetic heart. On the other hand, this study also provides evidence that cardiac NNCS exerted a compensatory effect against diastolic dysfunction in the *db/db* mice. This effect was evident by normalized ChAT and GLUT-4 expression at 24-weeks of age after an increase in cardiac NNCS activity (i.e., CHT1 and VAChT expression) at 20- and 24-weeks of age, suggesting an attempt to utilize glucose for ATP production in response to diastolic dysfunction (Figure 3.18).

The overall findings from this chapter suggest the potential for modulating cardiac NNCS as a therapeutic intervention to rectify cardiac metabolism and, hence preventing cardiac dysfunction. Thus, the next step is to demonstrate the effect of activating cardiac NNCS using an *in-vivo* model (Chapter 4). Activation of cardiac NNCS can be directly achieved by overexpressing *ChAT* gene, thereby increasing the ACh synthesis. The *in-vivo* study will provide evidence that cardiac NNCS prevents cardiovascular dysfunction and examine the underlying mechanism for the protective effect.

Chapter 4 : The effect of cardiac NNCS activation on cardiovascular function in the diabetic *db/db* mice

4.1 Introduction

The findings from Chapter 3 showed that the expression of the components of cardiac NNCS (i.e., ChAT, CHT1, VAChT, AChE, and M_2AChR) and GLUT-4 were dysregulated in the diabetic mouse and human heart. Further, the early dysregulation of cardiac NNCS preceded the decreased GLUT-4 expression in the diabetic *db/db* heart. These findings suggest that altered cardiac NNCS could be an additional mechanism to reduce GLUT-4 expression in T2DM. Thus, it may be possible that restoration of cardiac NNCS by increasing ACh synthesis or release could normalize the GLUT-4 expression in the diabetic heart. Therefore, in this chapter, I investigated if overexpression of the *ChAT* gene has beneficial effects on the cardiovascular function of the diabetic heart.

4.1.1 Inactivation of 5'-AMP-activated protein kinase (AMPK) in the diabetic heart

Flexibility in fuel substrate selection is essential for the heart to sustain ATP production and contractile function. This process is tightly regulated by 5'-AMP-activated protein kinase (AMPK), which is the energy sensor in the cardiomyocytes (reviewed in [220, 221]). AMPK is inactivated when the AMP/ATP ratio is low while it is activated when the AMP/ATP ratio is high [222]. Activation of the AMPK signaling cascade leads to the ATP-generating process by promoting FFA β-oxidation [223], glucose uptake [224], and glycolysis [225].

Apart from impaired insulin-stimulated glucose uptake [48, 61, 62, 154], AMPK inactivation is related to decreased glucose utilization in the diabetic heart [226, 227]. Viollet et al. [226] showed that genetic ablation of AMPKα2-catalytic subunit resulted in insulin resistance,

reduced insulin-stimulated glucose utilization, and increased circulating FFA in a mouse model [226]. Further, AMPK activators such as pterostilbene [228], metformin [229], and trimetazidine [227] have been shown to preserve the contractile function of the diabetic heart by activating AMPK signaling. Thus, these studies suggest the critical role of AMPK in regulating glucose metabolism in the diabetic heart.

4.1.2 Impaired coronary vascular function in the diabetic heart

Diabetic individuals present chest pain due to obstructive CAD [230] or CMVD without the presence of atherosclerotic plaques [231]. Such conditions are caused by endothelial dysfunction and atherosclerosis that impairs the function of epicardial coronary arteries and microvessels, restricting the blood delivery to the myocardium and myocardial perfusion, respectively [16, 232-236]. In this case, the availability of oxygen molecules for FFA oxidation is reduced, thereby halting ATP production and affecting the contractile function of the diabetic heart [21].

The underlying mechanism for endothelial dysfunction is multifactorial but remains unresolved. It has been demonstrated that increased reactive oxygen species (ROS) as a result of hyperglycemia or reduced nitric oxide (NO) bioavailability affects the endothelial function in diabetes [237-240]. Besides, the crosstalk between cardiomyocytes and endothelial cells mediated by paracrine factors is affected by diabetes. The cardiac-derived pro-angiogenic VEGF-A protein expression was found to be decreased in the diabetic human and diabetic *db/db* mouse model [137]. In line with this, Giordano et al. [241] demonstrated dilated and thin ventricular walls, hypovascularity, and contractile dysfunction in the mice with cardiac-specific knockout of VEGF-A protein. This evidence suggests that VEGF-A is crucial in maintaining vasculature in the diabetic heart.

4.1.3 Targeting cardiac NNCS in the diabetic heart

4.1.3.1 Glucose metabolism

Previous studies showed that rectification of cardiac metabolism by increasing GLUT-4 expression prevented the development of cardiac dysfunction in diabetic animal models [20, 69]. The findings from Chapter 3 suggests that dysregulation of cardiac NNCS could contribute to the decreased GLUT-4 expression in the diabetic heart. In this case, activation of cardiac NNCS to increase ACh bioavailability could be an approach to normalize GLUT-4 expression. The underlying mechanisms to increase GLUT-4 expression requires the ACh released from the cardiomyocytes to bind to the mAChR and mediate pro-survival PI3K/Akt/HIF1α signaling cascade [100, 120, 125]. Initiation of this signaling cascade increases the availability of HIF1α and allows it to dimerize with HIF1β to form HIF1 transcription factor [120]. HIF1 activates the transcription of *GLUT-4* gene, which subsequently increases GLUT-4 protein expression.

4.1.3.2 Angiogenesis

Kakinuma et al. [100] showed that activation of cardiac NNCS increased the number of endothelial cells in the *ChAT-tg* mice. These endothelial cells are either from the capillaries or arterioles, which suggest that the density of these microvessels was increased in the ventricular region [100]. Although the angiogenic factor was not identified in this study [100], VEGF-A could be related to this angiogenic effect since *VEGF-A* gene is a direct downstream target of HIF1 transcription factor (reviewed in [127]). The previous study from Katare laboratory showed that microvascular rarefaction, which was associated with decreased VEGF expression, was observed in the diabetic human and *db/db* mouse heart [137]. Interestingly, alteration of cardiac NNCS (8- to 16-weeks of age; from Chapter 3) preceded the decrease in VEGF expression (12-weeks of age) and microvascular rarefaction (20-weeks of age) in the *db/db* mice [137]. This result suggests that targeting cardiac NNCS could be an attractive approach to prevent vascular rarefaction in the diabetic heart. Such prevention could preserve coronary

artery blood flow and oxygen perfusion, in return, prevent contractile dysfunction of the diabetic heart.

4.2 Study aim

This chapter aims to determine the effect of overexpression of the *ChAT* gene on the cardiovascular function of the diabetic heart. Therefore, I hypothesized that ventricular-specific overexpression of *ChAT* gene would lead to activation of PI3K/Akt/HIF1α/GLUT-4 signaling pathway to promote glucose metabolism, thus improving cardiac function of the diabetic heart. Also, I hypothesized that overexpression of *ChAT* gene would in turn increase VEGF-A expression and promote angiogenesis, thus improving vascular function and in turn, enhance the cardiac function of the diabetic heart.

4.3 Materials and methods

This section only outlines the specific reagents, concentration, and conditions used for each of the general methodology as well as the specific methods applied to the study in this chapter (i.e., Section 4.3.2 - 4.3.4). Detailed experimental procedures for general methods are described in 'Chapter 2: General materials and methods'.

4.3.1 Type-2 diabetic *db/db* mouse with ventricular-specific overexpression of *ChAT* gene

Type-2 diabetic *db/db* mice with ventricular-specific overexpression of the *ChAT* gene (*db/db-ChAT-tg*) were used in this study to investigate the effect of cardiac NNCS activation on the diabetic heart. The body weight, blood glucose level, and LV function of *db/db* and *db/db-ChAT-tg* mice at 8-, 12-, 16- and 20-weeks of age were measured by Prof. Yoshihiko Kakinuma in Japan. The ventricular tissues were collected by Prof. Yoshihiko Kakinuma as described in

Chapter 2 (Figure 2.2). The lower part of the ventricular tissues were used for western blot analysis (i.e., ChAT, M_2AChR, Akt, HIF1α, GLUT-4, and AMPKα). The wild type non-diabetic (ND) mice were included for western blot analysis to allow comparison with *db/db* and *db/db-ChAT-tg* mice.

The assessment of *in-vivo* coronary vascular function was performed on *db/db* and *db/db-ChAT-tg* mice at 12- and 24-weeks of age in Super Photon ring-8 GeV (SPring-8) facility, Japan. The mice at 24-weeks of age were used in my study because a recent publication from Katare laboratory showed that the *db/db* mice exhibited vascular dysfunction and rarefaction at this age [16]. The 12-weeks old mice served as control as these mice had not developed cardiac and vascular dysfunction at this age. After Synchrotron radiation microangiography, the ventricular tissues were collected as described in Chapter 2 (Figure 2.2). The upper part of the ventricular tissues were used to assess the density of arterioles and capillaries in *ex-vivo* while the lower part of the ventricular tissues were used for western blot analysis (i.e., ChAT and VEGF-A). These mice, especially the 24-weeks old mice, were prepared for the experiments in SPring-8 facility, hence, the measurement of body weight, blood glucose level, and LV function were not possible to be performed in the facility. Although the lower part of ventricular tissues were collected for western blot analysis, the measurement of M_2AChR, Akt, HIF1α, GLUT-4, and AMPKα protein expression was not performed as there was no age-matched ND mice available for comparison.

4.3.2 Synchrotron radiation coronary microangiography

Synchrotron radiation microangiography was performed to evaluate the potential angiogenic effect of cardiac NNCS in the type-2 diabetic *db/db* mice. This method allows one to visualize the coronary circulation *in-vivo* and to assess vascular responsiveness. This experiment was performed in the SPring-8 facility, BL28B2 beamline, Hyogo, Japan, using established

protocols from the Katare laboratory [16]. The study was blinded to me by generating a unique ID to each mouse to avoid bias on sample type during the analysis.

4.3.2.1 Catheterization of the jugular vein and carotid artery

For this approach, *db/db-ChAT-tg* and *db/db* mice at the age of 12- and 24-weeks were used. Following anesthesia using isoflurane/oxygen (1.5-5%/1 L.min^{-1}), the mouse was positioned on a heating pad to maintain its body temperature at 37°C. The trachea was cannulated to ventilate the mouse mechanically. The jugular vein was cannulated with PE20 catheter for administration of fluid or drugs. The right common carotid artery was cannulated with a fine PE10 catheter for injection of iodinated contrast medium (Iomeron 350, Bracco-Eisai Co., Ltd.).

The carotid catheter was positioned close to the aortic valve to inject the contrast medium to the coronary vessels efficiently. Also, the carotid catheter was used to measure the arterial blood pressure intermittently. Following surgical preparation, the mouse was positioned supine in front of, and perpendicular to the SATICON X-ray detector (Hitachi Denshi Techno-system) to image the thorax in an alignment of 9.5 mm x 9.5 mm imaging field [16]. A 50 μm-thick tungsten filament was placed across the corner of the detector's window to be captured in all images and used as a reference to determine the size of the coronary vessels.

4.3.2.2 Infusion of drugs and imaging

A baseline angiogram of the coronary circulation was first recorded before the infusion of drugs. Then, the mouse was infused with the endothelium-dependent vasodilator ACh (10 μg/kg/min) for five minutes, followed by injecting the contrast medium to record the coronary circulation. Next, the mouse was infused with sodium nitroprusside (SNP, 10 μg/kg/min), an endothelium-independent vasodilator, for five minutes, and the same procedure was repeated to record the coronary circulation.

4.3.2.3 Angiogram data analysis

All analyses were performed using ImageJ software. The first analysis was performed to count the number of coronary vessel branches. The second analysis was done to measure the diameter of 2-4 vessels of each branch generation (i.e., first, second, and third-order vessels). The 50 μm-thick tungsten filament was used as a reference to measure the diameter of vessels. Finally, as the diameter of the first, second and third-order vessels may vary from mouse to mouse, the third analysis was performed to sort the vessels according to their diameter (0-100, 100-150, 150-200, and 200-350 μm). All the data are expressed as mean ± standard error of the mean, except the diameter of coronary vessels were expressed as the median in box and whisker to present the minimum and maximum distribution of data.

4.3.3 Western blot analysis

Western blot analysis was performed in Kakinuma laboratory in Nippon Medical School, Japan. Total protein extraction from the lower part of the mouse ventricular tissues was performed as described in Section 2.3.2.1. An equal amount of protein was loaded and electrophoresed and blotted for following protein targets, processed as described in Section 2.3.2.4. The band intensity of the target protein was normalized to a prominent band between 37 kDa and 50 kDa on the Ponceau S stained blot as described in Chapter 2 (section 2.3.2.5) [143, 144] and expressed as fold changes towards the control group [145]. As for the quantification of the phosphorylation of Akt and AMPKα, the band intensity of the phosphorylated protein was normalized to its respective total protein as well as to a prominent band between 37 kDa and 50 kDa on the Ponceau S stained blot. The rationale for the latter approach is that *(1)* total Akt and AMPKα expression were significantly decreased in the *db/db* mice (Section 4.4.2.2 & 4.4.2.3); *(2)* to further examine the phosphorylation status in a condition when the expression of normalizer is consistent among the ND, *db/db and db/db-ChAT-tg* mice. This particular approach has previously adopted by several research groups where they normalized to

normalizer such as β-actin or GAPDH that showed consistent expression in their study [242, 243]. Besides, the reason why total Akt and AMPKα expression were decreased in the *db/db* mice is not clear, however, this could be due to enhanced protein degradation that is associated with diabetes mellitus [146-150]. The information of each antibody are listed in Table 4.1. The full blot for each antibody is shown in Appendix 2.

Table 4.1 Primary and secondary antibodies for western blot

Antigen	Host/Clone	Dilution factor	Predicted molecular weight (kDa)	Manufacturer/ Catalogue number
Primary antibodies				
ChAT	Goat/polyclonal	1:1,000	70/74	Chemicon, AB144P
M_2AChR	Rabbit/monoclonal	1:2,000	52	Abcam, AB109226
GLUT-4	Rabbit/polyclonal	1:2,000	55	NovusBio, NBP1-49533
HIF1α	Mouse/monoclonal	1:500	93	NovusBio, NBP100-123
pAkt (Ser473)	Rabbit/polyclonal	1:1,000	60	Cell Signaling, 9271
Akt	Rabbit/polyclonal	1:2,000	60	Cell Signaling, 9272
pAMPKα (Thr172)	Rabbit/polyclonal	1:1,000	62	Cell Signaling, 2535
AMPKα	Rabbit/polyclonal	1:2,000	62	Cell Signaling, 2532
VEGF-A	Rabbit/polyclonal	1:1,000	21	Santa Cruz, SC-152
Secondary antibodies				
Anti-goat IgG, HRP conjugated	Donkey	1:2,000	-	Santa Cruz, SC2354
Anti-rabbit IgG, HRP conjugated	Goat	1:2,000	-	Cell Signaling, 7074
Anti-mouse IgG, HRP conjugated	Goat	1:1,000	-	Promega, W402B

Note: the predicted molecular weight of protein is recommended by the manufacturer

4.3.4 Immunofluorescence analysis

Double-labelling immunofluorescence staining was performed to detect the density of total capillaries and arterioles using the upper part of the mouse ventricular tissues, as described in Section 2.4. As there is a distinct structural difference between capillary and arteriole (i.e., a single endothelial layer in capillary versus endothelial and a smooth muscle cell layer in arteriole), specific antibody and lectin were used to differentiate capillaries and arterioles. The endothelial layer was detected by biotinylated *Griffonia simplicifolia* lectin-I (GSL-I) Isolectin

B4 while the smooth muscle cell layer was detected by Cy3™-conjugated α-smooth muscle actin antibody. DAPI was used to stain the nuclei. The density of capillaries was expressed as the number of Isolectin$^+$ cells/mm^2 of ventricular tissue. The density of small or large arterioles was expressed as the number of αSMA$^+$Isolectin$^+$ cells/mm^2 of ventricular tissue. Table 4.2 summarizes the dilution factor and the pairing of primary and secondary antibodies used in the experiment.

Table 4.2 Information on antibodies/lectin for double-labelling immunofluorescence

Antigen/lectin	Source	Dilution	Manufacturer/Catalogue number
Primary antibodies			
Isolectin B4 (Biotinylated)	*Griffonia simplicifolia*	1:200	Vector laboratories, B1205
α-smooth muscle actin (antibody is conjugated with Cy3™)	Mouse	1:800	Sigma-Aldrich, C6198)
Secondary reagent			
Streptavidin-AlexaFluor® 488	-	1:200	Invitrogen, S32354

4.3.5 Statistical analyses

All statistical analyses were performed using GraphPad Prism (version 7) in consultation with biostatistician Mr. Andrew Grey and Dr. Claire Cameron (Centre for Biostatistics, University of Otago). Data are expressed as the mean ± standard error of the mean. Two-way ANOVA followed by Sidak's test for multiple comparison test was performed to analyze body weight, blood glucose level, and all the cardiac functions. For the western blot data, as data from some specific age groups of the same protein target failed the normality test, a non-parametric Kruskal-Wallis test with Bunn's test (three groups comparison) or Mann-Whitney U test (two-group comparison) was used. The number of different order coronary vessels of two age groups failed the normality test. However, there is no single non-parametric test equivalent to Two-way ANOVA. Therefore, a non-parametric Mann-Whitney U test was used. The data for diameter, % changes of diameter in response to ACh and SNP, the density of small, large arterioles as well as total capillaries also failed the normality test. Thus, a non-parametric Mann-

Whitney U test was used. This particular approach was consulted with biostatistician Dr. Claire Cameron and Mr. Andrew Gray.

4.4 Results

4.4.1 Body weight and blood glucose level of *db/db-ChAT-tg* mice

The body weight of *db/db-ChAT-tg* mice at 12-weeks of age was significantly reduced in comparison to *db/db* mice (Figure 4.1A). However, there was no significant difference in the body weight of *db/db-ChAT-tg* mice at 8-, 16- and 20-weeks of age compared to the age-matched *db/db* mice. On the other hand, the 8- to 16-weeks old *db/db-ChAT-tg* mice showed a significant decrease in blood glucose levels in comparison to the *db/db* mice (Figure 4.1B). However, the decline in blood glucose level of 20-weeks old *db/db-ChAT-tg* mice was not statistically significant. The protocol for measuring blood glucose is described in Appendix 4.

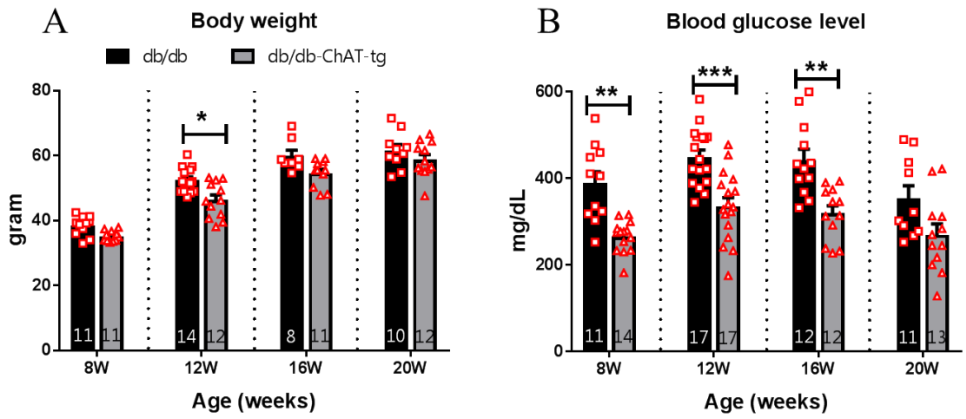

Figure 4.1 The body weight and blood glucose level in *db/db* and *db/db-ChAT-tg* mice.
Bar graphs with scatter plots showing the change of ***(A)*** *body weight and* ***(B)*** *blood glucose level in the db/db-ChAT-tg mice in comparison to the control age-matched db/db mice (DM). Data are expressed as mean ± SEM. Two-way ANOVA with Sidak's test for multiple comparison was performed. *p<0.05; **p<0.01; ***p<0.001 vs age-matched db/db mice. The number of samples per group is indicated in the figure.*

4.4.2 LV function of *db/db-ChAT-tg* mice

4.4.2.1 LV diastolic, systolic function and contractility

The overexpression of the *ChAT* gene in the ventricles of *db/db-ChAT-tg* mice improved the LV function. The indices of diastolic function such as end-diastolic pressure (EDP) and volume (EDV) were not statistically different in the *db/db-ChAT-tg* mice at 8- to 20-weeks of age compared to age-matched *db/db* mice (Figure 4.2A&B). However, *db/db-ChAT-tg* mice

showed better systolic function as demonstrated by a significant increase in the end-systolic pressure (ESP) at 8- to 20-weeks of age (Figure 4.2C) and a considerable decrease in the end-systolic volume (ESV) at 12- and 16-weeks of age compared to *db/db* mice (Figure 4.2D).

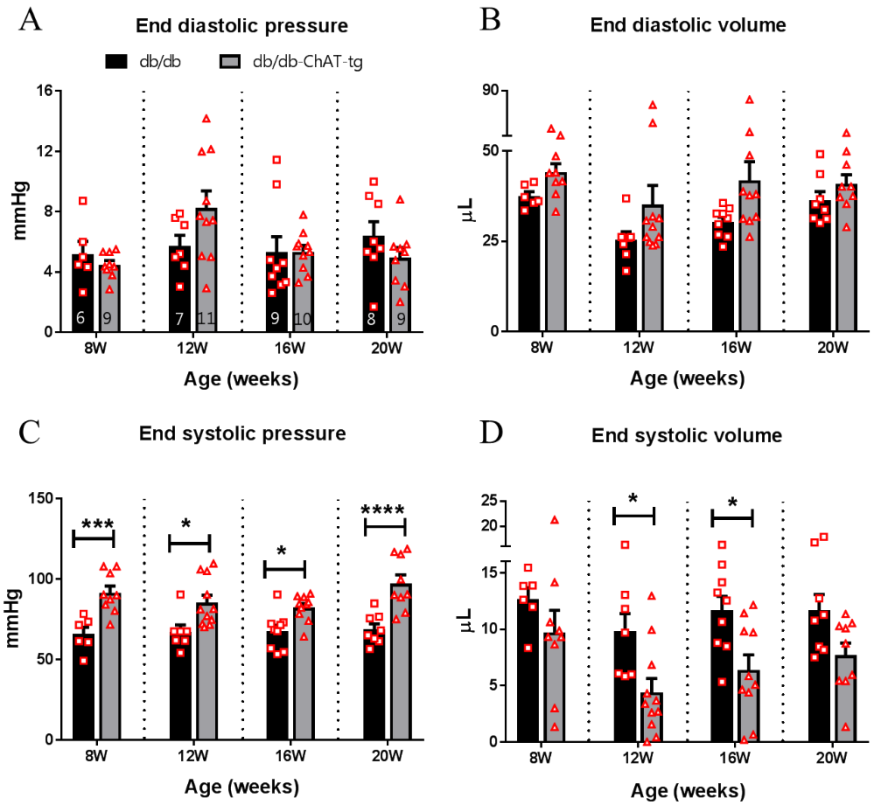

Figure 4.2 Activation of cardiac NNCS improved the systolic function of *db/db-ChAT-tg* mice.
Bar graphs with scatter plots showing the diastolic function as indicated by ***(A)*** *end-diastolic pressure and* ***(B)*** *end-diastolic volume as well as systolic function as indicated by* ***(C)*** *end-systolic pressure and* ***(D)*** *end-systolic volume of the db/db-ChAT-tg mice in comparison to the control age-matched db/db mice. Data are expressed as mean ± SEM. Two-way ANOVA with Sidak's test for multiple comparison was performed. *p<0.05; ***p<0.001; ****p<0.0001 VS age-matched db/db mice. The number of samples per group is indicated in figure A.*

The heart rate (HR) of *db/db-ChAT-tg* mice was unaltered at 8- to 20-weeks of age (Figure 4.3A). However, the stroke volume (SV) was significantly increased in the *db/db-ChAT-tg* mice at 16-weeks of age (Figure 4.3B). Further, the cardiac output (CO) and ejection fraction (EF) were considerably improved in the *db/db-ChAT-tg* mice at 12- to 20-weeks of age (Figure 4.3C&D). In summary, the overall findings indicate that the *db/db-ChAT-tg* mice exhibited superior LV systolic function and contractibility in comparison to the age-matched *db/db* mice. The protocol for measuring LV function is described in Appendix 4.

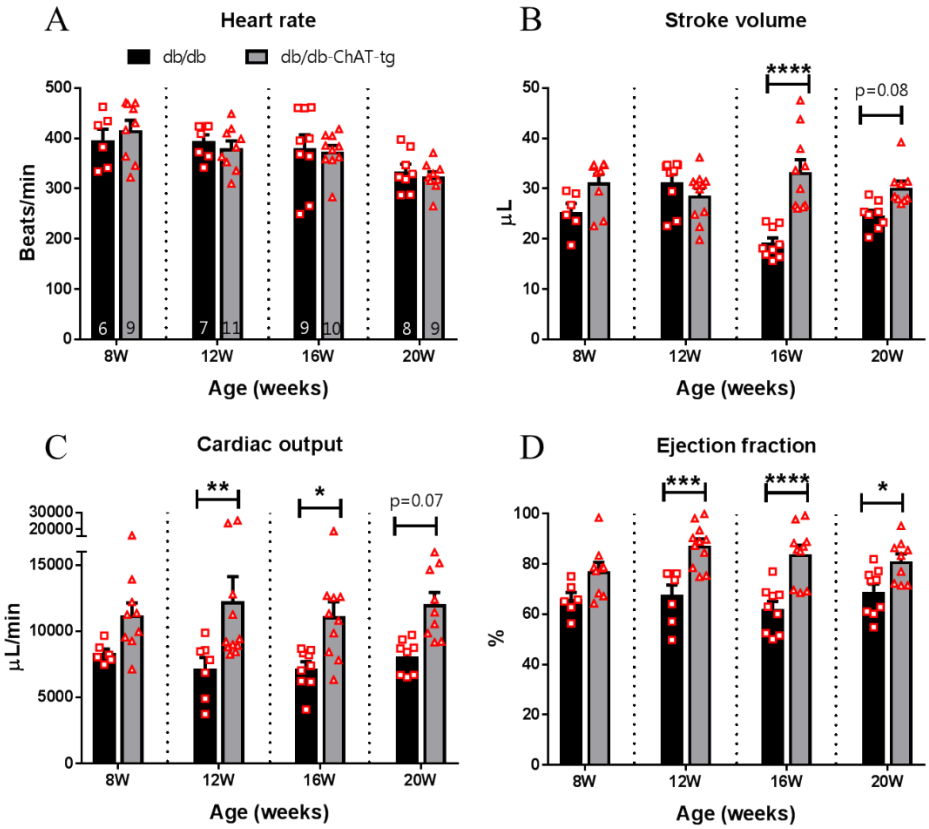

Figure 4.3 Activation of cardiac NNCS improved LV contractibility without altering heart rate in the *db/db-ChAT-tg* mice.

*Bar graphs with scatter plots showing the **(A)** heart rate, **(B)** stroke volume, **(C)** cardiac output and, **(D)** ejection fraction of the db/db-ChAT-tg mice in comparison to the control age-matched db/db mice. Data are expressed as mean ± SEM. Two-way ANOVA with Sidak's test for multiple comparisons was performed. *p<0.05; **p<0.01; ***p<0.001; ****p<0.0001 VS age-matched db/db mice. The number of samples per group is indicated in figure A.*

4.4.2.2 Molecular alterations associated with improved LV function

Since it is well established that ACh-mediated signaling promotes glucose metabolism and decrease energy demand [100], western blot analysis was performed to determine the protein expression of key targets involved in ACh signaling (ChAT and M_2AChR), ACh-mediated pro-survival PI3K/Akt/HIF1α/GLUT-4 signaling pathway (Akt, HIF1α and GLUT-4) as well as ATP homeostasis (AMPKα).

4.4.2.2.1 ChAT and M_2AChR

In comparison to age-matched ND mice, the ChAT protein expression in the *db/db* mice was unaltered at 8- to 20-weeks of age. Ventricular-specific overexpression of *ChAT* gene in the

db/db-ChAT-tg mice resulted in 1.7±0.2 to 2.0±0.1-fold increase in ChAT protein expression at 8-, 12-, 16- and 20-week of age (Figure 4.4).

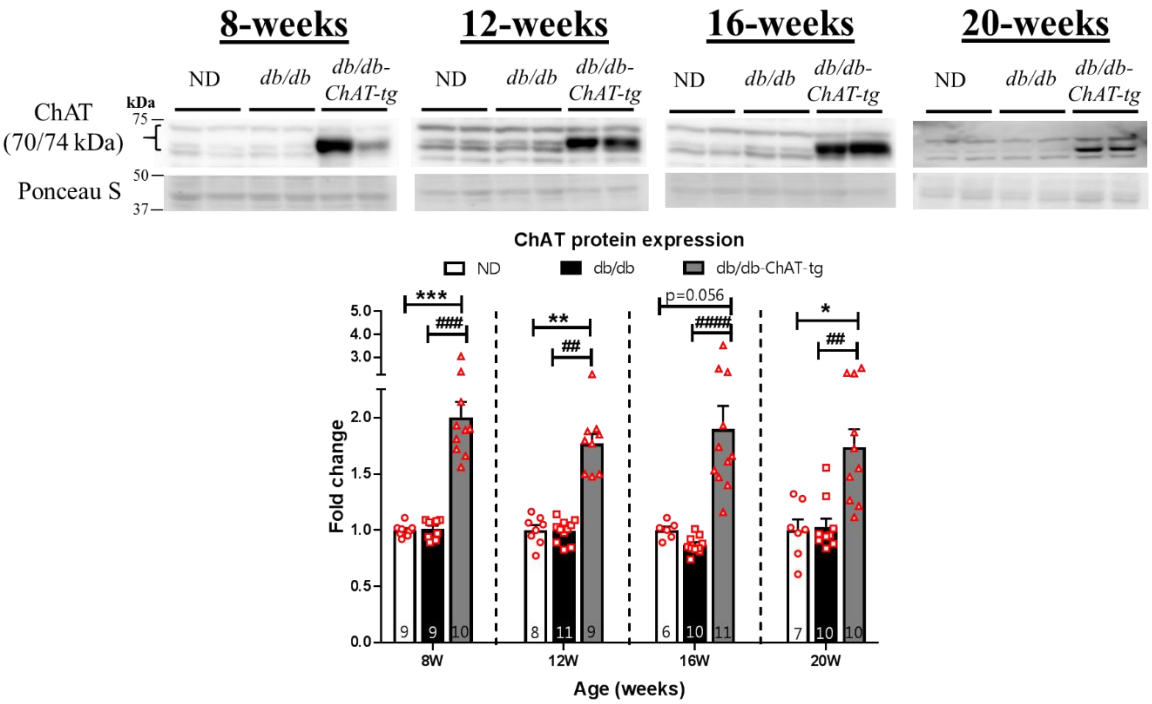

Figure 4.4 Increased ChAT protein expression in the *db/db-ChAT-tg* mice.
*Bar graphs with scatter plots showing the protein expression of ChAT in the ND, db/db, and db/db-ChAT-tg mice at 8-, 12-, 16- and 20-weeks of age. Data are presented as mean ± SEM. A non-parametric Kruskal-Wallis test with Bunn's test was performed. *p<0.05, **p<0.01, ***p<0.001 VS age-matched ND mice; ##p<0.01, ###p<0.001, ####p<0.0001 VS age-matched db/db mice. The number of samples per group is indicated in the figure.*

In comparison to the age-matched ND mice, the M_2AChR protein expression was significantly decreased in the heart of *db/db* mice at 8-weeks of age while the expression change in *db/db-ChAT-tg* mice was not statistically significant compared to ND mice (Figure 4.5). At 12-weeks of age, the M_2AChR protein expression was significantly decreased in the *db/db-ChAT-tg* mice while the expression was not statistically different in the *db/db* mice in spite of a downward trend as compared to the ND mice. At 16-weeks of age, the M_2AChR protein expression was unaltered in the *db/db* and *db/db-ChAT-tg* mice in comparison to the ND mice. At 20-weeks of age, the M_2AChR protein expression was significantly decreased in the *db/db* mice in comparison to the ND mice. However, this was prevented in the *db/db-ChAT-tg* mice, showing comparable expression to the corresponding age-matched ND mice.

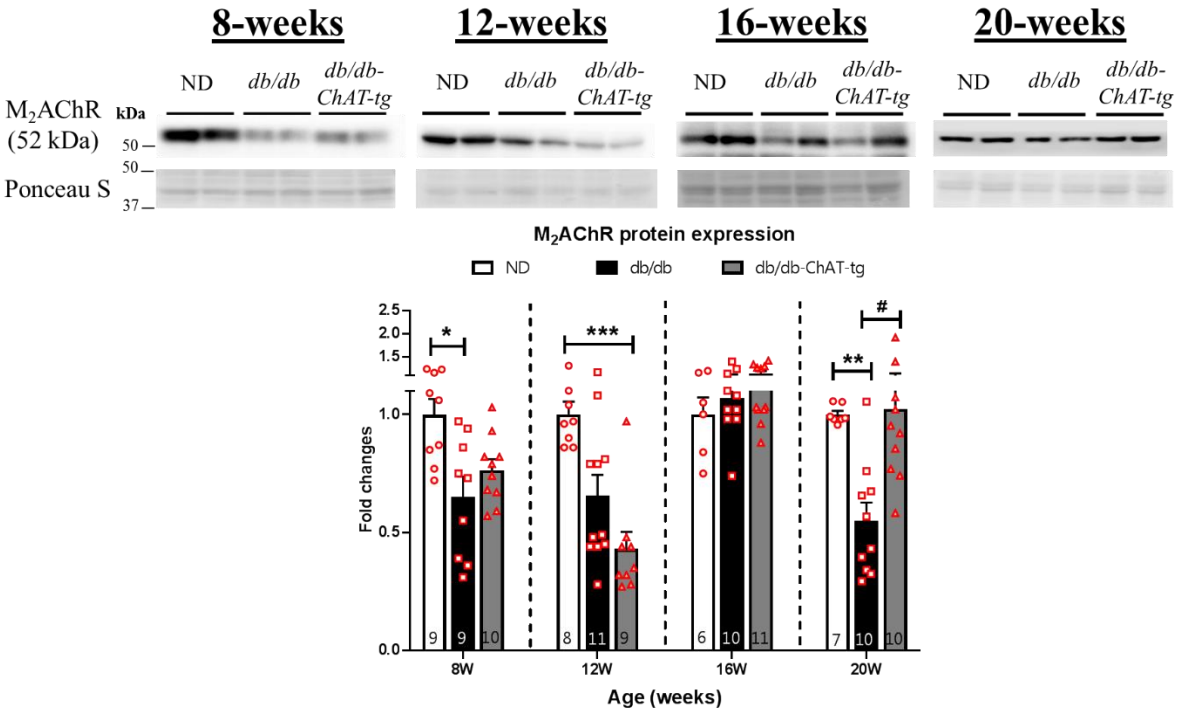

Figure 4.5 Prevention of decreased M_2AChR protein expression in the *db/db-ChAT-tg* mice.
*Representative blots and bar graphs with scatter plots showing the protein expression of M_2AChR in the ND, db/db, and db/db-ChAT-tg mice at 8-, 12-, 16- and 20-weeks of age. Data are expressed as mean ± SEM. A non-parametric Kruskal-Wallis test with Bunn's test was performed. *p<0.05, **p<0.01, ***p<0.001 VS age-matched ND mice; #p<0.05 VS age-matched db/db mice. The number of samples per group is indicated in the figure.*

4.4.2.2.2 Activation of pro-survival PI3K/Akt/HIF1α/GLUT-4 signaling pathway

To determine if cardiac NNCS-mediated PI3K/Akt/HIF1α/GLUT-4 signaling pathway plays a role in improved LV systolic function and contractility of the *db/db-ChAT-tg* heart, protein expression of Akt and its phosphorylated form (Ser473), HIF1α and GLUT-4 were investigated. Both anti-pAkt and anti-Akt antibodies are polyclonal, but it detected only one band at molecular weight of 60 kDa (Appendix 2, Figure S2.6). Based on the predicted molecular weight by manufacturer and UniProt, I identified this band as pAkt/Akt-positive. Besides, as two approaches were taken to quantify the phosphorylation level of Akt, the outcome was different in the mice at 8-weeks of age. By normalizing to the selected band between 37 kDa and 50 kDa on the Ponceau S stained blot, the phosphorylation level of Akt was unaltered in the *db/db* and *db/db-ChAT-tg* mice in comparison to the ND mice at 8-weeks of age (Figure 4.6). In contrast, by normalizing to the expression of total Akt expression, the phosphorylation

level of Akt was significantly increased in the *db/db* and *db/db-ChAT-tg* mice in comparison to the ND mice at 8-weeks of age. This difference is caused by a significant reduction in total Akt expression in the *db/db* and *db/db-ChAT-tg* mice. Further, the phosphorylation level of Akt showed similar trend in the *db/db and db/db-ChAT-tg* mice at 12- to 20-weeks after normalizing to total Akt expression or Ponceau S stained blot. In general, the phosphorylation level of Akt was significantly increased in *db/db-ChAT-tg* mice as compared to age-matched ND mice at 12- to 20-weeks of age. While *db/db* mice showed an increasing trend (normalized to Ponceau S stained blot) or significant increase (normalized to total Akt expression) in phosphorylated Akt expression in comparison to age-matched ND mice at 12- to 20-weeks of age.

The total Akt protein expression was significantly decreased in the *db/db* mice compared with the ND mice at 8- to 20-weeks of age. The *db/db-ChAT-tg* mice showed a similar decrease in total Akt protein expression at 8- and 12-weeks of age. However, at 16- and 20-weeks of age, the total Akt protein expression was significantly increased in the *db/db-ChAT-tg* compared with the *db/db* mice and was comparable to the ND mice.

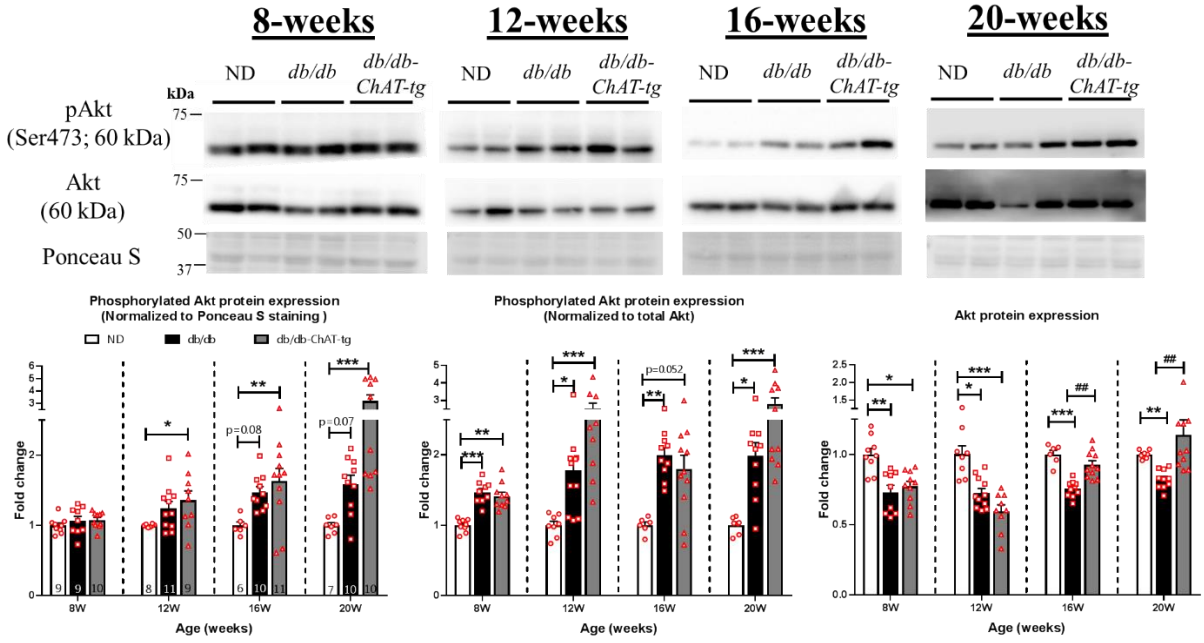

Figure 4.6 Modulation of total Akt protein expression and phosphorylated Akt at Ser473.
Representative blots and bar graphs with scatter plots showing the protein expression of total Akt and its phosphorylated form (Ser473) in the ND, db/db and db/db-ChAT-tg mice at 8-, 12-, 16- and 20-weeks of age. Data are presented as mean ± SEM. A non-parametric Kruskal-Wallis test with Bunn's test was

*performed. *p<0.05, **p<0.01, ***p<0.001 VS age-matched ND mice; ##p<0.01 VS age-matched db/db mice. The number of samples per group is indicated in the figure.*

Another pro-survival protein I investigated was HIF1α. The anti- HIF1α antibody is monoclonal, however, it detected multiple bands (Appendix 2, Figure S2.6). This could be partly due to the presence of isoforms ranged from 82 kDa to 96 kDa as well as post-translation modifications (https://www.uniprot.org/uniprot/Q16665). In my study, I observed a band with strong intensity above the 75 kDa. In line with this, Jablonska et al. [244] used the same antibody and reported HIF1α-positive band to be approximately 80 kDa. Therefore, I identified the band with strong intensity above 75 kDa as HIF1α-positive. Western blot analysis revealed that HIF1α expression was significantly increased in the *db/db-ChAT-tg* mice in comparison to the ND and *db/db* mice at 8-weeks of age (Figure 4.7). At 12- to 20-weeks of age, no significant changes in the HIF1α protein expression in the *db/db-ChAT-tg* mice in comparison to the age-matched ND and *db/db* mice.

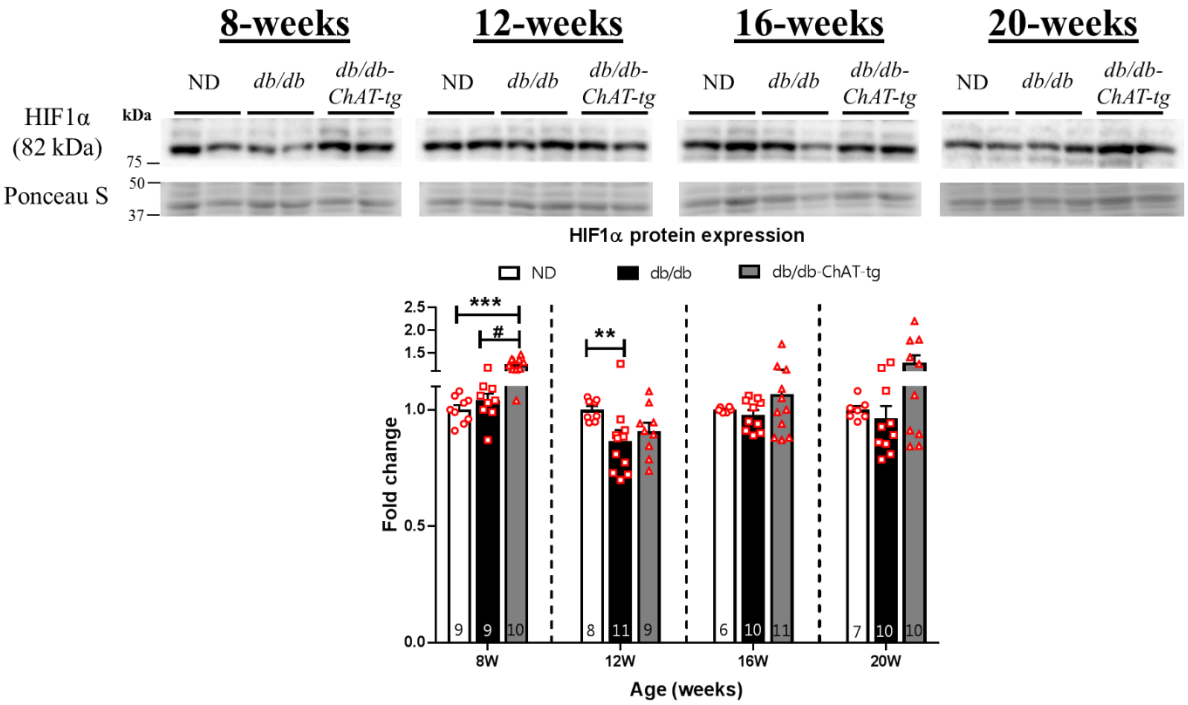

Figure 4.7 Modulation of HIF1α protein expression by activating cardiac NNCS.
*Representative blots and bar graphs with scatter plots showing the protein expression of HIF1α in the ND, db/db, and db/db-ChAT-tg mice at 8-, 12-, 16- and 20-weeks of age. Data are presented as mean ± SEM. A non-parametric Kruskal-Wallis test with Bunn's test was performed. **p<0.01, ***p<0.01 VS*

age-matched ND mice; #p<0.05 VS age-matched db/db mice. The number of samples per group is indicated in the figure.

Next, GLUT-4 expression was tested to determine if the activation of PI3K/Akt/HIFα signaling cascade shifted the cardiac metabolism to glucose oxidation. At the 8-weeks of age, the GLUT-4 protein expression was significantly increased in the *db/db* and *db/db-ChAT-tg* mice compared with ND mice (Figure 4.8). At 12- and 16-weeks of age, the GLUT-4 protein expression remained significantly higher in the *db/db-ChAT-tg* mice while the expression in the *db/db* mice was comparable to that of the age-matched ND mice. At the 20-weeks of age, there was a decreasing trend in GLUT-4 protein expression in the *db/db* mice (p=0.07) compared to the ND mice. Additionally, the GLUT-4 protein expression was unaltered in the *db/db-ChAT-tg* mice compared to ND mice, but the expression was significantly increased compared to the *db/db* mice. The overall findings indicate that overexpression of the *ChAT* gene activated PI3K/Akt/HIF1α/GLUT-4 signaling cascade in the ventricles of *db/db-ChAT-tg* mice. Initiation of this signaling cascade is likely to promote glucose uptake and oxidation in the ventricles of *db/db-ChAT-tg* mice.

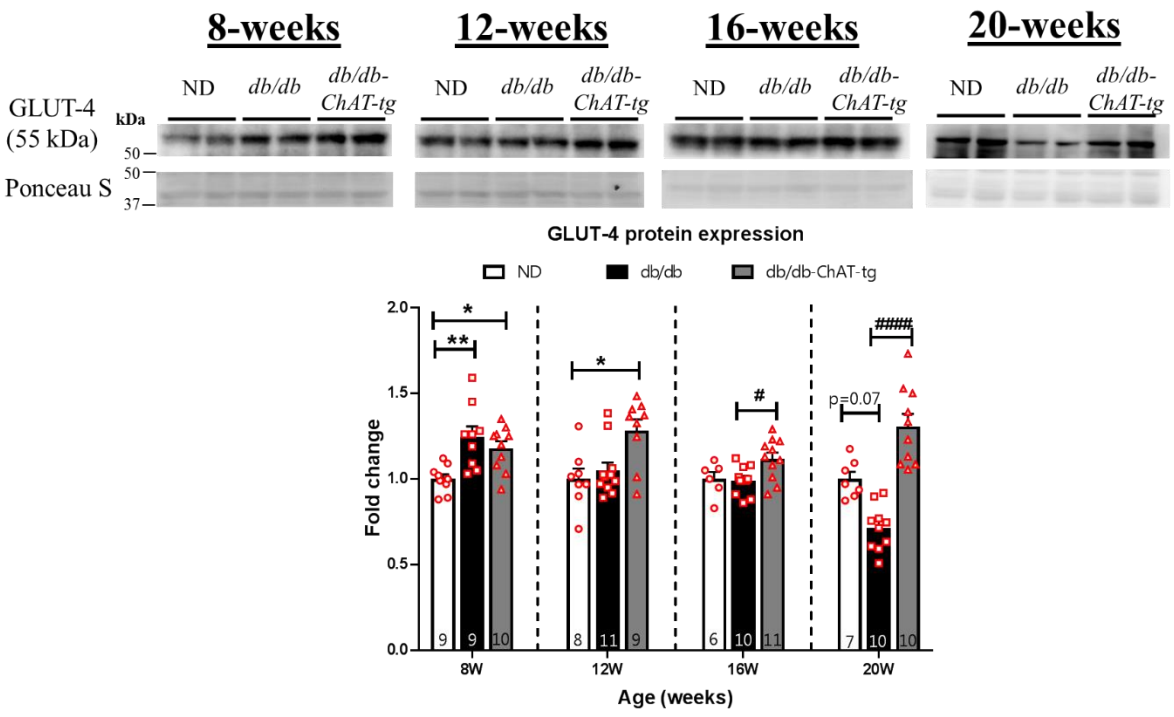

Figure 4.8 Normalization of GLUT-4 protein expression in the *db/db-ChAT-tg* mice.
*Representative blots and bar graphs with scatter plots showing the protein expression of GLUT-4 in the ND, db/db, and db/db-ChAT-tg mice at 8-, 12-, 16- and 20-weeks of age. Data are expressed as mean ± SEM. A non-parametric Kruskal-Wallis test with Bunn's test was performed. *p<0.05, **p<0.01 VS age-matched ND mice; #p<0.05, ####p<0.0001 VS age-matched db/db mice. The number of samples per group is indicated in the figure.*

4.4.2.2.3 ATP homeostasis - AMPKα

After confirming that PI3K/Akt/HIF1α/GLUT-4 signaling cascade was activated in the *db/db-ChAT-tg* mice's heart, the next aim was to examine if glucose oxidation increased the energy status in the ventricles. For this, the phosphorylation level and total protein expression of AMPKα, which is the catalytic subunit of energy regulator AMPK, was measured to reflect the energy status in the heart. The anti-pAMPKα and anti-AMPKα antibodies are polyclonal and resulted in multiple bands, however, a band with strong intensity with molecular weight of 60 kDa was detected (Appendix 2, Figure S2.7). Based on the predicted molecular weight indicated by manufacturer and UniProt, I identified this band as pAMPKα/AMPKα-positive.

Besides, the two approaches to quantify the phosphorylation of AMPKα generally resulted in similar trend in the mice at 8- to 16-weeks of age. In the *db/db-ChAT-tg* mice at 8- and 12-weeks of age, there was a decreasing trend in the phosphorylation level of AMPKα compared to ND mice (Figure 4.9). At 16-weeks of age, the phosphorylation level of AMPKα was significantly decreased in the heart of *db/db-ChAT-tg* mice compared to ND mice. As for *the db/db* mice, there was a decreasing trend in the phosphorylation level of AMPKα in at 8- and 16-weeks of age; however, the changes were not statistically significant.

At 20-weeks of age, by normalizing to Ponceau S stained blot, the phosphorylation level of AMPKα in the *db/db* showed an increasing trend while the phosphorylation level in the *db/db-ChAT-tg* mice was comparable to the ND mice. By normalizing to total AMPKα expression, the phosphorylation level of AMPKα in the *db/db* showed a decreasing trend (p=0.06) while the phosphorylation level in the *db/db-ChAT-tg* mice was comparable to the ND mice. In terms of the total AMPKα protein expression, the changes in the expression were not statistically

significant in both the *db/db* and *db/db-ChAT-tg* mice compared to the ND mice at 8- to 20-weeks of age. However, AMPKα protein expression was significantly increased in the *db/db-ChAT-tg* mice compared to that of *db/db* mice at 20-weeks of age. The overall findings suggest that AMPK was possibly inactivated in the *db/db* and *db/db-ChAT-tg* mice at 8- to 16-weeks of age, which may occur due to low AMP/ATP ratio. While in the *db/db* mice at 20-weeks of age, the result is not conclusive as the two different normalization methods resulted in opposite result.

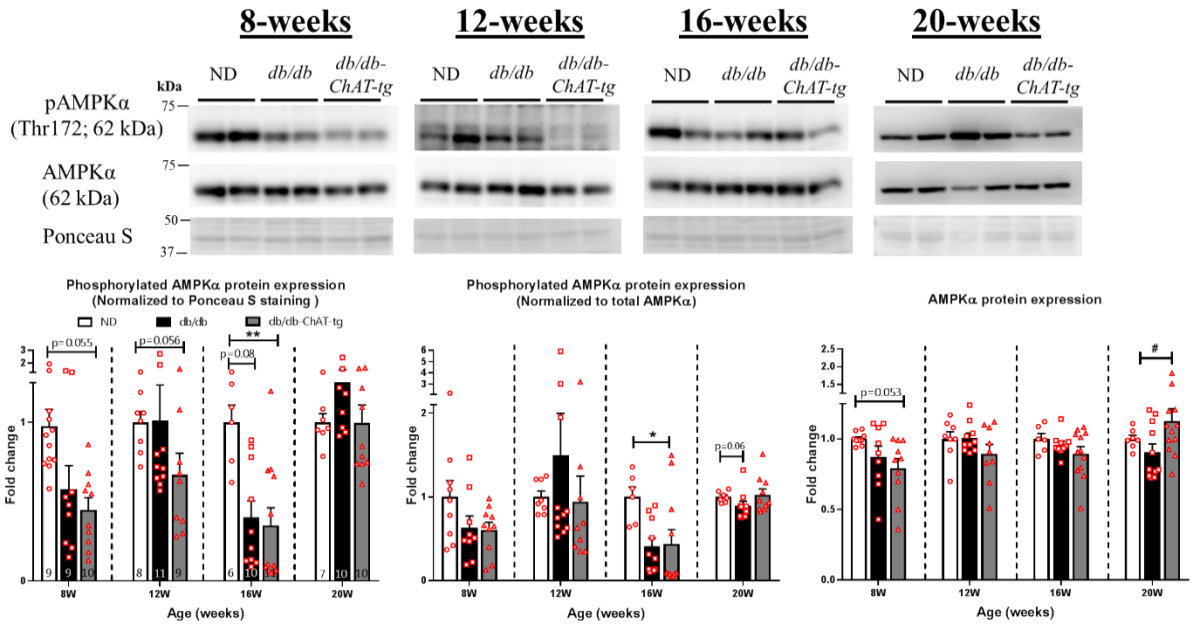

Figure 4.9 Modulation of total AMPKα protein expression and phosphorylated AMPKα at Thr172. *Representative blots and bar graphs with scatter plots showing the protein expression of total AMPKα and its phosphorylated form (Thr172) in the ND, db/db and db/db-ChAT-tg mice at 8-, 12-, 16- and 20-weeks of age. Data are presented as mean ± SEM. A non-parametric Kruskal-Wallis test with Bunn's test was performed. **p<0.01 VS age-matched ND mice; #p<0.05 VS age-matched db/db mice. The number of samples per group is indicated in the figure.*

4.4.3 Vascular function of *db/db-ChAT-tg* mice

4.4.3.1 *In-vivo* coronary circulation

Having demonstrated that *in-vivo* activation of cardiac NNCS improved the LV systolic function and contractility in the *db/db-ChAT-tg* mice, the next aim was to investigate the effect of cardiac NNCS in preventing diabetes-induced vascular dysfunction. This aim was tested by imaging the coronary circulation by Synchrotron radiation microangiography. The total number of first, second, third, and fourth-order coronary vessels on the angiogram was counted.

However, as the fourth-order coronary vessels were only visualized in a small number of mice (in particular only in the *db/db-ChAT-tg* mice), the number of fourth-order coronary vessels was combined with the number of third-order coronary vessels for analysis. The results showed that the difference in the total number of coronary vessels was not statistically significant in the *db/db-ChAT-tg* mice in comparison to the *db/db* mice at 12-weeks of age (Figure 4.10). However, at 24-weeks of age, the number of second-order coronary vessels was significantly increased in the *db/db-ChAT-tg* mice.

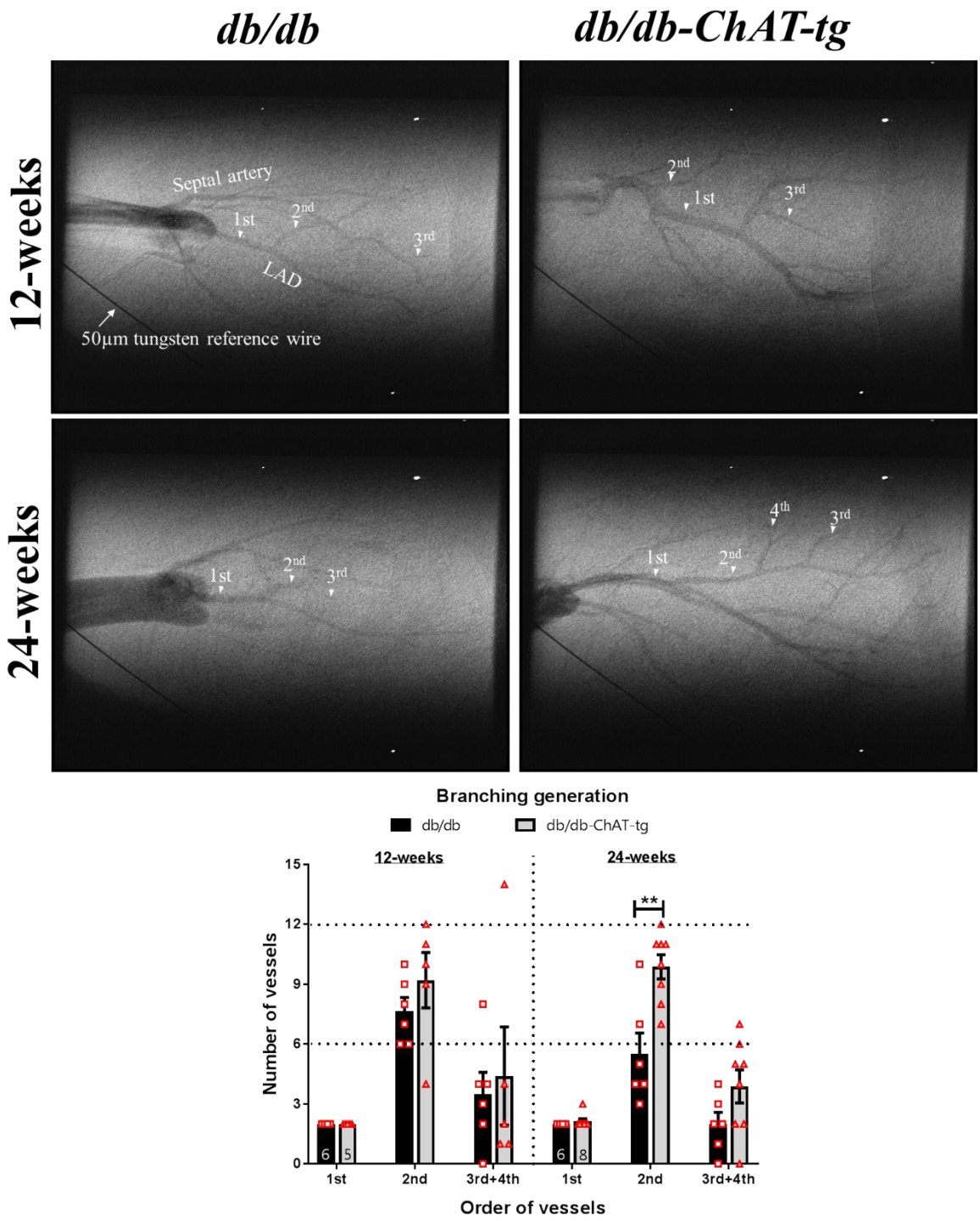

Figure 4.10 Effect of cardiac NNCS activation in maintaining vasculature.
*Representative microangiogram images and bar graphs with scatter plots showing the number of first, second, third and fourth-order coronary vessels in the db/db and db/db-ChAT-tg mice at 12- and 24-weeks of age. The 50 μm diameter tungsten wire in the bottom left corner of all angiogram frames serves as a reference. Data are presented as mean ± SEM. A non-parametric Mann-Whitney U test was performed. **p<0.01 VS age-matched db/db mice. The number of samples per group is indicated in the figure.*

The diameter of the coronary vessels was measured by using 50 μm tungsten wire as a reference.

The results showed an increasing trend in the diameter of coronary vessels (especially the third-

order vessels) in the *db/db-ChAT-tg* mice in comparison to the *db/db* mice at 12- and 24-weeks of age, however, this was not statistically significant (Figure 4.11 A&B).

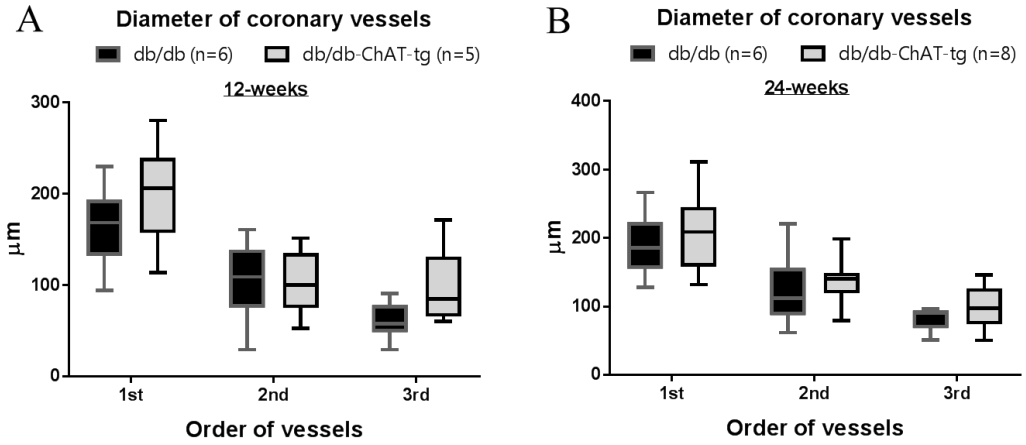

Figure 4.11 The range of vessel size in *db/db* and *db/db-ChAT-tg* mice.
*Box and whisker plots showing the internal diameter of first, second, and third coronary vessels in the **(A)** 12-weeks and **(B)** 24-weeks old db/db and db/db-ChAT-tg mice. Data are presented as a range. A non-parametric Mann-Whitney U test was performed. The number of samples per group is indicated in the figure.*

Next, to determine the endothelial function of the coronary vasculature, the mice were infused with ACh (10 µg/kg/min) and SNP (10 µg/kg/min) to examine the endothelial-dependent and -independent vasodilation, respectively. Measurement of diameter of first to third-order coronary vessels was performed. The diameter of coronary vessels was measured and further sorted according to vessel size of 0-100, 100-150, 150-200, 200-350 µm. After ACh infusion, the percentage change in diameter of the *db/db-ChAT-tg* mice was comparable to that of *db/db* mice at 12- and 24-weeks of age (Figure 4.12 A&B). Similarly, the percentage change in diameter after SNP infusion was similar between *db/db-ChAT-tg* and *db/db* mice at 12- and 24-weeks of age (Figure 4.12 C&D). Thus, there was no change in the diameter of coronary vessels in response to ACh and SNP in the *db/db-ChAT-tg* mice compared to the *db/db* mice at 12- and 24-weeks of age. These results suggest that endothelial-dependent and -independent vasodilation was not different between the *db/db* and *db/db-ChAT-tg* mice

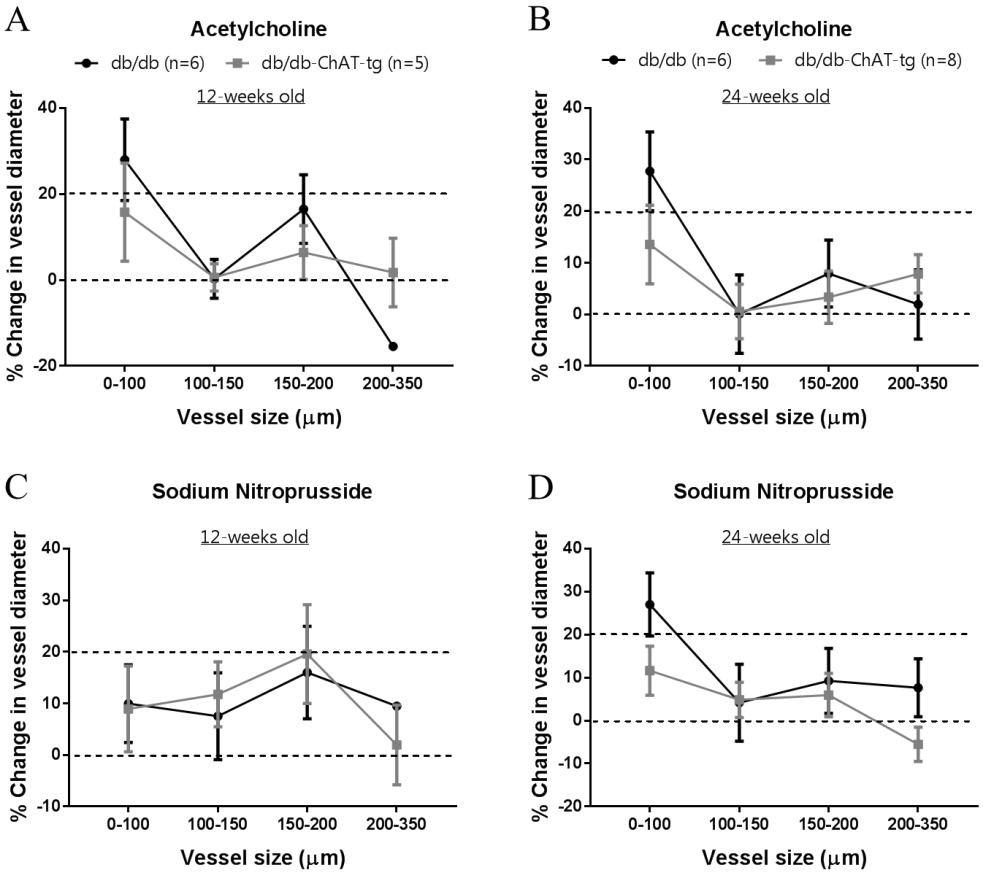

Figure 4.12 The effect of ACh and SNP on the diameter of coronary vessels in *db/db* and *db/db-ChAT-tg* mice.

*The line graphs showing **(A&B)** Acetylcholine (ACh; 10 µg/kg/min) and **(C&D)** Sodium nitroprusside (SNP; 10 µg/kg/min) in changing the diameter of coronary vessels. The percentage changes were sorted according to the coronary vessel size in the db/db and db/db-ChAT-tg mice at 12- and 24-weeks of age, respectively. Data are presented as mean ± SEM. A non-parametric Mann-Whitney U test was performed. The number of samples per group is indicated in the figure.*

The final measurement was performed to determine if ACh and SNP exerted its effect by recruiting small coronary vessels (i.e., third and fourth-order measured together). This measurement was only performed on the mice at 24-weeks of age as the decline in the number of coronary vessels was evident in the *db/db* mice at 24-weeks of age compared to the *db/db* mice at 12-weeks of age (Figure 4.10). The analysis revealed that the number of third and fourth-order coronary vessels of *db/db-ChAT-tg* mice was significantly increased after ACh (Figure 4.13B) and SNP infusion (Figure 4.13C) compared to that of the age-matched *db/db* mice. Thus, an increase in the number of third and fourth-order coronary vessels indicates preserved vascular responsiveness to ACh and SNP in the *db/db-ChAT-tg* mice.

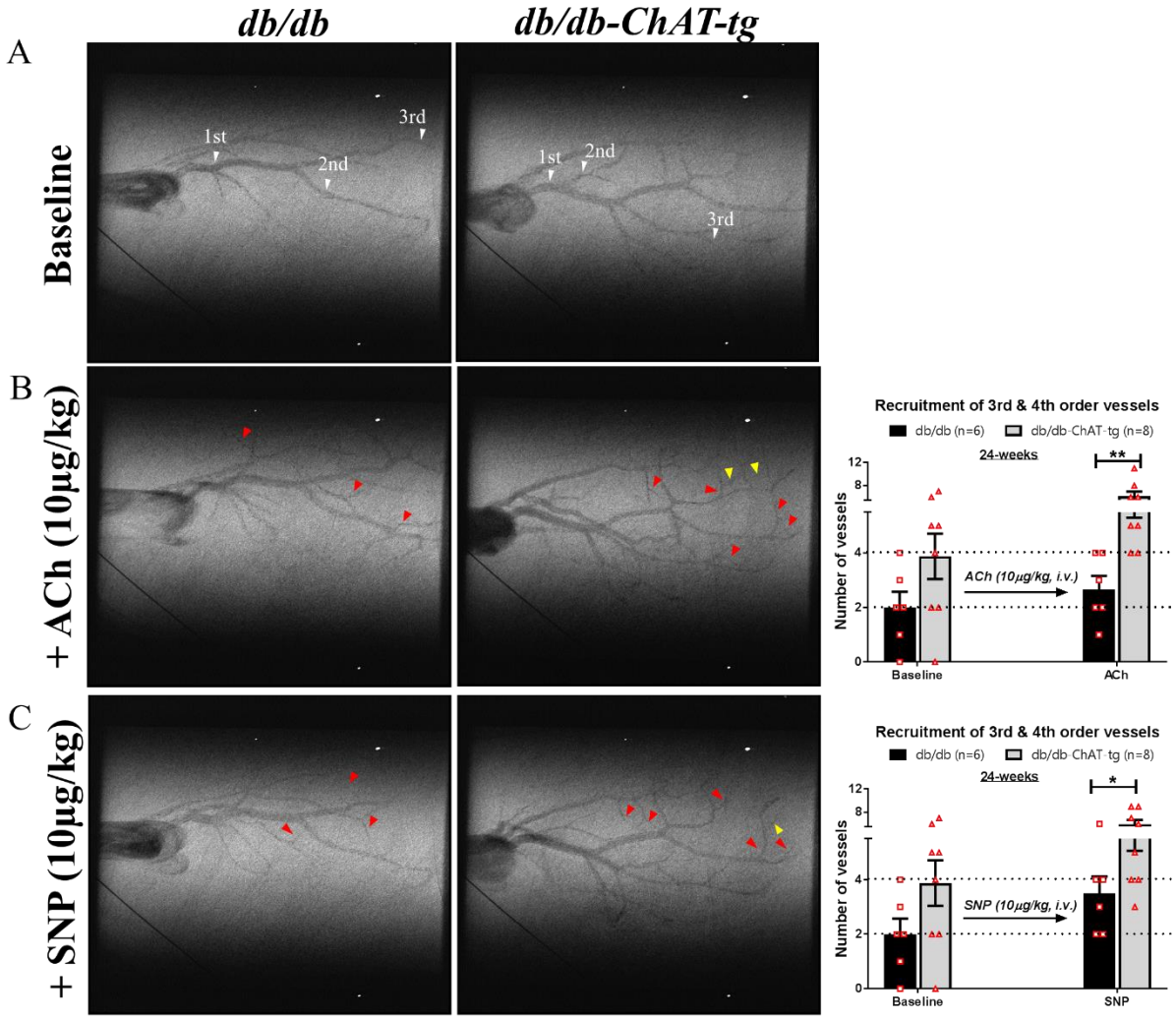

Figure 4.13 The effect of ACh and SNP on recruiting the small coronary vessels in *db/db* and *db/db-ChAT-tg* mice at 24-weeks of age.
Representative microangiogram images and bar graphs with scatter plots showing the number of third and fourth-order coronary vessels in the db/db and db/db-ChAT-tg mice at 24-weeks of age ***(A)*** *under baseline condition****, (B)*** *after ACh infusion (10 µg/kg/min) and* ***(C)*** *after SNP infusion (10 µg/kg/min). Red arrows indicate third-order coronary vessels, while yellow arrows indicate fourth-order coronary vessels. Data are presented as mean ± SEM. A non-parametric Mann-Whitney U test was performed. *p<0.05; **p<0.01 VS aged-matched db/db mice after ACh or SNP infusion. The number of samples per group is indicated in the figure.*

4.4.3.2 Coronary microvasculature

To further support the observation of an increased number of coronary vessels in the *db/db-ChAT-tg* mice, the microvascular density (i.e., the number of capillaries and arterioles) was examined by immunofluorescence analysis. This method was performed to accurately detect endothelial cells (Isolectin) as well as the smooth muscle cells (anti-αSMA antibody). Arterioles were identified by positive staining for Isolectin and αSMA, whereas capillaries were positive only for Isolectin.

The diameter of arterioles was measured and sorted into two groups – large arterioles (>50 μm) and small arterioles (<50 μm). The analysis revealed that the number of large arterioles was comparable between the *db/db* and *db/db-ChAT-tg* mice at 12- and 24-weeks of age (Figure 4.14). The number of small arterioles in the *db/db-ChAT-tg* mice was not different from the *db/db* mice at 12-weeks of age (Figure 4.14). There was an increasing trend in the number of small arterioles of the *db/db-ChAT-tg* mice compared to that of the *db/db* mice at 24-weeks of age. However, this was not statistically significant. The image of the secondary antibody-only control is shown in Appendix 4 (Figure S4.1).

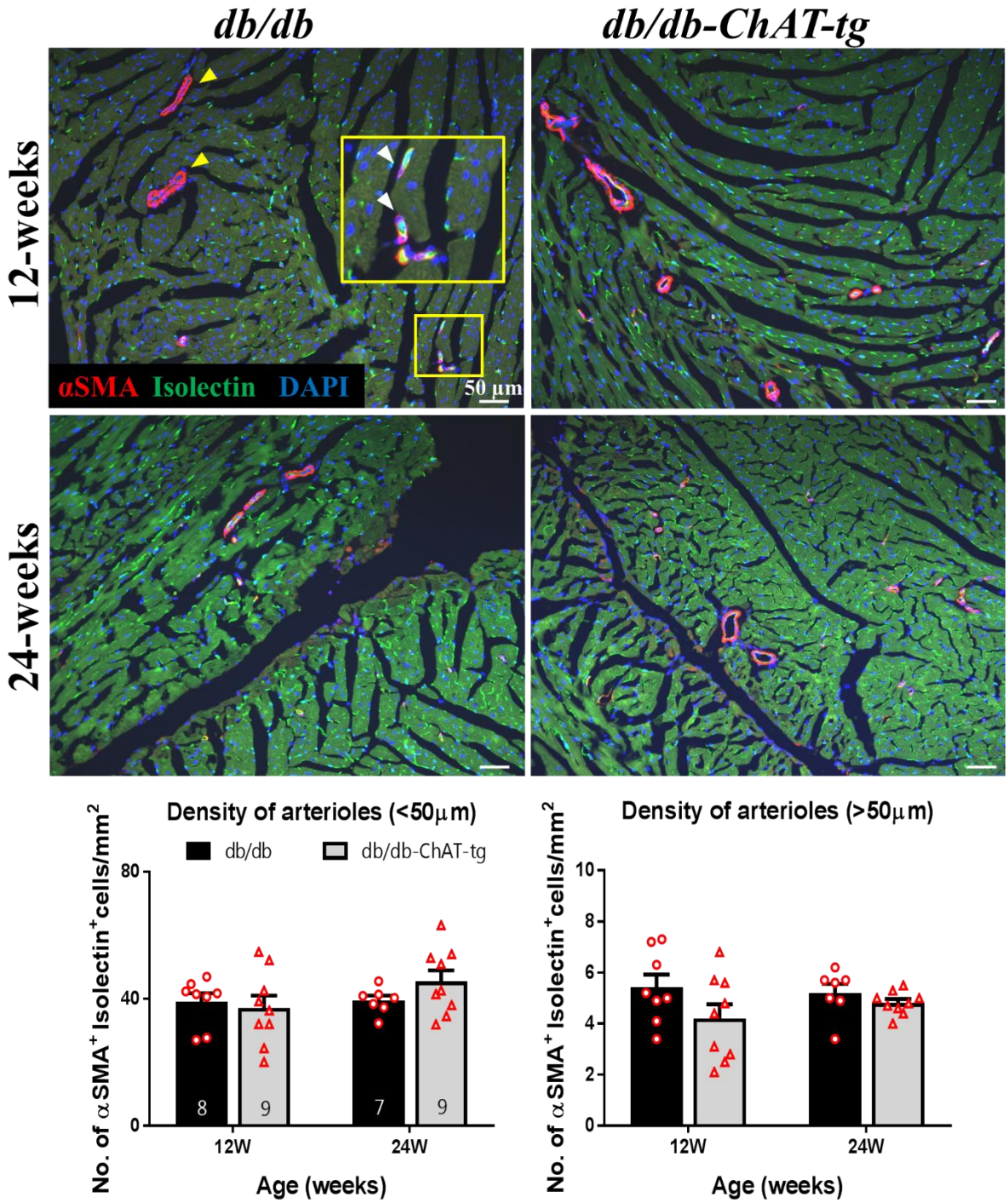

Figure 4.14 The effect of cardiac NNCS on the density of large and small arterioles.
Representative fluorescent images and bar graphs with scatter plots showing the density of large and small arterioles as indicated by the number of αSMA- and Isolectin-stained smooth muscle cells in the ventricular tissue of db/db and db/db-ChAT-tg mice at 12- and 24-weeks of age. Data are presented as mean ± SEM. A non-parametric Mann-Whitney U test was performed. Yellow arrows indicate large arterioles (>50 µm) while white arrows indicate small arterioles (<50 µm). The number of samples per group is indicated in the figure.

While the number of capillaries was comparable between the *db/db* and *db/db-ChAT-tg* mice at 12-weeks of age, this was significantly higher in the *db/db-ChAT-tg* mice at 24-weeks of age

(Figure 4.15). The image of the secondary antibody-only control is shown in Appendix 4 (Figure S4.1).

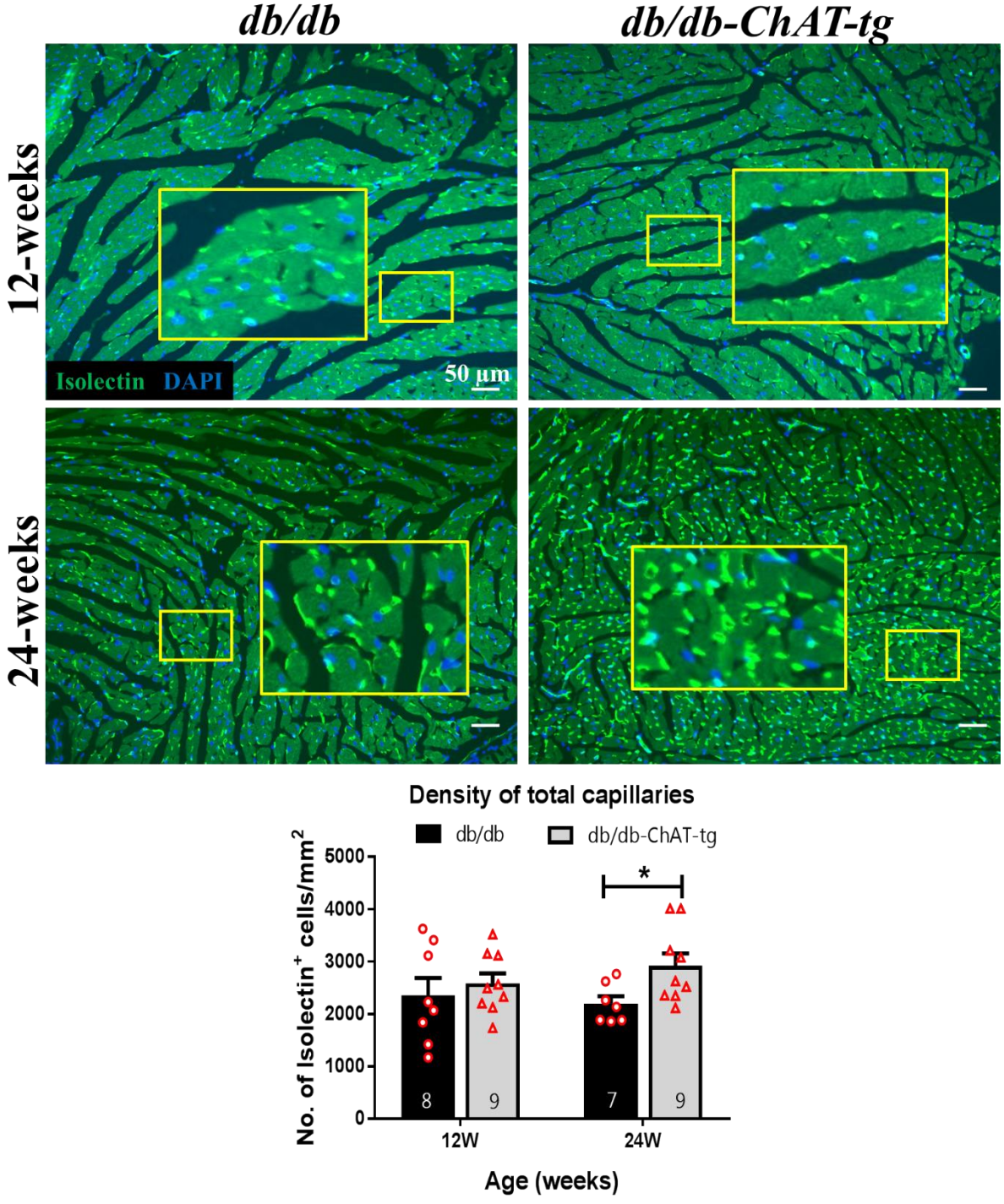

Figure 4.15 The effect of cardiac NNCS on the density of capillaries.
*Representative fluorescent images and bar graphs with scatter plots showing the density of capillaries which indicated by the number of Isolectin-stained endothelial cells in the ventricular tissues of db/db and db/db-ChAT-tg mice at 12- and 24-weeks of age. Data are presented as mean ± SEM. A non-parametric Mann-Whitney U test was performed. *p<0.05 VS aged-matched db/db mice. The number of samples per group is indicated in the figure.*

4.4.3.3 Molecular alterations associated with improved vascular function

Having demonstrated that increased number of coronary vessels and microvessels in the *db/db-ChAT-tg* mice, the next aim was to identify if VEGF-A contributed to the enhanced angiogenic effect since VEGF-A is a direct downstream target of a HIF1 transcription factor.

The anti-VEGF-A antibody used in my study is polyclonal and resulted in multiple bands on blot (Appendix 2, Figure S2.7). However, there was only a band with strong intensity detected in between 20 kDa and 25 kDa. Thus, I identified this band as VEGF-A positive. Data analysis revealed that VEGF-A protein expression was significantly increased by 0.1-fold in the *db/db-ChAT-tg* mice in comparison to the *db/db* mice at 12-weeks of age (Figure 4.16). The protein expression of VEGF-A in the ventricles of *db/db-ChAT-tg* mice was comparable to that of *db/db* mice at 24-weeks of age.

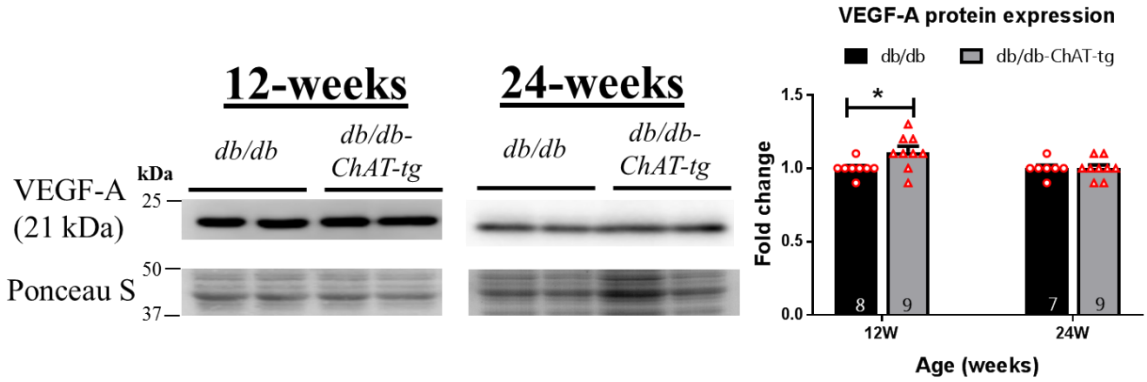

Figure 4.16 Activation of cardiac NNCS induced increased VEGF-A protein expression in 12-weeks old *db/db-ChAT-tg* mice.
*Representative blots and bar graphs with scatter plots showing the protein expression of VEGF-A in the db/db and db/db-ChAT-tg mice at 12- and 24-weeks of age. Data are presented as mean ± SEM. A non-parametric Mann-Whitney U test was performed. *p<0.05 VS age-matched db/db mice. The number of samples per group is indicated in the figure.*

4.5 Discussion

In this chapter, the *db/db-ChAT-tg* mouse model was used to examine the effect of overexpressing *ChAT* gene in the diabetic heart. The metabolic profile, such as body weight and blood glucose level of the *db/db-ChAT-tg* mice, was recorded. The LV function, vascular function as well as the key protein targets that are involved in cardiac NNCS-mediated signaling

(ChAT and M_2AChR), pro-survival signaling pathway (Akt, HIF1α, and GLUT-4), energy homeostasis (AMPKα) and angiogenesis (VEGF-A) were examined. I hypothesized that ventricular-specific overexpression of *ChAT* gene would lead to activation of PI3K/Akt/HIF1α/GLUT-4 signaling pathway to promote glucose metabolism, thus improving cardiac function of the diabetic heart. Also, I hypothesized that ventricular-specific overexpression of *ChAT* gene would lead to an increase in VEGF-A expression and promote angiogenesis, thus improving vascular function and in turn, enhancing the cardiac function of the diabetic heart. The main findings of this study can be summarized as follows:

1. **Metabolic profiles:**

- The body weight was significantly decreased in the *db/db-ChAT-tg* mice at 12-weeks of age.
- The blood glucose level was significantly decreased in the *db/db-ChAT-tg* mice at 8- to 16-weeks of age.

2. **Cardiac function:**

- LV systolic function (i.e., ESV and ESP) and contractility (i.e., SV, CO, and EF) were improved in the *db/db-ChAT-tg* mice at 8- to 20-weeks of age.
- Molecular alterations associated with improved LV function in the *db/db-ChAT-tg* mice:
    - Activation of cardiac NNCS and ACh-M_2AChR mediated signaling:
        - *Increased ChAT protein expression at 8- to 20-weeks of age*
        - *Prevention of decreased M_2AChR protein expression at 16- to 20-weeks of age*
    - Activation of cardiac NNCS-mediated pro-survival PI3K/Akt/HIFIα/GLUT-4 signaling cascade:
        - *Increased phosphorylation level of Akt at 8- to 20-weeks of age*

        - *Increased HIF1α protein expression at 8- and 20-weeks of age*
        - *Increased GLUT-4 protein expression at 8- to 20-weeks of age*
    - Energy homeostasis in the ventricles:
        - *Decreased phosphorylation level of AMPKα at 8- to 16-weeks of age*

3. **Vascular function:**

- The number of coronary vessels was increased in the *db/db-ChAT-tg* mice
- No significant increase in the diameter of coronary vessels in the *db/db-ChAT-tg* mice
- ACh and SNP did not change the diameter of coronary vessels in the *db/db-ChAT-tg* mice
- ACh and SNP-induced vasodilation revealed an increase in the number of third and fourth-order of coronary vessels in the *db/db-ChAT-tg* mice at 24-weeks of age.
- Increased number of capillaries in the *db/db-ChAT-tg* mice was observed at 24-weeks of age.
- This improved vascular function in the *db/db-ChAT-tg* mice was associated with increased VEGF-A protein expression at 12-weeks of age.

4.5.1 Activation of cardiac NNCS improved LV function of *db/db* mice

Kakinuma et al. [100] showed that ventricular-overexpression of *ChAT* gene in a normal heart did not alter the LV diastolic, systolic function, and contractility of *ChAT-tg* mice. While in my study, the ChAT transgene in the diabetic heart augmented the cardiac function (Figure 4.2 & 4.3). One possible reason for this could be because the *db/db* mice spontaneously developed cardiac dysfunction and hence the effect of ChAT transgene on cardiac function was evident in the *db/db-ChAT-tg* mice. Conversely, the effect of ChAT transgene was not evident in the mice that displayed normal cardiac function in the study performed by Kakinuma et al [100].

The clinical assessment of diastolic function relies on a few variables such as early and late mitral flow velocity (E' and A'), mitral annular early diastolic velocity (e'), E/A ratio, E/e' ratio as well as the deceleration time of E' [245-248], while the clinical assessment of systolic function is assessed by the measurement of EF, FS, CO and SV [249-251]. In my study, the measurement of diastolic function was based on EDV and EDP and there were not evident changes in these indices in the *db/db-ChAT-tg* mice (Figure 4.2A&B). However, the limitation of pressure-volume loop method is that it only measures the pressure and volume, and hence, these results may not be conclusive enough to determine the diastolic function of the *db/db-ChAT-tg* mice. Therefore, it would be crucial to perform echocardiography to assess the E/A ratio and deceleration time of E' on the *db/db-ChAT-tg* mice in future study. Apart from this, the LV systolic function (indicated by ESP and ESV; Figure 4.2C&D), as well as contractility (indicated by CO, SV, and EF; Figure 4.3B-D), were significantly enhanced in the *db/db-ChAT-tg* mice. Taken together, the overall findings suggest that activation of cardiac NNCS enhances the LV systolic function and contractility of the diabetic heart. The underlying mechanism for this beneficial effect is contributed by enhanced GLUT-4 and VEGF-A expression as induced by pro-survival PI3K/Akt/ HIF1α signaling pathway [100]. This is discussed in the following sections.

On a side note, the measurement of cardiac function was performed under 1% - 2% isoflurane via inhalation (Appendix 4). Isoflurane and other common inhalational anesthesia such as desflurane as well as intravenous anesthetics such as barbiturates are known to influence cardiac function and hemodynamics [252-255]. However, the influence of isoflurane to the cardiac function of mice used in this study should be minimal as previous studies showed that isoflurane concentration titrated between 0.5% - 2% did not induce significant effect on cardiac function [252, 253].

4.5.1.1 Cardiac NNCS activated PI3K/Akt/HIF1α/GLUT-4 signaling pathway

As discussed in Chapter 1 and 3, ACh-initiated mAChR signaling leads to the activation of pro-survival PI3K/Akt/HIF1α signaling pathway [100, 120, 125]. Although it is still not known which subtype of mAChR is responsible for initiating this signaling pathway, M_2AChR may involve in this as this subtype is the most abundant mAChR in the heart [111, 179, 186, 187]. Further, the non-neuronal effect of ACh-mAChR mediated signaling includes an increase in GLUT-4 expression via activation of PI3K/Akt/HIF1α signaling cascade [96, 100].

In the *db/db-ChAT-tg* mice, decreased M_2AChR expression was prevented at 16- and 20-weeks of age (Figure 4.5). Such prevention indicates that the non-neuronal effects mediated through ACh-M_2AChR interaction were possibly restored after activation of cardiac NNCS. Of note, normalization of M_2AChR expression was also observed in the *db/db* mice at 16-weeks. This finding contrasts with the outcome from Chapter 3 that showed a persistent reduction of M_2AChR expression in the *db/db* mice (Figure 3.7B). Although the reason for this is not known, this could be caused by the composition of food pellet used in the animal facility of University of Otago (**6.2% fat**, 3.5% fiber and 18.6% protein) that is different from the food pellet used in the Japanese animal facility (**4.5% fat**, 5.05% fiber and 25.1% protein). Thus, it is logical to postulate that the *db/db* mice that fed with lower fat content (in Japan) would develop diabetes-induced complications at a slower rate, and the molecular alteration may be different [256-258]. One possible future experiment could be performed is to feed the *db/db* mice originated from New Zealand and Japan with the food pellets used in New Zealand and Japanese animal facility, respectively. The outcome of this experiment could provide insight whether the composition of diet does influence the expression changes in M_2AChR.

Kakinuma et al. [100] showed that ventricular-specific overexpression of *ChAT* gene resulted in increased cardiac ACh content, the phosphorylation level of Akt (threonine 308), HIF1α and GLUT-4 expression in the *ChAT-tg* mice, indicating activation of PI3K/Akt/HIF1α/GLUT-4 signaling cascade mediated by ACh from the cardiomyocytes. In line with this, my study

showed an increase in the phosphorylation level of Akt (serine 473; Figure 4.6), HIF1α (Figure 4.7) and GLUT-4 expression (Figure 4.8) in the *db/db-ChAT-tg* mice compared to that of the age-matched WT and *db/db* mice. These findings support that the pro-survival PI3K/Akt/HIF1α/GLUT-4 signaling cascade was activated in the *db/db-ChAT-tg* mice.

On a side note, normalizing the phosphorylated protein expression to its respective total protein expression is generally a well-accepted approach. However, the outcome derives from this approach may not necessarily reflect the actual phosphorylated protein expression when the expression of total protein expression changes. In particular, the blot shows that the phosphorylation level of Akt was unchanged while total Akt expression was decreased in the *db/db* and *db/db-ChAT-tg* mice at 8-weeks of age (Figure 4.6 and additional image in Appendix 4, Figure S4.2). This suggests that T2DM decreases total Akt expression without affecting the phosphorylation capacity in the diabetic cardiomyocytes. To further confirm this, future study can consider performing enzyme-linked immunosorbent assay (ELISA) to detect the phosphorylated Akt or biochemical assay to detect the activity of Akt.

Besides, the phosphorylation level of Akt was increased in the *db/db* mice in comparison to the ND mice (Figure 4.6). In line with this, Cook et al. [61] showed that the basal phosphorylation level of Akt was increased in the *ob/ob* mouse model. Further, they demonstrated that GLUT-4 vesicle dysfunction contributed to the decreased sarcolemmal GLUT-4 expression in the T2DM patients and *ob/ob* mouse model, while the proximal insulin signaling was activated (i.e., IRS1 and PI3K) and functional in the diabetic heart [61]. However, the findings from my study and Cook et al. [61] are in contrast to other studies [259-261] that reported impaired insulin signaling cascade in the diabetic mouse model. The reason for this discrepancy is unknown, but this could relate to chronicity and severity of diabetes.

4.5.1.2 Normalization of GLUT-4 expression to restore glucose metabolism and energy level

Reduction in GLUT-4 expression decrease glucose uptake and oxidation in the diabetic heart [56-63, 79]. Previous studies showed that global overexpression of *GLUT-4* gene effectively decreased blood glucose level and alleviated insulin resistance in the *db/db* mice [20, 262] and diet-induced insulin resistance mice [263]. Further, increased GLUT-4 expression enhanced glycolysis and glucose oxidation as well as suppressed palmitate oxidation in the diabetic heart, and thereby preventing diabetes-induced cardiac dysfunction [20, 69]. Thus, this suggests that targeting GLUT-4 to rectify cardiac metabolism and prevent cardiac dysfunction can be a therapeutic option. In my study, GLUT-4 expression was significantly increased in the *db/db-ChAT-tg* mice (Figure 4.8) together with improved LV systolic function and contractility (Figure 4.2 & 4.3). Although cardiac glucose content, rate of glycolysis and glucose oxidation were not measured in the study, it is possible that increased GLUT-4 expression enhanced glucose metabolism and thus improving LV function in the *db/db-ChAT-tg* mice.

Besides, glucose metabolism augments ATP production in comparison to FFA metabolism, thus allowing the heart to cope with increased cardiac workload efficiently [264]. Although the cardiac ATP content was not measured in the present study, the phosphorylation level of AMPKα could provide a link to the energy status. The decreased phosphorylation level of AMPKα in the *db/db* and *db/db-ChAT-tg* mice (8- to 16-weeks of age) indicated that AMPK was inactivated possibly due to low AMP/ATP ratio (Figure 4.9) [222]. Notably, the phosphorylation level of AMPKα in *db/db-ChAT-tg* mice was further decreased in comparison to the age-matched *db/db* mice, suggesting that the AMP/ATP ratio was lower (i.e., energy preservation) and this could be associated with increased GLUT-4 expression. At 20-weeks of age when cardiac dysfunction began to develop in the *db/db* mice [1], the phosphorylation level of AMPKα in *db/db-ChAT-tg* mice was similar to that of the WT heart, and this again could be caused by increased GLUT-4 expression. Thus, this may support the postulation that the ATP

production could be augmented due to increased glucose uptake in the *db/db-ChAT-tg* mice. However, the measurement of cardiac ATP and glucose content is undoubtedly required to support this postulation.

Besides, previous studies reported that defective AMPK activation contributes to impaired glucose utilization in the diabetic heart [226, 227, 265, 266]. However, the phosphorylation of AMPKα in *db/db* mice at 20-week of age is not clear as two normalization approaches resulted in contradictory result. Whether T2DM induces an increase (in the case of normalizing to Ponceau S stained blot), or, a decrease in the phosphorylation of AMPKα (in the case of normalizing to total AMPKα expression), this need to be clearly examined in future. An ELISA assay to detect phosphorylated AMPKα or biochemical assay to detect the activity of AMPK can be considered.

4.5.2 Activation of cardiac NNCS preserved coronary vasculature and improved vascular function of *db/db* mice

The angiogram showed that the heart of *db/db-ChAT-tg* mice generally exhibited an increased number of coronary vessels as compared to the *db/db mice* at both 12- and 24-weeks of age (Figure 4.10). Importantly, there was a decreasing trend in the number of second, third and fourth-order coronary vessels in the 24-weeks old *db/db* mice compared to that of the 12-weeks old *db/db* mice. This observation was consistent with the study performed by Katare et al. [16] who showed a decreasing trend in the number of coronary vessels in the *db/db* mice with the progression of age. Conversely, the number of second, third, and fourth-order coronary vessels remained similar in the 24-weeks old *db/db-ChAT-tg* mice as compared to that of the 12-weeks old *db/db-ChAT-tg* mice. These results suggest that *in-vivo* activation of cardiac NNCS prevented a decline in the number of coronary vessels. Importantly, these findings also indicate that the blood and oxygen delivery to the myocardium was improved in the *db/db-ChAT-tg* mice in comparison to the *db/db* mice.

Apart from this, the diameter of coronary vessels in the *db/db-ChAT-tg* mice was increased in the baseline condition, although the changes were not statistically significant (Figure 4.11A&B). While the reason for this is not known, Oikawa et al. [267] showed that the cardiac ACh and nitric oxide (NO) were significantly increased after overexpression of the *ChAT* gene. An increase in NO production was resulted from the ACh-muscarinic receptor stimulation [99, 268, 269]. Although cardiac NO and ACh content were not measured in the present study, the effect of increased vascular diameter may indicate a possibility that endogenous ACh- and NO-induced vasodilation in the *db/db-ChAT-tg* mice under baseline condition [270, 271].

Previous studies demonstrated coronary endothelial dysfunction as indicated by blunted ACh-induced change in the diameter of coronary vessels in the *db/db* mice [16, 272, 273]. While in my study, the findings showed that exogenous addition of ACh- and SNP-induced diameter changes were comparable between the *db/db* and *db/db-ChAT-tg* at 12- and 24-weeks of age respectively (Figure 4.12). This result could again indicate that the diameter of coronary vessels in *db/db-ChAT-tg* mice may have already been increased under baseline condition, and thus, the changes induced by ACh and SNP were not evident. Therefore, future study should consider using vasoconstrictor such as phenylephrine to examine the magnitude of the diameter's changes, which in return will provide information on whether the coronary vessels are partially, or entirely wider in the *db/db-ChAT-tg* mice under baseline condition. Nonetheless, the exogenous addition of ACh and SNP did further increase the number of third and fourth-order coronary vessels in the *db/db* and *db/db-ChAT-tg* mice (Figure 4.13A&B). Notably, the increase in the number was minimal in the *db/db* mice after ACh infusion (Figure 4.13A), comparing to the increase in number after SNP infusion (Figure 4.13B). This result suggests endothelial dysfunction in the *db/db* mice. Conversely, the *db/db-ChAT-tg* mice exhibited a significant increase in the number of third and fourth-order coronary vessels after ACh and SNP infusion, indicating preserved endothelial function.

Hinkel et al. [274] reported the density of capillary was significantly reduced in the diabetic swine model and diabetic human with HF. In line with this, Teng et al. [275] reported that capillary rarefaction was observed in the pre-diabetic, T1DM, and T2DM mouse model. These findings indicate that microvascular rarefaction plays a role in the pathogenesis of DHD. While in my study, the density of capillaries was significantly increased in the *db/db-ChAT-tg* mice at 24-weeks of age in comparison to the *db/db* mice (Figure 4.15). This result suggests that the microvascular rarefaction was attenuated in the *db/db-ChAT-tg* mice. This result is also in agreement with Kakinuma et al. [100], who showed that activation of cardiac NNCS increased the number of endothelial cells in the ventricles, indicating enhanced microvasculature. Thus, my findings demonstrate that *in-vivo* activation of cardiac NNCS via overexpression of *ChAT* gene preserved endothelial function and maintained coronary macro- and microvasculature in the *db/db-ChAT-tg* mice.

4.5.2.1 Increased VEGF-A expression to maintain coronary vasculature

Coronary vascular rarefaction is associated with decreased proangiogenic factor VEGF expression in the diabetic animal model as well as diabetic human [137, 276, 277]. In particular, Rawal et al. [137] demonstrated that reduced VEGF-A protein expression (at 12-weeks of age) preceded the reduction in capillaries and small arterioles (<50 µm; at 20-weeks of age) in the *db/db* mice. In my study, the findings showed that the VEGF-A expression was significantly increased in the *db/db-ChAT-tg* mice at 12-weeks of age (Figure 4.16). As the improvements in coronary vasculature (Figure 4.10), endothelial function (Figure 4.12) and microvasculature (Figure 4.14 & 4.15) were only evident in the *db/db-ChAT-tg* mice at 24-weeks of age, but not the 12-weeks of age, these results suggest that early restoration of VEGF-A could prevent the development of vascular dysfunction and rarefaction in the diabetic heart.

The increase in VEGF-A expression was likely initiated by activation of PI3K/Akt/HIF1α signaling cascade through cardiac NNCS [100], as *VEGF-A* gene is the direct downstream

target of HIF transcription factor [100, 215, 269, 278]. In line with this, Xue et al. [215] demonstrated that cardiac-specific overexpression of *HIF1α* gene increased VEGF expression and the number of capillaries in the T1DM mice. Therefore, this supports that cardiac NNCS activation increased VEGF-A expression, which in turn mediates paracrine signaling in the endothelial cells and leads to angiogenesis in the *db/db-ChAT-tg* mice. Further, this molecular alteration may contribute to the improved LV function in the *db/db-ChAT-tg* mice by improving blood and oxygen delivery to the myocardium to sustain the myocardial perfusion.

4.5.3 Activation of cardiac NNCS reduced body weight and blood glucose level in the *db/db* mice

Another observation from my study was the reduction of bodyweight and blood glucose level in the *db/db-ChAT-tg* mice. In generally, the blood glucose level of a normal healthy mouse is typically 100 to 200 mg/dL [279]. In my study, the blood glucose level ranged from 353.8 to 449.9 mg/dL in *db/db* mice and 269.5 to 319.4 mg/dL in *db/db-ChAT-tg* mice at the age of 8- to 20-weeks old (Figure 4.1B).

The underlying mechanism of these extra-cardiac effects are not clear. Oikawa et al. [267, 280] reported that ventricular-specific overexpression of *ChAT* gene resulted in an activation of CNS via afferent vagus nerve. Such heart-brain crosstalk was evident by increased c-Fos signal in the medulla and increased norepinephrine (NE) level in the hypothalamus [267]. Previous studies showed that hypothalamic NE plays a role in suppressing food intake [281, 282]. Therefore, it may be logical to postulate that weight loss and decreased blood glucose level observed in the *db/db-ChAT-tg* mice could be due to suppressed food intake as a result of increased hypothalamic NE. Besides, recent report from Oikawa et al. [280] proposed that ventricular-specific overexpression of *ChAT* gene led to anti-inflammatory response by Kupffer cells in the liver through hepatic vagus nerve (i.e. heart-brain-liver crosstalk). Thus, I speculate that the heart-brain crosstalk may transmit efferent signal to peripheral organs to promote

glucose uptake, thereby reducing the blood glucose level. However, as this is out of the scope of the present study, more in-depth investigation is required to elucidate the underlying mechanism for these effects.

4.6 Limitations

4.6.1 Assessing the cardiac ACh, glucose and ATP content

The myocardial tissues from *db/db* and *db/db-ChAT-tg* mice were prioritized for western blot analysis instead of other analyses such as measurement of cardiac ACh, glucose, and ATP content. Thus, this study was not able to provide functional evidence that *in-vivo* activation of cardiac NNCS increases cardiac glucose content and preserves ATP in the diabetic heart.

4.6.2 Aging effect in the *db/db* and *db/db-ChAT-tg* mice

As explained in Chapter 3 (section 3.6.4), comparison of expression changes of the same protein target between different age groups had to be omitted as the experimental condition could vary from time to time. However, it is undeniable that aging is one of the factors that could alter the expression changes. Thus, the experimental setup of the future study should consider this factor.

4.6.3 Assessing the role of GLUT-1

It is well established that *GLUT-1* gene is the direct downstream target of HIF1 transcription factor [130] and Kakinuma et al. [100] has also reported that GLUT-1 protein expression was increased in the *ChAT-tg* mice via western blot analysis. Further, it has also been shown that cardiac-specific overexpression of GLUT-1 prevented the development of HF in the animal model, suggesting an essential role of GLUT-1 in cardiovascular disease [283]. However, as the present study only focused on the functional role of GLUT-4, the future study may consider assessing the role of GLUT-1.

4.6.4 Assessing membrane GLUT-4 expression

As explained in Chapter 3 (section 3.6.5), the measurement of membrane GLUT-4 expression could have provided further insight on the function of GLUT-4 in transporting glucose in the cardiomyocytes. However, the separation of cytosolic and membrane protein was not initially planned. Thus, this is one of the limitations of the study. Future study should carefully design the experimental layout and consider this factor.

4.6.5 Specificity of antibodies

For immunofluorescence analysis, anti-αSMA antibody conjugated with Cy3™ was used as a marker for smooth muscle cells. However, the specificity of this antibody was not tested as this antibody is no longer available in the laboratory. Thus, this is one of the limitations of the study. For western blot analysis, the identification/quantification of the ChAT-, M_2AChR- and GLUT-4-positive band was consistent as described in Chapter 3. However, due to limited resources and time, there was no additional control experiment to test the specificity of anti-GLUT-4 antibody as well as anti-pAKT, anti-AKT, anti-pAMPKα, anti-AMPKα, anti-HIF1α and anti-VEGF-A antibodies used in this study. This is one of the limitations of the study. Future study should consider testing the antibody on purified antigen, overexpressing or knockout tissue/cells.

4.6.6 Sample size

As specified in Chapter 3, power analysis was not performed prior to the experiments. This may explain why I often observed an increasing or decreasing trend in protein expression, the number of coronary vessels, diameter changes and density of arterioles, and yet, these changes were not statistically significant. For example, to effectively detect the significant changes in M_2AChR expression in the *db/db-ChAT-tg* mice in comparison to the ND mice at 8-weeks of age (Figure 4.5), power analysis revealed that 11 mice per groups are required (80% power).

Also, to effectively detect the significant changes in the number of second order coronary vessels in *db/db* mice at 12- and 24-weeks of age (Figure 4.10), power analysis revealed that nine mice per group are required (80% power; https://clincalc.com/stats/samplesize.aspx). Future study should consider performing power analysis to determine the sample size required to detect significant expression changes.

4.7 Conclusion

Based on the overall findings from this study, I confirm the hypothesis that ventricular-specific overexpression of *ChAT* gene would in turn mediates PI3K/Akt/HIF1α/GLUT-4 signaling pathway to promote glucose metabolism, thus improving cardiac function of the diabetic heart (Figure 4.17). In addition to this, I also confirm the hypothesis that ventricular-specific overexpression of *ChAT* gene would lead to an increase in VEGF-A expression and promote angiogenesis, thus improving vascular function and in turn enhancing the cardiac function of the diabetic heart (Figure 4.17). The use of this unique transgenic model confirms the potential for modulating cardiac NNCS to improve cardiovascular capacity and prevent the development of DHD. However, as the current study only focused on *db/db-ChAT-tg* mice at 8- to 24-weeks of age, further work is certainly required to examine how activation of cardiac NNCS could involve in the late progression of diabetes mellitus (or geriatric diabetic mice – 18 to 24 months old [284]).

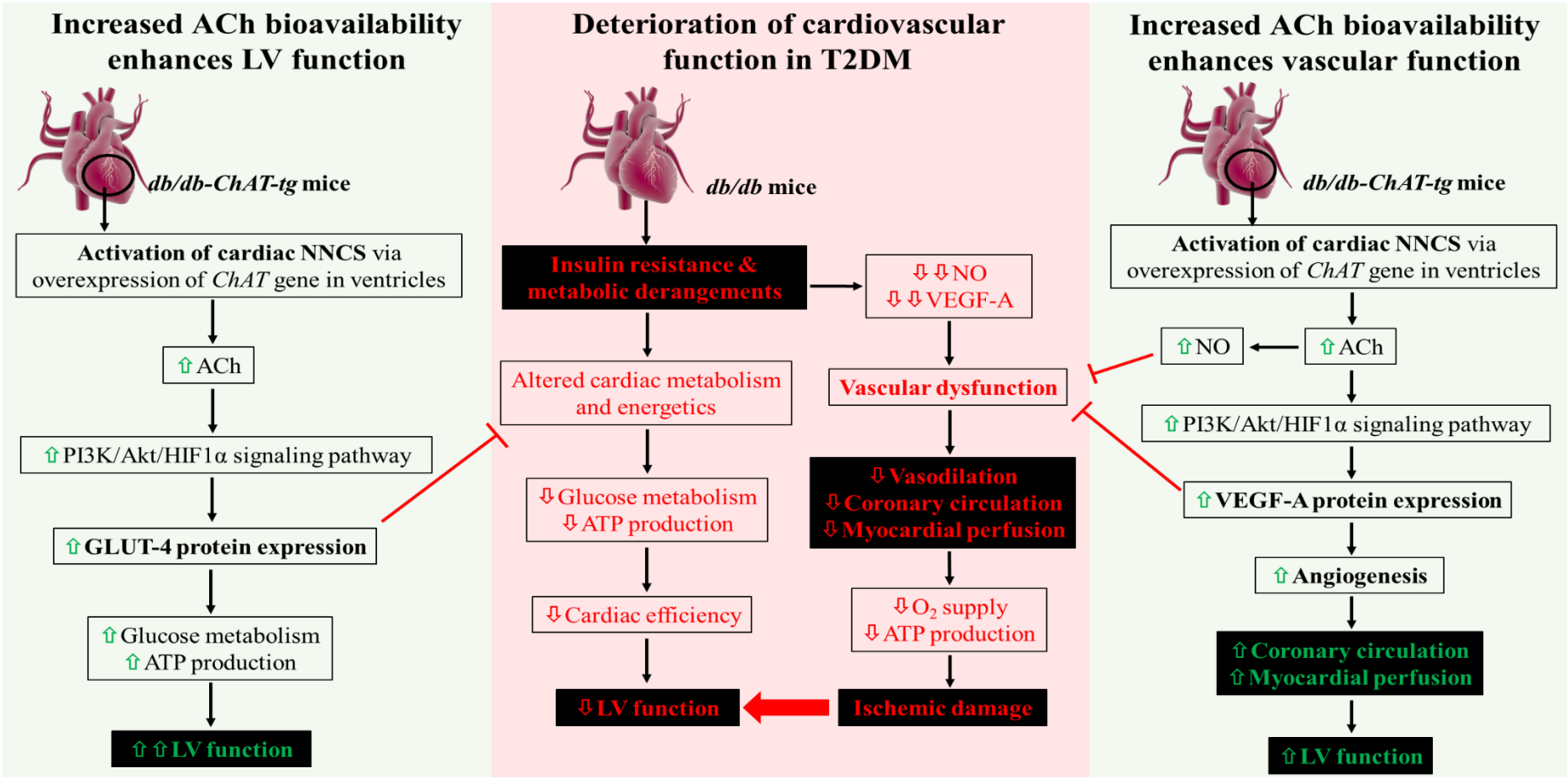

Figure 4.17 The beneficial effect of increased ACh bioavailability in the diabetic heart.

Activation of cardiac NNCS via overexpression of the ChAT gene in the ventricles increases ACh bioavailability, which in-return releases and binds to M_2AChR to mediate PI3K/Akt/HIF1α signaling cascade in an auto/paracrine manner. Initiation of this signaling cascade leads to increased GLUT-4 protein expression, which is responsible for glucose uptake in the heart. Such alteration restores the metabolic flexibility and rectifies the cardiac metabolism of diabetic cardiomyocytes, thus normalizing ATP production and maintaining the contractile function efficiently. Besides, the initiation of PI3K/Akt/HIF1α signaling cascade leads to increased VEGF-A protein expression, which is a paracrine mediator responsible for angiogenesis. Such alteration maintains vasculature and increases the number of macro- and micro-coronary vessels in the diabetic heart, thus improving coronary circulation and myocardial perfusion. The improved vascular function in-return improves the cardiac function of the diabetic heart.

Chapter 5 : The effect of cardiac NNCS activation in the diabetic AC16 cells in hypoxia

5.1 Introduction

The findings from Chapter 4 showed that activation of cardiac NNCS via overexpression of the *ChAT* gene enhanced the cardiovascular function of the diabetic mouse heart. However, it is not known if cardiac NNCS-induced upregulation of GLUT-4 could alleviate the damage in the diabetic heart in the event of myocardial ischemia. Therefore, in this chapter, the *in-vitro* study was designed to investigate the protective effect of cardiac NNCS activation in diabetic cardiomyocytes under the hypoxic condition to mimic ischemic insult.

5.1.1 Myocardial Insulin signaling pathway in the normal and diabetic heart

In the adult heart, GLUT-4 is the key glucose transporter for glucose uptake [285]. Under the basal condition, GLUT-4 resides in the intracellular vesicles, and it can be translocated to the membrane by insulin. As shown in Figure 5.1, insulin binds to the insulin receptor (IR) and leads to autophosphorylation of the receptor's β subunit (IRβ). The activated IR binds to and phosphorylates insulin receptor substrate family proteins (IRS1-3), which in turn binds and recruits PI3K to the cellular membrane. PI3K phosphorylates phosphatidylinositol 4,5-biphosphate (PIP_2) to phosphatidylinositol-3, 4,5-triphosphate (PIP_3), which in turn activates phosphoinositide-dependent protein kinase 1 (PDK1). PDK1 phosphorylates Akt and activated Akt subsequently phosphorylates Rab GTPase-activating protein AS160, causing dissociation of AS160 from GLUT-4 containing vesicles. This dissociation initiates GLUT-4 containing vesicles to translocate and fuse with the plasma membrane, thus promoting glucose uptake (reviewed in [175, 286]).

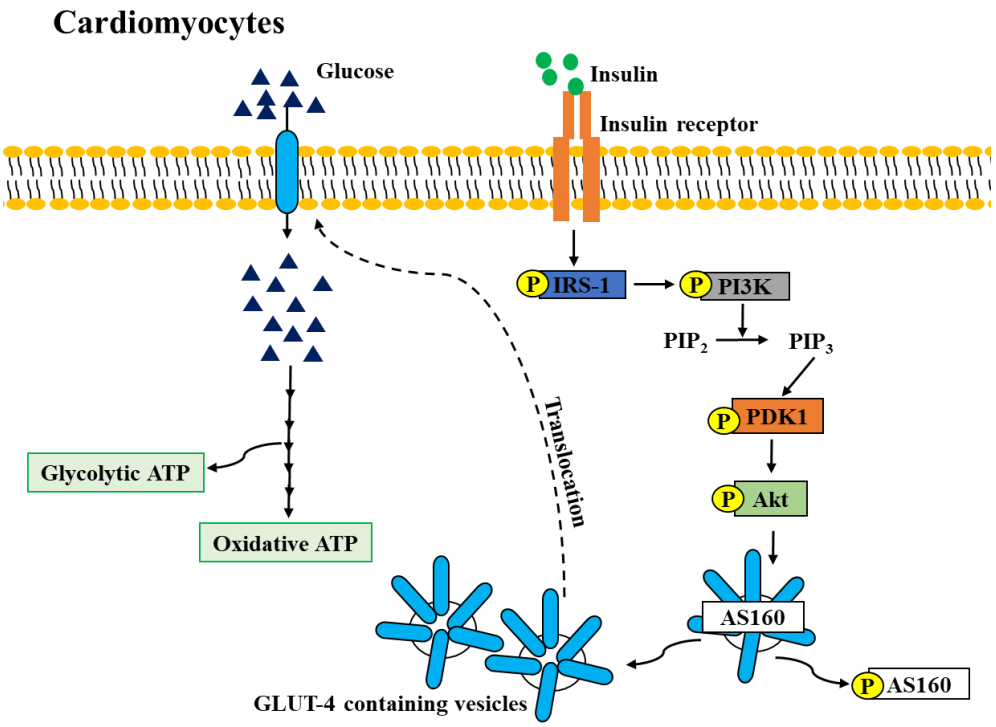

Figure 5.1 Insulin-mediated glucose uptake signaling pathway
Insulin binds to the IR and activates IRS1/PI3K/Akt signaling cascade. Activated Akt phosphorylates AS160, and thus dissociating AS160 from the GLUT-4 containing vesicles. This dissociation allows the vesicles to be translocated and fused with the plasma membrane to promote glucose uptake.

Myocardial insulin resistance is characterized by the impaired biologic response to insulin stimulation, thus decreasing insulin-stimulated glucose uptake in the diabetic heart [287]. This defect can be caused by decreased protein expression of IRβ and IRS1 [288], increased inhibitory phosphorylation of IRS1 [289], thereby reducing AKT activation [290] and blunting insulin-mediated signaling. Further, diabetes leads to a reduction in GLUT-4 expression and defective GLUT-4 translocation to the plasma membrane [58, 291, 292]. Collectively, impaired insulin signaling, as well as reduced GLUT-4 expression and activity, adversely affect glucose metabolism in the diabetic heart. In support of this, Belke et al. [20] showed that the overexpression of GLUT-4 improved glycolysis and cardiac contractile function in the diabetic *db/db* mice, suggesting an essential role of GLUT-4 in glucose metabolism in the diabetic heart.

5.1.2 Diabetic heart in ischemia

Metabolic derangement impairs vascular function and accelerates the formation of atherosclerotic plaques in the epicardial coronary arteries, thus causing CAD in diabetic individuals [7, 68, 293-296]. Additionally, endothelial dysfunction in the coronary microvessels impairs myocardial perfusion and results in chest pain syndromes similar to CAD in the absence of atherosclerotic plaques [297-299]. Both CAD and CMVD cause myocardial ischemia in the diabetic heart, thus limiting coronary blood flow and oxygen perfusion.

A healthy heart can switch to glucose metabolism for efficient ATP production during myocardial ischemia [42-45]. The glucose uptake is facilitated by GLUT-4 [300], and the mediator for ischemia-induced GLUT-4 membrane translocation is AMPK, which is activated by energy depletion (i.e., high AMP/ATP ratio) [44, 224, 228, 301-303]. However, the diabetic heart is unable to induce GLUT-4 membrane translocation due to insulin resistance and metabolic derangement [47-51, 55, 304]. On top of this, defective AMPK activation impairs glucose utilization in the diabetic heart [226, 227, 265, 266]. In this case, myocardial ischemia reduces oxygen availability to oxidize FFA in diabetic heart, thus halting ATP production and decreasing contractile function [21, 45, 80, 81].

5.1.3 Cardiac NNCS-induced glucose metabolism to protect the heart against ischemia

As outlined in the previous chapter, activation of cardiac NNCS promotes glucose metabolism through increasing GLUT-4 expression to transport glucose [100]. Further, Kakinuma et al. [100] showed that *ChAT-tg* mice had a higher survival rate after chronic ischemia induced by left artery descending (LAD) ligation. In addition to this, the *ChAT-tg* heart was resistant to ischemia-reperfusion injury induced using *ex-vivo* Langerdorff perfusion [100]. Kakinuma et al. [100] further showed that the intracellular ATP content was increased and accompanied by decreased mitochondrial activity in the primary cardiomyocyte isolated from the heart of *ChAT-*

tg mice [100]. Notably, glucose metabolism requires approximately 15% lesser oxygen molecules for oxidation to produce the same amount of ATP from FFA metabolism (reviewed in [305]). Thus, these results demonstrate the activation of cardiac NNCS promotes glucose metabolism, which in turn reduce oxygen demand and enhance ATP production during ischemia, thereby protecting the heart against ischemia-reperfusion injury.

5.2 Study aim

The aims of this chapter are to *(1)* establish an *in-vitro* diabetic cardiomyocytes model using AC16 cells (human ventricular cardiomyocytes), and *(2)* to investigate whether overexpression of *ChAT* gene has beneficial effects by preventing hypoxia-induced cell death. I hypothesized that palmitate and glucose treatment would impair insulin signaling cascade and induce insulin resistance in the AC16 cells. Further, I hypothesized that overexpression of *ChAT* gene in the diabetic AC16 cells would lead to an increase GLUT-4 expression, thus sustaining energy production and reducing apoptosis under hypoxic condition.

5.3 Materials and methods

This section only outlines the specific reagents, concentration, and conditions used for each general method. Detailed experimental procedures for general methods are described in 'Chapter 2: General materials and methods'.

5.3.1 Human ventricular cardiomyocyte cell line – AC16 cells

AC16 cells were maintained and grown in cell culture media composed of DMEM (Gibco, 31600034) with 5% FBS (Hyclone, SH30406.02) and 1X antibiotic-antimycotic solution (Gibco, 15240062), under 37ºC and 5% CO_2. The complete DMEM medium was changed every two days.

5.3.2 Overexpression of human ChAT gene in AC16 cells

The AC16 cells were seeded at a density of $0.75x10^5$ cells/cm^2, which resulted in approximately 90% confluency after overnight attachment. Then, the cells were transfected with pReceiver-M83 expression plasmid with the human *ChAT* gene (M83-hChAT) or without an open reading frame (M83-neg) as a negative control for 24 hours. The expression plasmid allows simultaneous expression of mCherry fluorescent protein to determine the transfection efficiency (Chapter 2, Section 2.6.3).

5.3.3 Induction of insulin resistance in AC16 cells

The AC16 cells were seeded at a density of $0.6x10^5$ cells/$cm^{2,}$ which resulted in approximately 70% confluency after overnight attachment. The cells were incubated in DMEM serum-free medium containing 400 μM palmitate/4% BSA complex, 30.5 mM glucose, and 1X antibiotic-antimycotic solution for 48 hours (addressed as diabetic cells) to induce insulin resistance [306]. The AC16 cells which served as a vehicle control were incubated in DMEM serum-free medium containing 5.5 mM glucose, 25 mM mannitol (osmotic control), non-conjugated 4% BSA solution and 1X antibiotic-antimycotic solution for the same duration (addressed as control cells; Chapter 2, Section 2.7).

5.3.4 Hypoxic condition

The cells were cultured in basal DMEM serum-free medium with 1X antibiotic-antimycotic solution under 37ºC, 5% CO_2 and 1% O_2 (nitrogen level was approximately 94%) or 24 hours to induce hypoxic injury.

5.3.5 Combined experimental protocol

The ultimate aim of this study was to investigate the protective effect of cardiac NNCS activation in the diabetic cells when exposed to the hypoxic condition. In this case, AC16 cells

were first subjected to 24 hours of transfection (Section 5.3.2), followed by 48 hours of palmitate and glucose treatment (Section 5.3.3) and finally exposing the cells to 24 hours of hypoxic condition (Section 5.3.4). The purpose of this combined experimental setup was to *(1)* activate cardiac NNCS via overexpression of *ChAT* gene first, then *(2)* induce insulin resistance, and finally *(3)* subjected the treated and transfected cells to the low oxygen environment.

5.3.6 Oil Red O (ORO) staining of AC16 cells

ORO staining was performed as described in Chapter 2 (Section 2.8) to visualize the palmitate deposition in the AC16 cells after 48 hours of vehicle or palmitate and glucose treatment.

5.3.7 Staining of IRX4, CTNI, ChAT, and GLUT-4 in AC16 cells

The staining of Iroquois homeobox 4 (IRX4; ventricular marker) and CTNI (cardiac marker) were performed to demonstrate AC16 cells are the cardiac-ventricular origin (Chapter 2, Section 2.4). Besides, to confirm that AC16 endogenously expression the key components of cardiac NNCS as well as the key glucose transporter, cells were immunostained for ChAT and GLUT-4 (along with DAPI at 1:1,000 for nuclei staining). The specificity of anti-ChAT and anti-CTNI antibodies were tested on ventricular tissue of *db/db-ChAT-tg* mouse (positive control; Appendix 3, Figure S3.1) and skeletal muscle tissue of ND mouse (negative control; Appendix 3, Figure S3.2). The specificity of anti-IRX4 antibody was tested by one of the Ph.D. students from Katare lab on undifferentiated iPSC and iPSC-induced ventricular cells. However, the specificity of anti-GLUT-4 antibody was not tested as explained in previous chapter, thus, this is one of the limitations of the study. Table 5.1 summarizes the information of each antibody/reagents used in the experiment.

Table 5.1 Information on antibodies/label for immunofluorescence

Antigen	Source	Dilution	Manufacturer/Catalogue number
Primary antibodies			
IRX4	Rabbit	1:100	Abcam, AB123542
CTNI (antibody is biotinylated)	Mouse	1:100	NovusBio, NB110-2546B
ChAT	Rabbit	1:100	Abcam, AB181023
GLUT-4 (antibody is conjugated with AlexaFluor® 488)	Rabbit	1:100	NovusBio, NBP1-49533AF488)
Secondary reagents			
AlexaFluor® 488 conjugated anti-rabbit IgG	Goat	1:200	Invitrogen, A32731
Streptavidin-AlexaFluor® 568	-	1:200	Invitrogen, S11226
AlexaFluor® 633 conjugated anti-rabbit IgG	Goat	1:100	Invitrogen, A21070

5.3.8 Western blot analysis

Total protein (Section 2.3.2.1), or cytosolic and membrane protein extraction (Section 2.3.2.2) from AC16 cells was performed. The cytosolic and membrane fraction of protein were separated as part of the experiments required to detect membrane-specific proteins. An equal amount of protein was loaded and electrophoresed and blotted for following protein targets, processed as described in Section 2.3.2.4. The protein expression of pan-cadherin (membrane protein) was detected via western blot analysis to confirm the successful separation of cytosolic and membrane protein (Appendix 5, Figure S5.1). The band intensity of the target protein was normalized to a prominent band between 37 kDa and 50 kDa on the Ponceau S stained blot as described in Chapter 2 (section 2.3.2.5) [143, 144] and expressed as fold changes towards the control group [145]. As explained in Chapter 4 (Section 4.3.3), the quantification of the phosphorylation of Akt and AMPKα was done by normalizing to its respective total protein as well as to a prominent band between 37 kDa and 50 kDa on the Ponceau S stained blot. The information of each antibody are listed in Table 5.2. The full blot for each antibody is shown in Appendix 2.

Table 5.2 Primary and secondary antibodies for western blot

Antigen	Host/Clone	Dilution factor	Predicted molecular weight (kDa)	Manufacturer/ Catalogue number
Primary antibodies				
pAkt (Ser473)	Rabbit/polyclonal	1:1,000	60	Cell Signaling, 9272
Akt	Rabbit/polyclonal	1:1,000	60	Cell Signaling, 9271
pAMPKα (Thr172)	Rabbit/polyclonal	1:1,000	62	Cell Signalling,2531
AMPKα	Rabbit/polyclonal	1:1,000	62	Cell Signaling, 2532
ChAT	Goat/polyclonal	1:1,000	70/74	Chemicon, AB144P
Cleaved caspase-3 (Asp175)	Rabbit/polyclonal	1:500	17/19	Cell Signaling, 9661
GLUT-4	Rabbit/polyclonal	1:2,500	55	NovusBio, NBP1-49533
Pan-cadherin	Mouse/monoclonal	1:1,000	125-140	Abcam, Ab6528
Secondary antibodies				
Anti-goat IgG, HRP conjugated	Mouse	1:3,000	-	Santa Cruz, SC2354
Anti-rabbit IgG, HRP conjugated	Goat	1:5,000	-	Sigma-Aldrich, A6154
Recombinant mouse IgGκ light chain binding protein, HRP conjugated	-	1:3,000	-	Santa Cruz, SC516102

Note: the predicted molecular weight of protein is recommended by the manufacturer

5.3.9 Statistical analyses

All statistical analyses were performed using GraphPad Prism (version 7) in consultation with biostatistician Mr. Andrew Grey and Dr. Claire Cameron (Centre for Biostatistics, University of Otago). Data are expressed as the mean ± SEM. Two-way ANOVA followed Tukey's test for multiple comparison test was performed to analyze the protein expression of all target. However, the total sample number in Figure 5.7 is too small for a normality test (n=4). Thus the protein expressions of ChAT, cytosolic, and membrane GLUT-4 protein expression were analyzed by a non-parametric Mann-Whitney U test.

5.4 Results

5.4.1 ChAT and GLUT-4 are endogenously expressed in the human ventricular AC16 cells

AC16 cell line is a fusion of non-proliferating primary cultures of human adult ventricular heart tissues with SV40 transformed human fibroblasts [141]. The immunofluorescence analysis was performed to demonstrate the cardiac-ventricular origin of AC16 cells by detecting IRX4 (ventricular marker) and CTNI (cardiac marker). The results showed the expression of CTNI was localized in the cytoplasm (Figure 5.2A), and IRX4 was localized in the perinuclear region (Figure 5.2B) of the AC16 cells. Next, immunofluorescence analysis was performed to demonstrate if AC16 cells endogenously express ChAT to synthesize ACh and GLUT-4 to transport glucose. The findings showed perinuclear localization of ChAT (Figure 5.2C) and both cytoplasmic and perinuclear localization of GLUT-4 in the AC16 cells (Figure 5.2D). The immunofluorescent images for secondary antibody-only control for staining of CTNI, IRX4, ChAT, and GLUT-4 are in Appendix 5 (Figure S5.2). The overall findings indicate that the ventricular AC16 cells are a suitable model to study cardiac NNCS as these cells endogenously express ChAT and GLUT-4 expression that was required to serve as a control to compare with the effect derived from overexpression of *ChAT* gene in the AC16 cells.

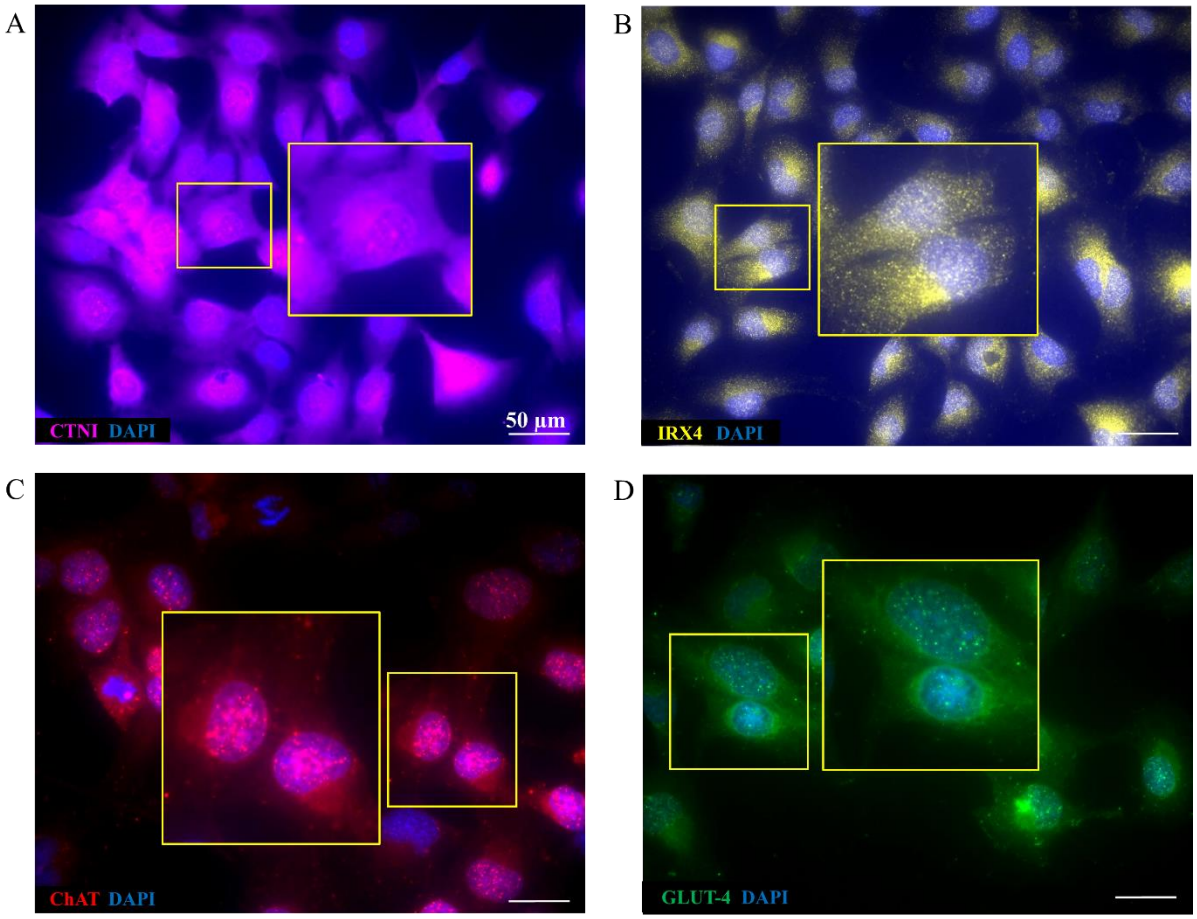

Figure 5.2 Immunostaining of CTNI, IRX4, ChAT, and GLUT-4 in AC16 cells.
Representative fluorescent images showing the staining of ***(A)*** *cardiac marker, CTNI;* ***(B)*** *ventricular marker, IRX4;* ***(C)*** *cardiac NNCS marker, ChAT; and* ***(D)*** *GLUT-4 in AC16 cells.*

5.4.2 Establishment and validation of the *in-vitro* diabetic model

An *in-vitro* diabetic model was established to study the role of cardiac NNCS in diabetic condition. AC16 cells were either treated with 400 µM palmitate and 30.5 mM glucose (diabetic) or vehicle treatment (no palmitate and 5.5 mM glucose; control) for 48 hours. Forty-eight hours was chosen as there was no significant decrease in insulin-stimulated membrane GLUT-4 translocation after 24 hours of treatment (Appendix 5, Figure S5.3). ORO staining was performed to visualize the intracellular deposition of palmitate in the AC16 cell to confirm palmitate uptake in the AC16 cells (Figure 5.3A). The analysis showed that incubation with 400 µM palmitate resulted in approximately 73% of ORO-positive diabetic cells, and about 45%

of viable cells remained compared to the control cells without palmitate treatment (Appendix 5, Figure S5.4).

As palmitate is known to impair insulin signaling cascade by inhibiting Akt phosphorylation [306, 307], the next experiment was to measure the phosphorylated and total expression of Akt in the cytosolic fraction. Also, as explained in Chapter 4, two approaches of normalization were performed to examine the phosphorylation level of Akt. In generally, these two approaches showed identical results. The basal phosphorylation level of Akt was significantly decreased in the diabetic cells compared to that of the control cells (Figure 5.3B). The control and diabetic cells were stimulated with 500 nM insulin for 30- and 60-mins to examine the insulin responsiveness after palmitate and glucose treatment. Five hundred nanomolar of insulin was chosen based on the optimization experiment to induce membrane GLUT-4 translocation (Appendix 5, Figure S5.5). The findings revealed that the phosphorylation level of Akt was significantly increased after stimulating the control and diabetic cells with insulin (Figure 5.3B). However, the phosphorylation level of Akt was lower in the diabetic AC16 cells in comparison to the control AC16 cells after 60-mins of insulin stimulation (Figure 5.3B), suggesting reduced insulin responsiveness after palmitate and glucose treatment. The total Akt protein expression was not altered in control AC16 cells. However, after 60-mins of insulin stimulation, the total Akt protein expression was significantly decreased in the diabetic AC16 cells. Thus, this could indicate that palmitate and glucose treatment reduced the availability of Akt for phosphorylation, thereby reducing the insulin responsiveness.

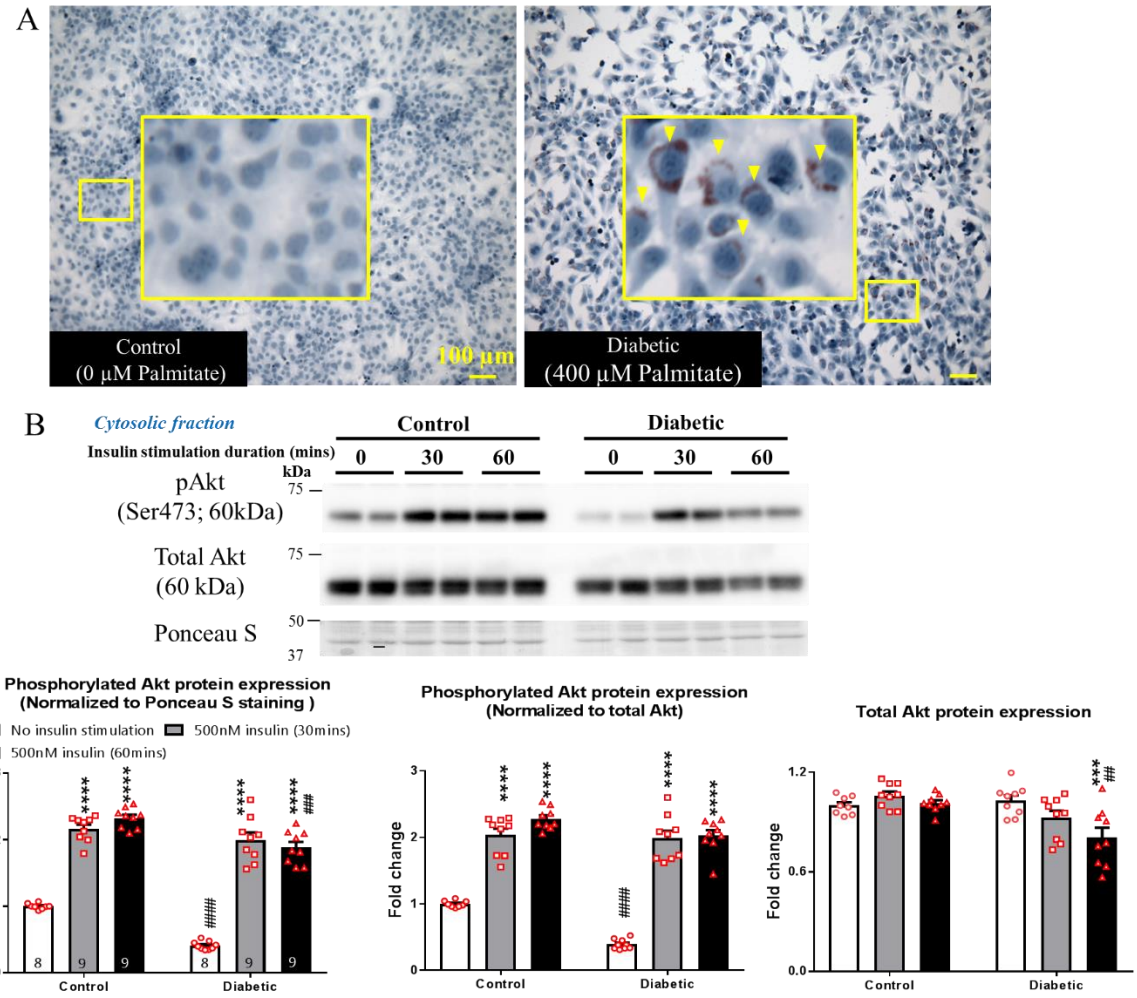

Figure 5.3 Decreased insulin responsiveness in the diabetic AC16 cells.
(A) *Representative images showing the ORO staining of control and diabetic AC16 cells after 48 hours of treatment. The hematoxylin-stained nuclei are in blue while the ORO-stained palmitate appears in red. Yellow arrows indicate ORO-positive cells. The diabetic cells showed palmitate deposition, while the control cells did not show palmitate deposition after treatment.* ***(B)*** *Representative blots and bar graphs with scatter plots showing the phosphorylated (Ser473) and total Akt protein expression in AC16 cells after 48 hours of vehicle or palmitate and glucose treatment. After treatment, the cells were stimulated with 500 nM of insulin for 30- and 60-mins to test the insulin responsiveness. Data are expressed as mean ± SEM. Two-way ANOVA with Tukey's multiple comparisons test was performed. ***p<0.001, ****p<0.0001 VS respective control or diabetic AC16 cells treated with 0 nM insulin; ##p<0.01, ###p<0.001, ####p<0.0001 VS respective control AC16 cells with same insulin stimulation duration. The number of samples per group is indicated in the figure. The total number of samples was derived from three independent experiments.*

The protein expression of membrane GLUT-4 was measured to examine if impaired Akt activation correlates with insulin-stimulated GLUT-4 membrane translocation. Thirty and sixty minutes (mins) of insulin stimulation gradually increased the membrane GLUT-4 expression in control AC16 cells; however, the increase in expression was not statistically significant (Figure 5.4A). The diabetic AC16 cells exhibited a gradual decrease in membrane GLUT-4 expression

after 30-mins of insulin stimulation. After 60-mins of stimulation, membrane GLUT-4 protein expression was significantly decreased (Figure 5.4A). This observation suggests decreased GLUT-4 membrane translocation in diabetic AC16 cells, which is in agreement with reduced insulin responsiveness. The cytosolic GLUT-4 expression in the control and diabetic cells did not change after 30- and 60-mins of insulin stimulation (Figure 5.4B). These findings suggest that decreased membrane GLUT-4 protein expression in the diabetic cells could possibly due to a retention of GLUT-4 in the intracellular vesicles after palmitate and glucose treatment.

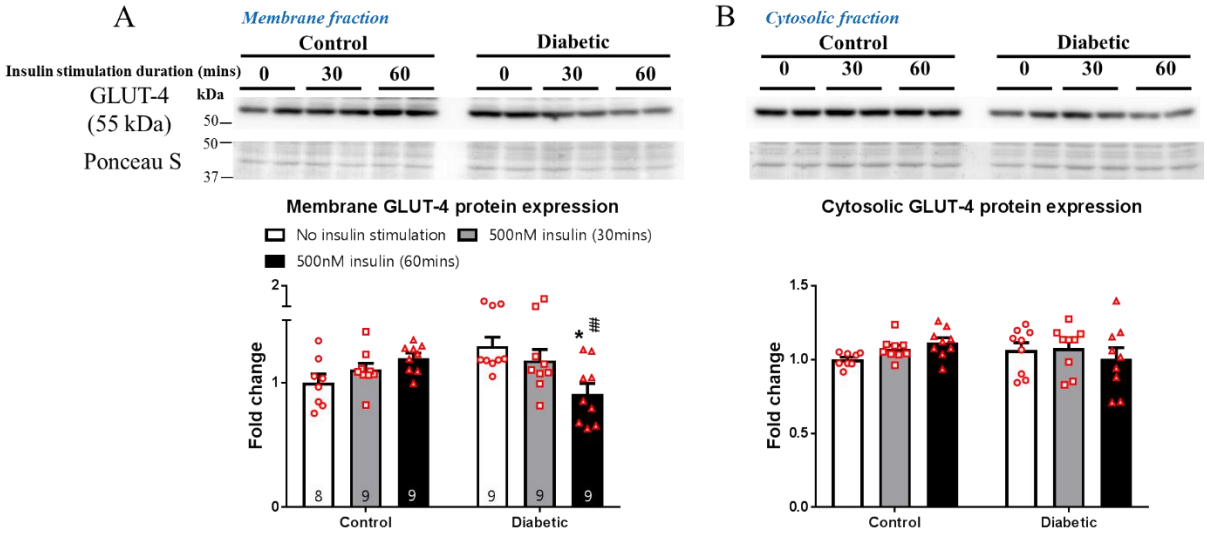

Figure 5.4 Decreased membrane GLUT-4 protein expression in the diabetic AC16 cells.
*Representative blots and bar graphs with scatter plots showing the **(A)** membrane GLUT-4 protein expression and **(B)** cytosolic GLUT-4 protein expression in AC16 cells after 48 hours of vehicle or palmitate and glucose treatment. After treatment, the cells were stimulated with 500 nM of insulin for 30- and 60-mins to test the insulin responsiveness in translocating GLUT-4 to the plasma membrane. Data are expressed as mean ± SEM. Two-way ANOVA with Tukey's multiple comparisons test was performed. *p<0.05 VS diabetic AC16 cells treated with 0 nM insulin; ##p<0.01 VS control AC16 cells with same insulin stimulation duration. The number of samples per group is indicated in the figure. The total number of samples was derived from three independent experiments.*

ChAT protein expression was measured to examine the effect of palmitate and glucose treatment on ACh synthesis. The basal ChAT protein expression was unaltered in both the control and diabetic AC16 cells (Figure 5.5). In response to 30- and 60-mins of insulin stimulation, the control AC16 cells showed an increasing trend in the ChAT protein expression, however, these changes were not statistically significant. While the diabetic cells showed an

increasing trend in ChAT expression, this was absent after 60-mins of insulin stimulation (Figure 5.5).

Taken together, the overall findings from this section indicate that palmitate and glucose treatment significantly decreased Akt phosphorylation, insulin-stimulated GLUT-4 membrane translocation in the diabetic AC16 cells. Therefore, this model can be used to investigate the effect of activation of cardiac NNCS via overexpression of the *ChAT* gene in regulating GLUT-4 expression.

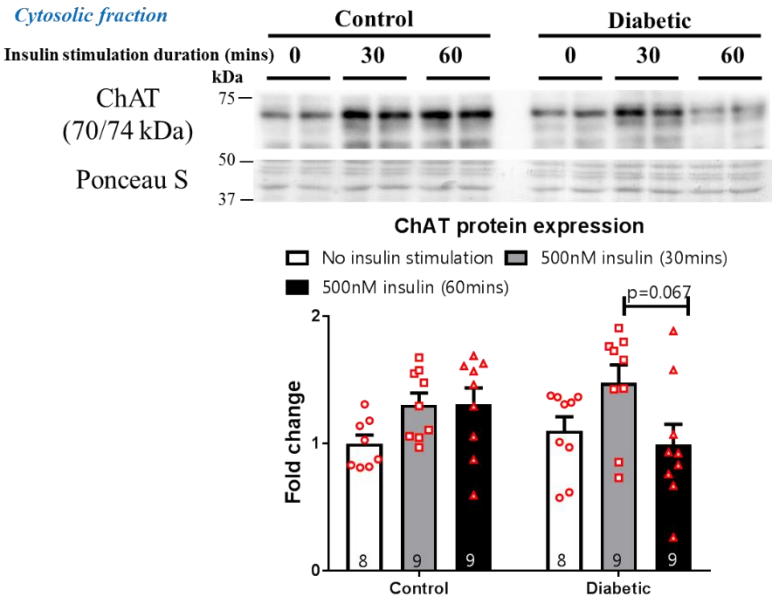

Figure 5.5 Insulin stimulation modulated ChAT expression in AC16 cells.
Representative blots and bar graphs with scatter plots showing the ChAT protein expression in AC16 cells after 48 hours of vehicle or palmitate and glucose treatment. Data are expressed as mean ± SEM. Two-way ANOVA with Tukey's multiple comparisons test was performed. The number of samples per group is indicated in the figure. The total number of samples was derived from three independent experiments.

5.4.3 Overexpression of *ChAT* gene in the AC16 cells

AC16 cells were transfected with M83-hChAT plasmid to overexpress human *ChAT* gene (hChAT) while the cells transfected with M83-neg plasmid served as a negative control (WT). Both expression plasmids allowed simultaneous expression of mCherry fluorescent protein to determine the transfection efficiency. The transfection efficiency was approximately 40% (Appendix 5, Figure S5.6). The immunofluorescent analysis confirmed increased ChAT and

GLUT-4 fluorescent intensity in the hChAT transfected cells compared to that of the WT cells (Figure 5.6 A). The immunofluorescent images of secondary antibody-only control for ChAT and GLUT-4 staining are in Appendix 5 (Figure S5.7). Further, western blot analysis revealed that overexpression of the *ChAT* gene resulted in an approximately 10.2±2.8-fold increase in the ChAT protein expression in the hChAT transfected cells (Figure 5.6B). Also, the total GLUT-4 protein expression was significantly increased in the hChAT cells. The increase in GLUT-4 protein expression is likely to be mediated by PI3K/Akt/HIF1α/GLUT-4 signaling pathway via cardiac NNCS as a result of overexpression of *ChAT* gene, as discussed in Chapter 4 and by Kakinuma et al. [100].

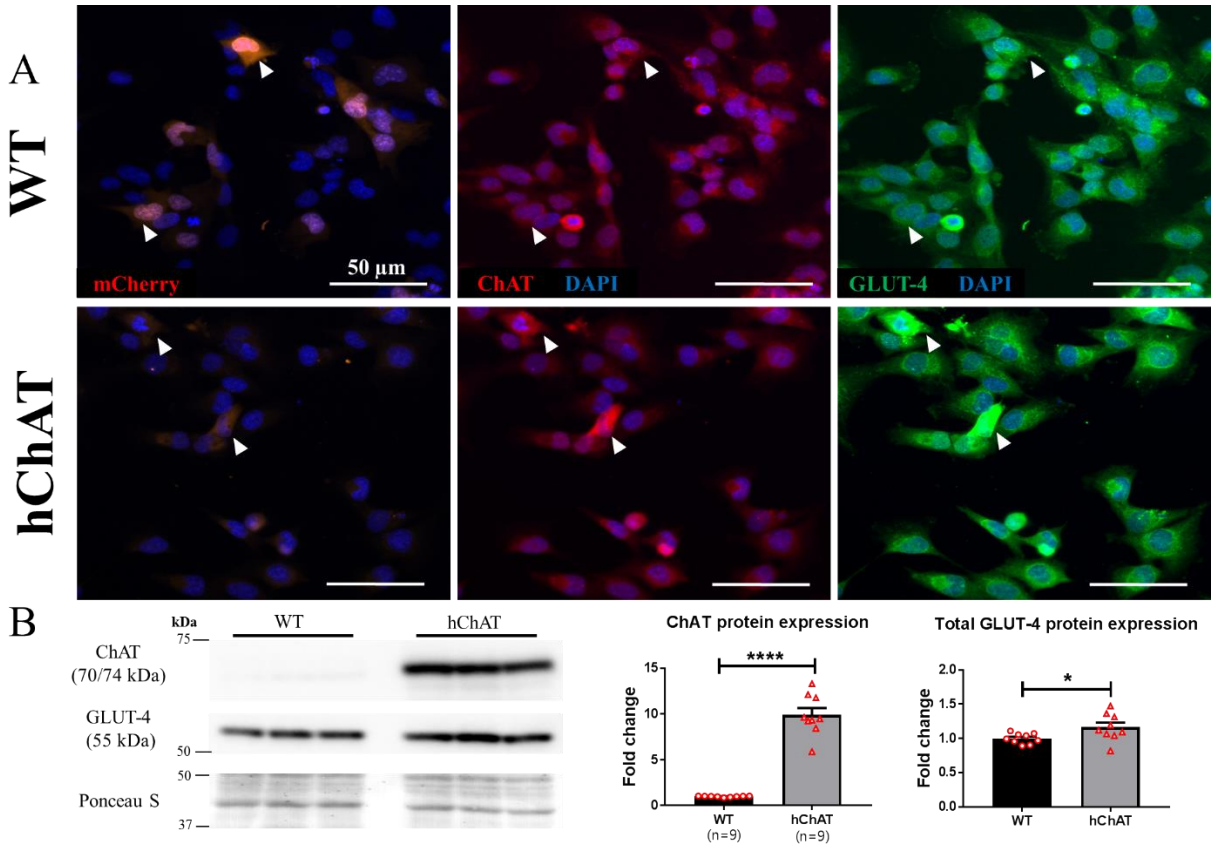

Figure 5.6 ChAT and GLUT-4 protein expression in the transfected AC16 cells.
(A) *Representative confocal images showing the expression of mCherry fluorescent proteins and staining of ChAT and GLUT-4 proteins in the WT and hChAT transfected cells.* ***(B)*** *Representative blots and bar graphs with scatter plots showing the protein expression of ChAT and total GLUT-4 protein expression in the WT and hChAT transfected AC16 cells. Data are expressed as mean ± SEM. Unpaired T-test was performed. *p<0.05, ****p<0.0001 VS WT AC16 cells. White arrows indicated transfected AC16 cells. The number of samples per group is indicated in the figure. The total number of samples was derived from three independent experiments.*

To further investigate if the hChAT transfected cells express increased GLUT-4 protein expression in the plasma membrane, the cytosolic and membrane fraction of protein lysates were separated and analyzed. Western blot analysis revealed that membrane GLUT-4 protein expression was significantly increased in the hChAT transfected cells (Figure 5.7). The decrease in cytosolic GLUT-4 protein expression in hChAT transfected cells was not statistically significant. However, the decreasing trend supports that GLUT-4 proteins in the intracellular vesicles have translocated to the plasma membrane.

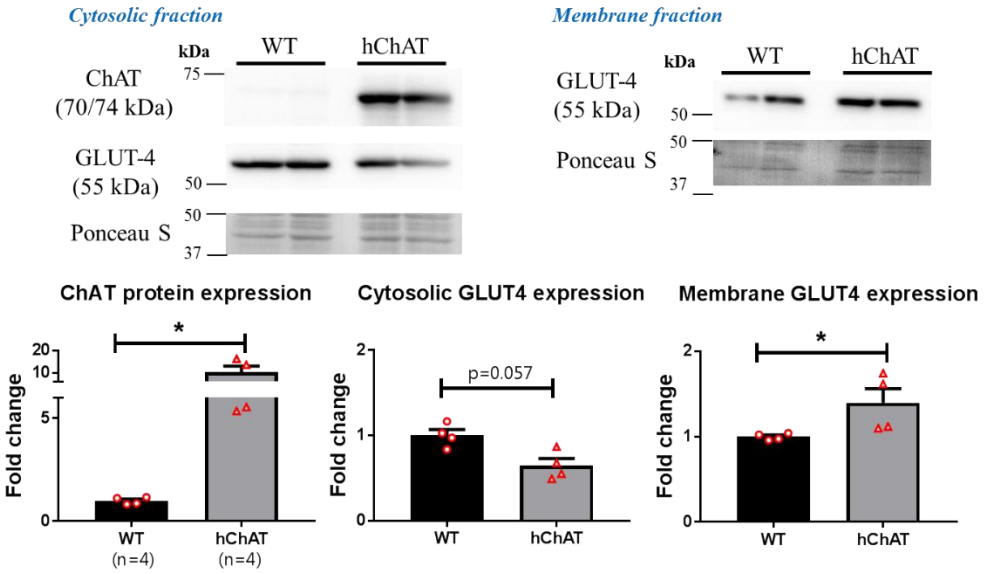

Figure 5.7 ChAT, membrane and cytosolic GLUT-4 protein expression in the hChAT transfected AC16 cells.

*Representative blots and bar graphs with scatter plots showing the protein expression of ChAT, cytosolic, and membrane GLUT-4 protein expression in the M83-neg and M83-hChAT transfected cells. Data are expressed as mean ± SEM. A non-parametric Mann-Whitney test was performed. *p<0.05 VS WT AC16 cells. The number of samples per group is indicated in the figure. The total number of samples was derived from two independent experiments.*

5.4.4. The role of cardiac NNCS in diabetic AC16 cells under hypoxic condition

The protein expression of ChAT was measured to examine whether the palmitate and glucose treatment, as well as hypoxic condition, affects the cardiac NNCS. Western blot analysis showed no difference in the endogenous ChAT expression between the control and diabetic WT cells in both normoxic (Appendix 5, Figure S5.8) and hypoxic condition (Figure 5.8),

respectively. However, diabetic WT cells showed a significant decrease in the endogenous ChAT expression following hypoxia (Appendix 5, Figure S5.8). Similarly, the control and diabetic hChAT transfected cells showed a substantial decrease in the ChAT expression following hypoxia (Appendix 5, Figure S5.8). Thus, these results suggest that hypoxia decreased ChAT expression. Further, diabetic hChAT transfected cells showed an only 2.2±0.3-fold increase in the ChAT expression in hypoxic condition. The decrease in ChAT expression was caused by the combinational effect of palmitate and glucose treatment, as well as hypoxia (Figure 5.8; Appendix 5, Figure S5.8). Therefore, the overall findings suggest that ACh synthesis was reduced in the diabetic cells in hypoxic condition, which may reduce the activation of ACh-mediated pro-survival signaling cascade.

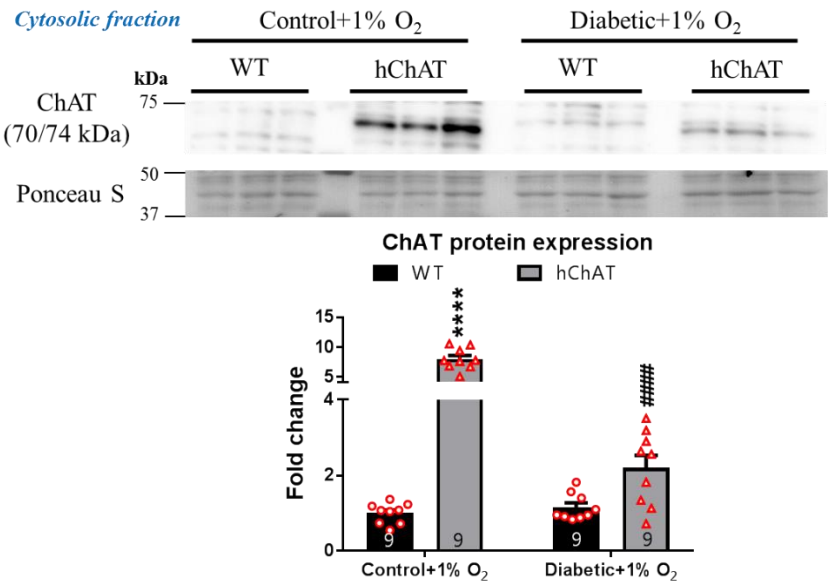

Figure 5.8 Palmitate and glucose treatment decreased ChAT protein expression in the hChAT transfected AC16 cells under hypoxic condition.
*Representative blots and bar graphs with scatter plots showing the protein expression of ChAT in the control/diabetic and WT/hChAT AC16 transfected cells after 24 hours of 1% O_2 hypoxic condition. Data are expressed as mean ± SEM. Two-way ANOVA with Tukey's multiple comparisons test was performed. ****p<0.0001 VS control WT cells; $^{\#\#\#\#}$p<0.0001 VS control hChAT transfected cells. The number of samples per group is indicated in the figure. The total number of samples was derived from three independent experiments.*

To examine if GLUT-4 expression was also decreased due to reduced ChAT expression in the diabetic hChAT transfected cells in hypoxic condition, the expression level of the membrane

and cytosolic GLUT-4 protein expression were examined. Western blot analysis revealed that there were no significant changes in the membrane and cytosolic GLUT-4 expression in the control hChAT transfected AC16 cells (Figure 5.9A&B). However, there was a substantial decrease in the membrane GLUT-4 protein expression in the diabetic WT cells (Figure 5.9A), suggesting reduced translocation of GLUT-4 to the membrane and possibly decreased glucose uptake. There was no significant change in the cytosolic GLUT-4 expression in the diabetic WT cells (Figure 5.9B). In contrast, the membrane GLUT-4 expression was unaltered while the cytosolic GLUT-4 expression was significantly reduced in the diabetic hChAT transfected cells (Figure 5.9A&B). This result suggests that diabetic hChAT transfected cells prevented the decrease in membrane GLUT-4 possibly by translocating the cytosolic GLUT-4 to plasma membrane under hypoxic condition. Thus, the overall findings suggest that cardiac NNCS was still activated in the diabetic cells, and activation of cardiac NNCS preserved membrane GLUT-4 expression when exposed to hypoxia.

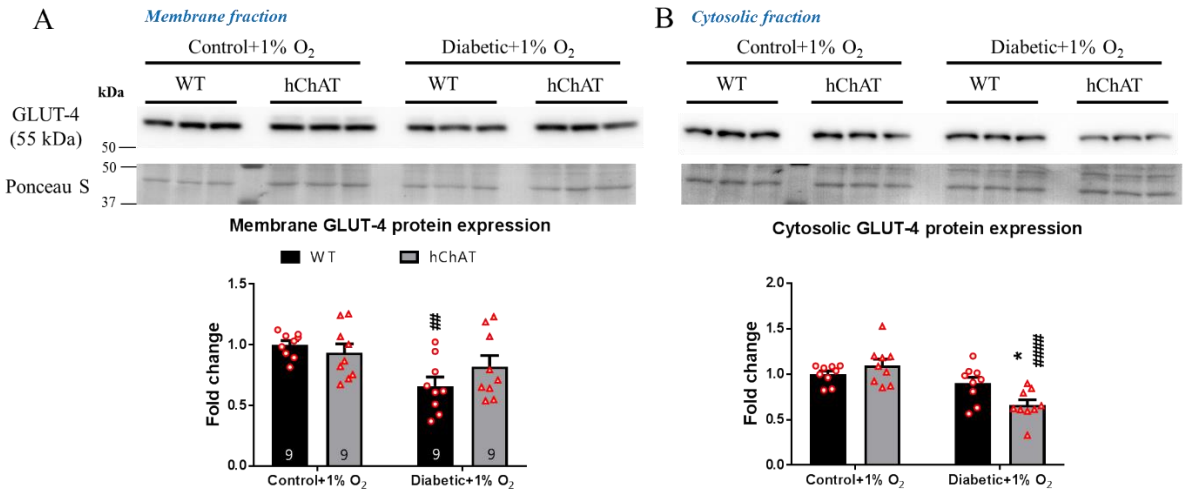

Figure 5.9 Normalized membrane GLUT-4 protein expression in the diabetic hChAT transfected AC16 cells under hypoxic condition.

*Representative blots and bar graphs with scatter plots showing the **(A)** membrane GLUT-4 protein expression and **(B)** cytosolic GLUT-4 protein expression in the control/diabetic and WT/hChAT transfected AC16 cells after 24 hours of 1% O_2 hypoxic condition. Data are expressed as mean ± SEM. Two-way ANOVA with Tukey's multiple comparisons test was performed. *p<0.05 VS diabetic WT cells; $^{\#}p<0.05$, $^{\#\#\#\#}p<0.0001$ VS respective control WT or hChAT transfected cells. The number of samples per group is indicated in the figure. The total number of samples was derived from three independent experiments.*

Previous studies showed that improved glucose transport under ischemic condition alleviates ischemic damage and prevents cell death [224, 308]. Since diabetic hChAT transfected cells preserved membrane translocation of GLUT-4 under hypoxic condition, the next aim was to determine if hypoxia-induced apoptosis could be alleviated. Western blot analysis was performed to measure the protein expression of pro-apoptotic marker cleaved caspase-3. The anti-cleaved caspase 3 antibody is polyclonal and resulted in multiple bands. However, based on the predicted molecular weight recommended by the manufacturer, I identified the two bands at/above molecular weight of 17 kDa as cleaved-caspase 3 positive (17/19 kDa; Appendix 2, Figure S2.8). The analysis showed that palmitate and glucose treatment significantly increased the protein expression of cleaved caspase-3 in both the diabetic WT and hChAT transfected cells in comparison to that of the control WT and hChAT transfected cells respectively (Figure 5.10). There was no difference between the diabetic WT and diabetic hChAT transfected cells after palmitate and glucose treatment. This result suggests that the extent of the hypoxic injury was not altered by overexpression of the *ChAT* gene in the AC16 cells. *(Note: Figure 5.10 shows a total of 12 samples per group derived from four independent experiments. However, three protein samples isolated from one of the independent experiments had low protein amount, and hence I was only able to perform western blot analysis for cleaved caspase-3 protein, but not other protein targets shown as in Figure 5.8, 5.9 & 5.11)*

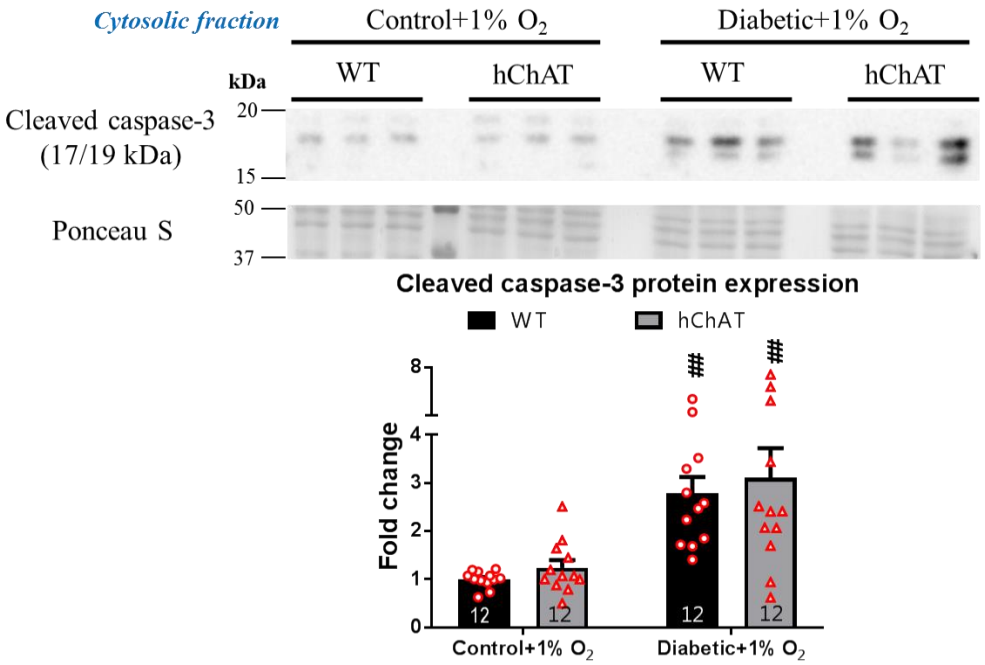

Figure 5.10 Increased cleaved caspase-3 protein expression in the diabetic cells under hypoxic condition.
Representative blots and bar graphs with scatter plots showing the cleaved caspase-3 protein expression in the control/diabetic and WT/hChAT transfected AC16 transfected cells after 24 hours of 1% O_2 hypoxic condition. Data are expressed as mean ± SEM. Two-way ANOVA with Tukey's multiple comparisons test was performed. $^{\#\#}p<0.01$ VS respective control WT or hChAT transfected AC16 cells. The number of samples per group is indicated in the figure. The total number of samples was derived from four independent experiments.

One reason for the failure to reduce the hypoxia-induced apoptosis by activation of cardiac NNCS in the diabetic cells could be due to impaired ATP production under hypoxic condition. Thus, the next aim was to examine if the ATP homeostasis regulated by AMPK was affected by palmitate and glucose in the hypoxic condition. As explained in Chapter 4, two approaches of normalization were taken to examine the phosphorylation level of AMPKα. However, such normalizations resulted in two different sets of result. By normalizing to the selected band between 37 kDa and 50 kDa on the Ponceau S stained blot, the phosphorylation level of AMPKα was significantly decreased in the diabetic WT and hChAT transfected cells under hypoxic condition (Figure 5.11). Conversely, by normalizing to total AMPKα expression, the phosphorylation level of AMPKα was unchanged in diabetic WT and hChAT transfected cells under hypoxic condition. Further, the analysis showed a significant decrease in the total protein

of AMPKα in the diabetic WT and hChAT transfected cells under hypoxic condition (Figure 5.11).

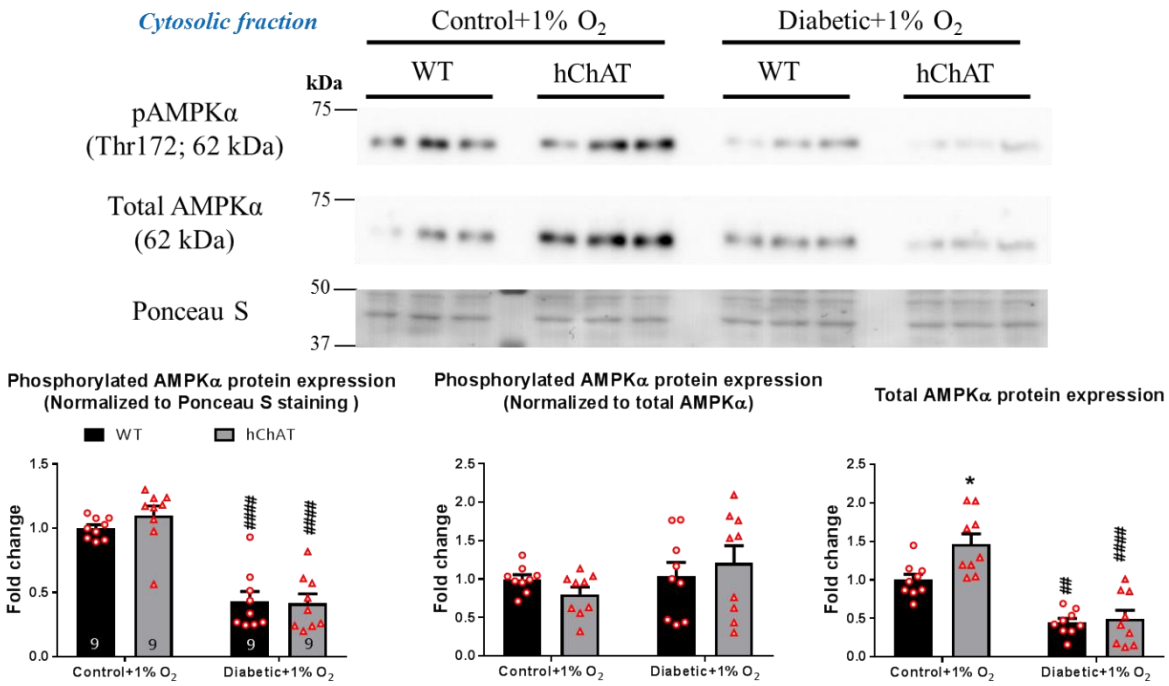

Figure 5.11 Decreased AMPK activation in the diabetic cells under hypoxic condition.
*Representative blots and bar graphs with scatter plots showing the phosphorylated (Thr172) and total AMPKα protein expression in control/diabetic and WT/hChAT transfected AC16 cells after 24 hours of 1% O_2 hypoxic condition. Data are expressed as mean ± SEM. Two-way ANOVA with Tukey's multiple comparisons test was performed. *p<0.05 VS control WT cells; $^{\#\#}$p<0.01, $^{\#\#\#\#}$p<0.0001 VS respective control WT or hChAT transfected AC16 cells. The number of samples per group is indicated in the figure. The total number of samples was derived from three independent experiments.*

5.5 Discussion

In this chapter, the *in-vitro* diabetic AC16 cell model was first established. This purpose of developing this model was to investigate the role of cardiac NNCS under "diabetic" condition. Human ventricular-origin AC16 cell line is a suitable model to study the role of cardiac NNCS in regulating glucose metabolism as it expresses ChAT and GLUT-4 endogenously. To investigate the effect of cardiac NNCS in protecting the diabetic AC16 cells in hypoxic condition, the experiments were carried out in three steps: *(1)* 24 hours of transfection to overexpress human *ChAT* gene in AC16 cells, then *(2)* 48 hours of palmitate and glucose treatment to induce diabetic effect, and finally *(3)* 24 hours of incubation in 1% O_2 hypoxic condition. I hypothesized that palmitate and glucose treatment would impair insulin signaling cascade and induce insulin resistance in the AC16 cells. Further, I hypothesized that overexpression of *ChAT* gene in the diabetic AC16 cells would lead to an increase GLUT-4 expression, thus sustaining energy production and reducing apoptosis under hypoxic condition. The main findings of this study can be summarized as follows:

1. **Diabetic AC16 cells:**
    - Palmitate and glucose treatment impaired insulin signaling cascade as evidenced by decreased basal and the insulin-stimulated phosphorylation level of Akt expression and insulin-stimulated membrane GLUT-4 protein expression.
    - The basal ChAT protein expression was unaffected. However, the insulin-induced increased ChAT protein expression was abolished in the diabetic AC16 cells.

2. **hChAT transfected AC16 cells:**
    - Overexpression of the *ChAT* gene resulted in increased membrane GLUT-4 protein expression.

3. **Diabetic hChAT transfected AC16 cells in hypoxic condition:**
    - The decrease in membrane GLUT-4 protein expression was prevented in comparison to diabetic WT AC16 cells.
    - The hypoxic injury was not alleviated as cleaved caspase-3 protein expression was similar to the diabetic WT cells.
    - The phosphorylation level of AMPKα is not clear. Thus, it is not clear if AMPK inactivation contributes to the hypoxic injury.

5.5.1 *In-vitro* diabetic AC16 cells

In cardiovascular research, the establishment of the *in-vitro* diabetic model mainly involves the use of high glucose [1, 137, 309], palmitate [306, 307], insulin [310] or a combination of palmitate and insulin [311] to mimic the *in-vivo* insulin resistance. Particularly, palmitate desensitizes the insulin-mediated glucose uptake by inhibiting Akt phosphorylation [306, 311]. In the study performed by Chokshi et al. [312], the diabetic AC16 cells exhibited decreased basal and insulin-stimulated Akt phosphorylation after 16 hours of palmitate treatment. However, Chokshi et al. [312] did not examine the GLUT-4 membrane translocation in the diabetic model. My study showed similar results with a reduction in both basal and insulin-stimulated Akt phosphorylation in the diabetic cells (Figure 5.3B). Also, my study further demonstrated a reduction in insulin-stimulated GLUT-4 membrane translocation in diabetic AC16 cells, supporting that the insulin signaling cascade was impaired in the model (Figure 5.4A).

The use of diabetic AC16 cells can provide mechanistic insight on how cardiac NNCS is specifically altered in the condition of insulin resistance. This is one of the advantages of using an *in-vitro* model over the *in-vivo* models that typically display a complex pathophysiology when different systems and cell types interact with each other. In my study, palmitate and glucose treatment did not alter the basal ChAT expression in the diabetic AC16 cells (Figure

5.5 & Appendix 5, Figure S5.8). However, insulin stimulation increased ChAT expression (not statistically significant) in control AC16 cells while this effect was abolished in the diabetic cells (Figure 5.5). To the best of my knowledge, this is the first study observed the effect of insulin in regulating ChAT expression specifically in the ventricular cardiomyocytes. This particular effect of insulin was previously demonstrated in neuronal cell lines and the frontal lobe and cerebellum of animal model [313-315]. Further, the streptozotocin-induced diabetic rats showed decreased ChAT expression in the hippocampus [316]. Taking all these information and my results into consideration, metabolic derangements and insulin resistance may suppress ChAT expression in the ventricular cardiomyocytes, and hence preventing the activation of cardiac NNCS in T2DM.

5.5.2 Activation of cardiac NNCS did not alleviate hypoxia-induced apoptosis in the diabetic AC16 cells

The previous study showed that glucose oxidation plays a vital role to maintain contractile function in mild-to-moderate ischemia (i.e., 60% reduction in LAD coronary blood flow) [45]. Tian et al. [300] showed that GLUT-4 is essential to transport glucose into the cardiomyocytes for ATP generation in ischemic condition. Notably, Kakinuma et al. [100] showed that activation of cardiac NNCS increased GLUT-4 expression, cardiac glucose, and ATP content, thereby reducing ischemia-reperfusion injury to the WT *ChAT-tg* heart. In my study, I questioned whether activation of cardiac NNCS could increase the membrane translocation of GLUT-4, which in turn could allow efficient ATP production and prevent hypoxia-induced apoptosis in the diabetic AC16 cells.

The overexpression of the *ChAT* gene did not increase the membrane GLUT-4 translocation in the control and diabetic hChAT transfected cells in hypoxia. This outcome could be due to the reduction of ChAT expression by palmitate and glucose treatment as well as hypoxia (Appendix 5, Figure S5.8). However, the expression level of ChAT was sufficient to prevent the decrease

in membrane GLUT-4 translocation in the diabetic cells (Figure 5.9 A&B). In spite of this, hypoxia-induced apoptosis was similar between the diabetic WT and hChAT transfected cells (Figure 5.10). Vanoverschelde et al. [317] showed that the rate of glycolysis is invesely proportional to ischemic damage in the heart, suggesting that a high rate of glycolysis is undoubtedly needed to protect the cardiomyocytes against hypoxia-induced apoptosis.

Besides, previous studies showed that ischemia-induced activation of AMPK protects the heart against ischemia-reperfusion injury [44, 224, 228, 301-303]. Notably, activation of AMPK signaling cascade enhanced glucose uptake and oxidation, thus reducing apoptosis in the heart [224, 303]. In my study, I was unable to conclude the phosphorylation level of AMPKα as the outcome of the result was different depending on the way the data were analyzed (Figure 5.11). Whether the phosphorylation level of AMPKα is decreased or unaltered after palmitate and hypoxic treatment, this requires further investigation. An ELISA assay to detect phosphorylated AMPKα or biochemical assay to detect the activity of AMPK could also be considered in the future. However, previous studied showed that palmitate treatment impaired AMPK activation in the cardiomyocytes [318] and endothelial cells [319, 320]. Thus, based on these information, it may be considered that AMPK-mediated glucose uptake could be prevented by palmitate treatment, thus increasing apoptosis following hypoxia. On a side note, the mechanism of cardiac NNCS-induced GLUT-4 membrane translocation is likely to be independent on AMPK activation in hypoxia, as preserved GLUT-4 membrane translocation was observed in the diabetic cells (Figure 5.9A).

Besides, my results showed that the ChAT expression has to be at least a 10-fold increase to enhance membrane GLUT-4 expression in an *in-vitro* setting (Figure 5.6&5.7). Considering that the transfection efficiency was approximately 40% (Appendix 5, Figure S5.6), and due to the fact that palmitate and glucose treatment as well as hypoxia decrease ChAT expression (Figure 5.8, Appendix 5, Figure S5.8), this suggests that the number of hChAT transfected cells must be increased to be accounted for the reduction in ChAT expression caused by the

treatments. Thus, a longer transfection duration to increase transfection efficiency could be considered in the future study. However, this was not performed in the present study due to time constraint. Additionally, as the current study performed transient overexpression of the *ChAT* gene in AC16 cells, the future study could consider generating AC16 cells that are stably overexpressing *ChAT* gene as an alternative. Having the ChAT-overexpressing stable cell line would omit the lipofectamine transfection step that could also induce cell loss during the experimental process.

5.6 Limitations

5.6.1 The use of the *in-vitro* diabetic model

The *in-vitro* diabetic AC16 established in my study exhibited impaired insulin signaling cascade. This allows one to examine how cardiac NNCS is specifically altered under the condition of insulin resistance. However, the impaired insulin signaling cascade only represents a subset of the pathophysiology of T2DM. Thus, this indicates the limitation of the *in-vitro* diabetic model as it cannot completely mimic the *in-vivo* insulin resistance in T2DM.

5.6.2 Assessing intracellular ACh, glucose and ATP content

Due to time constraint, the measurement of intracellular ACh, glucose content, and ATP content were not performed. Measurement of these functional parameters would support the findings derived from western blot analysis.

5.6.3 Transfection efficiency

In the present study, lipofectamine-mediated transfection was optimized in the AC16 cells in normoxic condition, and this resulted in approximately 40% transfection efficiency. As both palmitate and glucose treatment, as well as hypoxia, decreased ChAT expression, higher

transfection efficiency is needed to account for the reduction in ChAT expression due to cell loss. However, this was not done due to time constraints.

5.6.4 Specificity of antibodies

As specified in previous chapter, due to limited resources and time, additional control experiments were not performed to test the specificity of anti-GLUT-4, anti-pAKT, anti-AKT, anti-pAMPKα, anti-AMPKα and anti-cleaved caspase 3 antibodies used in this study. This is one of the limitations of the study. Future study should consider testing the antibody on purified antigen, overexpressing or knockout tissue/cells.

5.6.5 Sample size

The present study only collected nine samples from three independent experiments due to time constraints. Thus, future study should consider increasing the number of samples to confidently detect the expression changes.

5.7 Conclusion

In summary, I confirm the hypothesis that palmitate and glucose treatment would impair insulin signaling cascade and induce insulin resistance in the AC16 cells. However, I do not confirm the hypothesis that overexpression of *ChAT* gene in the diabetic AC16 cells would lead to an increase in GLUT-4 expression, thus sustaining energy production and reducing apoptosis under hypoxic condition. The reason is that membrane GLUT-4 expression was not increased, and hypoxia-induced apoptosis was not alleviated in the diabetic hChAT transfected cells. One possible reason could be the ChAT expression was not durable enough to increase the membrane GLUT-4 expression in the diabetic hChAT transfected cells in hypoxic condition. This is because the results from optimization showed at least a 10-fold increase in ChAT expression is needed to induce increase membrane GLUT-4 expression. Thus, a longer

transfection duration may be required to increase the transfection efficiency or generation of stable ChAT-overexpressing cell line may be favorable in the future study. Apart from this, my results also suggest that insulin resistance prevents an insulin-stimulated upregulation of ChAT. This result further supports that findings from Chapter 3 that dysregulation of cardiac NNCS is caused by metabolic derangement and insulin resistance before the onset of DHD. Nevertheless, more in-depth studies are needed to elucidate the underlying mechanism of how metabolic derangement and insulin resistance suppress ChAT expression.

Chapter 6 : General discussion

6.1 Overview of key findings

The main findings of my thesis are:

1. Chapter 3: Changes in cardiac NNCS is associated with the development of DHD

- **Time-dependent increase or decrease in the expression of the components of cardiac NNCS (i.e., ChAT, CHT1, VAChT, AChE, and M_2AChR) in the diabetic heart.** In the *db/db* mice, increased AChE and decreased M_2AChR expression was observed in the early stage of T2DM (8-, 12- and 16-weeks of age), followed by increased VAChT and CHT1 expression as well as decreased AChE and M_2AChR expression at 20- and 24-weeks of age. Subsequently, decreased ChAT, AChE, and M_2AChR expression as well as increased VAChT expression at 28- and 32-weeks of age (Figure 3.18). Further, decreased CHT1 expression was observed in the diabetic human heart. These novel findings provide evidence that cardiac NNCS is dysregulated in T2DM, and the changes in the components of cardiac NNCS may play a role in the diabetic heart.

- **Decreased GLUT-1 and GLUT-4 expression in the diabetic heart.** Previous studies showed that GLUT-1 and GLUT-4 expression were decreased in the diabetic heart [20, 58, 61, 63, 153, 215]. In line with this, my study showed that GLUT-1 and GLUT-4 expression was decreased in the *db/db* mice at 16- and 20-weeks of age, respectively. The GLUT-1 expression remained decreased till 32-weeks of age. On the other hand, GLUT-4 expression was normalized at 24-weeks of age, and the expression was subsequently decreased in the *db/db* mice at 28- and 32-weeks of age. Also, the GLUT-4 expression, but not GLUT-1 expression, was reduced in the diabetic human heart. The findings from my study support that T2DM decreases GLUT-1 and GLUT-4 expression [58, 63, 321], and thereby decreasing glucose uptake [48, 154] and oxidation [62] in the

diabetic heart. Further, to the best of my knowledge, this is the first study to demonstrate the time-dependent expression changes in GLUT-1 and GLUT-4.

- **Changes in cardiac NNCS is associated with a decrease in GLUT-4 expression and diastolic dysfunction in the diabetic heart.** Kakinuma et al. [100] showed that cardiac NNCS plays a role in glucose metabolism by regulating GLUT-4 expression. Further, previous studies showed that decreased glucose metabolism and basal myocardial energy status contributed to cardiac dysfunction in the diabetic heart [19-21, 65-68, 70-72]. In my study, diabetes increased AChE expression and decreased M_2AChR expression in the *db/db* mice at 8- to 16-weeks of age, while GLUT-4 expression and diastolic function were decreased at 20-weeks of age [1]. This suggests that altered cardiac NNCS could contribute to decreased GLUT-4 expression and cardiac dysfunction in diabetes.

- **Changes in cardiac NNCS is associated with cardiac hypertrophy and remodeling in the diabetic heart.** Previous studies reported that cardiac NNCS prevents cardiac hypertrophy and remodeling [97, 99, 101, 124]. In my study, altered cardiac NNCS preceded the cardiac hypertrophy and remodeling [1], suggesting cardiac NNCS plays a role in offsetting hypertrophic signals in the diabetic heart.

2. Chapter 4: Activation of cardiac NNCS is beneficial to the diabetic heart

- **Activation of cardiac NNCS increased GLUT-4 expression and enhanced LV systolic function and contractility of the diabetic heart.** Belke et al. [20] showed that global overexpression of *GLUT-4* gene increased glycolysis and glucose oxidation in the diabetic heart, and ultimately attenuated diabetes-induced cardiac dysfunction. My study demonstrated that the LV functions of the diabetic heart were enhanced after

activation of cardiac NNCS in the ventricles. Further, my study showed that the improved LV functions were associated with increased GLUT-4 expression initiated by pro-survival PI3K/Akt/HIF1α/GLUT-4 signaling cascade through cardiac NNCS (Figure 4.17). Taken together, the findings from my study support the essential role of cardiac NNCS in enhancing GLUT-4 expression to regulate cardiac glucose metabolism and prevent deterioration of cardiac function in diabetes.

- **Activation of cardiac NNCS increased VEGF-A expression and preserved coronary vasculature and enhanced the vascular function of the diabetic heart.** Rawal et al. [137] demonstrated that decreased VEGF-A expression preceded the microvascular rarefaction in the *db/db* mice. Further, Hinkel et al. [322] showed that treatment with VEGF-A stimulated angiogenesis and restored capillary density as well as cardiac function in the diabetic swine model. Thus, the findings from these studies [241, 322] and my study support that cardiac-derived VEGF-A is essential to prevent vasculature rarefaction in the diabetic heart (Figure 4.17). My results also underscore the critical role of cardiac NNCS in angiogenesis.

3. Chapter 5: Transient activation of cardiac NNCS is not effective to protect diabetic cardiomyocytes in hypoxia

- **Preservation of membrane GLUT-4 expression was insufficient to alleviate hypoxia-induced apoptosis in diabetic AC16 cardiomyocytes model overexpressed with *ChAT* gene.** My findings showed that preservation of membrane GLUT-4 expression alone was not sufficient to protect the diabetic cells from hypoxic injury. Vanoverschelde et al. [317] demonstrated that a high rate of glycolysis is necessarily needed to reduce the ischemic injury.

- **Insulin resistance prevented the activation of cardiac NNCS.** Previous studies showed that insulin stimulation increased ChAT and CHT1 expression in the neuronal cell lines and rodent's brain [313, 314]. Further, ChAT expression was decreased in the hippocampus of T1DM rat model [316]. In line with this, insulin stimulation increased ChAT expression in control AC16 cells. However, this was abolished in the diabetic AC16 cells. The result suggests that insulin resistance possibly prevents activation of cardiac NNCS, thereby contributing to reduced GLUT-4 expression.

In summary, this thesis provides evidence that changes in cardiac NNCS may contribute to the development of DHD. Also, activation of cardiac NNCS by increasing ACh bioavailability is beneficial to the cardiovascular function of the diabetic heart (Figure 6.1). Further, a transient activation of cardiac NNCS is not adequate to reduce hypoxic injury in the diabetic cardiomyocytes (Figure 6.1).

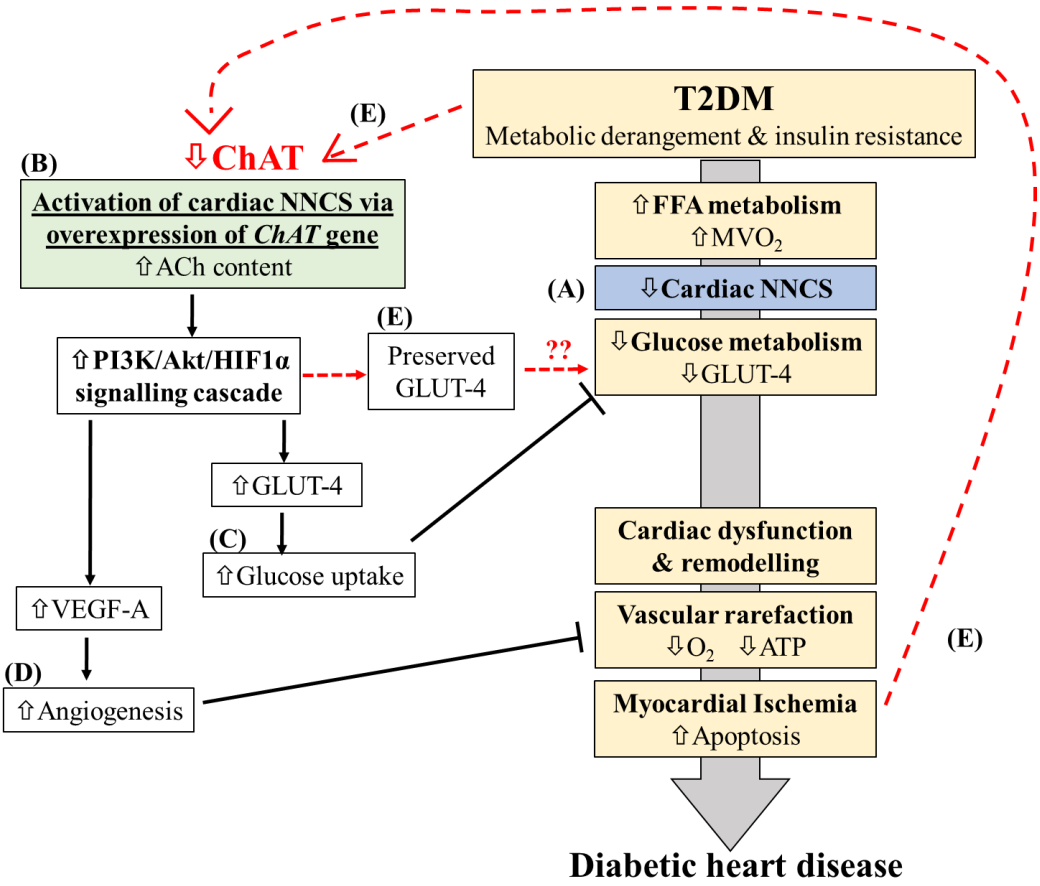

Figure 6.1 The role of cardiac NNCS in the diabetic heart.
(A) *Cardiac NNCS expression is decreased in the diabetic heart.* ***(B)*** *Activation of cardiac NNCS via overexpression of the ChAT gene increases ACh synthesis in the diabetic heart. The ACh is released and bound to M_2AChR, and thus activating PI3K/Akt/HIF1α signaling cascade* ***(C)*** *Initiation of this pathway leads to increased GLUT-4 expression, and thereby increasing glucose uptake and normalizing cardiac metabolism and cardiac efficiency in the diabetic heart. Hence, this could prevent the development of cardiac dysfunction.* ***(D)*** *Initiation of PI3K/Akt/HIF1α signaling pathway leads to an increase in VEGF-A expression, and thereby promoting angiogenesis in the diabetic heart. Hence, this could prevent diabetes-induced vascular rarefaction.* ***(E)*** *However, the combination of hypoxia as well as palmitate and glucose treatment decreased ChAT expression in the in-vitro diabetic cardiomyocytes that overexpressing ChAT gene. Thus, the membrane GLUT-4 expression was not increased, but it was preserved in hypoxia. In this case, the hypoxia-induced apoptosis was not alleviated.*

6.2 Can cardiac NNCS be a therapeutic target?

As outlined in Chapter 1, glucose metabolism is suppressed due to reduced GLUT-4 expression in the diabetic heart [58, 63, 153, 321]. This was consistently observed in the diabetic mouse and human heart samples used in my study (Chapter 3). Besides, previous studies showed that cardiac NNCS regulates glucose metabolism by modulating GLUT-4 expression, thereby enhancing glucose uptake and ATP production in the heart [122, 323]. In line with this, my findings showed dysregulation of cardiac NNCS in the diabetic mouse and human heart,

suggesting dysregulation of cardiac NNCS, which together with insulin resistance, contributes to decreased GLUT-4 expression in diabetes (Chapter 3). Further, GLUT-4 expression, as well as LV function, was enhanced after activating cardiac NNCS via overexpression of the *ChAT* gene in the diabetic heart (Chapter 4). These findings are in agreement with Belke et al. [20] that global overexpression of *GLUT-4* gene prevents cardiac dysfunction by increasing glucose uptake and oxidation in the diabetic heart. These findings strongly support the notion for therapeutically targeting cardiac NNCS as a metabolic intervention to restore glucose metabolism in the diabetic heart.

Although this thesis was initially set to investigate the role of cardiac NNCS in regulating glucose metabolism in the diabetic heart, my findings newly revealed that cardiac NNCS plays a role in angiogenesis in the diabetic heart (Chapter 4). In T2DM, endothelial dysfunction is associated with decreased NO bioavailability [237-240]. Previous studies reported that cardiomyocytes produce NO via ACh-muscarinic receptor stimulation [99, 268, 269]. Therefore, targeting cardiac NNCS to increase ACh production could be an attractive approach to restore NO bioavailability. This notion was evident in the previous study by Oikawa et al. [267], using WT *ChAT-tg* mice, where overexpression of *ChAT* gene resulted in increased NO bioavailability in the heart. Although cardiac NO content was not measured in my study, the enhanced vascular function observed in the diabetic heart may indicate the possibility that NO bioavailability was either preserved or increased. In addition to NO availability, reduction of proangiogenic factor VEGF-A contributes to coronary vascular rarefaction in diabetes, thus impairing vascular function [137]. Previous studies showed that VEGF-A treatment stimulated angiogenesis in the diabetic swine heart [322] as well as infarcted myocardium [324]. My findings are in agreement with these studies that increased VEGF-A preserved coronary vasculature in the diabetic heart (Chapter 4). Therefore, these findings further strengthen the notion of cardiac NNCS as a therapeutic target in the diabetic heart.

Cardiac autonomic neuropathy (CAN) is a severe complication of diabetes [325]. It is caused by damage to the nerve fibers that innervate the heart and blood vessels, thus increasing the risk of developing cardiovascular disease in the diabetic population (reviewed in [326]). The early development of CAN is characterized by increased sympathetic and decreased parasympathetic tone on the cardiac function such as HR and contraction (reviewed in [327]). Further, the decreased parasympathetic tone is associated with decreased ACh secretion [328]. At present, no clinically available therapy aims to deliver ACh to the heart directly. Therefore, targeting cardiac NNCS via overexpression of the *ChAT* gene could be an attractive approach to restore the ACh bioavailability in the diabetic heart, thereby normalizing parasympathetic control of cardiac functions.

In summary, the overall findings position cardiac NNCS as a therapeutic target to normalize GLUT-4 expression (metabolic effect), VEGF-A expression (angiogenic effect), and neuronal cholinergic effects (parasympathetic effect).

6.3 Strategies to target cardiac NNCS

In this section, I propose strategies such as gene therapy, pharmacological therapy, microRNA therapy, stem cell therapy, and vagal nerve stimulation to target cardiac NNCS to enrich the heart with ACh. (*The content presented in this section has been modified from the published literature review in the Journal of Molecular and Cellular Cardiology [102]).*

6.3.1 Gene therapy

My study utilized a genetic approach to overexpress *ChAT* gene to activate cardiac NNCS, however, targeting other components such as CHT1 and VAChT can be equally useful to enable cardiac NNCS (Figure 6.2). This notion is because CHT1 is involved in reuptake of choline for ACh synthesis, and VAChT is involved in the release of ACh [101]. While my study used transgenic mouse model, to translate the results to the clinic, it is important to carefully identify

the suitable vector (i.e., non-viral and viral vector) for efficient delivery of a gene to the heart. This is because a different type of vector would result in different duration of transgene expression and transfection efficiency (reviewed in [329]). For instance, Rengo et al. [330] reported that the cardiac expression of transgene lasted for up to 12-weeks via adeno-associated viral vector and such long duration of transgene expression was able to prevent MI-induced HF and normalized the neurohormonal axis. In contrast, Giordano et al. [331] demonstrated transient transgene expression with an adenoviral vector was sufficient to promote angiogenesis and therefore ameliorating the myocardial contractile dysfunction by improving blood flow. Due to the chronic nature of diabetes, a vector that can induce long term gene expression may be required. On the other hand, viral vectors have been demonstrated to induce inflammatory responses (reviewed in [329]). Therefore, future studies should be carefully designed to identify and test the best vector to deliver the gene to activate NNCS in the diabetic heart.

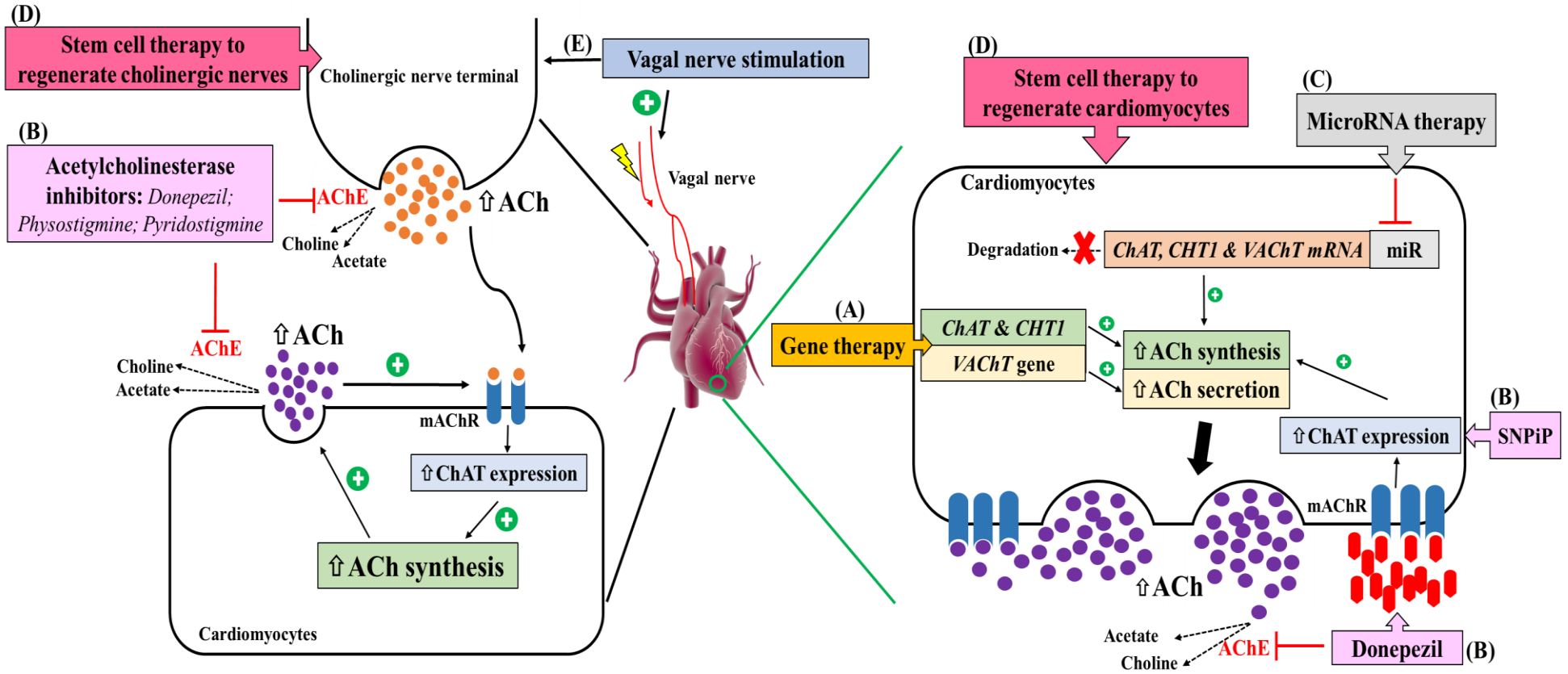

Figure 6.2 The proposed therapeutic strategies to target cardiac NNCS to elevate ACh production to protect the heart against cardiovascular disease. ***(A)*** *Gene therapy where cholinergic genes such as ChAT, CHT1, and VAChT can be delivered to the cardiomyocytes and therefore increasing the expression of these markers that are responsible for ACh synthesis and secretion.* ***(B)*** *The pharmacological approach by using AChE inhibitors can prolong the ACh effect in the extracellular space. Notably, donepezil and SNPiP can increase ChAT transcriptional activity and protein expression.* ***(C)*** *Inhibiting the cardiac miRNAs that promotes degradation of the cholinergic mRNAs.* ***(D)*** *Stem cells therapy to repopulate the cholinergic neurons or to replace the damaged cardiomyocytes with differentiated cholinergic neurons and cardiomyocytes, respectively.* ***(E)*** *Vagal nerve stimulation to electrically activate the vagal nerve to produce and release ACh, and these ACh can, in return, enable cardiac NNCS.*

6.3.2 Pharmacological therapy

The abundant presence of AChE in the extracellular space rapidly hydrolyze ACh and therefore terminating its effect. Previous studies demonstrated the use of AChE inhibitors such as donepezil, physostigmine, and pyridostigmine as effective agents in improving cardiac function in animal models [332-336] as well as HF patients [337-344]. Inhibition of AChE increases the availability of extracellular ACh which in turn acts as an activator to stimulate the cardiomyocytes to synthesize and release ACh in a positive feedback manner [96, 99, 123] (Figure 6.2). Further, donepezil can directly increase the cardiac ChAT gene and protein expression [96]. Increased ChAT expression was also observed in donepezil-treated neuronal cells *in-vitro* [345] and *in-vivo* [346] as well as human umbilical vein endothelial cells (HUVECs; [123]), suggesting that donepezil functions as an AChE inhibitor as well as NNCS inducer. Although the exact molecular mechanism of donepezil in upregulating ChAT expression is unknown, Kakinuma et al. [96] showed that muscarinic ACh receptor is required for donepezil's action as atropine reduced the ChAT expression and intracellular ACh concentration. However, whether donepezil would be effective for the diabetic heart is not known as my findings showed decreased M_2AChR expression in the *db/db* mice (Chapter 3 and 4). Besides, a recent report showed that novel nitric oxide donor S-Nitroso-NPivaloyl-D-Penicillamine (SNPiP) activated cardiac NNCS by increasing ChAT expression [347]. However, the underlying mechanism of how SNPiP leads to an increased ChAT expression is not clear. Although donepezil and SNPiP seem to be a promising agent to induce cardiac NNCS, further investigations are needed to determine the short- and long-term efficacy in the diabetic heart as well as the safety of these drugs.

6.3.3 MicroRNA therapy

MicroRNAs (miRNAs) have been recognized as an essential regulator of gene expression in nearly all biological processes. miRNAs are short non-coding transcript which binds to the 3'

untranslated region of targeted mRNA to inhibit translation and to induce degradation of mRNA (reviewed in [348]). Oikawa et al. [349] reported that miR-345 as the regulator for ChAT mRNA in the murine heart. They demonstrated that the expression pattern of miR-345 was reciprocal to the expression pattern of ChAT mRNA (i.e., high miR-345 expression and low ChAT mRNA expression) in the murine heart as well as in the miR-345 transfected cell lines. However, previous studies showed that dysregulation of microRNA contributed to the pathophysiology of the diabetic heart [1, 137, 350, 351]. Thus, it is not known whether diabetes would affect the expression of miR-345. Nevertheless, a synthetic inhibitor (also known as anti-miR) that has the reverse complement to the miR-345 can be designed to bind to miR-345 and deplete its abundance to prevent degradation of ChAT mRNA and eventually increase the ChAT protein expression and ACh synthesis (Figure 6.2).

6.3.4 Stem cell therapy

Chronic exposure to metabolic derangement induces apoptosis of cardiomyocytes [352, 353]. Thus, the population of cardiomyocytes that remains healthy and able to produce and release ACh is lesser as diabetes progresses. In this case, stem cell therapy is an attractive option, as stem cells can either differentiate into or activate the regeneration of new functional cardiomyocytes to compensate those lost due to diabetes. In particular, an attempt to use resident cardiac stem cells to regenerate the cardiomyocytes has increasingly received great attention along with controversies [354-356]. Regeneration of lost cardiomyocytes will restore their numbers, and this will indirectly increase the population of cells able to produce and release ACh. (Figure 6.2)

Withdrawal of parasympathetic cholinergic tone as a result of CAN is commonly seen in the diabetic population (reviewed in [326]). In this case, stem cell therapy can be used to repopulate the cholinergic neurons, specifically in the medulla oblongata where all the preganglionic cholinergic neurons project through the vagal nerve to the heart and therefore normalizing the

autonomic system in diabetes. While this therapeutic option has not been explored and tested in the cardiovascular disease model, it has been demonstrated to be beneficial in an Alzheimer's disease mouse model [357]. The mice received stem cells therapy showed increased mature cholinergic neurons that functionally integrated into the endogenous basal forebrain cholinergic projection system and eventually improved learning and memory performance. Thus, stem cell therapy to repopulate the cardiomyocytes or cholinergic neurons would be worthwhile to explore in the future as a successful outcome could also be a significant breakthrough in cardiovascular disease.

6.3.5 Autonomic regulation therapy via vagal nerve stimulation

Vagal nerve stimulation has been proposed as an adjunctive treatment to stimulate the neuronal cholinergic nerves to produce ACh. This treatment is achieved by surgically implanting a stimulator that connects to the cervical vagal nerve [358-360]. Since the cardiac NNCS activity can be directly influenced by the neuronal cholinergic system (Chapter 1, Section 1.2.4), electrical stimulation of the vagal nerves to produce and release ACh would in return activate the cardiac NNCS in the cardiomyocytes (Figure 6.2). However, the long-term efficacy of vagal nerve stimulation has been controversial, as NECTAR-HF [361, 362] and INOVATE-HF [363] clinical trials reported no improvement up to 18-month of therapy while ANTHEM-HF clinical trial [364-367] reported an increase in LVEF after 42-month of treatment. Although Malbert et al. [368] showed that vagal nerve stimulation improved skeletal glucose uptake, it is not known if this therapy would be beneficial to the diabetic heart. Nevertheless, the risks and post-surgery side effects associated with this procedure have to be considered as it may not be favorable in individuals with compromised cardiac function and advanced age.

6.4 Future directions

The overall findings from this thesis extend the knowledge of cardiac NNCS in regulating glucose metabolism and vasculature in the diabetic heart. The study's limitations stated in Chapter 3 to 5 provide suggestions to improve the present study. Apart from this, the following future experiments could further strengthen and support the role of cardiac NNCS as a therapeutic target in diabetes.

I. Donepezil [96] and SNPiP [347] enhance ChAT expression in the heart. In a future study, it would be interesting to treat the *db/db* mice with donepezil or SNPiP to assess whether this strategy improves cardiovascular functions in comparison to the non-treated *db/db* mice. The use of *db/db* mice with different age groups could provide valuable insight into the treatment. For example, treating the *db/db* mice before established cardiac dysfunction would demonstrate whether the donepezil or SNPiP could prevent the manifestation of DHD. Treating the *db/db* mice after established cardiac function would confirm whether donepezil or SNPiP are effective in ameliorating the effect of DHD. The outcome would further position the role of donepezil or SNPiP as a prophylactic or therapeutic treatment when translating to the clinics.

II. Reduction of ChAT expression by loss-of-function through knocking out the *ChAT* gene. The experiment could be performed in *in-vitro* and *in-vivo* diabetic models where deterioration of LV and vascular function, severe impairment in glucose utilization and metabolism as well as increased apoptosis might be observed. The outcome from the experiments will complement the findings derived from the present study and further strengthen the role of cardiac NNCS in diabetes.

6.5 Conclusion

An early rectification of cardiac metabolism prevents the development of DHD in the diabetic heart. In this thesis, I demonstrated that dysregulation of cardiac NNCS is associated with altered cardiac metabolism in diabetic heart and hence, the development of DHD. Further, I showed that the activation of cardiac NNCS prevents the development of DHD. However, transient activation of cardiac NNCS is not adequate to alleviate hypoxic injury in diabetic cardiomyocytes. Last but not least, this thesis provides a strong foundation that targeting cardiac NNCS could be a potential therapeutic target for the diabetic heart.

.

References

1. Rawal, S., et al., Early dysregulation of cardiac-specific microRNA-208a is linked to maladaptive cardiac remodelling in diabetic myocardium. Cardiovascular Diabetology, 2019. **18**(1): p. 13.
2. American Diabetes, A., Diagnosis and classification of diabetes mellitus. Diabetes care, 2010. **33 Suppl 1**(Suppl 1): p. S62-S69.
3. IDF. IDF Diabetes Atlas 2017; 8th [Available from: http://www.diabetesatlas.org/.
4. Taylor, R., Insulin Resistance and Type 2 Diabetes. Diabetes, 2012. **61**(4): p. 778.
5. Skyler, J.S., et al., Differentiation of Diabetes by Pathophysiology, Natural History, and Prognosis. Diabetes, 2017. **66**(2): p. 241.
6. Garcia, M.J., et al., Morbidity and Mortality in Diabetics In the Framingham Population: Sixteen Year Follow-up Study. Diabetes, 1974. **23**(2): p. 105-111.
7. Kannel, W.B. and D.L. McGee, Diabetes and cardiovascular risk factors: the Framingham study. Circulation, 1979. **59**(1): p. 8-13.
8. Galderisi, M., et al., Echocardiographic evidence for the existence of a distinct diabetic cardiomyopathy (the Framingham Heart Study). Am J Cardiol, 1991. **68**(1): p. 85-9.
9. Kannel, W.B. and D.L. McGee, Diabetes and cardiovascular disease. The Framingham study. Jama, 1979. **241**(19): p. 2035-8.
10. Marwick, T.H., Diabetic heart disease. Heart, 2006. **92**(3): p. 296.
11. MacDonald, M.R., et al., Impact of diabetes on outcomes in patients with low and preserved ejection fraction heart failure: an analysis of the Candesartan in Heart failure: Assessment of Reduction in Mortality and morbidity (CHARM) programme. European Heart Journal, 2008. **29**(11): p. 1377-85.
12. Cubbon, R.M., et al., Diabetes mellitus is associated with adverse prognosis in chronic heart failure of ischaemic and non-ischaemic aetiology. Diab Vasc Dis Res, 2013. **10**(4): p. 330-6.
13. Kannel, W.B., Framingham Study Insights on Diabetes and Cardiovascular Disease. Clinical Chemistry, 2011. **57**(2): p. 338.
14. Brands Michael, W. and E. Hopkins Timothy, Poor Glycemic Control Induces Hypertension in Diabetes Mellitus. Hypertension, 1996. **27**(3): p. 735-739.
15. Bryson, C.L., et al., Association between Gestational Diabetes and Pregnancy-induced Hypertension. American Journal of Epidemiology, 2003. **158**(12): p. 1148-1153.
16. Katare, R., et al., Progressive Decrease in Coronary Vascular Function Associated With Type 2 Diabetic Heart Disease. Frontiers in physiology, 2018. **9**: p. 696-696.

17. Sarwar, N., et al., Diabetes mellitus, fasting blood glucose concentration, and risk of vascular disease: a collaborative meta-analysis of 102 prospective studies. Lancet, 2010. **375**(9733): p. 2215-22.

18. Lind, M., et al., Glycaemic control and incidence of heart failure in 20,985 patients with type 1 diabetes: an observational study. Lancet, 2011. **378**(9786): p. 140-6.

19. Scheuermann-Freestone, M., et al., Abnormal cardiac and skeletal muscle energy metabolism in patients with type 2 diabetes. Circulation, 2003. **107**(24): p. 3040-6.

20. Belke, D.D., et al., Altered metabolism causes cardiac dysfunction in perfused hearts from diabetic (db/db) mice. American Journal of Physiology. Endocrinology and Metabolism, 2000. **279**(5): p. E1104-1113.

21. Levelt, E., et al., Cardiac energetics, oxygenation, and perfusion during increased workload in patients with type 2 diabetes mellitus. European Heart Journal, 2016. **37**(46): p. 3461-3469.

22. Wang, Y., et al., Prediction of heart failure in patients with type 2 diabetes mellitus- a systematic review and meta-analysis. Diabetes Res Clin Pract, 2015. **108**(1): p. 55-66.

23. Zhou, Y.T., et al., Lipotoxic heart disease in obese rats: implications for human obesity. Proc Natl Acad Sci U S A, 2000. **97**(4): p. 1784-9.

24. Stanley, W.C., G.D. Lopaschuk, and J.G. McCormack, Regulation of energy substrate metabolism in the diabetic heart. Cardiovasc Res, 1997. **34**(1): p. 25-33.

25. Sacre, J.W., et al., Association of cardiac autonomic neuropathy with subclinical myocardial dysfunction in type 2 diabetes. JACC Cardiovasc Imaging, 2010. **3**(12): p. 1207-15.

26. Giacco, F. and M. Brownlee, Oxidative stress and diabetic complications. Circulation Research, 2010. **107**(9): p. 1058-70.

27. Matsushima, S., et al., Increased myocardial NAD(P)H oxidase-derived superoxide causes the exacerbation of postinfarct heart failure in type 2 diabetes. Am J Physiol Heart Circ Physiol, 2009. **297**(1): p. H409-16.

28. Shipp, J.C., L.H. Opie, and D. Challoner, Fatty Acid and Glucose Metabolism in the Perfused Heart. Nature, 1961. **189**: p. 1018.

29. Rothlin, M.E. and R.J. Bing, Extraction and release of individual free fatty acids by the heart and fat depots. J Clin Invest, 1961. **40**: p. 1380-6.

30. Adeva-Andany, M.M., et al., Mitochondrial beta-oxidation of saturated fatty acids in humans. Mitochondrion, 2019. **46**: p. 73-90.

31. Chong, C.-R., K. Clarke, and E. Levelt, Metabolic remodelling in diabetic cardiomyopathy. Cardiovascular Research, 2017. **113**(4): p. 422-430.

32. Wentz, A.E., et al., Adaptation of myocardial substrate metabolism to a ketogenic nutrient environment. J Biol Chem, 2010. **285**(32): p. 24447-56.
33. Kaijser, L. and B. Berglund, Myocardial lactate extraction and release at rest and during heavy exercise in healthy men. Acta Physiol Scand, 1992. **144**(1): p. 39-45.
34. Goodwin, G.W. and H. Taegtmeyer, Improved energy homeostasis of the heart in the metabolic state of exercise. Am J Physiol Heart Circ Physiol, 2000. **279**(4): p. H1490-501.
35. Boudina, S., et al., Mitochondrial energetics in the heart in obesity-related diabetes: direct evidence for increased uncoupled respiration and activation of uncoupling proteins. Diabetes, 2007. **56**(10): p. 2457-66.
36. Nascimben, L., et al., Mechanisms for increased glycolysis in the hypertrophied rat heart. Hypertension, 2004. **44**(5): p. 662-7.
37. Allard, M.F., et al., Contribution of oxidative metabolism and glycolysis to ATP production in hypertrophied hearts. Am J Physiol, 1994. **267**(2 Pt 2): p. H742-50.
38. Schonekess, B.O., Competition between lactate and fatty acids as sources of ATP in the isolated working rat heart. Journal of Molecular and Cellular Cardiology, 1997. **29**(10): p. 2725-33.
39. Maki, M.T., et al., Free fatty acid uptake in the myocardium and skeletal muscle using fluorine-18-fluoro-6-thia-heptadecanoic acid. J Nucl Med, 1998. **39**(8): p. 1320-7.
40. Liepinsh, E., et al., The heart is better protected against myocardial infarction in the fed state compared to the fasted state. Metabolism, 2014. **63**(1): p. 127-36.
41. Gertz, E.W., et al., Myocardial substrate utilization during exercise in humans. Dual carbon-labeled carbohydrate isotope experiments. J Clin Invest, 1988. **82**(6): p. 2017-25.
42. Sun, D., et al., Ischemia induces translocation of the insulin-responsive glucose transporter GLUT4 to the plasma membrane of cardiac myocytes. Circulation, 1994. **89**(2): p. 793-8.
43. Stanley, W.C., et al., Acute myocardial ischemia causes a transmural gradient in glucose extraction but not glucose uptake. Am J Physiol, 1992. **262**(1 Pt 2): p. H91-6.
44. Xing, Y., et al., Glucose metabolism and energy homeostasis in mouse hearts overexpressing dominant negative alpha2 subunit of AMP-activated protein kinase. J Biol Chem, 2003. **278**(31): p. 28372-7.
45. Zhou, L., et al., Impact of anaerobic glycolysis and oxidative substrate selection on contractile function and mechanical efficiency during moderate severity ischemia. Am J Physiol Heart Circ Physiol, 2008. **295**(3): p. H939-h945.
46. Fillmore, N. and G.D. Lopaschuk, Impact of fatty acid oxidation on cardiac efficiency. Heart and Metabolism, 2011(53): p. 33-37.

47. Iozzo, P., et al., Independent Association of Type 2 Diabetes and Coronary Artery Disease With Myocardial Insulin Resistance. Diabetes, 2002. **51**(10): p. 3020.
48. Yokoyama, I., et al., Role of insulin resistance in heart and skeletal muscle F-18 fluorodeoxyglucose uptake in patients with noninsulin-dependent diabetes mellitus. Journal of Nuclear Cardiology, 2000. **7**(3): p. 242-248.
49. Peterson, L.R., et al., Fatty acids and insulin modulate myocardial substrate metabolism in humans with type 1 diabetes. Diabetes, 2008. **57**(1): p. 32-40.
50. Labbe, S.M., et al., Increased myocardial uptake of dietary fatty acids linked to cardiac dysfunction in glucose-intolerant humans. Diabetes, 2012. **61**(11): p. 2701-10.
51. Young, M.E., et al., Impaired long-chain fatty acid oxidation and contractile dysfunction in the obese Zucker rat heart. Diabetes, 2002. **51**(8): p. 2587-95.
52. Chakrabarti, P., et al., Insulin inhibits lipolysis in adipocytes via the evolutionarily conserved mTORC1-Egr1-ATGL-mediated pathway. Mol Cell Biol, 2013. **33**(18): p. 3659-66.
53. Ellis, B.A., et al., Long-chain acyl-CoA esters as indicators of lipid metabolism and insulin sensitivity in rat and human muscle. Am J Physiol Endocrinol Metab, 2000. **279**(3): p. E554-60.
54. Itani, S.I., et al., Lipid-induced insulin resistance in human muscle is associated with changes in diacylglycerol, protein kinase C, and IkappaB-alpha. Diabetes, 2002. **51**(7): p. 2005-11.
55. Randle, P.J., et al., The glucose fatty-acid cycle. Its role in insulin sensitivity and the metabolic disturbances of diabetes mellitus. Lancet, 1963. **1**(7285): p. 785-9.
56. Finck, B.N., et al., The cardiac phenotype induced by PPARalpha overexpression mimics that caused by diabetes mellitus. J Clin Invest, 2002. **109**(1): p. 121-30.
57. Gulick, T., et al., The peroxisome proliferator-activated receptor regulates mitochondrial fatty acid oxidative enzyme gene expression. Proc Natl Acad Sci U S A, 1994. **91**(23): p. 11012-6.
58. Garvey, W.T., et al., Effects of diabetes on myocardial glucose transport system in rats: implications for diabetic cardiomyopathy. Am J Physiol, 1993. **264**(3 Pt 2): p. H837-44.
59. Rijzewijk, L.J., et al., Effects of hepatic triglyceride content on myocardial metabolism in type 2 diabetes. J Am Coll Cardiol, 2010. **56**(3): p. 225-33.
60. Sidell, R.J., et al., Thiazolidinedione Treatment Normalizes Insulin Resistance and Ischemic Injury in the Zucker Fatty Rat Heart. Diabetes, 2002. **51**(4): p. 1110.
61. Cook, S.A., et al., Abnormal myocardial insulin signalling in type 2 diabetes and left-ventricular dysfunction. European Heart Journal, 2010. **31**(1): p. 100-111.

62. Rijzewijk, L.J., et al., Altered myocardial substrate metabolism and decreased diastolic function in nonischemic human diabetic cardiomyopathy: studies with cardiac positron emission tomography and magnetic resonance imaging. J Am Coll Cardiol, 2009. **54**(16): p. 1524-32.

63. Huang, J.-P., et al., Impairment of insulin-stimulated Akt/GLUT4 signaling is associated with cardiac contractile dysfunction and aggravates I/R injury in STZ-diabetic rats. Journal of biomedical science, 2009. **16**(1): p. 77-77.

64. Chatham, J.C. and A.-M.L. Seymour, Cardiac carbohydrate metabolism in Zucker diabetic fatty rats. Cardiovascular Research, 2002. **55**(1): p. 104-112.

65. Mazumder, P.K., et al., Impaired cardiac efficiency and increased fatty acid oxidation in insulin-resistant ob/ob mouse hearts. Diabetes, 2004. **53**(9): p. 2366-74.

66. Buchanan, J., et al., Reduced cardiac efficiency and altered substrate metabolism precedes the onset of hyperglycemia and contractile dysfunction in two mouse models of insulin resistance and obesity. Endocrinology, 2005. **146**(12): p. 5341-9.

67. How, O.J., et al., Increased myocardial oxygen consumption reduces cardiac efficiency in diabetic mice. Diabetes, 2006. **55**(2): p. 466-73.

68. Levelt, E., et al., Cardiac energetics, oxygenation, and perfusion during increased workload in patients with type 2 diabetes mellitus. Eur Heart J, 2016. **37**(46): p. 3461-3469.

69. Semeniuk, L.M., A.J. Kryski, and D.L. Severson, Echocardiographic assessment of cardiac function in diabetic db/db and transgenic db/db-hGLUT4 mice. Am J Physiol Heart Circ Physiol, 2002. **283**(3): p. H976-82.

70. Luptak, I., et al., Decreased ATP production and myocardial contractile reserve in metabolic heart disease. Journal of Molecular and Cellular Cardiology, 2018. **116**: p. 106-114.

71. Bashir, A., A.R. Coggan, and R.J. Gropler, In vivo creatine kinase reaction kinetics at rest and stress in type II diabetic rat heart. Physiol Rep, 2015. **3**(1).

72. Diamant, M., et al., Diastolic dysfunction is associated with altered myocardial metabolism in asymptomatic normotensive patients with well-controlled type 2 diabetes mellitus. J Am Coll Cardiol, 2003. **42**(2): p. 328-35.

73. Young, M.E., et al., Uncoupling protein 3 transcription is regulated by peroxisome proliferator-activated receptor α in the adult rodent heart. The FASEB Journal, 2001. **15**(3): p. 833-845.

74. Tong, M., et al., Mitophagy Is Essential for Maintaining Cardiac Function During High Fat Diet-Induced Diabetic Cardiomyopathy. Circulation Research, 2019. **124**(9): p. 1360-1371.

75. Boudina, S., et al., Reduced mitochondrial oxidative capacity and increased mitochondrial uncoupling impair myocardial energetics in obesity. Circulation, 2005. **112**(17): p. 2686-95.
76. Anderson, E.J., et al., Substrate-specific derangements in mitochondrial metabolism and redox balance in the atrium of the type 2 diabetic human heart. J Am Coll Cardiol, 2009. **54**(20): p. 1891-8.
77. Ceradini, D.J., et al., Decreasing intracellular superoxide corrects defective ischemia-induced new vessel formation in diabetic mice. J Biol Chem, 2008. **283**(16): p. 10930-8.
78. Xiang, L., et al., Chronic hyperglycemia impairs functional vasodilation via increasing thromboxane-receptor-mediated vasoconstriction. American Journal of Physiology-Heart and Circulatory Physiology, 2007. **292**(1): p. H231-H236.
79. Chatham, J.C. and A.M. Seymour, Cardiac carbohydrate metabolism in Zucker diabetic fatty rats. Cardiovascular Research, 2002. **55**(1): p. 104-12.
80. Mjos, O.D., Effect of free fatty acids on myocardial function and oxygen consumption in intact dogs. J Clin Invest, 1971. **50**(7): p. 1386-9.
81. Burkhoff, D., et al., Influence of metabolic substrate on rat heart function and metabolism at different coronary flows. Am J Physiol, 1991. **261**(3 Pt 2): p. H741-50.
82. Lopaschuk, G.D., et al., Myocardial fatty acid metabolism in health and disease. Physiol Rev, 2010. **90**(1): p. 207-58.
83. Kantor, P.F., et al., The antianginal drug trimetazidine shifts cardiac energy metabolism from fatty acid oxidation to glucose oxidation by inhibiting mitochondrial long-chain 3-ketoacyl coenzyme A thiolase. Circ Res, 2000. **86**(5): p. 580-8.
84. Lopaschuk, G.D., et al., Beneficial effects of trimetazidine in ex vivo working ischemic hearts are due to a stimulation of glucose oxidation secondary to inhibition of long-chain 3-ketoacyl coenzyme a thiolase. Circ Res, 2003. **93**(3): p. e33-7.
85. Abozguia, K., et al., Metabolic modulator perhexiline corrects energy deficiency and improves exercise capacity in symptomatic hypertrophic cardiomyopathy. Circulation, 2010. **122**(16): p. 1562-9.
86. Bebernitz, G.R., et al., Anilides of (R)-Trifluoro-2-hydroxy-2-methylpropionic Acid as Inhibitors of Pyruvate Dehydrogenase Kinase. Journal of Medicinal Chemistry, 2000. **43**(11): p. 2248-2257.
87. Fath-Ordoubadi, F. and J. Beatt Kevin, Glucose-Insulin-Potassium Therapy for Treatment of Acute Myocardial Infarction. Circulation, 1997. **96**(4): p. 1152-1156.

88. Mamas, M.A., L. Neyses, and F. Fath-Ordoubadi, A meta-analysis of glucose-insulin-potassium therapy for treatment of acute myocardial infarction. Experimental and clinical cardiology, 2010. **15**(2): p. e20-e24.

89. Liu, B., et al., Cardiac Efficiency Is Improved After Ischemia by Altering Both the Source and Fate of Protons. Circulation Research, 1996. **79**(5): p. 940-948.

90. Wu, C.Y., et al., A novel inhibitor of pyruvate dehydrogenase kinase stimulates myocardial carbohydrate oxidation in diet-induced obesity. J Biol Chem, 2018. **293**(25): p. 9604-9613.

91. Wallhaus Thomas, R., et al., Myocardial Free Fatty Acid and Glucose Use After Carvedilol Treatment in Patients With Congestive Heart Failure. Circulation, 2001. **103**(20): p. 2441-2446.

92. Igarashi, N., et al., Influence of beta-adrenoceptor blockade on the myocardial accumulation of fatty acid tracer and its intracellular metabolism in the heart after ischemia-reperfusion injury. Circ J, 2006. **70**(11): p. 1509-14.

93. Cook, W.S., et al., Less extrahepatic induction of fatty acid beta-oxidation enzymes by PPAR alpha. Biochem Biophys Res Commun, 2000. **278**(1): p. 250-7.

94. Schoonjans, K., et al., Acyl-CoA synthetase mRNA expression is controlled by fibric-acid derivatives, feeding and liver proliferation. Eur J Biochem, 1993. **216**(2): p. 615-22.

95. Schmitz, F.J., P. Rosen, and H. Reinauer, Improvement of myocardial function and metabolism in diabetic rats by the carnitine palmitoyl transferase inhibitor Etomoxir. Horm Metab Res, 1995. **27**(12): p. 515-22.

96. Kakinuma, Y., T. Akiyama, and T. Sato, Cholinoceptive and cholinergic properties of cardiomyocytes involving an amplification mechanism for vagal efferent effects in sparsely innervated ventricular myocardium. FEBS journal, 2009. **276**(18): p. 5111-5125.

97. Roy, A., et al., Cardiomyocyte-secreted acetylcholine is required for maintenance of homeostasis in the heart. FASEB journal, 2013. **27**(12): p. 5072-5082.

98. Kakinuma, Y., et al., A non-neuronal cardiac cholinergic system plays a protective role in myocardium salvage during ischemic insults. PLOS ONE, 2012. **7**(11): p. e50761.

99. Rocha-Resende, C., et al., Non-neuronal cholinergic machinery present in cardiomyocytes offsets hypertrophic signals. Journal of Molecular and Cellular Cardiology, 2012. **53**(2): p. 206-216.

100. Kakinuma, Y., et al., Heart-specific overexpression of choline acetyltransferase gene protects murine heart against ischemia through hypoxia-inducible factor-1α-related defense mechanisms. Journal of the American Heart Association, 2013. **2**(1): p. e004887.

101. Roy, A., et al., Cardiac acetylcholine inhibits ventricular remodeling and dysfunction under pathologic conditions. FASEB journal, 2015. **30**(2): p. 688-701.
102. Saw, E.L., et al., The non-neuronal cholinergic system in the heart: A comprehensive review. J Mol Cell Cardiol, 2018. **125**: p. 129-139.
103. Parsons, S.M., C. Prior, and I.G. Marshall, Acetylcholine transport, storage, and release. Int Rev Neurobiol, 1993. **35**: p. 279-390.
104. Nguyen, M.L., G.D. Cox, and S.M. Parsons, Kinetic Parameters for the Vesicular Acetylcholine Transporter: Two Protons Are Exchanged for One Acetylcholine. Biochemistry, 1998. **37**(38): p. 13400-13410.
105. Kuhar, M.J. and L.C. Murrin, Sodium-dependent, high affinity choline uptake. Journal of Neurochemistry, 1978. **30**(1): p. 15-21.
106. Koelle, G.B., The histochemical localization of cholinesterases in the central nervous system of the rat. J Comp Neurol, 1954. **100**(1): p. 211-35.
107. Massoulié, J., et al., Molecular and cellular biology of cholinesterases. Progress in Neurobiology, 1993. **41**(1): p. 31-91.
108. Rana, O.R., et al., Acetylcholine as an age-dependent non-neuronal source in the heart. Autonomic Neuroscience: Basic & Clinical, 2010. **156**(1-2): p. 82-89.
109. Dhein, S., C.J. van Koppen, and O.E. Brodde, Muscarinic receptors in the mammalian heart. Pharmacological Research, 2001. **44**(3): p. 161-182.
110. Krejčí, A. and S. Tuček, Quantitation of mRNAs for M1 to M5 Subtypes of Muscarinic Receptors in Rat Heart and Brain Cortex. Mol Pharmacology, 2002. **61**(6): p. 1267.
111. Kitazawa, T., et al., M3 muscarinic receptors mediate positive inotropic responses in mouse atria: a study with muscarinic receptor knockout mice. J Pharmacol Exp Ther, 2009. **330**(2): p. 487-93.
112. Wang, H., et al., Expression of multiple subtypes of muscarinic receptors and cellular distribution in the human heart. Mol Pharmacology, 2001. **59**(5): p. 1029-36.
113. Soejima, M. and A. Noma, Mode of regulation of the ACh-sensitive K-channel by the muscarinic receptor in rabbit atrial cells. Pflügers Archiv: European Journal of Physiology, 1984. **400**(4): p. 424-431.
114. Accili, E.A., et al., From funny current to HCN channels: 20 years of excitation. News in Physiological Sciences: An International Journal of Physiology Produced Jointly by the International Union of Physiological Sciences and the American Physiological Society, 2002. **17**: p. 32-37.

115. Hartzell, H.C., Regulation of cardiac ion channels by catecholamines, acetylcholine and second messenger systems. Progress in Biophysics and Molecular Biology, 1988. **52**(3): p. 165-247.

116. Harvey, R.D. and A.E. Belevych, Muscarinic regulation of cardiac ion channels. British Journal of Pharmacology, 2003. **139**(6): p. 1074-1084.

117. Giles, W. and S.J. Noble, Changes in membrane currents in bullfrog atrium produced by acetylcholine. The Journal of Physiology, 1976. **261**(1): p. 103-123.

118. Dhein, S., et al., Autocrine control of angiogenesis by endogenous acetylcholine in an in vitro model using human endothelial cells: evidence for an autocrine cholinergic system in endothelial cells. Journal of Cardiovascular Pharmacology, 2015. **65**(5): p. 508-515.

119. Vanhaesebroeck, B. and M.D. Waterfield, Signaling by distinct classes of phosphoinositide 3-kinases. Exp Cell Res, 1999. **253**(1): p. 239-54.

120. Kakinuma, Y., et al., Acetylcholine from vagal stimulation protects cardiomyocytes against ischemia and hypoxia involving additive non-hypoxic induction of HIF-1alpha. FEBS letters, 2005. **579**(10): p. 2111-2118.

121. Miao, Y., et al., Acetylcholine inhibits tumor necrosis factor α activated endoplasmic reticulum apoptotic pathway via EGFR-PI3K signaling in cardiomyocytes. Journal of Cellular Physiology, 2015. **230**(4): p. 767-774.

122. Oikawa, S., M. Iketani, and Y. Kakinuma, A non-neuronal cholinergic system regulates cellular ATP levels to maintain cell viability. Cellular Physiology and Biochemistry, 2014. **34**(3): p. 781-789.

123. Kakinuma, Y., et al., Donepezil, an acetylcholinesterase inhibitor against Alzheimer's dementia, promotes angiogenesis in an ischemic hindlimb model. Journal of Molecular and Cellular Cardiology, 2010. **48**(4): p. 680-693.

124. Gavioli, M., et al., Cholinergic signaling exerts protective effects in models of sympathetic hyperactivity-induced cardiac dysfunction. PLOS ONE, 2014. **9**(7): p. e100179.

125. Hirota, K., et al., Induction of hypoxia-inducible factor 1 activity by muscarinic acetylcholine receptor signaling. J Biol Chem, 2004. **279**(40): p. 41521-8.

126. Maxwell, P.H., et al., The tumour suppressor protein VHL targets hypoxia-inducible factors for oxygen-dependent proteolysis. Nature, 1999. **399**(6733): p. 271-5.

127. Semenza, G.L., Hypoxia-inducible factor 1 and cardiovascular disease. Annu Rev Physiol, 2014. **76**: p. 39-56.

128. Xue, W., et al., Cardiac-specific overexpression of HIF-1{alpha} prevents deterioration of glycolytic pathway and cardiac remodeling in streptozotocin-induced diabetic mice. The American journal of pathology, 2010. **177**(1): p. 97-105.

129. Piantadosi, C.A. and H.B. Suliman, Transcriptional Regulation of SDHa flavoprotein by nuclear respiratory factor-1 prevents pseudo-hypoxia in aerobic cardiac cells. J Biol Chem, 2008. **283**(16): p. 10967-77.

130. Date, T., et al., Expression of constitutively stable hybrid hypoxia-inducible factor-1alpha protects cultured rat cardiomyocytes against simulated ischemia-reperfusion injury. Am J Physiol Cell Physiol, 2005. **288**(2): p. C314-20.

131. Royer, C., et al., Effects of gestational hypoxia on mRNA levels of Glut3 and Glut4 transporters, hypoxia inducible factor-1 and thyroid hormone receptors in developing rat brain. Brain Res, 2000. **856**(1-2): p. 119-28.

132. Aerni-Flessner, L., et al., GLUT4, GLUT1, and GLUT8 are the dominant GLUT transcripts expressed in the murine left ventricle. Cardiovascular Diabetology, 2012. **11**: p. 63.

133. Wang, C. and S.M. Hu, Developmental regulation in the expression of rat heart glucose transporters. Biochem Biophys Res Commun, 1991. **177**(3): p. 1095-100.

134. Association, A.D., 8. Cardiovascular Disease and Risk Management. Diabetes Care, 2015. **38**(Supplement 1): p. S49-S57.

135. Morrish, N.J., et al., Mortality and causes of death in the WHO Multinational Study of Vascular Disease in Diabetes. Diabetologia, 2001. **44 Suppl 2**: p. S14-21.

136. Burke, S.J., et al., db/db Mice Exhibit Features of Human Type 2 Diabetes That Are Not Present in Weight-Matched C57BL/6J Mice Fed a Western Diet. J Diabetes Res, 2017. **2017**: p. 8503754.

137. Rawal, S., et al., Down-regulation of proangiogenic microRNA-126 and microRNA-132 are early modulators of diabetic cardiac microangiopathy. Cardiovascular Research, 2017. **113**(1): p. 90-101.

138. Jung, H., H. Nam, and J.-G. Suh, Rapid and efficient identification of the mouse leptin receptor mutation (C57BL/KsJ-db/db) by tetra-primer amplification refractory mutation system-polymerase chain reaction (ARMS-PCR) analysis. Laboratory animal research, 2016. **32**(1): p. 70-73.

139. Laboratory, T.J. BKS.Cg-Dock7m+/+Leprdb/J. 17/07/2019]; Available from: https://www.jax.org/strain/000697.

140. Organization, G.W.H., 2. Glycated haemoglobin (HbA1c) for the diagnosis of diabetes, in Use of Glycated Haemoglobin (HbA1c) in the Diagnosis of Diabetes Mellitus: Abbreviated Report of a WHO Consultation. 2011.

141. Davidson, M.M., et al., Novel cell lines derived from adult human ventricular cardiomyocytes. Journal of Molecular and Cellular Cardiology, 2005. **39**(1): p. 133-47.

142. Livak, K.J. and T.D. Schmittgen, Analysis of relative gene expression data using real-time quantitative PCR and the 2(-Delta Delta C(T)) Method. Methods, 2001. **25**(4): p. 402-408.
143. Rain, S., et al., Protein changes contributing to right ventricular cardiomyocyte diastolic dysfunction in pulmonary arterial hypertension. Journal of the American Heart Association, 2014. **3**(3): p. e000716-e000716.
144. Pinto-Junior, D.C., et al., Advanced glycation end products-induced insulin resistance involves repression of skeletal muscle GLUT4 expression. Scientific Reports, 2018. **8**(1): p. 8109.
145. Katare, R., et al., Ghrelin Promotes Functional Angiogenesis in a Mouse Model of Critical Limb Ischemia Through Activation of Proangiogenic MicroRNAs. Endocrinology, 2016. **157**(2): p. 432-445.
146. Dice, J.F., et al., General characteristics of protein degradation in diabetes and starvation. Proceedings of the National Academy of Sciences of the United States of America, 1978. **75**(5): p. 2093-2097.
147. Smith, O.L., C.Y. Wong, and R.A. Gelfand, Skeletal muscle proteolysis in rats with acute streptozocin-induced diabetes. Diabetes, 1989. **38**(9): p. 1117-22.
148. Liu, Z., et al., The Ubiquitin-Proteasome Proteolytic Pathway in Heart vs Skeletal Muscle: Effects of Acute Diabetes. Biochemical and Biophysical Research Communications, 2000. **276**(3): p. 1255-1260.
149. Siew, E.D., et al., Insulin resistance is associated with skeletal muscle protein breakdown in non-diabetic chronic hemodialysis patients. Kidney Int, 2007. **71**(2): p. 146-52.
150. Hu, J., et al., Cardiac muscle protein catabolism in diabetes mellitus: activation of the ubiquitin-proteasome system by insulin deficiency. Endocrinology, 2008. **149**(11): p. 5384-5390.
151. Cousin, S.P., et al., Free fatty acid-induced inhibition of glucose and insulin-like growth factor I-induced deoxyribonucleic acid synthesis in the pancreatic beta-cell line INS-1. Endocrinology, 2001. **142**(1): p. 229-40.
152. Kinkel, A.D., et al., Oil red-O stains non-adipogenic cells: a precautionary note. Cytotechnology, 2004. **46**(1): p. 49-56.
153. Leguisamo, N.M., et al., GLUT4 content decreases along with insulin resistance and high levels of inflammatory markers in rats with metabolic syndrome. Cardiovascular Diabetology, 2012. **11**: p. 100-100.
154. Ohtake, T., et al., Myocardial glucose metabolism in noninsulin-dependent diabetes mellitus patients evaluated by FDG-PET. J Nucl Med, 1995. **36**(3): p. 456-63.

155. Boyer, J.K., et al., Prevalence of ventricular diastolic dysfunction in asymptomatic, normotensive patients with diabetes mellitus. Am J Cardiol, 2004. **93**(7): p. 870-5.
156. Patil, V.C., et al., Diastolic dysfunction in asymptomatic type 2 diabetes mellitus with normal systolic function. Journal of cardiovascular disease research, 2011. **2**(4): p. 213-222.
157. Bouthoorn, S., et al., Prevalence of left ventricular systolic dysfunction and heart failure with reduced ejection fraction in men and women with type 2 diabetes mellitus: a systematic review and meta-analysis. Cardiovascular diabetology, 2018. **17**(1): p. 58-58.
158. Zoppini, G., et al., Association between subclinical left ventricular systolic dysfunction and glycemic control in asymptomatic type 2 diabetic patients with preserved left ventricular function. J Diabetes Complications, 2017. **31**(6): p. 1035-1040.
159. Buchanan, J., et al., Reduced Cardiac Efficiency and Altered Substrate Metabolism Precedes the Onset of Hyperglycemia and Contractile Dysfunction in Two Mouse Models of Insulin Resistance and Obesity. Endocrinology, 2005. **146**(12): p. 5341-5349.
160. Araz, M., A. Bayrac, and H. Ciftci, The impact of diabetes on left ventricular diastolic function in patients with arterial hypertension. Northern clinics of Istanbul, 2015. **2**(3): p. 177-181.
161. Poirier, P., et al., Diastolic Dysfunction in Normotensive Men with Well-Controlled Type 2 Diabetes. Diabetes Care, 2001. **24**(1): p. 5.
162. Romano, S., et al., Early diagnosis of left ventricular diastolic dysfunction in diabetic patients: a possible role for natriuretic peptides. Cardiovascular Diabetology, 2010. **9**(1): p. 89.
163. Rayner, J.J., et al., The relative contribution of metabolic and structural abnormalities to diastolic dysfunction in obesity. International Journal Of Obesity, 2017. **42**: p. 441.
164. Gopal, K., et al., Cardiac-Specific Deletion of Pyruvate Dehydrogenase Impairs Glucose Oxidation Rates and Induces Diastolic Dysfunction. Frontiers in Cardiovascular Medicine, 2018. **5**(17).
165. Shamhart, P.E., et al., Hyperglycemia enhances function and differentiation of adult rat cardiac fibroblasts. Can J Physiol Pharmacol, 2014. **92**(7): p. 598-604.
166. Schannwell, C.M., et al., Left ventricular diastolic dysfunction as an early manifestation of diabetic cardiomyopathy. Cardiology, 2002. **98**(1-2): p. 33-9.
167. Zhao, L.M., et al., Advanced glycation end products promote proliferation of cardiac fibroblasts by upregulation of KCa3.1 channels. Pflugers Arch, 2012. **464**(6): p. 613-21.
168. Nielsen, J.M., et al., Blockage of receptor for advanced glycation end products prevents development of cardiac dysfunction in db/db type 2 diabetic mice. Eur J Heart Fail, 2009. **11**(7): p. 638-47.

169. Korosoglou, G., et al., Left ventricular diastolic function in type 2 diabetes mellitus is associated with myocardial triglyceride content but not with impaired myocardial perfusion reserve. J Magn Reson Imaging, 2012. **35**(4): p. 804-11.

170. Vinereanu, D., et al., Subclinical left ventricular dysfunction in asymptomatic patients with Type II diabetes mellitus, related to serum lipids and glycated haemoglobin. Clin Sci (Lond), 2003. **105**(5): p. 591-9.

171. Devereux, R.B., et al., Impact of diabetes on cardiac structure and function: the strong heart study. Circulation, 2000. **101**(19): p. 2271-6.

172. Velagaleti, R.S., et al., Relations of insulin resistance and glycemic abnormalities to cardiovascular magnetic resonance measures of cardiac structure and function: the Framingham Heart Study. Circ Cardiovasc Imaging, 2010. **3**(3): p. 257-63.

173. Heckbert, S.R., et al., Traditional cardiovascular risk factors in relation to left ventricular mass, volume, and systolic function by cardiac magnetic resonance imaging: the Multiethnic Study of Atherosclerosis. J Am Coll Cardiol, 2006. **48**(11): p. 2285-92.

174. Levelt, E., et al., Relationship Between Left Ventricular Structural and Metabolic Remodeling in Type 2 Diabetes. Diabetes, 2016. **65**(1): p. 44-52.

175. Shao, D. and R. Tian, Glucose Transporters in Cardiac Metabolism and Hypertrophy. Comprehensive Physiology, 2015. **6**(1): p. 331-351.

176. Maria, Z., A.R. Campolo, and V.A. Lacombe, Diabetes Alters the Expression and Translocation of the Insulin-Sensitive Glucose Transporters 4 and 8 in the Atria. PLOS ONE, 2015. **10**(12).

177. Mueckler, M., R.C. Hresko, and M. Sato, Structure, function and biosynthesis of GLUT1. Biochem Soc Trans, 1997. **25**(3): p. 951-4.

178. Haga, T., Molecular properties of the high-affinity choline transporter CHT1. J Biochem, 2014. **156**(4): p. 181-94.

179. Krejčí, A. and S. Tuček, Quantitation of mRNAs for M1 to M5 Subtypes of Muscarinic Receptors in Rat Heart and Brain Cortex. Molecular Pharmacology, 2002. **61**(6): p. 1267.

180. LaCroix, C., et al., Deficiency of M2 muscarinic acetylcholine receptors increases susceptibility of ventricular function to chronic adrenergic stress. American Journal of Physiology-Heart and Circulatory Physiology, 2008. **294**(2): p. H810-H820.

181. Kent, K.M., et al., Cholinergic Innervation of the Canine and Human Ventricular Conducting System Anatomic and Electrophysiologic Correlations. Circulation, 1974. **50**(5): p. 948-955.

182. Hoover, D.B., et al., Localization of cholinergic innervation in guinea pig heart by immunohistochemistry for high-affinity choline transporters. Cardiovascular Research, 2004. **62**(1): p. 112-21.

183. Kawano, H., R. Okada, and K. Yano, Histological study on the distribution of autonomic nerves in the human heart. Heart Vessels, 2003. **18**(1): p. 32-9.

184. Clavijo, L.C., et al., Metabolic syndrome in patients with acute myocardial infarction is associated with increased infarct size and in-hospital complications. Cardiovasc Revasc Med, 2006. **7**(1): p. 7-11.

185. Mabe, A.M., et al., Localization of cholinergic innervation and neurturin receptors in adult mouse heart and expression of the neurturin gene. Cell and Tissue Research, 2006. **326**(1): p. 57-67.

186. Woo, S.H., et al., Excitatory effect of M1 muscarinic acetylcholine receptor on automaticity of mouse heart. Arch Pharm Res, 2005. **28**(8): p. 930-5.

187. Wang, H., Y. Lu, and Z. Wang, Function of cardiac M3 receptors. Auton Autacoid Pharmacol, 2007. **27**(1): p. 1-11.

188. Guzman, M.S., et al., Elimination of the Vesicular Acetylcholine Transporter in the Striatum Reveals Regulation of Behaviour by Cholinergic-Glutamatergic Co-Transmission. PLOS Biology, 2011. **9**(11): p. e1001194.

189. Grisaru, D., et al., Structural roles of acetylcholinesterase variants in biology and pathology. Eur J Biochem, 1999. **264**(3): p. 672-86.

190. Dingová, D., Neuschlová, Study of the cholinergic system in the heart and its potential pharmacological targeting. 2015, Université Sorbonne Paris Cité
Univerzita Komenského (Bratislava).

191. Linz, D., et al., Cardiac remodeling and myocardial dysfunction in obese spontaneously hypertensive rats. Journal of Translational Medicine, 2012. **10**(1): p. 187.

192. Association, A.D., Screening for Type 2 Diabetes. Diabetes Care, 2004. **27**(suppl 1): p. s11.

193. Nickerson, H.D. and S. Dutta, Diabetic complications: current challenges and opportunities. Journal of cardiovascular translational research, 2012. **5**(4): p. 375-379.

194. Lew, J.K.S., et al., Exercise mediated protection of diabetic heart through modulation of microRNA mediated molecular pathways. Cardiovascular diabetology, 2017. **16**(1): p. 10-10.

195. Ulphani, J.S., et al., Quantitative analysis of parasympathetic innervation of the porcine heart. Heart Rhythm, 2010. **7**(8): p. 1113-9.

196. Crick, S.J., et al., Localisation and quantitation of autonomic innervation in the porcine heart II: endocardium, myocardium and epicardium. J Anat, 1999. **195 (Pt 3)**: p. 359-73.
197. Marron, K., et al., Human endocardial innervation and its relationship to the endothelium: an immunohistochemical, histochemical, and quantitative study. Cardiovascular Research, 1994. **28**(10): p. 1490-9.
198. Marron, K., et al., Distribution, morphology, and neurochemistry of endocardial and epicardial nerve terminal arborizations in the human heart. Circulation, 1995. **92**(8): p. 2343-51.
199. Pauza, D.H., et al., Morphology, distribution, and variability of the epicardiac neural ganglionated subplexuses in the human heart. The Anatomical Record, 2000. **259**(4): p. 353-382.
200. Saburkina, I., et al., Epicardial neural ganglionated plexus of ovine heart: Anatomic basis for experimental cardiac electrophysiology and nerve protective cardiac surgery. Heart Rhythm. **7**(7): p. 942-950.
201. Rysevaite, K., et al., Immunohistochemical characterization of the intrinsic cardiac neural plexus in whole-mount mouse heart preparations. Heart Rhythm: The Official Journal of the Heart Rhythm Society, 2011. **8**(5): p. 731-738.
202. Narayanan, K., et al., Left ventricular diameter and risk stratification for sudden cardiac death. Journal of the American Heart Association, 2014. **3**(5): p. e001193-e001193.
203. Khattar, R.S., Effects of ACE-inhibitors and beta-blockers on left ventricular remodeling in chronic heart failure. Minerva Cardioangiol, 2003. **51**(2): p. 143-54.
204. Yoshiyama, M., et al., Angiotensin converting enzyme inhibitor prevents left ventricular remodelling after myocardial infarction in angiotensin II type 1 receptor knockout mice. Heart (British Cardiac Society), 2005. **91**(8): p. 1080-1085.
205. Eguchi, K., et al., Type 2 diabetes is associated with left ventricular concentric remodeling in hypertensive patients. Am J Hypertens, 2005. **18**(1): p. 23-9.
206. Krumholz, H.M., M. Larson, and D. Levy, Prognosis of left ventricular geometric patterns in the Framingham Heart Study. J Am Coll Cardiol, 1995. **25**(4): p. 879-84.
207. Kanazawa, H., et al., Heart failure causes cholinergic transdifferentiation of cardiac sympathetic nerves via gp130-signaling cytokines in rodents. J Clin Invest, 2010. **120**(2): p. 408-21.
208. Shamir, M., et al., SnapShot: Timescales in Cell Biology. Cell, 2016. **164**(6): p. 1302-1302.e1.

209. Oikawa, S., et al., Various Regulatory Modes for Circadian Rhythmicity and Sexual Dimorphism in the Non-Neuronal Cardiac Cholinergic System. J Cardiovasc Transl Res, 2017. **10**(4): p. 411-422.

210. Han, L., et al., Free fatty acid can induce cardiac dysfunction and alter insulin signaling pathways in the heart. Lipids in health and disease, 2018. **17**(1): p. 185-185.

211. Aasum, E., et al., Age-Dependent Changes in Metabolism, Contractile Function, and Ischemic Sensitivity in Hearts From db/db Mice. Diabetes, 2003. **52**(2): p. 434.

212. Feng, X.T., et al., Palmitate contributes to insulin resistance through downregulation of the Src-mediated phosphorylation of Akt in C2C12 myotubes. Biosci Biotechnol Biochem, 2012. **76**(7): p. 1356-61.

213. Vettor, R., et al., Changes in FAT/CD36, UCP2, UCP3 and GLUT4 gene expression during lipid infusion in rat skeletal and heart muscle. Int J Obes Relat Metab Disord, 2002. **26**(6): p. 838-47.

214. Armoni, M., et al., Free Fatty Acids Repress the GLUT4 Gene Expression in Cardiac Muscle via Novel Response Elements. Journal of Biological Chemistry, 2005. **280**(41): p. 34786-34795.

215. Xue, W., et al., Cardiac-Specific Overexpression of HIF-1α Prevents Deterioration of Glycolytic Pathway and Cardiac Remodeling in Streptozotocin-Induced Diabetic Mice. The American Journal of Pathology, 2010. **177**(1): p. 97-105.

216. Wessler, I., et al., Release of non-neuronal acetylcholine from the isolated human placenta is mediated by organic cation transporters. Br J Pharmacol, 2001. **134**(5): p. 951-6.

217. Lips, K.S., et al., Acetylcholine and molecular components of its synthesis and release machinery in the urothelium. European Urology, 2007. **51**(4): p. 1042-1053.

218. Kummer, W., et al., Role of acetylcholine and polyspecific cation transporters in serotonin-induced bronchoconstriction in the mouse. Respir Res, 2006. **7**: p. 65.

219. Chatonnet, A. and O. Lockridge, Comparison of butyrylcholinesterase and acetylcholinesterase. The Biochemical journal, 1989. **260**(3): p. 625-634.

220. Arad, M., E. Seidman Christine, and J.G. Seidman, AMP-Activated Protein Kinase in the Heart. Circulation Research, 2007. **100**(4): p. 474-488.

221. Xiao, B., et al., Structure of mammalian AMPK and its regulation by ADP. Nature, 2011. **472**(7342): p. 230-233.

222. Frederich, M. and J.A. Balschi, The Relationship between AMP-activated Protein Kinase Activity and AMP Concentration in the Isolated Perfused Rat Heart. Journal of Biological Chemistry, 2002. **277**(3): p. 1928-1932.

223. Kudo, N., et al., High rates of fatty acid oxidation during reperfusion of ischemic hearts are associated with a decrease in malonyl-CoA levels due to an increase in 5'-AMP-activated protein kinase inhibition of acetyl-CoA carboxylase. J Biol Chem, 1995. **270**(29): p. 17513-20.
224. Russell, R.R., 3rd, et al., AMP-activated protein kinase mediates ischemic glucose uptake and prevents postischemic cardiac dysfunction, apoptosis, and injury. J Clin Invest, 2004. **114**(4): p. 495-503.
225. Marsin, A.S., et al., Phosphorylation and activation of heart PFK-2 by AMPK has a role in the stimulation of glycolysis during ischaemia. Curr Biol, 2000. **10**(20): p. 1247-55.
226. Viollet, B., et al., The AMP-activated protein kinase alpha2 catalytic subunit controls whole-body insulin sensitivity. J Clin Invest, 2003. **111**(1): p. 91-8.
227. Li, Y.J., et al., Improvement of mechanical heart function by trimetazidine in db/db mice. Acta Pharmacol Sin, 2010. **31**(5): p. 560-9.
228. Kosuru, R., et al., AMPK Contributes to Cardioprotective Effects of Pterostilbene Against Myocardial Ischemia- Reperfusion Injury in Diabetic Rats by Suppressing Cardiac Oxidative Stress and Apoptosis. Cellular Physiology and Biochemistry, 2018. **46**(4): p. 1381-1397.
229. Zhang, Y., et al., Metformin Activates AMPK Signaling but Inhibits Mitophagy in the Mouse Heart. Diabetes, 2018. **67**(Supplement 1): p. 1226-P.
230. Krul, M.M.G., et al., Coronary artery disease in patients with atypical chest pain with and without diabetes mellitus assessed with coronary CT angiography. BMJ Open Diabetes Research & Care, 2014. **2**(1): p. e000004.
231. Sara, J.D., et al., Coronary microvascular dysfunction is associated with poor glycemic control amongst female diabetics with chest pain and non-obstructive coronary artery disease. Cardiovascular Diabetology, 2019. **18**(1): p. 22.
232. Prasad, A., et al., Abnormal coronary microvascular endothelial function in humans with asymptomatic left ventricular dysfunction. Am Heart J, 2003. **146**(3): p. 549-54.
233. Cai, X., et al., Myocardial perfusion at rest in uncomplicated type 2 diabetes patients without coronary artery disease evaluated by 320-multidetector computed tomography: A pilot study. Medicine, 2018. **97**(5).
234. Liu, X., et al., Left ventricular subclinical myocardial dysfunction in uncomplicated type 2 diabetes mellitus is associated with impaired myocardial perfusion: a contrast-enhanced cardiovascular magnetic resonance study. Cardiovascular Diabetology, 2018. **17**(1): p. 139.
235. Boodhwani, M., et al., Insulin treatment enhances the myocardial angiogenic response in diabetes. The Journal of Thoracic and Cardiovascular Surgery, 2007. **134**(6): p. 1453-1460.

236. Prior John, O., et al., Coronary Circulatory Dysfunction in Insulin Resistance, Impaired Glucose Tolerance, and Type 2 Diabetes Mellitus. Circulation, 2005. **111**(18): p. 2291-2298.
237. Tessari, P., et al., Nitric oxide synthesis is reduced in subjects with type 2 diabetes and nephropathy. Diabetes, 2010. **59**(9): p. 2152-2159.
238. Kashyap, S.R., et al., Insulin Resistance Is Associated with Impaired Nitric Oxide Synthase Activity in Skeletal Muscle of Type 2 Diabetic Subjects. The Journal of Clinical Endocrinology & Metabolism, 2005. **90**(2): p. 1100-1105.
239. Cai, S., et al., Endothelial nitric oxide synthase dysfunction in diabetic mice: importance of tetrahydrobiopterin in eNOS dimerisation. Diabetologia, 2005. **48**(9): p. 1933-40.
240. Alp Nicholas, J. and M. Channon Keith, Regulation of Endothelial Nitric Oxide Synthase by Tetrahydrobiopterin in Vascular Disease. Arteriosclerosis, Thrombosis, and Vascular Biology, 2004. **24**(3): p. 413-420.
241. Giordano, F.J., et al., A cardiac myocyte vascular endothelial growth factor paracrine pathway is required to maintain cardiac function. Proc Natl Acad Sci U S A, 2001. **98**(10): p. 5780-5.
242. Ishii, M., et al., Palmitate induces insulin resistance in human HepG2 hepatocytes by enhancing ubiquitination and proteasomal degradation of key insulin signaling molecules. Arch Biochem Biophys, 2015. **566**: p. 26-35.
243. Benzler, M., et al., "Insulin-like" effects of palmitate compromise insulin signalling in hypothalamic neurons. Journal of Comparative Physiology B, 2019. **189**(3): p. 413-424.
244. Jablonska, B., et al., Sirt1 regulates glial progenitor proliferation and regeneration in white matter after neonatal brain injury. Nature communications, 2016. **7**: p. 13866-13866.
245. Nagueh, S.F., et al., Recommendations for the Evaluation of Left Ventricular Diastolic Function by Echocardiography: An Update from the American Society of Echocardiography and the European Association of Cardiovascular Imaging. J Am Soc Echocardiogr, 2016. **29**(4): p. 277-314.
246. Little William, C. and K. Oh Jae, Echocardiographic Evaluation of Diastolic Function Can Be Used to Guide Clinical Care. Circulation, 2009. **120**(9): p. 802-809.
247. Zile Michael, R. and L. Brutsaert Dirk, New Concepts in Diastolic Dysfunction and Diastolic Heart Failure: Part II. Circulation, 2002. **105**(12): p. 1503-1508.
248. Zile Michael, R. and L. Brutsaert Dirk, New Concepts in Diastolic Dysfunction and Diastolic Heart Failure: Part I. Circulation, 2002. **105**(11): p. 1387-1393.
249. McMurray, J.J., et al., ESC guidelines for the diagnosis and treatment of acute and chronic heart failure 2012: The Task Force for the Diagnosis and Treatment of Acute and

Chronic Heart Failure 2012 of the European Society of Cardiology. Developed in collaboration with the Heart Failure Association (HFA) of the ESC. Eur J Heart Fail, 2012. **14**(8): p. 803-69.
250. Paulus, W.J., et al., How to diagnose diastolic heart failure: a consensus statement on the diagnosis of heart failure with normal left ventricular ejection fraction by the Heart Failure and Echocardiography Associations of the European Society of Cardiology. Eur Heart J, 2007. **28**(20): p. 2539-50.
251. Ponikowski, P., et al., 2016 ESC Guidelines for the diagnosis and treatment of acute and chronic heart failure: The Task Force for the diagnosis and treatment of acute and chronic heart failure of the European Society of Cardiology (ESC)Developed with the special contribution of the Heart Failure Association (HFA) of the ESC. European Heart Journal, 2016. **37**(27): p. 2129-2200.
252. Sawey, E., S. Hollenberg, and S. Zanotti, Effects of Isoflurane Anesthesia on Cardiac Function in a Murine Model. CHEST, 2012. **142**(4): p. 398A.
253. Yang, C.-F., et al., Dose-dependent effects of isoflurane on cardiovascular function in rats. Tzu Chi Medical Journal, 2014. **26**(3): p. 119-122.
254. Johnson, J.S. and M.K. Loushin, The Effects of Anesthetic Agents on Cardiac Function, in Handbook of Cardiac Anatomy, Physiology, and Devices, P.A. Iaizzo, Editor. 2015, Springer International Publishing: Cham. p. 295-306.
255. Patel, S., Cardiovascular Effects of Intravenous Anesthetics. International Anesthesiology Clinics, 2002. **40**(1).
256. Fleming, R.M., The effect of high-, moderate-, and low-fat diets on weight loss and cardiovascular disease risk factors. Prev Cardiol, 2002. **5**(3): p. 110-8.
257. Snell-Bergeon, J.K., et al., Adults with type 1 diabetes eat a high-fat atherogenic diet that is associated with coronary artery calcium. Diabetologia, 2009. **52**(5): p. 801-809.
258. Kohsaka, A., et al., High-Fat Diet Disrupts Behavioral and Molecular Circadian Rhythms in Mice. Cell Metabolism, 2007. **6**(5): p. 414-421.
259. Lu, Z., et al., Increased persistent sodium current due to decreased PI3K signaling contributes to QT prolongation in the diabetic heart. Diabetes, 2013. **62**(12): p. 4257-4265.
260. Carroll, R., et al., Metabolic effects of insulin on cardiomyocytes from control and diabetic db/db mouse hearts. Am J Physiol Endocrinol Metab, 2005. **288**(5): p. E900-6.
261. Gu, J., et al., Metallothionein Preserves Akt2 Activity and Cardiac Function via Inhibiting TRB3 in Diabetic Hearts. Diabetes, 2018. **67**(3): p. 507.
262. Gibbs, E.M., et al., Glycemic improvement in diabetic db/db mice by overexpression of the human insulin-regulatable glucose transporter (GLUT4). J Clin Invest, 1995. **95**(4): p. 1512-8.

263. Atkinson, B.J., et al., Moderate GLUT4 Overexpression Improves Insulin Sensitivity and Fasting Triglyceridemia in High-Fat Diet–Fed Transgenic Mice. Diabetes, 2013. **62**(7): p. 2249.

264. Collins-Nakai, R.L., D. Noseworthy, and G.D. Lopaschuk, Epinephrine increases ATP production in hearts by preferentially increasing glucose metabolism. Am J Physiol, 1994. **267**(5 Pt 2): p. H1862-71.

265. Kanamori, H., et al., Autophagic adaptations in diabetic cardiomyopathy differ between type 1 and type 2 diabetes. Autophagy, 2015. **11**(7): p. 1146-1160.

266. Plante, E., et al., Oxytocin Treatment Prevents the Cardiomyopathy Observed in Obese Diabetic Male db/db Mice. Endocrinology, 2015. **156**(4): p. 1416-1428.

267. Oikawa, S., et al., Non-neuronal cardiac cholinergic system influences CNS via the vagus nerve to acquire a stress-refractory propensity. Clin Sci (Lond), 2016. **130**(21): p. 1913-28.

268. Dedkova, E.N., et al., Signaling Mechanisms That Mediate Nitric Oxide Production Induced by Acetylcholine Exposure and Withdrawal in Cat Atrial Myocytes. Circulation Research, 2003. **93**(12): p. 1233.

269. Kuwabara, M., et al., Nitric oxide stimulates vascular endothelial growth factor production in cardiomyocytes involved in angiogenesis. J Physiol Sci, 2006. **56**(1): p. 95-101.

270. Quyyumi Arshed, A., et al., Contribution of Nitric Oxide to Metabolic Coronary Vasodilation in the Human Heart. Circulation, 1995. **92**(3): p. 320-326.

271. Dharmashankar, K., et al., Nitric Oxide Synthase-Dependent Vasodilation of Human Subcutaneous Arterioles Correlates With Noninvasive Measurements of Endothelial Function. American Journal of Hypertension, 2012. **25**(5): p. 528-534.

272. Zhang, C., et al., Maturation-induces endothelial dysfunction via vascular inflammation in diabetic mice. Basic Res Cardiol, 2008. **103**(5): p. 407-16.

273. Lee, J., et al., Interaction of IL-6 and TNF-α contributes to endothelial dysfunction in type 2 diabetic mouse hearts. PLOS ONE, 2017. **12**(11): p. e0187189.

274. Hinkel, R., et al., Diabetes Mellitus–Induced Microvascular Destabilization in the Myocardium. Journal of the American College of Cardiology, 2017. **69**(2): p. 131-143.

275. Teng, X., et al., Selective deletion of endothelial cell calpain in mice reduces diabetic cardiomyopathy by improving angiogenesis. Diabetologia, 2019. **62**(5): p. 860-872.

276. Chen, J.-X. and A. Stinnett, Disruption of Ang-1/Tie-2 Signaling Contributes to the Impaired Myocardial Vascular Maturation and Angiogenesis in Type II Diabetic Mice. Arteriosclerosis, Thrombosis, and Vascular Biology, 2008. **28**(9): p. 1606-1613.

277. Marfella, R., et al., Myocardial infarction in diabetic rats: role of hyperglycaemia on infarct size and early expression of hypoxia-inducible factor 1. Diabetologia, 2002. **45**.

278. Katare, R.G., et al., Vagal nerve stimulation prevents reperfusion injury through inhibition of opening of mitochondrial permeability transition pore independent of the bradycardiac effect. The Journal of Thoracic and Cardiovascular Surgery, 2009. **137**(1): p. 223-231.

279. Bogdanov, P., et al., The db/db Mouse: A Useful Model for the Study of Diabetic Retinal Neurodegeneration. PLOS ONE, 2014. **9**(5): p. e97302.

280. Oikawa, S., et al., Potentiating a non-neuronal cardiac cholinergic system reinforces the functional integrity of the blood brain barrier associated with systemic anti-inflammatory responses. Brain Behav Immun, 2019. **81**: p. 122-137.

281. Gehlert, D.R., et al., The Selective Norepinephrine Reuptake Inhibitor, LY368975, Reduces Food Consumption in Animal Models of Feeding. Journal of Pharmacology and Experimental Therapeutics, 1998. **287**(1): p. 122.

282. Wong, D.T., et al., LY248686, A New Inhibitor of Serotonin and Norepinephrine Uptake. Neuropsychopharmacology, 1993. **8**(1): p. 23-33.

283. Liao, R., et al., Cardiac-specific overexpression of GLUT1 prevents the development of heart failure attributable to pressure overload in mice. Circulation, 2002. **106**(16): p. 2125-31.

284. Laboratory, T.J. Life span as a biomarker. [cited 2019 2/7/2019]; Available from: https://www.jax.org/research-and-faculty/research-labs/the-harrison-lab/gerontology/life-span-as-a-biomarker.

285. Fukumoto, H., et al., Cloning and characterization of the major insulin-responsive glucose transporter expressed in human skeletal muscle and other insulin-responsive tissues. J Biol Chem, 1989. **264**(14): p. 7776-9.

286. Montessuit, C. and R. Lerch, Regulation and dysregulation of glucose transport in cardiomyocytes. Biochimica Et Biophysica Acta, 2013. **1833**(4): p. 848-856.

287. Freeman, A.S.-F., K.; Pennings, N. Insulin resistance. 10/05/2019; Available from: https://www.ncbi.nlm.nih.gov/books/NBK507839/.

288. Desrois, M., et al., Initial steps of insulin signaling and glucose transport are defective in the type 2 diabetic rat heart. Cardiovascular Research, 2004. **61**(2): p. 288-96.

289. Huisamen, B., Protein kinase B in the diabetic heart. Mol Cell Biochem, 2003. **249**(1-2): p. 31-8.

290. Battiprolu, P.K., et al., Metabolic stress-induced activation of FoxO1 triggers diabetic cardiomyopathy in mice. J Clin Invest, 2012. **122**(3): p. 1109-18.

291. Uphues, I., et al., Failure of insulin-regulated recruitment of the glucose transporter GLUT4 in cardiac muscle of obese Zucker rats is associated with alterations of small-molecular-mass GTP-binding proteins. Biochem J, 1995. **311 (Pt 1)**: p. 161-6.

292. Leguisamo, N.M., et al., GLUT4 content decreases along with insulin resistance and high levels of inflammatory markers in rats with metabolic syndrome. Cardiovascular Diabetology, 2012. **11**(1): p. 100.

293. Hodis, H.N. and W.J. Mack, Triglyceride-rich lipoproteins and the progression of coronary artery disease. Curr Opin Lipidol, 1995. **6**(4): p. 209-14.

294. Turner, R.C., et al., Risk factors for coronary artery disease in non-insulin dependent diabetes mellitus: United Kingdom Prospective Diabetes Study (UKPDS: 23). BMJ, 1998. **316**(7134): p. 823-8.

295. Hiukka, A., et al., Alterations of lipids and apolipoprotein CIII in very low density lipoprotein subspecies in type 2 diabetes. Diabetologia, 2005. **48**(6): p. 1207-15.

296. Farmer, J.A., Diabetic dyslipidemia and atherosclerosis: evidence from clinical trials. Curr Atheroscler Rep, 2007. **9**(2): p. 162-8.

297. Camici, P.G., G. d'Amati, and O. Rimoldi, Coronary microvascular dysfunction: mechanisms and functional assessment. Nat Rev Cardiol, 2015. **12**(1): p. 48-62.

298. Crea, F., P.G. Camici, and C.N. Bairey Merz, Coronary microvascular dysfunction: an update. Eur Heart J, 2014. **35**(17): p. 1101-11.

299. Shivu, G.N., et al., Relationship Between Coronary Microvascular Dysfunction and Cardiac Energetics Impairment in Type 1 Diabetes Mellitus. Circulation, 2010. **121**(10): p. 1209-1215.

300. Tian, R. and E.D. Abel, Responses of GLUT4-Deficient Hearts to Ischemia Underscore the Importance of Glycolysis. Circulation, 2001. **103**(24): p. 2961-2966.

301. Altarejos, J.Y., et al., Myocardial Ischemia Differentially Regulates LKB1 and an Alternate 5′-AMP-activated Protein Kinase Kinase. Journal of Biological Chemistry, 2005. **280**(1): p. 183-190.

302. Paiva, M.A., et al., Enhancing AMPK activation during ischemia protects the diabetic heart against reperfusion injury. American journal of physiology. Heart and circulatory physiology, 2011. **300**(6): p. H2123-H2134.

303. Hu, H., et al., The cardioprotective effects of carvedilol on ischemia and reperfusion injury by AMPK signaling pathway. Biomed Pharmacother, 2019. **117**: p. 109106.

304. Chakrabarti, G., et al., Reduced Cardiac Efficiency and Altered Substrate Metabolism Precedes the Onset of Hyperglycemia and Contractile Dysfunction in Two Mouse Models of Insulin Resistance and Obesity. Endocrinology, 2005. **146**(12): p. 5341-5349.

305. Nagoshi, T., et al., Optimization of cardiac metabolism in heart failure. Current pharmaceutical design, 2011. **17**(35): p. 3846-3853.
306. Chokshi, A., et al., Ventricular assist device implantation corrects myocardial lipotoxicity, reverses insulin resistance, and normalizes cardiac metabolism in patients with advanced heart failure. Circulation, 2012. **125**(23): p. 2844-53.
307. Tsuchiya, Y., et al., Palmitate-induced down-regulation of sortilin and impaired GLUT4 trafficking in C2C12 myotubes. J Biol Chem, 2010. **285**(45): p. 34371-81.
308. Malhotra, R. and F.C. Brosius, Glucose Uptake and Glycolysis Reduce Hypoxia-induced Apoptosis in Cultured Neonatal Rat Cardiac Myocytes. Journal of Biological Chemistry, 1999. **274**(18): p. 12567-12575.
309. Davidoff, A.J., et al., Diabetic cardiomyocyte dysfunction and myocyte insulin resistance: role of glucose-induced PKC activity. Mol Cell Biochem, 2004. **262**(1-2): p. 155-63.
310. Bertrand, L., et al., AMPK activation restores the stimulation of glucose uptake in an in vitro model of insulin-resistant cardiomyocytes via the activation of protein kinase B. Am J Physiol Heart Circ Physiol, 2006. **291**(1): p. H239-50.
311. Schwenk, R.W., et al., Overexpression of vesicle-associated membrane protein (VAMP) 3, but not VAMP2, protects glucose transporter (GLUT) 4 protein translocation in an in vitro model of cardiac insulin resistance. Journal of Biological Chemistry, 2012. **287**(44): p. 37530-37539.
312. Chokshi, A., et al., Ventricular Assist Device Implantation Corrects Myocardial Lipotoxicity, Reverses Insulin Resistance, and Normalizes Cardiac Metabolism in Patients With Advanced Heart Failure. Circulation, 2012. **125**(23): p. 2844-2853.
313. Fishwick, K.J. and R.J. Rylett, Insulin Regulates the Activity of the High-Affinity Choline Transporter CHT. PLOS ONE, 2015. **10**(7): p. e0132934.
314. Rivera, E.J., et al., Insulin and insulin-like growth factor expression and function deteriorate with progression of Alzheimer's disease: link to brain reductions in acetylcholine. J Alzheimers Dis, 2005. **8**(3): p. 247-68.
315. de la Monte, S.M., et al., si-RNA inhibition of brain insulin or insulin-like growth factor receptors causes developmental cerebellar abnormalities: relevance to fetal alcohol spectrum disorder. Molecular Brain, 2011. **4**(1): p. 13.
316. Sherin, A., et al., Cholinergic and GABAergic receptor functional deficit in the hippocampus of insulin-induced hypoglycemic and streptozotocin-induced diabetic rats. Neuroscience, 2012. **202**: p. 69-76.

317. Vanoverschelde, J.L., et al., Rate of glycolysis during ischemia determines extent of ischemic injury and functional recovery after reperfusion. American Journal of Physiology-Heart and Circulatory Physiology, 1994. **267**(5): p. H1785-H1794.
318. Spillmann, F., et al., High-density lipoproteins reduce palmitate-induced cardiomyocyte apoptosis in an AMPK-dependent manner. Biochemical and Biophysical Research Communications, 2015. **466**(2): p. 272-277.
319. Weikel, K.A., et al., Glucose and palmitate uncouple AMPK from autophagy in human aortic endothelial cells. American Journal of Physiology-Cell Physiology, 2014. **308**(3): p. C249-C263.
320. Wu, Y., et al., Activation of protein phosphatase 2A by palmitate inhibits AMP-activated protein kinase. J Biol Chem, 2007. **282**(13): p. 9777-88.
321. Faramoushi, M., et al., Cardiac fibrosis and down regulation of GLUT4 in experimental diabetic cardiomyopathy are ameliorated by chronic exposures to intermittent altitude. Journal of cardiovascular and thoracic research, 2016. **8**(1): p. 26-33.
322. Hinkel, R., et al., Diabetes Mellitus-Induced Microvascular Destabilization in the Myocardium. J Am Coll Cardiol, 2017. **69**(2): p. 131-143.
323. Kakinuma, Y., et al., A HIF-1alpha-related gene involved in cell protection from hypoxia by suppression of mitochondrial function. FEBS letters, 2008. **582**(2): p. 332-340.
324. Zhao, T., et al., Vascular endothelial growth factor (VEGF)-A: role on cardiac angiogenesis following myocardial infarction. Microvascular research, 2010. **80**(2): p. 188-194.
325. Yun, J.-S., et al., Progression of cardiovascular autonomic neuropathy and cardiovascular disease in type 2 diabetes. Cardiovascular Diabetology, 2018. **17**(1): p. 109.
326. Vinik, A.I., et al., Cardiac Autonomic Neuropathy in Diabetes: A Predictor of Cardiometabolic Events. Frontiers in Neuroscience, 2018. **12**: p. 591.
327. Pop-Busui, R., Cardiac autonomic neuropathy in diabetes: a clinical perspective. Diabetes Care, 2010. **33**(2): p. 434-441.
328. Lara, A., et al., Dysautonomia Due to Reduced Cholinergic Neurotransmission Causes Cardiac Remodeling and Heart Failure. Molecular and Cellular Biology, 2010. **30**(7): p. 1746.
329. Rincon, M.Y., T. VandenDriessche, and M.K. Chuah, Gene therapy for cardiovascular disease: advances in vector development, targeting, and delivery for clinical translation. Cardiovascular Research, 2015. **108**(1): p. 4-20.
330. Rengo, G., et al., Myocardial Adeno-Associated Virus Serotype 6–βARKct Gene Therapy Improves Cardiac Function and Normalizes the Neurohormonal Axis in Chronic Heart Failure. Circulation, 2009. **119**(1): p. 89-98.

331. Giordano, F.J., et al., Intracoronary gene transfer of fibroblast growth factor–5 increases blood flow and contractile function in an ischemic region of the heart. Nature Medicine, 1996. **2**: p. 534.

332. Sabino, J.P.J., et al., The treatment with pyridostigmine improves the cardiocirculatory function in rats with chronic heart failure. Autonomic Neuroscience, 2013. **173**(1): p. 58-64.

333. Sabino, J.P., et al., Parasympathetic activation by pyridostigmine on chemoreflex sensitivity in heart-failure rats. Autonomic Neuroscience, 2013. **179**(1-2): p. 43-8.

334. Lataro, R.M., et al., Increase in parasympathetic tone by pyridostigmine prevents ventricular dysfunction during the onset of heart failure. Am J Physiol Regul Integr Comp Physiol, 2013. **305**(8): p. R908-16.

335. Li, M., et al., Adding the acetylcholinesterase inhibitor, donepezil, to losartan treatment markedly improves long-term survival in rats with chronic heart failure. Eur J Heart Fail, 2014. **16**(10): p. 1056-65.

336. Santos-Almeida, F.M., et al., Cholinergic stimulation with pyridostigmine protects myocardial infarcted rats against ischemic-induced arrhythmias and preserves connexin43 protein. Am J Physiol Heart Circ Physiol, 2015. **308**(2): p. H101-7.

337. Castro, R.R.T., et al., Cholinergic stimulation with pyridostigmine protects against exercise induced myocardial ischaemia. Heart, 2004. **90**(10): p. 1119-1123.

338. Androne, A.S., et al., Acetylcholinesterase inhibition with pyridostigmine improves heart rate recovery after maximal exercise in patients with chronic heart failure. Heart, 2003. **89**(8): p. 854-8.

339. Kubo, T., et al., Influences of Donepezil on Cardiovascular System—Possible Therapeutic Benefits for Heart Failure—DOnepezil Cardiac TEst Registry (DOCTER) Study. Journal of Cardiovascular Pharmacology, 2012. **60**(3): p. 310-314.

340. Serra, S.M., et al., Cholinergic stimulation improves autonomic and hemodynamic profile during dynamic exercise in patients with heart failure. J Card Fail, 2009. **15**(2): p. 124-9.

341. Behling, A., et al., Cholinergic stimulation with pyridostigmine reduces ventricular arrhythmia and enhances heart rate variability in heart failure. Am Heart J, 2003. **146**(3): p. 494-500.

342. Nordstrom, P., et al., The use of cholinesterase inhibitors and the risk of myocardial infarction and death: a nationwide cohort study in subjects with Alzheimer's disease. European Heart Journal, 2013. **34**(33): p. 2585-91.

343. Sato, K., et al., The Effect of Donepezil Treatment on Cardiovascular Mortality. Clinical pharmacology and therapeutics, 2010. **88**(3): p. 335-338.

344. Wu, P.-H., et al., Impact of acetylcholinesterase inhibitors on the occurrence of acute coronary syndrome in patients with dementia. Scientific Reports, 2015. **5**: p. 15451.
345. Kato, K., et al., TAK-147, an acetylcholinesterase inhibitor, increases choline acetyltransferase activity in cultured rat septal cholinergic neurons. Neurosci Lett, 1999. **260**(1): p. 5-8.
346. Hernandez, C.M., et al., Comparison of galantamine and donepezil for effects on nerve growth factor, cholinergic markers, and memory performance in aged rats. J Pharmacol Exp Ther, 2006. **316**(2): p. 679-94.
347. Oikawa, S., et al., A Novel Nitric Oxide Donor, S-Nitroso-NPivaloyl-D-Penicillamine, Activates a Non-Neuronal Cardiac Cholinergic System to Synthesize Acetylcholine and Augments Cardiac Function. Cell Physiol Biochem, 2019. **52**(4): p. 922-934.
348. Ha, M. and V.N. Kim, Regulation of microRNA biogenesis. Nature Reviews Molecular Cell Biology, 2014. **15**: p. 509.
349. Oikawa, S., et al., Various Regulatory Modes for Circadian Rhythmicity and Sexual Dimorphism in the Non-Neuronal Cardiac Cholinergic System. J Cardiovasc Transl Res, 2017.
350. Rawal, S., et al., Differential expression pattern of cardiovascular microRNAs in the human type-2 diabetic heart with normal ejection fraction. International Journal of Cardiology, 2016. **202**: p. 40-43.
351. Rawal, S., et al., Downregulation of miR-15a/b accelerates fibrotic remodelling in the type-2 diabetic human and mouse heart. Clinical Science, 2017: p. CS20160916.
352. Cai, L., et al., Hyperglycemia-Induced Apoptosis in Mouse Myocardium. Diabetes, 2002. **51**(6): p. 1938.
353. Chowdhry, M.F., H.A. Vohra, and M. Galiñanes, Diabetes increases apoptosis and necrosis in both ischemic and nonischemic human myocardium: Role of caspases and poly–adenosine diphosphate–ribose polymerase. The Journal of Thoracic and Cardiovascular Surgery, 2007. **134**(1): p. 124-131.e3.
354. Messina, E., et al., Isolation and expansion of adult cardiac stem cells from human and murine heart. Circulation Research, 2004. **95**(9): p. 911-21.
355. Smith, R.R., et al., Regenerative potential of cardiosphere-derived cells expanded from percutaneous endomyocardial biopsy specimens. Circulation, 2007. **115**(7): p. 896-908.
356. Hsieh, P.C., et al., Evidence from a genetic fate-mapping study that stem cells refresh adult mammalian cardiomyocytes after injury. Nat Med, 2007. **13**(8): p. 970-4.
357. Yue, W., et al., ESC-Derived Basal Forebrain Cholinergic Neurons Ameliorate the Cognitive Symptoms Associated with Alzheimer's Disease in Mouse Models. Stem Cell Reports, 2015. **5**(5): p. 776-790.

358. De Ferrari, G.M., et al., Chronic vagus nerve stimulation: a new and promising therapeutic approach for chronic heart failure. European Heart Journal, 2011. **32**(7): p. 847-855.
359. Hauptman, P.J., et al., Rationale and study design of the increase of vagal tone in heart failure study: INOVATE-HF. American Heart Journal, 2012. **163**(6): p. 954-962.e1.
360. Dicarlo, L., et al., Autonomic regulation therapy for the improvement of left ventricular function and heart failure symptoms: the ANTHEM-HF study. Journal of Cardiac Failure, 2013. **19**(9): p. 655-660.
361. Zannad, F., et al., Chronic vagal stimulation for the treatment of low ejection fraction heart failure: results of the NEural Cardiac TherApy foR Heart Failure (NECTAR-HF) randomized controlled trial. European Heart Journal, 2015. **36**(7): p. 425-433.
362. De Ferrari, G.M., et al., Long-term vagal stimulation for heart failure: Eighteen month results from the NEural Cardiac TherApy foR Heart Failure (NECTAR-HF) trial. International Journal of Cardiology, 2017. **244**: p. 229-234.
363. Gold, M.R., et al., Vagus Nerve Stimulation for the Treatment of Heart Failure: The INOVATE-HF Trial. Journal of the American College of Cardiology, 2016. **68**(2): p. 149-158.
364. Premchand, R.K., et al., Autonomic regulation therapy via left or right cervical vagus nerve stimulation in patients with chronic heart failure: results of the ANTHEM-HF trial. Journal of Cardiac Failure, 2014. **20**(11): p. 808-816.
365. Libbus, I., et al., Autonomic regulation therapy suppresses quantitative T-wave alternans and improves baroreflex sensitivity in patients with heart failure enrolled in the ANTHEM-HF study. Heart Rhythm, 2016. **13**(3): p. 721-728.
366. Premchand, R.K., et al., Extended Follow-Up of Patients With Heart Failure Receiving Autonomic Regulation Therapy in the ANTHEM-HF Study. Journal of Cardiac Failure, 2016. **22**(8): p. 639-642.
367. Premchand, R.K., et al., LONG-TERM FOLLOW-UP OF REDUCED EJECTION FRACTION HEART FAILURE PATIENTS RECEIVING AUTONOMIC REGULATION THERAPY IN THE ANTHEM-HF PILOT STUDY. Journal of the American College of Cardiology, 2019. **73**(9 Supplement 1): p. 770.
368. Malbert, C.-H., et al., Obesity-Associated Alterations in Glucose Metabolism Are Reversed by Chronic Bilateral Stimulation of the Abdominal Vagus Nerve. Diabetes, 2017. **66**(4): p. 848.

Appendix 1

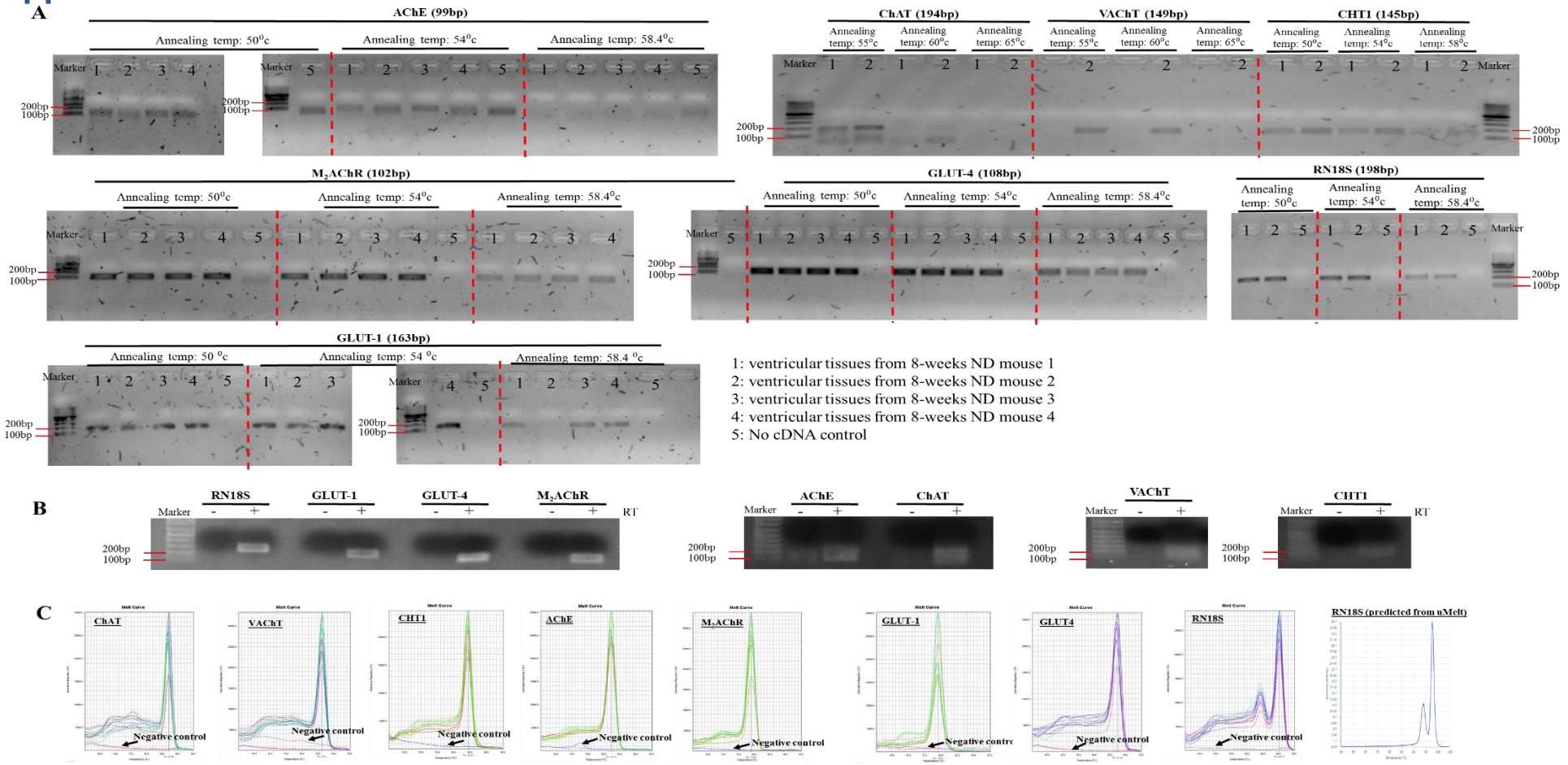

Figure S1.1 Optimization and controls for RT-qPCR analysis.

(A) *Gradient PCR was performed to optimize the annealing temperature (50°C, 54°C, 58.4°C or 55°C, 60°C and 65°C) of each primers ;* ***(B)*** *PCR was performed with (+) and without (-; serving as negative control) reverse transcription of rDNase treated RNA.* ***(C)*** *Melting curve analysis showed the melting temperature of each PCR amplicon which was also serve as a quality control for specific amplification. The PCR amplicon of RN18S shows two melting temperatures which is likely due to the GC rich region in the amplicon. This was confirmed by using Umelt software (https://www.dna.utah.edu/umelt/umelt.html) to predict the melt curve profile based on the amplicon sequences.*

Appendix 2

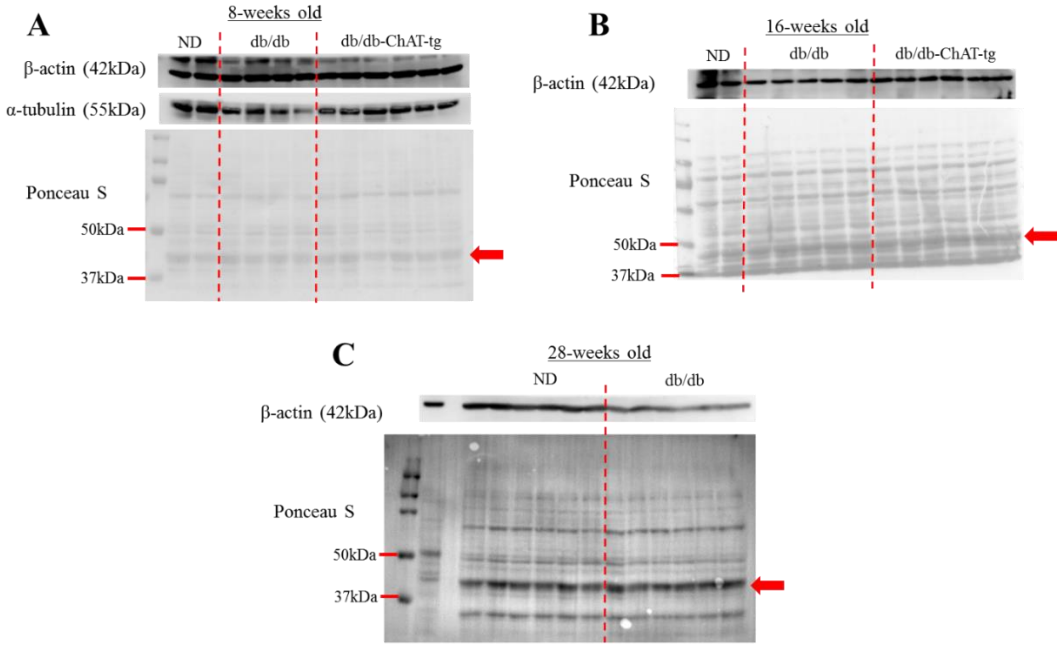

Figure S2.1 The protein expression of α-tubulin, β-actin and total protein from Ponceau S staining of the mouse ventricular tissues.

*Representative blots showing **(A)** a decreasing trend in α-tubulin expression in the db/db mice at 8-weeks of age while β-actin expression and total protein as well as the selected band (red arrow) from Ponceau S staining showed consistent expression in all samples; **(B & C)** a decreasing trend in β-actin expression in the db/db mice at 16- and 20-weeks of age while total protein as well as selected band (red arrow) from Ponceau S staining showed relatively consistent expression in all samples.*

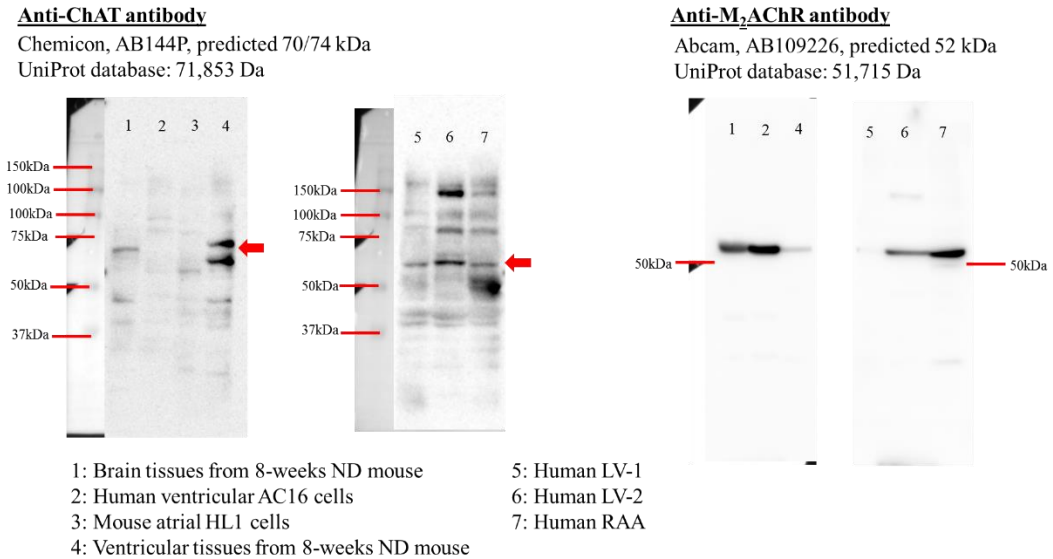

Figure S2.2 Examination of the specificity of anti-ChAT and anti-M_2AChR antibodies

Representative full blots showing the specificity of anti-ChAT and anti-M_2AChR antibodies tested on protein lysates from mouse brain tissue (positive control), AC16 cells, HL1 cells (mouse atrial cardiomyocytes cells), mouse ventricular tissues, human LV and right atrial appendage (RAA).

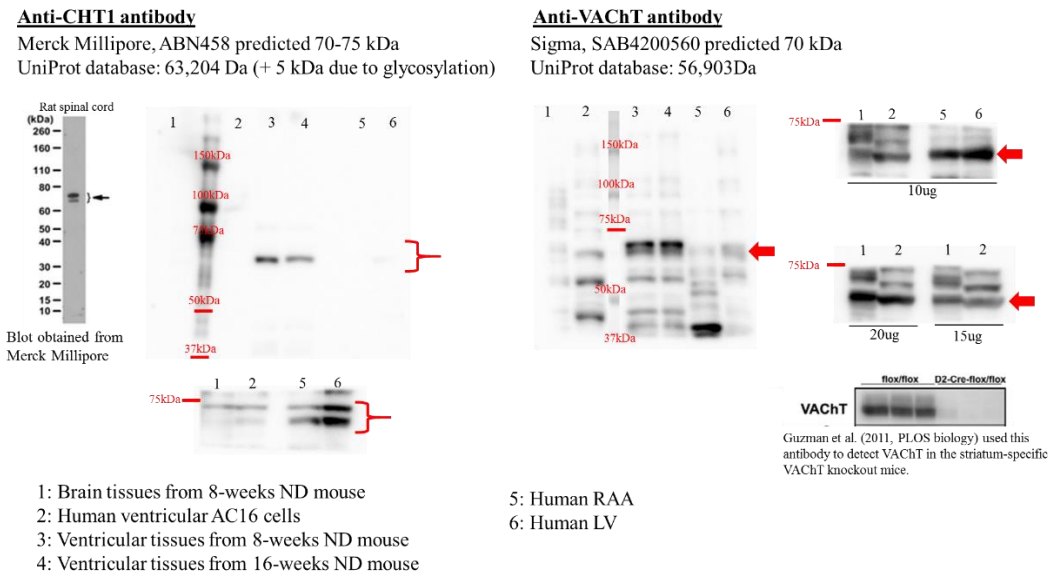

Figure S2.3 Examination of the specificity of anti-CHT1 and anti-VAChT antibodies

Representative full blots showing the specificity of anti-CHT1 and anti-VAChT antibodies tested on protein lysates from mouse brain tissue (positive control), AC16 cells, HL1 cells (mouse atrial cardiomyocytes cells), mouse ventricular tissues, human LV and right atrial appendage (RAA).

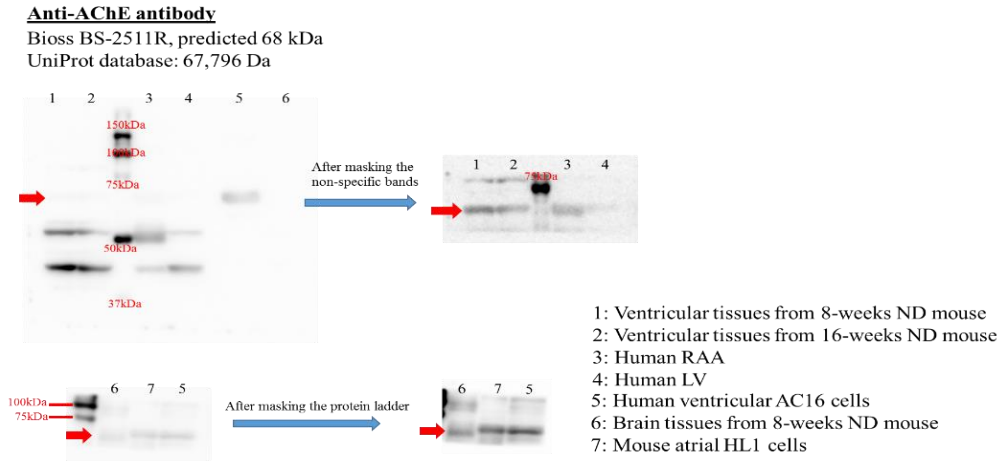

Figure S2.4 Examination of the specificity of anti-AChE antibody

Representative full blots showing the specificity of anti-AChE antibody tested on protein lysates from mouse brain tissue (positive control), AC16 cells, HL1 cells (mouse atrial cardiomyocytes cells), mouse ventricular tissues, human LV and right atrial appendage (RAA).

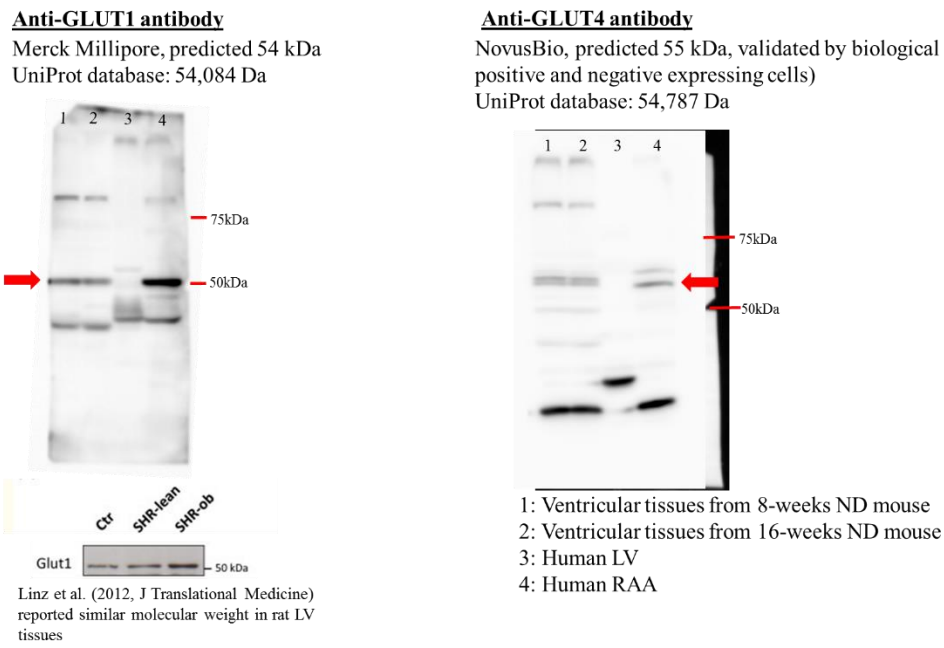

Figure S2.5 Examination of the specificity of anti-GLUT-1 and anti-GLUT-4 antibodies
Representative full blots showing the specificity of anti-GLUT-1 and anti-GLUT-4 antibodies tested on protein lysates from mouse ventricular tissues, human LV and right atrial appendage (RAA).

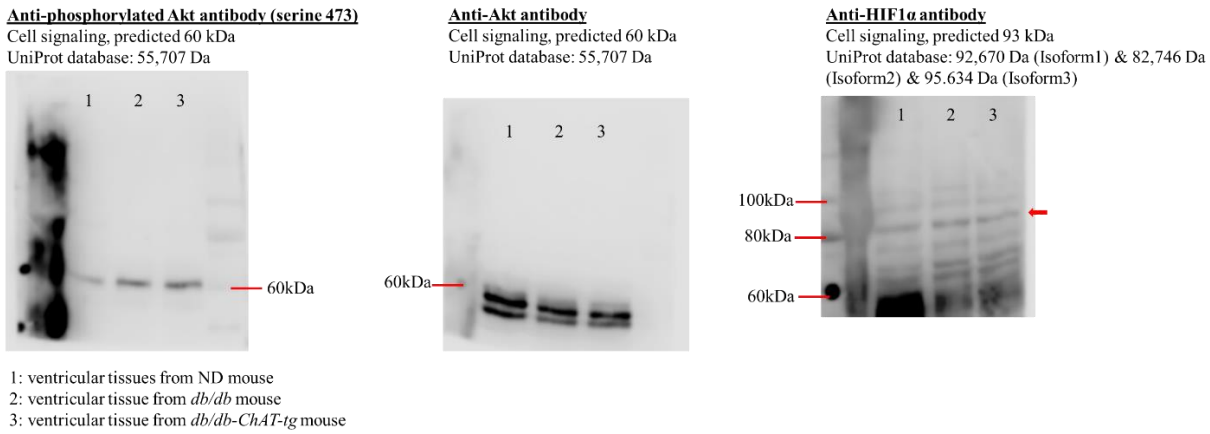

Figure S2.6 Examination of the specificity of anti-pAkt, anti-Akt and anti-HIF1α antibodies
Representative full blots showing the specificity of anti-pAkt (serine 473), anti-Akt and anti-HIF1α antibodies tested on protein lysates from mouse ventricular tissues of ND, db/db and db/db-ChAT-tg mouse. There are three isoforms of HIF1α. Isoform 2 that has approximately 83 kDa was identified as HIF1α-positive as the band intensity appeared to be more prominent that other isoforms in the ventricular tissues.

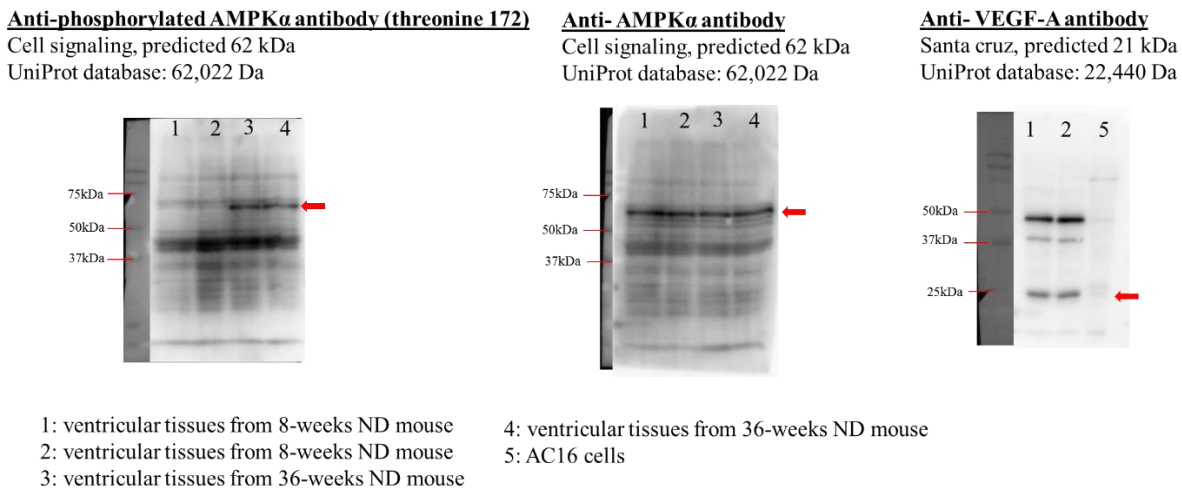

Figure S2.7 Examination of the specificity of anti-pAMPkα, anti-AMPKα and anti-VEGF-A antibodies

Representative blots showing the specificity of anti-pAMPKα (threonine 172), anti-AMPKα and anti-VEGF-A antibodies tested on protein lysates from mouse ventricular tissues of ND at 8-, 36-weeks of age as well as AC16 cells.

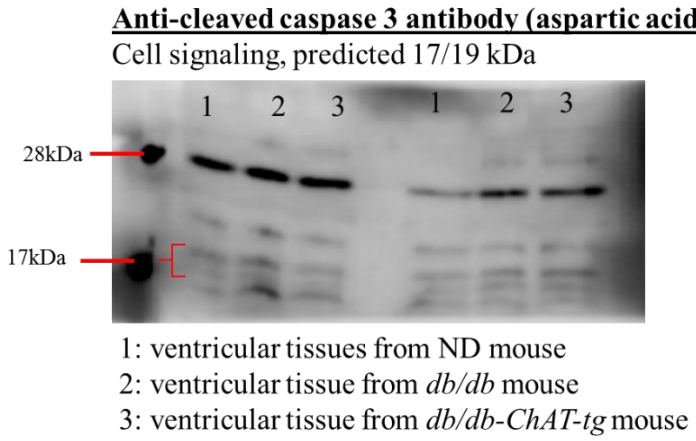

Figure S2.8 Examination of the specificity of anti-VEGF-A and anti-cleaved caspase 3 antibodies

Representative blots showing the specificity of anti-VEGF-A and anti-cleaved caspase 3 antibodies tested on protein lysates from mouse ventricular tissues of ND, db/db and db/db-ChAT-tg mice.

Appendix 3

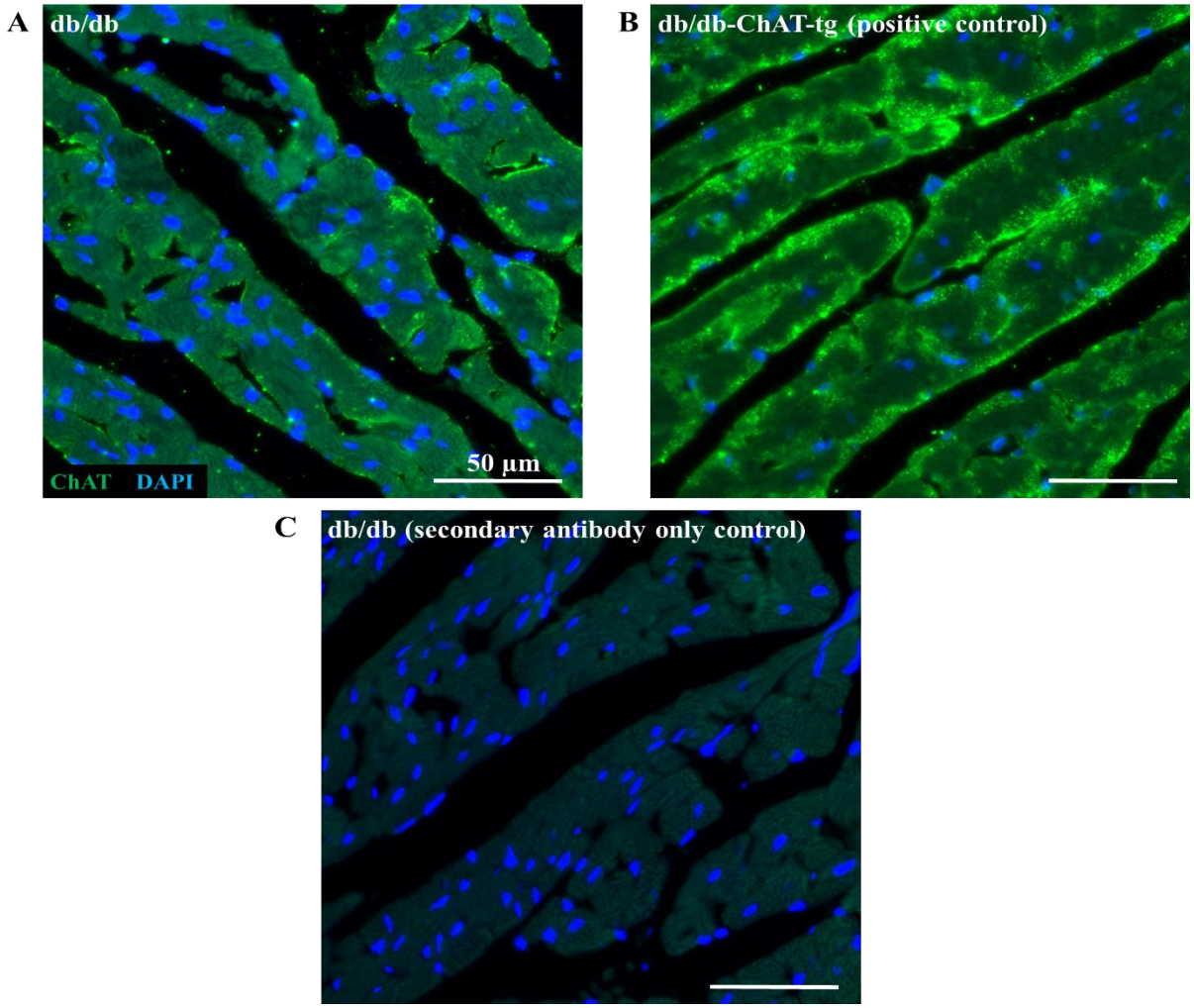

Figure S3.1 Examination of the specificity of anti-ChAT antibody
*Representative confocal images showing positive ChAT staining in the ventricular tissue from **(A)** db/db mouse and **(B)** db/db-ChAT-tg mouse. The intensity of ChAT is stronger in the db/db-ChAT-tg mice due to overexpression of ChAT gene. **(C)** No staining in the secondary antibody only control performed on the ventricular tissue of db/db mouse.*

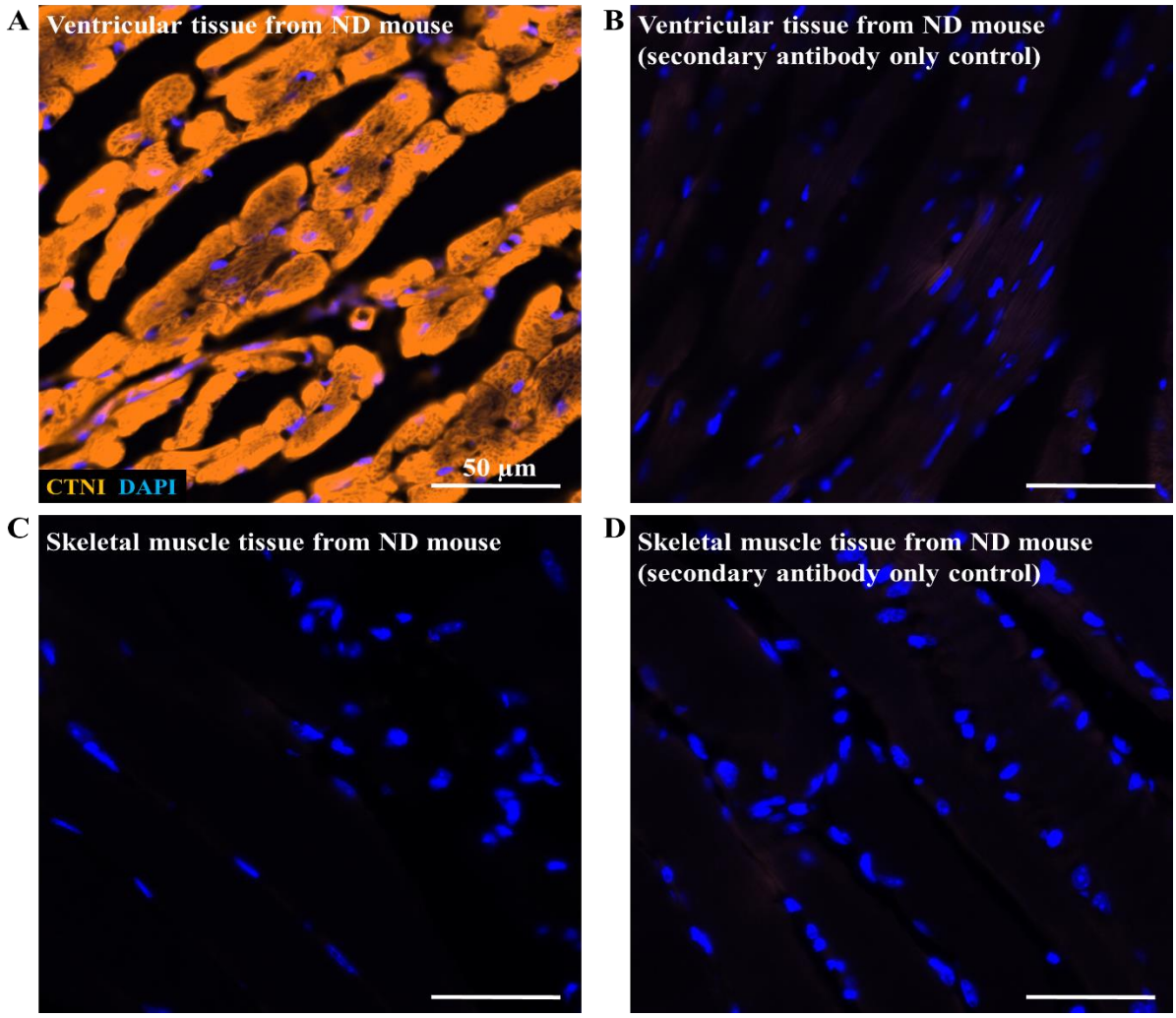

Figure S3.2 Examination of the specificity of anti-CTNI antibody

*Representative confocal images showing **(A)** positive CTNI staining in the ventricular tissue from ND mouse and **(B)** negatvie CTNI staining in the secondary antibody only control performed on the ventricular tissues from ND mouse. **(C)** No staining detected in the skeletal muscle tissues from ND mouse in the presence and **(D)** absence of anti-CTNI antibody.*

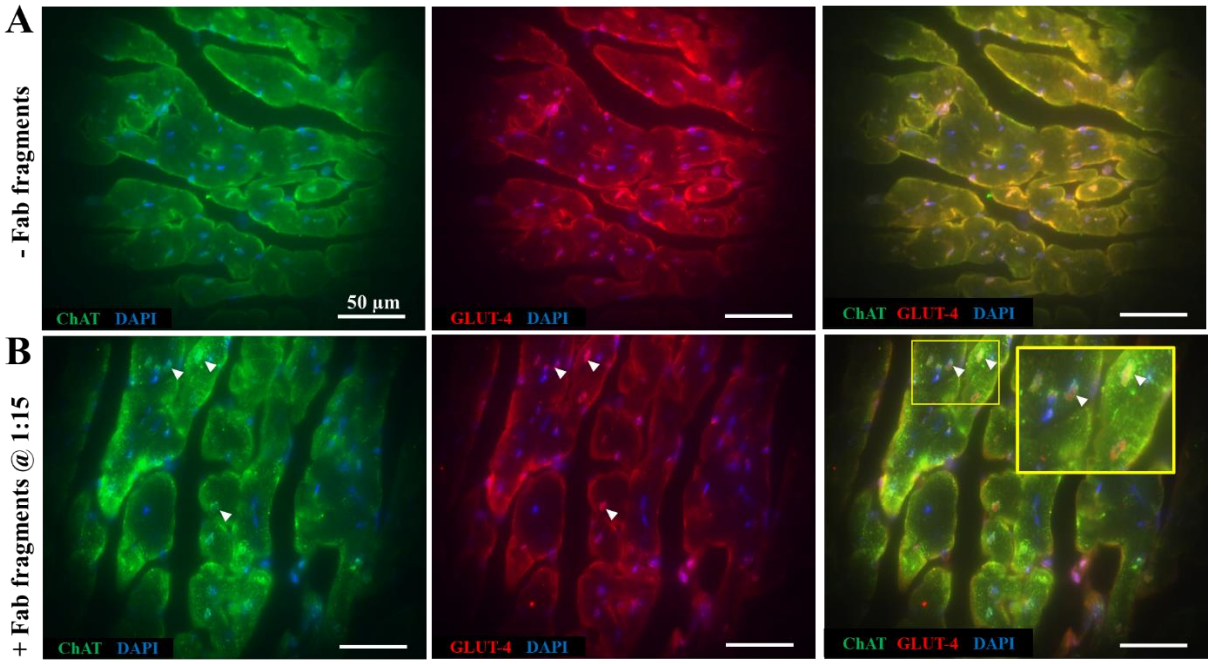

Figure S3.3 The co-staining of ChAT and GLUT-4 on the same ventricular tissue in the absence and presence of AffiniPure anti-rabbit Fab fragments

Representative fluorescent images showing co-staining of ChAT and GLUT-4 ***(A)*** *in the absence and* ***(B)*** *in the presence of AffiniPure anti-rabbit Fab fragments. The anti-rabbit Fab fragments successfully blocked the crossreactivity as ChAT and intracellular GLUT-4 vesicles (white arrows) can be clearly differentiated in the cardiomyocytes.*

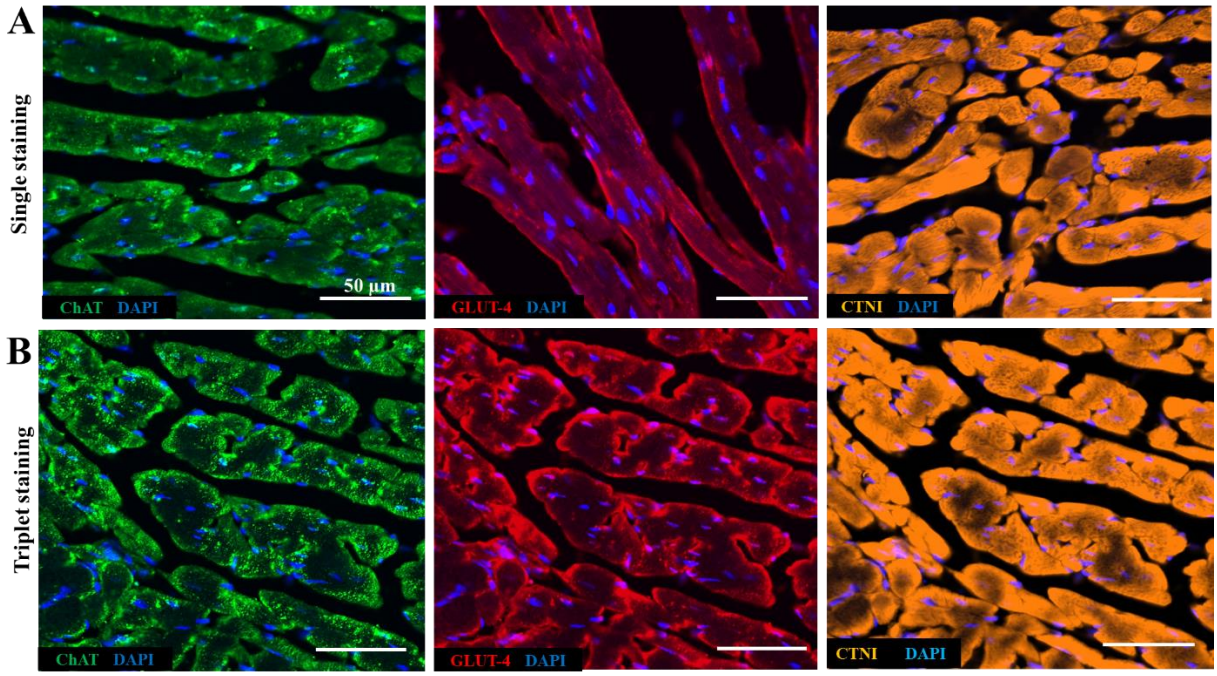

Figure S3.4 Single and triplet staining of ChAT, GLUT-4 and CTNI on mouse ventricular tissues

Representative confocal images showing (A) single staining on different mouse ventricular tissue and ***(B)*** *triplet staining of ChAT, GLUT-4 and CTNI in the same mouse ventricular tissue. This images from single staining served as a control for comparison with the images from triplet staining.*

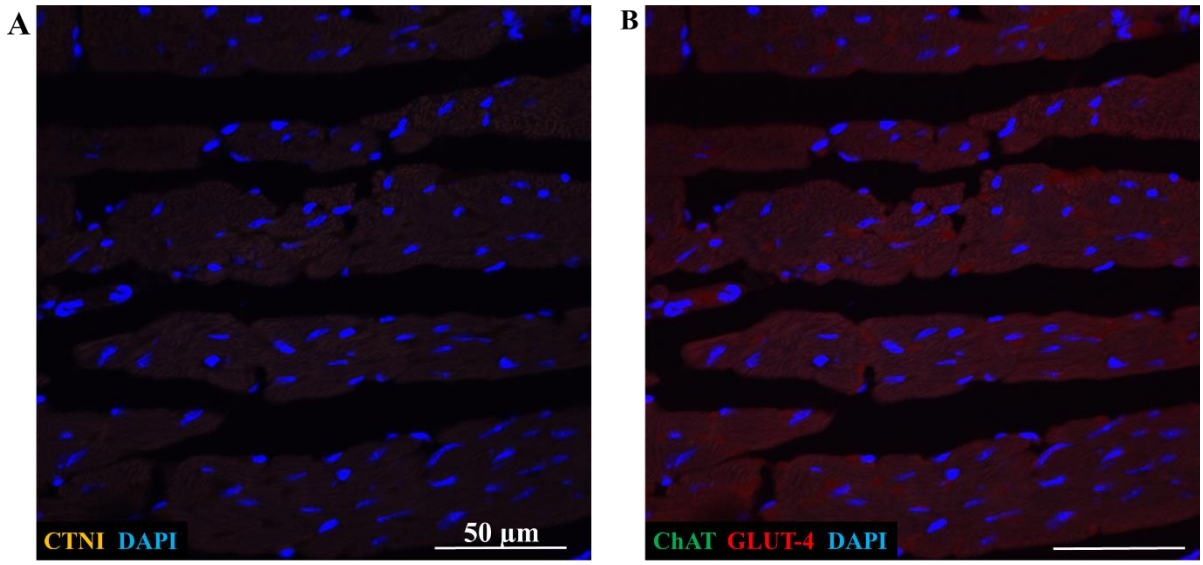

Figure S3.5 The secondary-antibody only control for CTNI, ChAT, GLUT-4 in mouse ventricular tissue

Representative confocal images showing secondary-antibody only control of ***(A)*** *CTNI and* ***(B)*** *ChAT, GLUT-4 in the same mouse ventricular tissue.*

Appendix 4

Measurement of blood glucose level

Accu-Chek Performa blood glucose device kit (Roche) was used to measure the blood glucose level of the *db/db* and *db/db-ChAT-tg* mice. The measurement was taken between 9 am to 10 am to minimize fluctuation of blood glucose level due to the mice's activity at different time. A lancing device was used to prick the tail of the mice to obtain blood. The blood drop was touched on the end of the test strip that has been inserted into the blood glucose meter. The results were expressed as mg/dL.

Measurement of LV function using pressure-volume (PV) catheter

LV function was measured as described by Oikawa et al. [267]. Briefly, the mice were anesthetized with 1% - 2% isoflurane at a flow rate of 0.5-1.0 L/min. The incision was made into the abdominal cavity to allow the PV catheter to be inserted into the apex of the heart via the diaphragm. The catheter was connected to an ADVantage PV system control box (Transonic Systems) and a data acquisition system (iWorx System). Hemodynamic parameters were measured using LabScribe2 software (iWorx System).

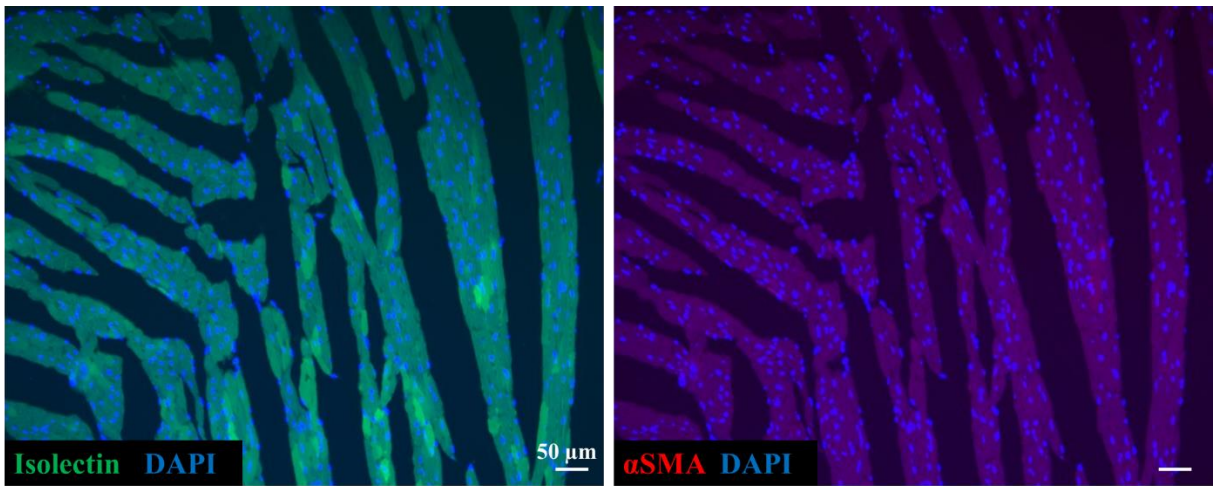

Figure S4.1 The secondary antibody-only control for staining of endothelial cells and smooth muscle cells.
Representative fluorescent images showing secondary antibody-only control for Isolectin B4 and anti-αSMA antibody staining as well as staining of nuclei in the ventricular tissue.

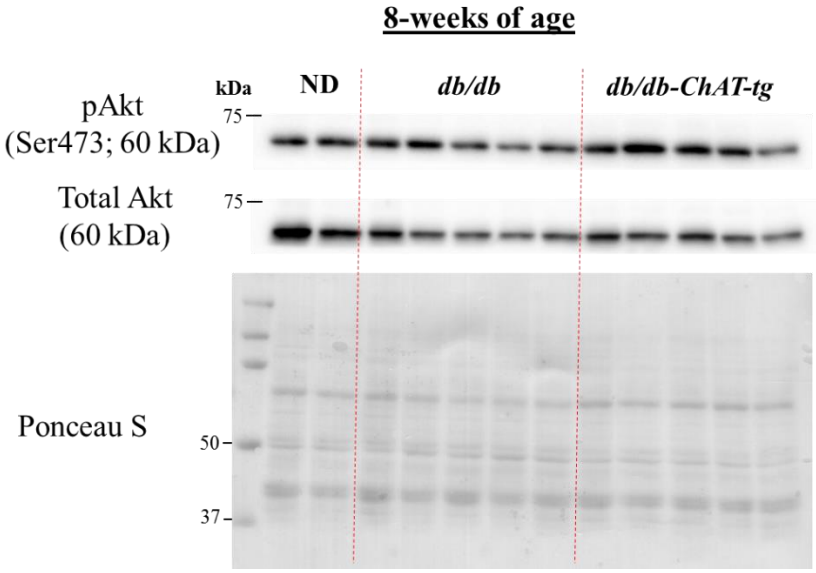

Figure S4.2 The protein expression of pAkt and total Akt in ND, *db/db* and *db/db-ChAT-tg* mice at 8-weeks of age.
Representative blots showing the protein expression of pAkt (serine 473), total Akt as well as total protein expression from Ponceau S staining from the ND, db/db and db/db-ChAT-tg micea t 8-weeks of age.

Appendix 5

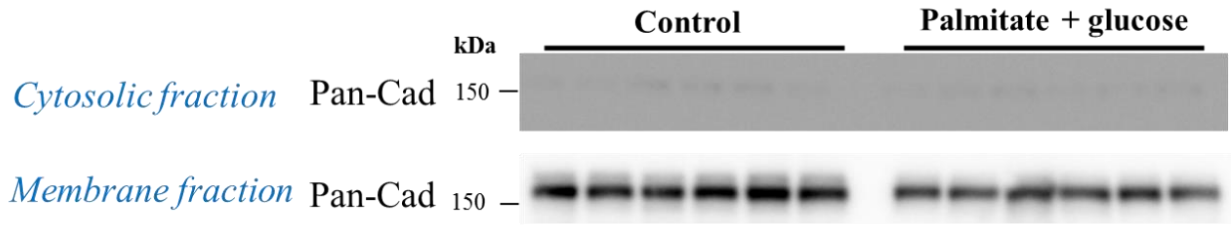

Figure S5.1 Fraction of cytosolic and membrane protein from AC16 cells.
Representative blots showing the protein expression of Pan-Cad (membrane protein) in cytosolic and membrane fraction. Low protein expression of Pan-Cad in cytosolic fraction indicates the successful separation of cytosolic and membrane proteins.

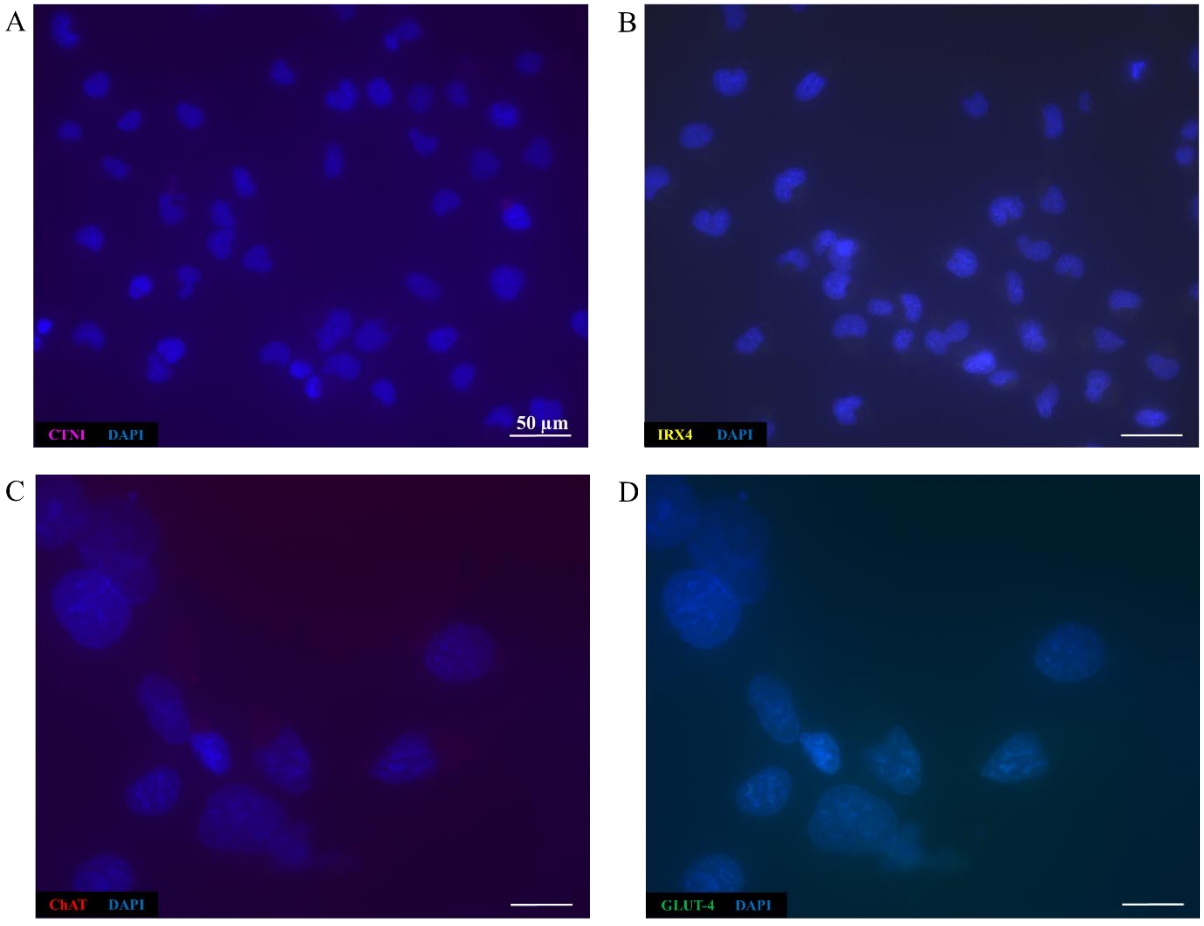

Figure S5.2 Secondary antibody-only control for CTNI, IRX4, ChAT, and GLUT-4 staining.
*Representative fluorescent images showing the secondary antibody-only control for **(A)** CTNI, **(B)** IRX4, **(C)** ChAT, and **(D)** GLUT-4 staining in AC16 cells.*

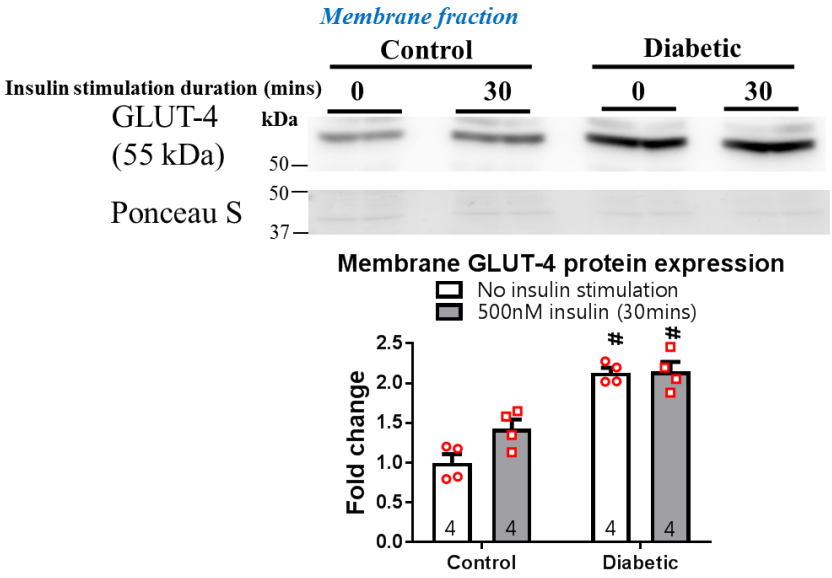

Figure S5.3 24-hours of palmitate and glucose treatment did not impair insulin-stimulated GLUT-4 membrane translocation

Representative blots and bar graphs with scatter blots showing the membrane GLUT-4 protein expression in AC16 cells after 24 hours of vehicle or palmitate and glucose treatment. After treatment, the cells were stimulated with 500nM of insulin for 30-mins to test the insulin responsiveness. Data are expressed as mean ± SEM. A non-parametric Mann-Whitney test was performed. $^{\#}p<0.05$ VS control AC16 cells with the same insulin treatment. The number of samples per group is indicated in the figure. The total number of samples was derived from two independent experiments.

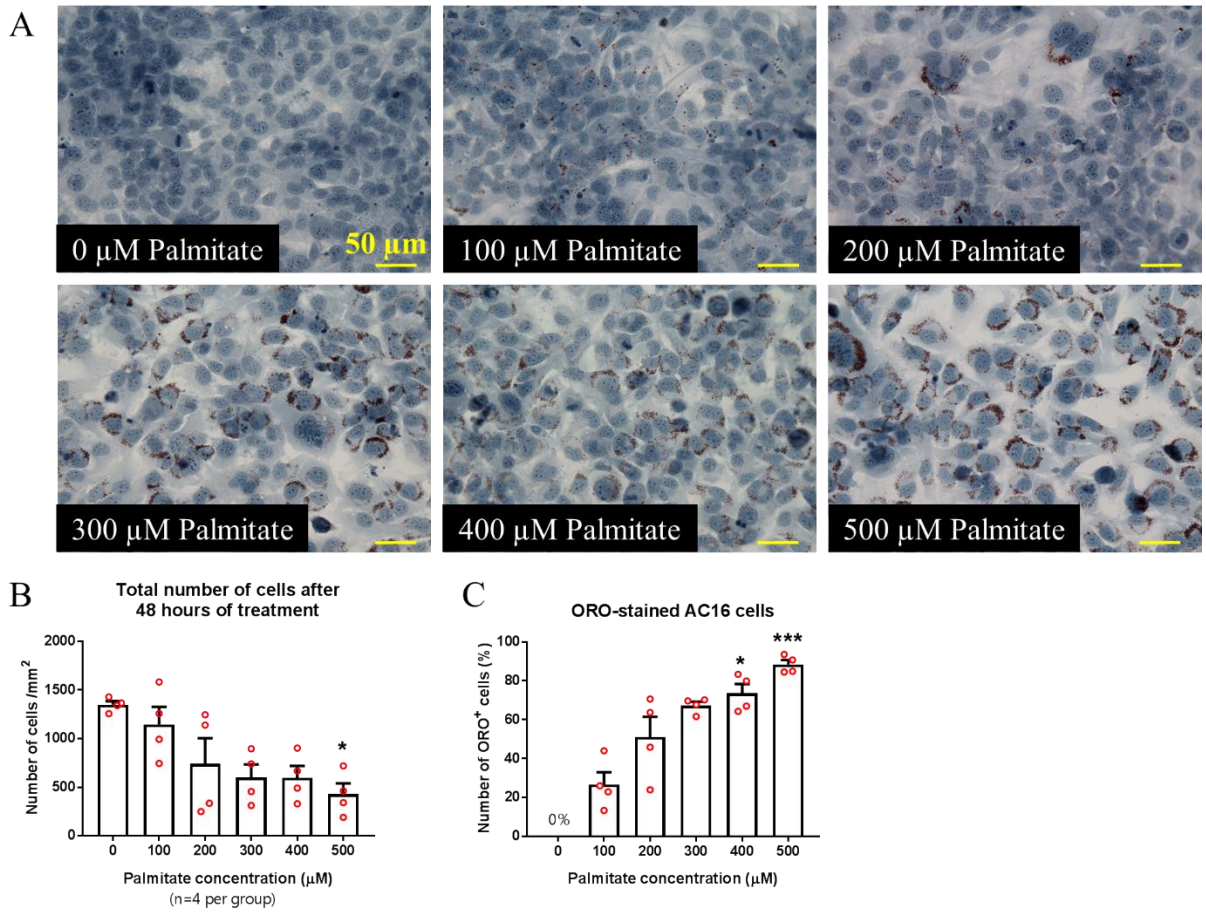

Figure S5.4 Optimization of palmitate concentration to induce palmitate uptake.

(A) *Representative images showing the ORO staining of AC16 cells treated with 100, 200, 300, 400 and 500µM of palmitate for 48 hours. The hematoxylin-stained nuclei are in blue while the ORO-stained palmitate appears in red. Yellow arrows indicate ORO-positive cells. Bar graphs with scatter plots showing the* ***(B)*** *total number of viable cells/mm^2 remained and* ***(C)*** *percentage of ORO-positive cells per total cells after 48 hours of treatment. A non-parametric Kruskal-Wallis test with Dunn's multiple comparison test was performed. For figure B: *p<0.05 VS AC16 cells treated with 0µM of palmitate; For figure C: *p<0.05; ***p<0.001 VS AC16 cells treated with 100µM of palmitate. The number of samples per group is indicated in the figure. The total number of samples was derived from two independent experiments.*

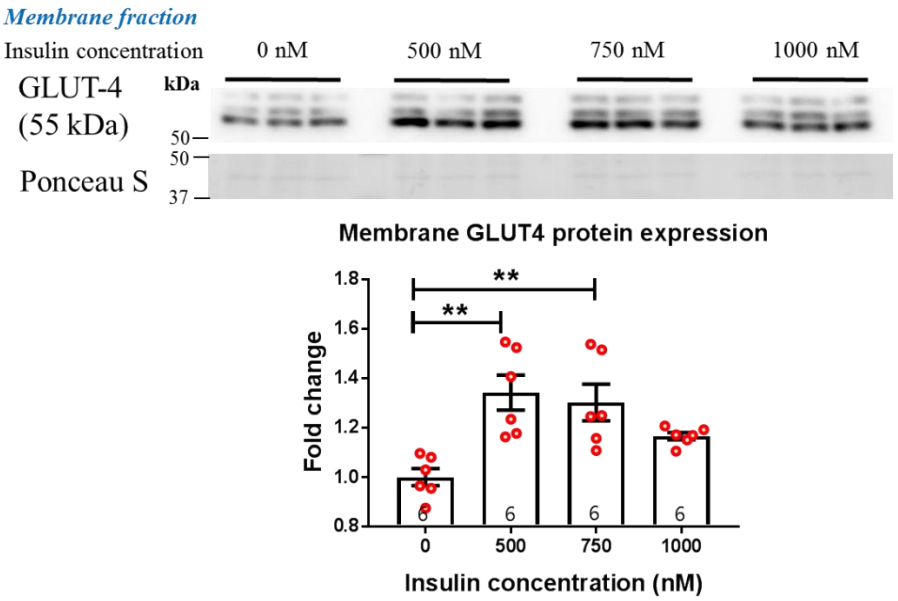

Figure S5.5 Stimulation of AC16 cells with various concentration of insulin to mediate GLUT-4 membrane translocation.

*Representative blots and bar graphs with scatter blots showing the protein expression of GLUT-4 at the plasma membrane in response to stimulation with 0, 500, 750 and 1,000 nM of insulin concentration for 60-mins. Data are expressed as mean ± SEM. One-way ANOVA with Dunnett's multiple comparisons test was performed. **p<0.01 VS AC16 cells treated with 0nM insulin. The number of samples per group is indicated in the figure. The total number of samples was derived from two independent experiments.*

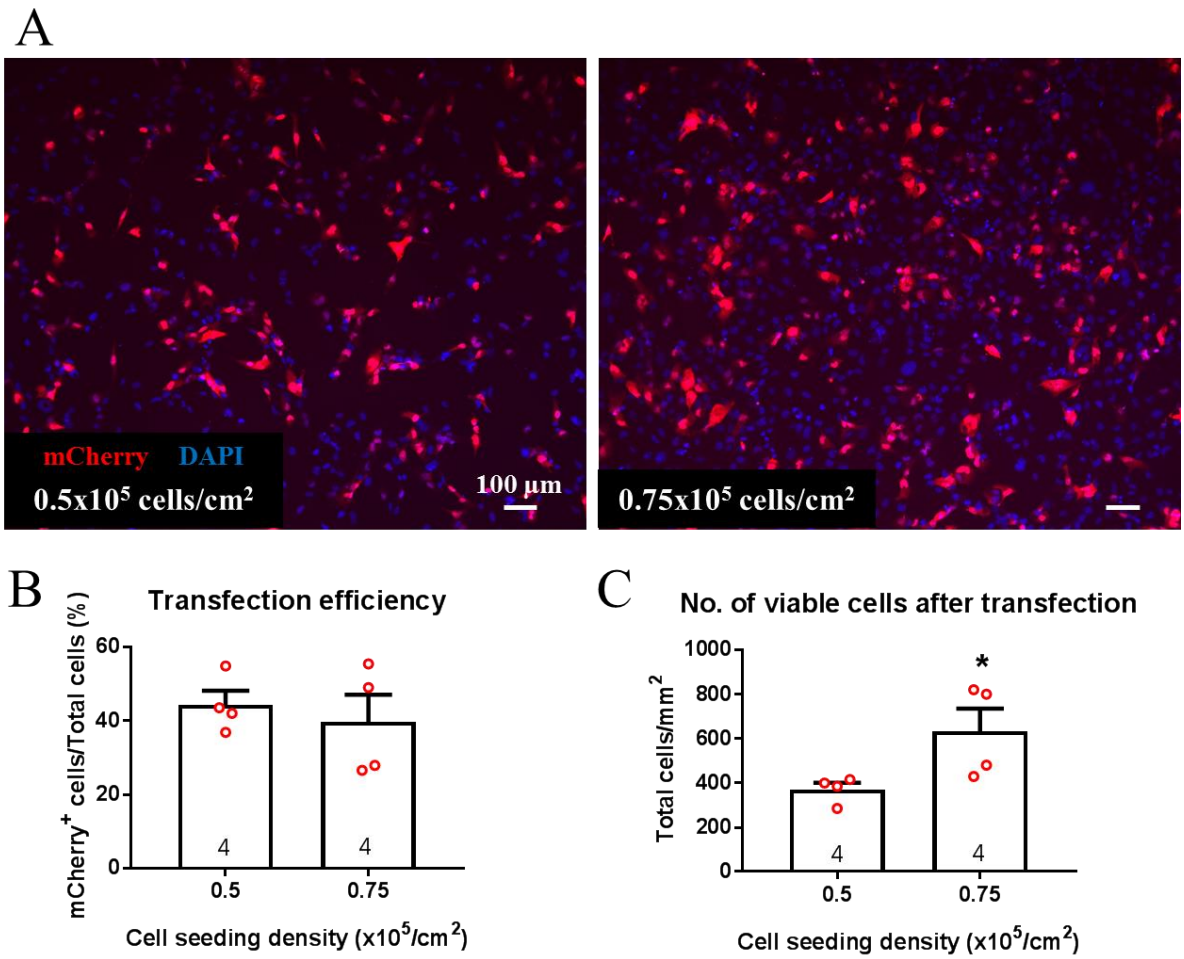

Figure S5.6 Optimization of cell seeding density for lipofectamine transfection
(A) *Representative fluorescent images showing the expression of mCherry fluorescent proteins and staining of nuclei by DAPI in the AC16 cells after 24 hours of transfection. Bar graphs with scatter plots showing the* ***(B)*** *transfection efficiency determined by the percentage of mCherry-positive cells per total cells and* ***(C)*** *total number of viable cells remained after 24 hours of transfection. A non-parametric Mann-Whitney test was performed. *p<0.05 VS AC16 cells seeded in density of 0.5x10^5 cell/cm^2. The number of samples per group is indicated in the figure. The total number of samples was derived from two independent experiments.*

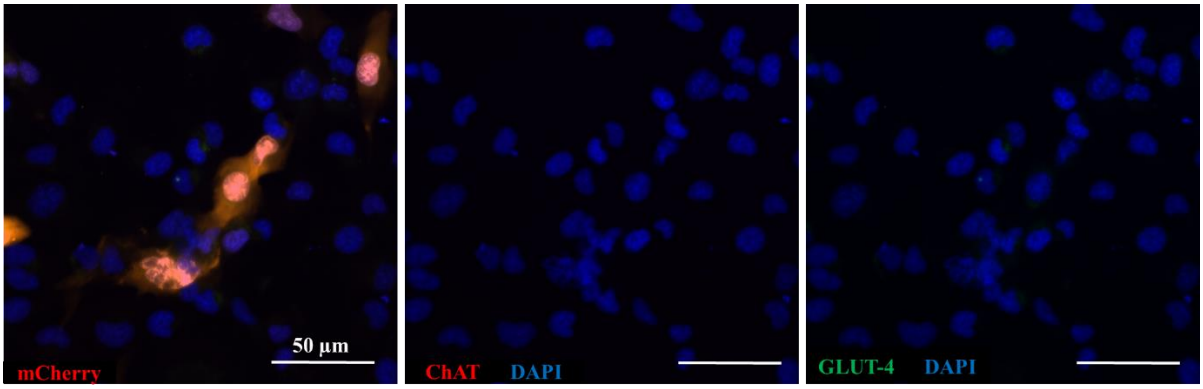

Figure S5.7 Secondary antibody-only control for ChAT and GLUT-4 in the transfected AC16 cells
Representative confocal images showing the endogenous mCherry fluorescent protein as well as secondary antibody-only control for co-staining of ChAT and GLUT-4 in the transfected AC16 cells.

In order to compare *(1)* the expression changes in endogenous ChAT in the control or diabetic WT cells in normoxic and hypoxic condition OR *(2)* the expression changes in ChAT in the control or diabetic hChAT transfected cells in normoxic and hypoxic condition (Appendix 3, S5.8), the protein samples from these cells should have grouped and processed in one PAGE gel for western blot analysis. However, as the protein amount from the diabetic cells were insufficient, I was not able to handle these samples together. Thus, the comparison of ChAT expression changes was made in separate blots. For this reason, I expressed the data as a ratio between ChAT and total protein (relative expression) rather than fold change.

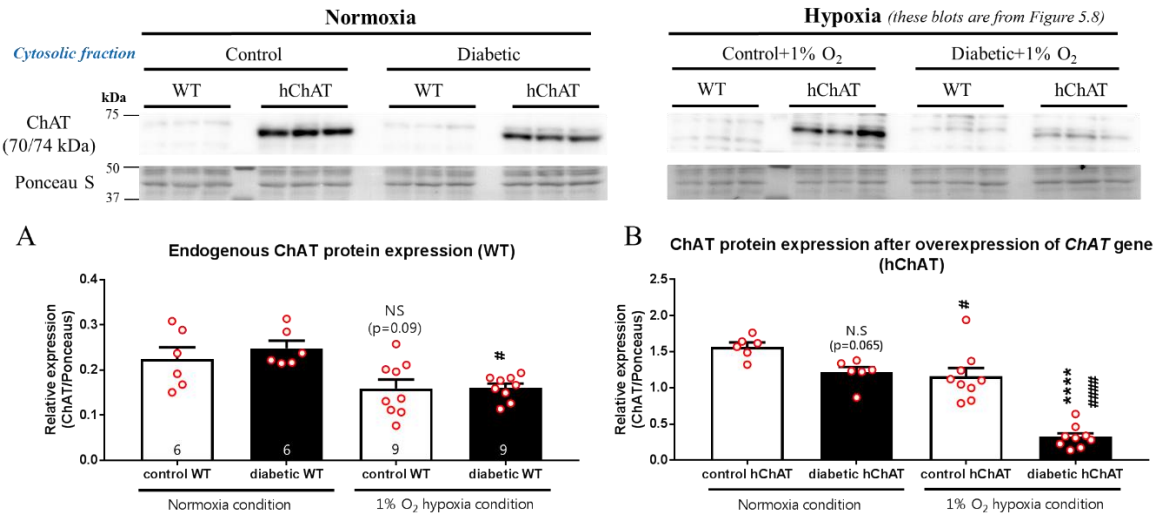

Figure S5.8 ChAT expression in control and diabetic transfected AC16 cells in normoxic and hypoxic condition.

Representative blots and bar graphs with scatter plots showing ***(A)*** *the endogenous ChAT expression from control and diabetic AC16 cells and* ***(B)*** *the ChAT expression after overexpression of ChAT gene from control and diabetic in normoxic and hypoxic condition. Data are expressed as mean ± SEM. One-way ANOVA test with Tukey's comparison test was performed. ****$p<0.0001$ VS control hChAT transfected cells AC16 cells; $^{\#}p<0.05$, $^{\#\#\#\#}p<0.0001$ VS respective control or diabetic AC16 cells in normoxic condition. The number of samples per group is indicated in the figure. The total number of samples in the normoxic condition was derived from two independent experiments, while the total number of samples in the hypoxic condition was derived from three independent experiments.*